

Microorganism and process engineering for biosynthesis

Edited by

Qi Xianghui, Jiandong Cui, Hossain M. Zayed
and Md Mofijur Rahman

Published in

Frontiers in Bioengineering and Biotechnology



FRONTIERS EBOOK COPYRIGHT STATEMENT

The copyright in the text of individual articles in this ebook is the property of their respective authors or their respective institutions or funders. The copyright in graphics and images within each article may be subject to copyright of other parties. In both cases this is subject to a license granted to Frontiers.

The compilation of articles constituting this ebook is the property of Frontiers.

Each article within this ebook, and the ebook itself, are published under the most recent version of the Creative Commons CC-BY licence. The version current at the date of publication of this ebook is CC-BY 4.0. If the CC-BY licence is updated, the licence granted by Frontiers is automatically updated to the new version.

When exercising any right under the CC-BY licence, Frontiers must be attributed as the original publisher of the article or ebook, as applicable.

Authors have the responsibility of ensuring that any graphics or other materials which are the property of others may be included in the CC-BY licence, but this should be checked before relying on the CC-BY licence to reproduce those materials. Any copyright notices relating to those materials must be complied with.

Copyright and source acknowledgement notices may not be removed and must be displayed in any copy, derivative work or partial copy which includes the elements in question.

All copyright, and all rights therein, are protected by national and international copyright laws. The above represents a summary only. For further information please read Frontiers' Conditions for Website Use and Copyright Statement, and the applicable CC-BY licence.

ISSN 1664-8714
ISBN 978-2-8325-3016-0
DOI 10.3389/978-2-8325-3016-0

About Frontiers

Frontiers is more than just an open access publisher of scholarly articles: it is a pioneering approach to the world of academia, radically improving the way scholarly research is managed. The grand vision of Frontiers is a world where all people have an equal opportunity to seek, share and generate knowledge. Frontiers provides immediate and permanent online open access to all its publications, but this alone is not enough to realize our grand goals.

Frontiers journal series

The Frontiers journal series is a multi-tier and interdisciplinary set of open-access, online journals, promising a paradigm shift from the current review, selection and dissemination processes in academic publishing. All Frontiers journals are driven by researchers for researchers; therefore, they constitute a service to the scholarly community. At the same time, the *Frontiers journal series* operates on a revolutionary invention, the tiered publishing system, initially addressing specific communities of scholars, and gradually climbing up to broader public understanding, thus serving the interests of the lay society, too.

Dedication to quality

Each Frontiers article is a landmark of the highest quality, thanks to genuinely collaborative interactions between authors and review editors, who include some of the world's best academicians. Research must be certified by peers before entering a stream of knowledge that may eventually reach the public - and shape society; therefore, Frontiers only applies the most rigorous and unbiased reviews. Frontiers revolutionizes research publishing by freely delivering the most outstanding research, evaluated with no bias from both the academic and social point of view. By applying the most advanced information technologies, Frontiers is catapulting scholarly publishing into a new generation.

What are Frontiers Research Topics?

Frontiers Research Topics are very popular trademarks of the *Frontiers journals series*: they are collections of at least ten articles, all centered on a particular subject. With their unique mix of varied contributions from Original Research to Review Articles, Frontiers Research Topics unify the most influential researchers, the latest key findings and historical advances in a hot research area.

Find out more on how to host your own Frontiers Research Topic or contribute to one as an author by contacting the Frontiers editorial office: frontiersin.org/about/contact

Microorganism and process engineering for biosynthesis

Topic editors

Qi Xianghui — Jiangsu University, China

Jiandong Cui — Tianjin University of Science and Technology, China

Hossain M. Zayed — Jiangsu University, China

Md Mofijur Rahman — University of Technology Sydney, Australia

Citation

Xianghui, Q., Cui, J., Zayed, H. M., Rahman, M. M., eds. (2023). *Microorganism and process engineering for biosynthesis*. Lausanne: Frontiers Media SA.
doi: 10.3389/978-2-8325-3016-0

Table of contents

- 04 **Editorial: Microorganism and process engineering for biosynthesis**
Xianghui Qi, Jiandong Cui, M. Mofijur and Hossain M. Zabed
- 07 **Process study of ceramic membrane-coupled mixed-cell fermentation for the production of adenine**
Pengjie Sun, Changgeng Li, Yu Gong, Jinduo Wang and Qingyang Xu
- 19 **The potential of caproate (hexanoate) production using *Clostridium kluyveri* syntrophic cocultures with *Clostridium acetobutylicum* or *Clostridium saccharolyticum***
Jonathan K. Otten, Yin Zou and Eleftherios T. Papoutsakis
- 33 **Genetic engineering for enhanced production of a novel alkaline protease BSP-1 in *Bacillus amyloliquefaciens***
Cong Jiang, Changwen Ye, Yongfeng Liu, Kuo Huang, Xuedeng Jiang, Dian Zou, Lu Li, Wenyan Han and Xuetuan Wei
- 45 **A facile and efficient synthesis approach of salidroside esters by whole-cell biocatalysts in organic solvents**
Rongling Yang, Yu Wang, Xiangjie Zhao, Zheng Tong, Qianlin Zhu, Xiaoxi He, Zhaoyu Wang, Hongzhen Luo and Fang Fang
- 53 **Engineering the glyoxylate cycle for chemical bioproduction**
Peng Yang, Wenjing Liu, Yanan Chen and An-Dong Gong
- 69 **One-pot encapsulation of lactate dehydrogenase and Fe₃O₄ nanoparticles into a metal–organic framework: A novel magnetic recyclable biocatalyst for the synthesis of D-phenyllactic acid**
Xiaolong Sun, Jiahuan Hu, Yifeng Wang, Xi Luo, He Huang and Yongqian Fu
- 79 **Engineering *Bacillus subtilis* for production of 3-hydroxypropanoic acid**
Abhroop Garg, Carsten Jers, Hee Jin Hwang, Aida Kalantari, Ildze Ventina and Ivan Mijakovic
- 87 **Enhancing and stabilizing monoclonal antibody production by Chinese hamster ovary (CHO) cells with optimized perfusion culture strategies**
Kexue Liang, Hongzhen Luo and Qi Li
- 97 **System metabolic engineering of *Escherichia coli* W for the production of 2-ketoisovalerate using unconventional feedstock**
Darwin Carranza-Saavedra, Jesús Torres-Bacete, Blas Blázquez, Claudia Patricia Sánchez Henao, José Edgar Zapata Montoya and Juan Nogales
- 111 **Improved laccase production by *Trametes versicolor* using Copper-Glycyl-L-Histidyl-L-Lysine as a novel and high-efficient inducer**
Feng Wang, Xiaolei Yu, Zhuo Yu, Yi Cui, Ling Xu, Shuhao Huo, Zhongyang Ding, Liting Zhao, Lizhi Du and Yanguo Qiu



OPEN ACCESS

EDITED AND REVIEWED BY
Georg M. Guebitz,
University of Natural Resources and Life
Sciences Vienna, Austria

*CORRESPONDENCE

Xianghui Qi,
✉ qxh@ujs.edu.cn,
✉ bioqxh@163.com
Hossain M. Zayed,
✉ zayedctgbd@yahoo.com

RECEIVED 14 June 2023

ACCEPTED 26 June 2023

PUBLISHED 03 July 2023

CITATION

Qi X, Cui J, Mofijur M and Zayed HM
(2023), Editorial: Microorganism and
process engineering for biosynthesis.
Front. Bioeng. Biotechnol. 11:1239991.
doi: 10.3389/fbioe.2023.1239991

COPYRIGHT

© 2023 Qi, Cui, Mofijur and Zayed. This is
an open-access article distributed under
the terms of the [Creative Commons
Attribution License \(CC BY\)](#). The use,
distribution or reproduction in other
forums is permitted, provided the original
author(s) and the copyright owner(s) are
credited and that the original publication
in this journal is cited, in accordance with
accepted academic practice. No use,
distribution or reproduction is permitted
which does not comply with these terms.

Editorial: Microorganism and process engineering for biosynthesis

Xianghui Qi^{1,2*}, Jiandong Cui³, M. Mofijur^{4,5} and
Hossain M. Zayed^{1,2*}

¹School of Life Sciences, Guangzhou University, Guangzhou, Guangdong, China, ²School of Food and Biological Engineering, Jiangsu University, Zhenjiang, Jiangsu, China, ³State Key Laboratory of Food Nutrition and Safety, Laboratory of Industrial Fermentation Microbiology, Ministry of Education, Tianjin University of Science and Technology, Tianjin Economic and Technological Development Area (TEDA), Tianjin, China, ⁴Faculty of Engineering and IT, University of Technology Sydney, Sydney, NSW, Australia, ⁵Mechanical Engineering Department, Prince Mohammad Bin Fahd University, Al Khobar, Saudi Arabia

KEYWORDS

microbial biosynthesis, biocatalysis, cell factory, fermentation, bioprocessing

Editorial on the Research Topic

Microorganism and process engineering for biosynthesis

Introduction

Recent years have observed a significant surge in research and industrial focus on the biosynthesis of valuable chemicals and natural products. This trend has been primarily driven by the increasing demand for green manufacturing of pharmaceuticals, food ingredients, agricultural products, bioplastics, and important chemicals. Microorganisms play a central role in biosynthesis, and the effectiveness of biocatalysts determines the overall success and acceptance of biosynthesis technologies. With substantial research efforts in strain and bioprocess engineering, there have been significant developments in biosynthesis. Nevertheless, many of the developed technologies for biosynthesis have not been explored commercially due to their low competitiveness and inadequate production performance metrics. The primary challenges include the low stability and tolerance of microorganisms to stressors, slow growth rate, unbalanced metabolic pathways, and inefficient distribution of carbon flux, leading to unwanted byproducts.

Overcoming these challenges requires multidisciplinary and multidimensional efforts, and hence, there has been a growing interest in the exploration of novel strains and metabolic engineering strategies to develop efficient cell factories. These approaches particularly aimed to modulate pathways and engineer strains to enhance the performance of biocatalysts beyond what is observed in their wild counterparts. Furthermore, considerable attention has been devoted to the midstream step, which involves fermentation and requires careful configuration and simulation to achieve the desired levels of titer, yield, and productivity for the target product.

The objective of this Research Topic (RT) was to provide valuable insights into recent advancements in engineering strategies for the development of cell factories and bioprocesses, leading to the establishment of sustainable biosynthesis technologies. With

a compilation of 10 articles, this RT offers an up-to-date overview of various aspects, including microbial hosts as cell factories, metabolic pathways, product streams, bioprocessing strategies, and optimization techniques used in biosynthesis. The published articles were authored by researchers affiliated with esteemed institutions across the globe, including countries like the United States, China, Denmark, Sweden, South Korea, Colombia, and Spain. The editorial team expresses sincere gratitude to all the authors for their valuable contributions to this RT.

Biocatalysts and microbial hosts as cell factories

Biosynthesis of value-added chemicals primarily involves biocatalysts, which are generally categorized into enzymatic and microbial biocatalysts. In a study, a novel enzymatic biocatalyst was developed for D-phenyllactic acid biosynthesis by immobilizing lactate dehydrogenase with Fe_3O_4 nanoparticles on a metal-organic framework (Sun et al.). However, microbial systems are generally more convenient and cost-effective compared to biocatalysts. Microorganisms play a central role in biosynthesis, where a wide range of hosts have been explored. The selection of a suitable host depends on factors such as feasibility, genomic knowledge, available engineering tools, and the intended use of the target product. For instance, the model host *E. coli* is frequently used in target product biosynthesis due to its extensive genetic information and engineering capabilities, as demonstrated in Carranza-Saavedra et al. Nevertheless, if the synthesized product is intended for use in food preparations, the use of *E. coli* as a cell factory may raise safety concerns. In such cases, attention may shift to generally recognized as safe (GRAS) strains, as reported in a study by using *Bacillus subtilis* for 3-hydroxypropionic acid (3-HP) biosynthesis (Garg et al.).

The development of a cell factory for the target host requires the construction of a pathway, which can be native or heterologous, and may consist of either product-specific or general pathways. For example, a *B. subtilis* cell factory containing the 3-HP producing pathway was used to biosynthesize 3-HP from glycerol (Garg et al.), while a general pathway like the glyoxylate cycle (GOC) is capable of producing various value-added compounds. This RT published a review on GOC that comprehensively discussed the metabolic regulation of GOC and advancements in biosynthesis performed with this pathway (Yang et al.).

Product streams

To date, a wide range of value-added and platform chemicals have been reported to be produced by microbial biosynthesis from inexpensive and non-fossil fuel-based substrates with competitive titer and productivity. For example, caproate (hexanoate), which is a valuable platform chemical with its applications in various fields, was biosynthesized from sugars (Otten et al.). Using clostridial cell factories, the authors reported up to 200 mM titer and 8.1 mM/h productivity of caproate. Likewise, biosynthesis of several other platform chemicals was also reported in this RT, including 3-HP (Garg et al.) and 2-ketoisovalerate (Carranza-Saavedra et al.). Apart

from platform chemicals, the production of enzymes has also gained attention. For example, alkaline protease, which has widespread industrial applications, was successfully produced by microorganisms heterologously expressing a relevant gene from *B. subtilis* into *B. amyloliquefaciens* (Jiang et al.). Similarly, laccase production has been reported using *Trametes versicolor* and a novel inducer called copper-glycyl-L-histidyl-L-lysine (GHK-Cu) (Wang et al.). Another group of products is dedicated to food or health-related applications, and this RT has reported biosynthesis of several such products, including adenine (Sun et al.), D-phenyllactic acid (Sun et al.), and monoclonal antibodies (Liang et al.).

Engineering cell factories and bioprocesses

Recent advancements in microbial biosynthesis have utilized advanced technologies to obtain efficient microbial systems and bioprocesses. Coculture technology is one of them that has received significant attention recently. In one study, a novel coculture system was designed for caproate biosynthesis using clostridial species, specifically *Clostridium kluyveri* and *C. saccharolyticum* (Otten et al.). This system exhibited notably higher titers and productivity than monoculture systems. Once a cell factory is developed, the next step is bioprocessing of appropriate substrates, typically involving fermentation. However, this technology presents certain challenges, such as the non-targeted flow of carbon flux. Additionally, achieving optimal efficiency during fermentation can be difficult due to varying conditions between cell growth and product synthesis. In this context, resting cell or whole cell technology has gained attention in recent years. This technology was applied in a study on salidroside biosynthesis, which is a plant-derived bioactive compound (Yang et al.). The authors optimized the conditions and reported excellent conversion efficiency and regioselectivity using the whole cells of *Aspergillus oryzae*. In another attempt, chemical and enzymatic synthesis methods were replaced for adenine by exploring fermentation and enzymatic approaches. A fermentation system coupled with a ceramic membrane was employed to enhance permeability (Sun et al.). This technology led to significant improvements in cell viability and product recovery, with an average adenine titer of 14 g/L.

Conclusion and outlook

Over the past two decades, there has been a significant research focus on the biosynthesis of valuable compounds with microorganisms playing a crucial role. The aim has been to develop efficient cell factories and bioprocess technologies for sustainable biosynthesis. This RT presents a compilation of 10 high-quality articles, showcasing various research efforts. These articles cover essential aspects such as cell factories, host streams, product ranges, and emerging technological strategies. However, to fully unlock the potential of these biosynthesis technologies, it is imperative to address the challenges associated with microorganisms and bioprocessing through further innovative

research. By doing so, we can pave the way for the widespread adoption of biosynthesis and drive the development of sustainable and efficient production methods across a wide range of applications.

Author contributions

XQ, HZ, JC, and MM conceptualized and designed the study. XQ and HZ wrote the initial draft, while other authors carefully reviewed the draft. All authors contributed to the article and approved the submitted version.

Acknowledgments

The authors are thankful to the National Natural Science Foundation of China (grant no. 32272284), the Foreign Expert Program, Ministry of Science and Technology, China (no.

QN2022014005L), and the Innovation and Entrepreneurship Program of Jiangsu Province (no. SSCBS20210929).

Conflict of interest

The authors declare that the research was conducted in the absence of any commercial or financial relationships that could be construed as a potential conflict of interest.

Publisher's note

All claims expressed in this article are solely those of the authors and do not necessarily represent those of their affiliated organizations, or those of the publisher, the editors, and the reviewers. Any product that may be evaluated in this article, or claim that may be made by its manufacturer, is not guaranteed or endorsed by the publisher.



OPEN ACCESS

EDITED BY

Hossain M. Zayed,
Jiangsu University, China

REVIEWED BY

Shams Forruque Ahmed,
Asian University for Women, Bangladesh
Parveen Fatemeh Rupani,
KU Leuven, Belgium

*CORRESPONDENCE

Qingyang Xu,
xuqingyang@tust.edu.cn

SPECIALTY SECTION

This article was submitted to Industrial
Biotechnology,
a section of the journal
Frontiers in Bioengineering and
Biotechnology

RECEIVED 15 June 2022

ACCEPTED 14 July 2022

PUBLISHED 10 August 2022

CITATION

Sun P, Li C, Gong Y, Wang J and Xu Q
(2022), Process study of ceramic
membrane-coupled mixed-cell
fermentation for the production
of adenine.
Front. Bioeng. Biotechnol. 10:969668.
doi: 10.3389/fbioe.2022.969668

COPYRIGHT

© 2022 Sun, Li, Gong, Wang and Xu. This
is an open-access article distributed
under the terms of the [Creative
Commons Attribution License \(CC BY\)](#).
The use, distribution or reproduction in
other forums is permitted, provided the
original author(s) and the copyright
owner(s) are credited and that the
original publication in this journal is
cited, in accordance with accepted
academic practice. No use, distribution
or reproduction is permitted which does
not comply with these terms.

Process study of ceramic membrane-coupled mixed-cell fermentation for the production of adenine

Pengjie Sun^{1,2}, Changgeng Li^{1,2}, Yu Gong^{1,2}, Jinduo Wang^{1,2} and Qingyang Xu^{1,2*}

¹National and Local United Engineering Lab of Metabolic Control Fermentation Technology, Tianjin University of Science and Technology, Tianjin, China, ²College of Biotechnology, Tianjin University of Science and Technology, Tianjin, China

In order to solve the problems of high complexity, many by-products, high pollution and difficult extraction of the existing adenine production process, in this study, ceramic membrane-coupled mixed cell fermentation was used to produce adenine while reducing the synthesis of by-products and simplifying the production process of adenine. Nucleoside hydrolase (encoded by the *rihC* gene) was used to produce adenine by coordinated fermentation with the adenosine-producing bacterium *Bacillus Subtilis* XGL. The adenosine hydrolase (AdHy)-expressing strain *Escherichia coli* BL21-AdHy was successfully employed and the highest activity of the crude enzyme solution was found by orthogonal experiments at 170 W power, 42% duty cycle, and 8 min of sonication. The highest AdHy activity was found after 18 h of induction incubation. *E. coli* BL21-AdHy was induced for 18 h and sonicated under the above ultrasonic conditions and the resulting crude enzyme solution was used for co-fermentation of the strain and enzyme. Moreover, 15% (v/v) of the AdHy crude enzyme solution was added to fermentation of *B. subtilis* XGL after 35 h. Finally, the whole fermentation system was dialyzed using coupled ceramic membranes for 45 and 75 h, followed by the addition of fresh medium. In contrast, the AdHy crude enzyme solution was added after 35, 65, and 90 h of *B. subtilis* fermentation, with three additions of 15, 15, and 10% of the *B. subtilis* XGL fermentation system. The process was validated in a 5 L fermenter and 14 ± 0.25 g/L of adenine was obtained, with no accumulation of adenosine and D-ribose as by-products. The enzymatic activity of the AdHy crude solution treated with ultrasound was greatly improved. It also reduced the cellular activity of *E. coli* BL21-AdHy and reduced effects on bacterial co-fermentation. Membrane-coupled dialysis solved the problem of decreased yield due to poor bacterial survival and decreased viability, and eliminated inhibition of the product synthesis pathway by adenosine. The batch addition of crude enzyme broth allowed the continuous conversion of adenosine to adenine. This production method provides the highest yield of biologically produced adenine reported to date, reduces the cost of adenine production, and has positive implications for the industrial production of adenine by fermentation. And it provides a reference for producing other high-value-added products made by fermentation.

KEYWORDS

adenine, adenosine, ceramic membrane, *Bacillus subtilis*, nucleoside hydrolase

Introduction

Adenine is one of the four basic bases of nucleic acids, which are essential molecules for life and evolution (Zhao et al., 2018). It is used in the treatment of granulocyte deficiency and neutropenia (Takeuchi et al., 2015) and can indirectly provide energy to red blood cells during blood storage (Paglia et al., 2016; Hess and Greenwalt, 2005). Adenine is also an intermediate in the production of many drugs and is used in the synthesis of phytohormone I, vitamins, adefovir, and vinegar. Owing to the wide range of applications of adenine, its use has been increasing worldwide in recent years.

Nowadays, the main methods for producing adenine are chemical synthesis and enzymatic catalysis. Li et al. (2016) prepared adenine from malononitrile and thiourea by cyclization in the presence of sodium alcohol, followed by oxidation, nitrosation and reduction; You et al. (2013) prepared adenine from acetyl hypoxanthine by chlorination and amination. Both of the above methods for preparing adenine by chemical synthesis suffer from harsh reaction conditions, complex reaction steps and environmental pollution. Lv and Fu (2008) prepared adenine by hydrolysis of adenosine at high temperature and pressure at 170–210°C. Yue et al. (2020) used adenosine as raw material and hydrolyzed adenosine into adenine and D-ribose under the combined action of adenosine hydrolase and neutral protease. Xie et al. (2018) successfully constructed an adenine-producing strain by introducing the gene encoding adenosine hydrolase, *rihC*, from *E. coli* into the original adenosine-producing bacteria. However, the fermentation cycle was long, with 44 h of fermentation production and a yield of only 6.38 g/L.

The rapid progress in the field of biotechnology constantly attracts new methods and solutions for further development of bioprocess performances. In the last decade, ultrasound has been widely used for enzyme-catalyzed biotransformations to enhance the reaction process and obtain higher product yields in a short period, as ultrasound can enhance enzyme activity by altering favourable conformational changes of proteins without changing their structural integrity. However, the tolerance of enzymes to ultrasound depends on the physiological properties of the enzymes themselves. Ladole et al. (2017) showed a 3.6-fold increase in the catalytic activity of cellulase compared to the control by incubating the enzyme at 24 kHz, 36 W power and 6 min ultrasound. *Pseudostelium antarcticum* lipase B activity increased 1.5-fold at 22 kHz, 15.48 W cm⁻² and 66.67% duty cycle (Nadar and Rathod, 2017). In recent years, the coupling of fermentation systems with other biotechnologies has been used as a new form of fermentation to increase product yields. He et al. (2021) increased the activities of three key enzymes in glycolytic metabolism (hexokinase, phosphofructokinase and pyruvate

kinase) by adding an ultrasound device to the fermentation of brewer's yeast for ethanol production at 280 w/L. 59.02, 109.05 and 87.27%, respectively, and the ethanol production increased by 30.79%. Coupling a butterfly centrifuge during the L-tyrosine fermentation process and cycling the fermentation system to fractionate the fermentation process increased L-tyrosine yield by 44.1% (Li et al., 2021).

In this study, a bacterial and enzyme-linked ceramic membrane co-fermentation method was used for the preparation of adenine. The conversion of adenosine to adenine and D-ribose was first achieved by adding AdHy crude enzyme solution to the production of adenosine by fermentation in *B. subtilis*. The batch addition of AdHy crude enzyme solution ensured the continuous conversion of adenosine. The D-ribose is involved in cellular energy metabolism (Teitelbaum et al., 2006) and can also be reused as a high-quality carbon source for *B. subtilis* XGL, thus reducing sugar consumption. Continuous production of adenosine is ensured by coupling ceramic membranes and adding nutrient flow to enhance strain viability and release the product from inhibition of the synthetic pathway. Nowadays, with the rise of biological methods, most nucleosides can be produced by biological processes. However, direct fermentation to produce adenosine has not been reported due to the strict feedback regulation of the purine synthesis pathway by adenosine. This method combines enzymatic and fermentation methods to successfully produce adenine by reusing D-ribose's by-product. Compared with the previous adenine production method, the present method has the advantages of high adenine yield, low environmental pollution, low by-products and low production costs, and it is suitable for the industrial production of adenine.

Materials and methods

Strains, plasmids, primers, and media

In this study, *E. coli* DH5α was used as a host strain for cloning and plasmid construction. *E. coli* BL21 was used as a host strain for enzyme expression, and pET-28a plasmid was used as an expression vector bearing the selectable kanamycin sulfate screening marker. Recombinant plasmids were constructed using the One Step Cloning Kit from Vazyme Biotech Co., Ltd (Nanjing, China). *E. coli* cells were cultured and screened on LB medium (1% peptone, 0.5% yeast powder, 1% NaCl) at 37 °C with the addition of 100 µg/ml ampicillin. The *E. coli* BL21-AdHy strain induction expression medium is presented in Supplementary Table S1. In this study, *B. subtilis* XGL (this isolate was screened by UV mutagenesis and was histidine- and xanthine-deficient) was used as the adenosine producing strain in

B. subtilis XGL medium (see [Supplementary Table S2](#) for the specific formulation), and the medium added after dialysis was the same (all reagents purchased from Sinopharm Chemical Reagent, Tianjin, China). The strains and plasmids used in this study are listed in [Supplementary Table S3](#) pET-28a identification primers synthesized by Genewiz (Jiangsu, China) are listed in [Supplementary Table S4](#). Plasmid extraction was performed using the plasmid rapid extraction kit from Omega Bio-tek Co. (Shanghai, China).

Construction of *E. coli* BL21-AdHy

We used pET-28a with a T7/lac-inducible strong promoter (induced by Isopropyl β -D-1-Thiogalactopyranoside (IPTG); for initiation). The nucleoside hydrolase used in this study (encoded by the *rihC* gene, GenBank ID: WP112886990.1), designed with the *rihC* fragment in pET-28a that has overlapping parts with the enzymatic sites EcoRI and HindIII, was synthesized by Genewiz (Jiangsu, China). Details of plasmid and strain construction are given in [Arivett et al. \(2014\)](#).

Culture of *E. coli* BL21-AdHy

E. coli BL21-AdHy cells were transferred from glycerol preservative tubes into strain activation medium (see [Supplementary Table S1](#)) for activated culture (two generations of activation) with the temperature maintained at 37°C. Activated strains were inoculated by aseptic manipulation into 5 L fermenters and incubated at a pH of approximately 6.7–7.0, a temperature of 37°C with 35–50% dissolved oxygen. The induction of AdHy expression was initiated by adding IPTG (0.1 mmol/L) within 4–5 h of incubation. (*E. coli* BL21-AdHy induction medium is presented in [Supplementary Table S1](#)).

Preparation of AdHy crude enzyme solution employed an ultrasonic bar with a power of 170 W and a frequency of 25 kHz was chosen to treat the bacteria, specifically, working its way through the process by working for 8 min with a duty cycle of 42%, during which time the temperature was controlled at 4°C and the final solution was stored in a 4°C tank for backup until the end of the overall fermentation process.

Culture of *B. subtilis* XGL

B. subtilis XGL was inoculated from glycerol-preserved tubes into activation medium (two generations of activation culture) and incubated at 34°C for 10–12 h. The activated strains were transferred to seed jars at 34°C, pH 6.7–7.0, with 30–50% dissolved oxygen. When the cells reached the middle of the exponential growth phase (OD_{600} : optical density at 600 nm; $OD_{600} = 15$ –20), the seed culture was introduced into the

fermenter as a 20% inoculum. Temperature was maintained at 34°C, with dissolved oxygen at 30–50% and pH 6.7–7.0 at the start of fermentation, with pH controlled at 6.4–6.7 from mid-fermentation ($OD_{600} > 30$). After 10 h of fermentation, flow-through of complex nutrients at a rate of 0.3 g/L/h was initiated (detailed composition of the medium is listed in [Supplementary Table S2](#)).

Bacterial and enzyme mixed coupling ceramic membrane fermentation

The hybrid coupled ceramic membrane fermentation system for bacteria and enzymes consisted of a fermenter (Shanghai Baoxing Biological Equipment Engineering Co., Ltd., Shanghai, China), a multi-frequency power ultrasound device (Hebei Handan He Tao Machinery Technology Co., Ltd., Hebei Handan, China) and a ceramic membrane circulation system. The ceramic membrane circulation system consisted of a centrifugal pump (Nanfeng Pump Co., Ltd., Jiangsu, China), a ceramic membrane (Shanghai Gaubire Environmental Engineering Co., Ltd., Shanghai, China) and a storage tank (Shanghai Baoxing Biological Equipment Engineering Co., Ltd., Shanghai, China). Adding AdHy crude enzyme solution to *B. subtilis* fermentation system, and two dialysis operations were performed during fermentation. The pH was maintained at 6.4–6.6 (pH adjusted by flow-through addition of ammonia), with dissolved oxygen at 40–60% and a temperature of 36°C. The process of coordinated dialysis fermentation with biomass is illustrated in [Figure 1](#).

Analytical methods

Detection of fermentation process

Determination of biomass: the optical absorbance at 600 nm was measured using a UV spectrophotometer (Beijing Pu-analysis General Instrument Co., Ltd., Beijing, China) after diluting the sample 10–100 times.

Determination of residual sugar content during fermentation: 1 ml of fermentation broth was sampled, centrifuged at 13,000 r/min for 2 min, the supernatant was diluted 100 times and the sugar content of the fermentation broth was determined using an SBA-40E biosensor (Institute of Biology, Shandong Academy of Sciences, Jinan, China).

Verification method of strain construction

Colony PCR amplification validation method: The single colonies cultured overnight were inoculated into 15 μ L colony PCR system for reaction. At the end of the reaction, agarose gel electrophoresis was used to verify the size of the band (refer to [Petersen and Møller, 2001](#), for specific steps.).

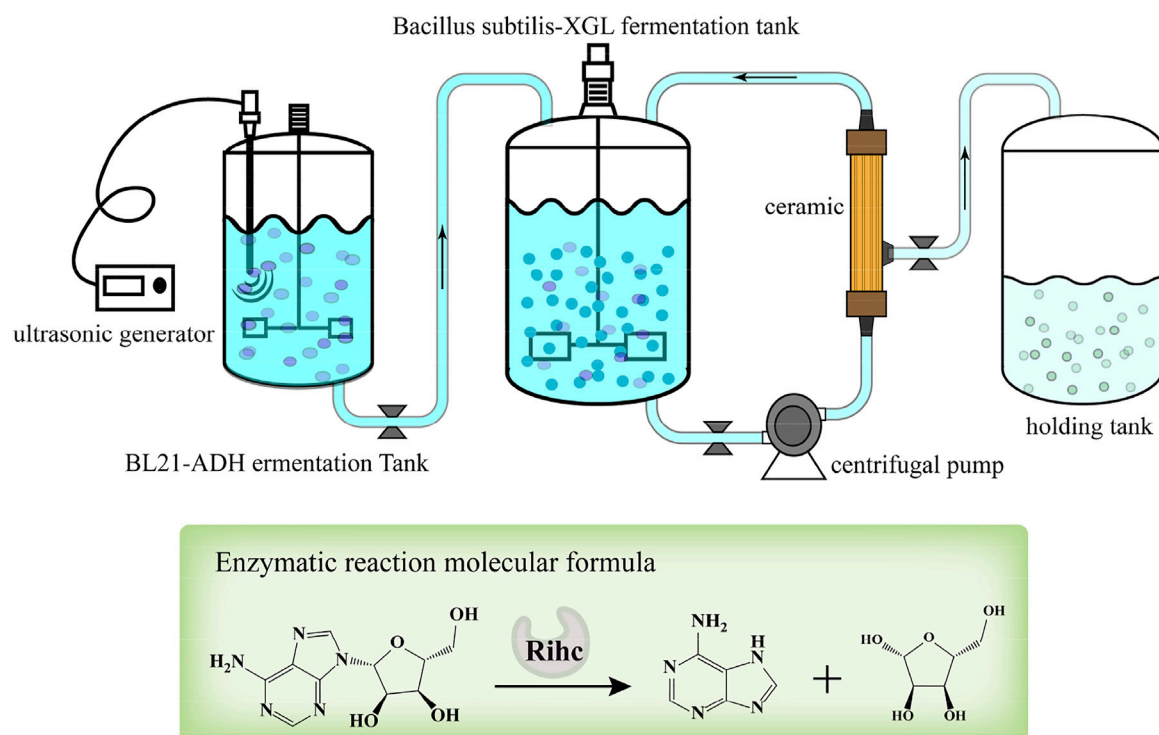


FIGURE 1

Schematic diagram of the production of adenine by ceramic membrane coupled mixed cell fermentation.

SDS-PAGE analysis: refer to (García-Fraga et al., 2015) for specific procedures. Nucleic acid and protein electrophoresis apparatus (Beijing Liuyi Instrument Factory, China).

AdHy enzyme activity identification

Enzyme activity assay method: 2 ml of bacterial solution was sampled after ultrasonication and 100 μL was added to 10 ml of enzyme reaction system (adenosine 15 g/L, PBS buffer 4.9 ml) and the reaction was terminated by boiling for 20 min, after which the adenine yield was determined by high performance liquid chromatography (HPLC).

Definition of enzyme activity unit: The amount of enzyme required to catalyse the production of 1 mol/L of adenine from the substrate adenosine in 1 min under standard enzyme activity assay conditions was defined as one enzyme activity unit, i.e. 1 U.

Product detection method

Product determination: Determination of products by HPLC (Shimadzu, Japan), chromatographic conditions were as follows; Liquid chromatography separation conditions: column temperature 30 $^{\circ}\text{C}$, detection wavelength 259 nm, total mobile phase flow rate 0.8 ml/min, mobile phase 10% (v/v) acetonitrile

and 0.05% (v/v) trifluoroacetic acid, column: Kromasil C18 column (250 mm \times 4.6 mm \times 5 μm USA).

Results and discussion

Construction of *E. coli* BL21-AdHy

Pet-28a-*rihC* plasmid construction

The results of colony polymerase chain reaction (PCR) on the successfully constructed *E. coli* DH5 α cells containing pET28a-*rihC* recombinant plasmid are shown in Figure 2A. The expected bands appeared around 1,221 bp; the recombinant plasmid was verified by enzymatic digestion using EcoRI and HindIII, as shown in Figure 2A. The bands appeared around 5,350 bp and 912 bp. The linearized plasmid and the target gene showed consistent bands, which indicated that the Pet-28a-*rihC* plasmid was successfully constructed, with two verifications.

Construction of *E. coli*-BL21-AdHy

The *E. coli* BL21-AdHy strain was subjected to SDS-PAGE analysis and the results are shown in Figure 2B. The supernatant of the homogenized bacteria showed the expected band (around 33 kDa), demonstrating that the protein could be stably expressed by the recombinant strain.

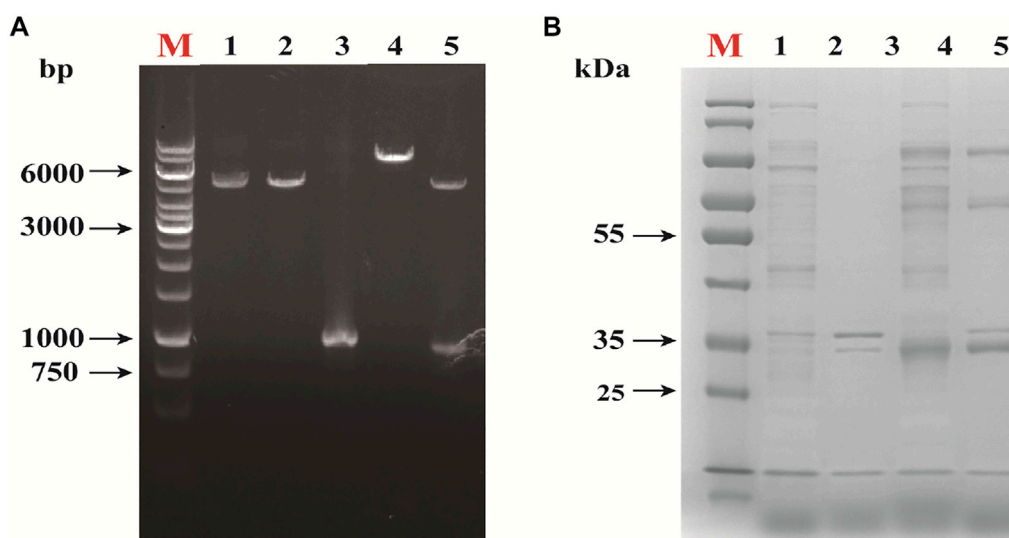


FIGURE 2

Validation of Recombinant Expression of Nucleoside Hydrolase *rihC*. (A) Restriction map of recombinant plasmid. M: DNA marker; 1: *EcoR* I single enzyme digestion of pET-28a; 2: pET-28a was digested by *EcoR* I and *Hind* III. 3: target gene fragment; 4: *EcoR* I single enzyme digestion of pET-28a-*rihC*; 5: pET-28a-*rihC* was digested with *EcoR* I and *Hind* III. (B) SDS-PAGE analysis of the recombinant protein. M: protein marker; 1: *E. coli* pET-28a cell lysate supernatant sample; 2: *E. coli* pET-28a cell lysate precipitation sample; 3: *E. coli* pET-28a-*rihC* cell lysate supernatant sample; 4: Sedimentation in cell lysate of *E. coli* pET-28a-*rihC*.

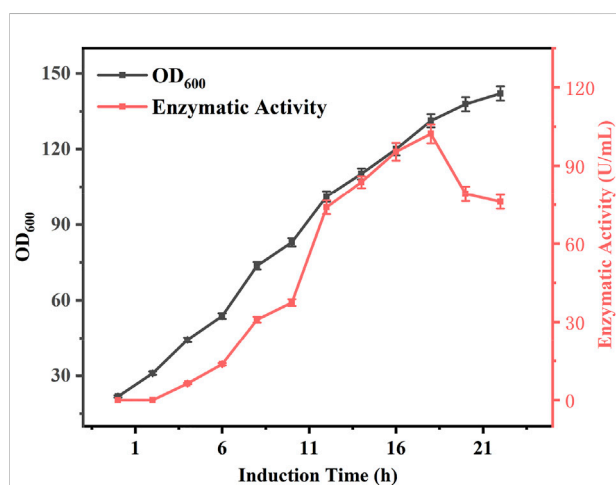


FIGURE 3

Changes in enzyme activity and biomass during induction culture.

Effects of incubation time and ultrasound treatment on enzyme and cell activity

Effect of incubation time on enzyme expression

During induction culture of the bacteria, the enzyme activity is positively correlated with the incubation time of the bacterium for a certain period of time. However,

prolonged incubation periods can also affect enzyme activity. To investigate the relationship between induction culture time and enzyme activity, *E. coli* BL21-AdHy were induced in 5 L fermenters and their biomass and enzyme activity were examined, the results of which are shown in Figure 3. At the beginning of induction, the biomass was 21.8, and the enzyme activity was 0 U/mL. Both biomass and enzyme activity increased significantly with the extension of induction time, and the enzyme activity was the highest at 18 h. At this time, the biomass was 131.2, and the enzyme activity was 102.2 U/mL. With the passage of time, the biomass still increased, whereas enzyme activity exhibited a decreasing trend. Analysis suggested that the increase in enzyme activity during the early stages was due to the lack of induced expression of the enzyme and the low biomass per unit volume, such that enzyme activity continued to increase in the first 18 h. It is known that longer induction times increase protein expression, but may also jeopardise protein stability or induce protein hydrolysis (García-Fraga et al., 2015); alternatively, studies have shown that at high biomass levels, the availability of dissolved oxygen decreases and various substances affecting protein stability are produced (Olaofe et al., 2010; Hu et al., 2015), leading to a decrease in enzyme activity. However, after 18 h of induction culture, AdHy enzymatic activity tended to decrease with increasing induction time. Therefore, an 18 h period for induction culture of *E. coli* BL21-AdHy was selected to produce a crude enzyme broth.

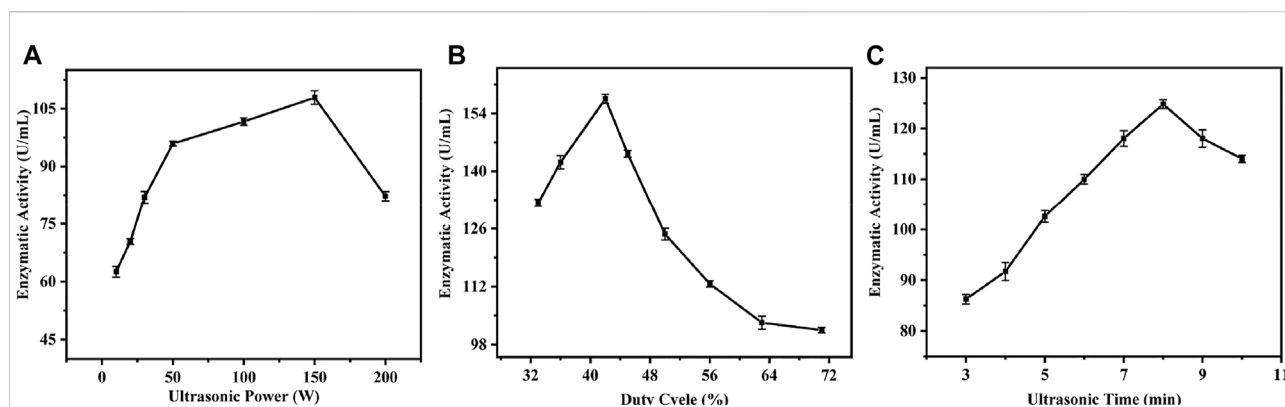


FIGURE 4

Single factor experiment of ultrasonic parameters. (A) Effect of ultrasonic power on enzyme activity; (B) Effect of Duty Ratio on Enzyme Activity; (C) Effect of ultrasonic time on enzyme activity.

Effects of different ultrasound treatment modes on enzyme activity

Ultrasound is now widely used for cleaning, lithotripsy, and sterilization because of its good directionality and penetrating power. Extreme ultrasound treatment can cause loss of enzyme activity (O'Donnell et al., 2010), whereas low frequency ultrasound can enhance enzyme activity by altering favorable conformational changes in proteins without altering their structural integrity (Duan et al., 2011). The tolerance of enzymes to ultrasound depends on the physiological properties of the enzyme and ultrasound parameters, such as ultrasound power, duty cycle, and treatment time, which can directly affect catalytic activity of the enzyme (Kentish and Ashokkumar, 2011; Gonçalves et al., 2015). Therefore, in order to investigate the effects of different sonication conditions on the activity of nucleoside hydrolase crude enzyme solution, sonication time, sonication power, and duty cycle were used here as conditions for investigation, and specific experiments and experimental results are shown in Figure 4.

To investigate the effects of different sonication power on the activity of crude enzyme solution, a duty cycle of 62% and a sonication time of 5 min were chosen, and different sonication powers were selected for single-factor experiments. The experimental results are shown in Figure 4A. Under low power sonication, the activity of crude enzyme solution increased with increasing sonication power; the highest activity of 107 U/mL was achieved under the treatment condition of 150 W. However, with further increases in power, the activity showed a trend of weakening. Analysis showed that low-power ultrasound could induce stable cavitation in the surrounding liquid, and the generation and extinction of cavitation bubbles can cause oscillations in the liquid (Rao and Rathod, 2014; Gonçalves et al., 2015), which in turn causes changes in the structure of the cell membrane,

increasing its permeability to some extent and even disrupting it, causing enzyme molecules to flow from inside the cell to outside the cell (Zhang et al., 2021), and ultrasound produces benign changes in the structure of enzyme molecules (Wang et al., 2012), leading to further increases in enzyme activity. As a result, enzyme activity tends to increase. However, with further increase in ultrasound power, the enzyme activity shows a gradual decrease, which may be due to the high power of ultrasound, which also carries higher energy and displays significant shearing in the surrounding liquid (Neslihan et al., 2006), in which case peptide chains of the enzyme molecule are disrupted, leading to loss of enzyme activity (Huang et al., 2017).

To investigate the effects of different duty cycles on the activity of the crude enzyme solution, ultrasound power of 100 W and ultrasound time of 5 min were selected, and eight different gradients in the duty cycle of 38–83% were selected for single-factor experiments, and the results are shown in Supplementary Figure S4B. As the duty cycle increased, the activity of the crude enzyme solution gradually increased and reached the highest level of 157 U/mL at 42% duty cycle; with further increase in the duty cycle, the activity showed a decreasing trend. This increase in activity is presumed to be due to the increase in exposure time of the enzyme molecules undergoing sonication and the effective modification of the enzyme (Nadar and Rathod, 2017) and was highest at 42% duty cycle; however, further increases in duty cycle revealed decreasing enzyme activity. This is presumed to be due to the fact that higher duty cycles result in greater heat being generated around the enzyme molecules, and the higher heat generation causes a loss of enzyme activity (O'Donnell et al., 2010).

In order to investigate the effects of different sonication times on the activity of the crude enzyme solution, the sonication power was chosen to be 100 W, the duty cycle was 63% and eight different treatment times were selected between 3 and 10 min for

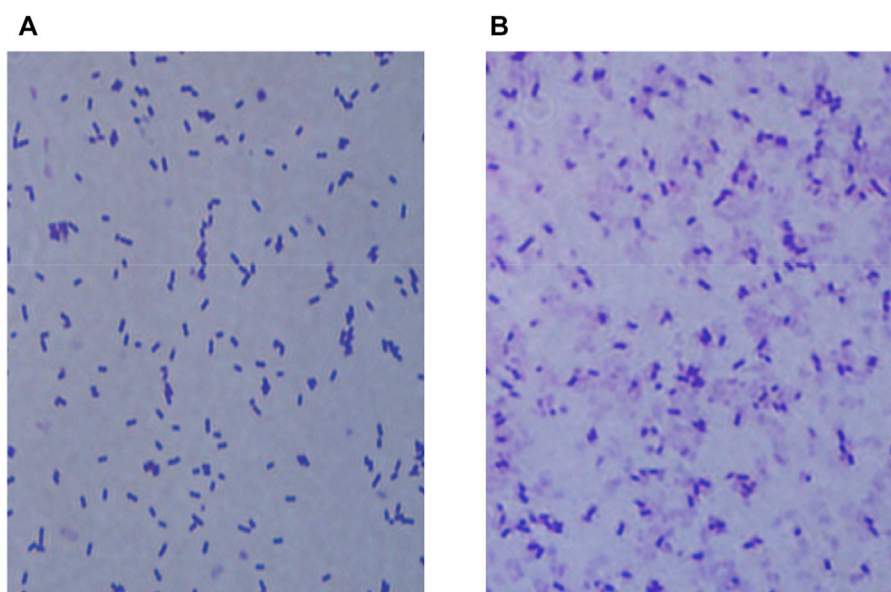


FIGURE 5

Morphological changes in *E. coli* BL21-AdHy under optimized ultrasound conditions. (A) Normal bacterial morphology; (B) Changes in bacterial morphology under ultrasound treatment.

single-factor tests. The results are shown in [Supplementary Figure S4C](#). The activity of the crude enzyme solution gradually increased with increasing sonication time, reaching a maximum of 124 U/mL after 8 min of treatment. It is hypothesized that this trend is caused by the duration of exposure of the enzyme molecule to sonication, and the effective modification of the enzyme molecule by such treatment ([Nadar and Rathod, 2017](#)).

Optimization of orthogonal experiments

In order to obtain higher enzymatic activity, the orthogonal experiments of L_9 (3^3) were performed to further optimize the sonication parameters by combining the previous single-factor experiments of sonication power, sonication time and duty cycle. The specific experiments and results are shown in [Supplementary Table S5](#). The experimental data showed that the enzyme activity of the crude enzyme solution was the highest at 207 U/mL when the power was 170 W, the duty cycle was 42%, and the treatment time was 8 min.

Changes to *E. coli* BL21-AdHy under ultrasound treatment

Normal and sonicated bacteria were stained separately using Gram staining and observed by electron microscopy (100 ×) for comparison (as shown in [Figure 5](#)). It was hypothesized from the cell morphology that ultrasound treatment caused great structural damage to the cell membrane of *E. coli* BL21-AdHy, which in turn led to a significant decrease in cellular activity. The

detrimental effect on the synergistic fermentation of bacteria and enzymes due to the addition of crude enzyme solution was reduced.

Synergistic fermentation of bacteria and enzymes coupling ceramic membranes to produce adenine

Effects of timing of crude enzyme solution addition on synergistic fermentation of bacteria and enzymes

In this study, it was found that mixing a certain percentage of sonicated AdHy crude enzyme solution during the fermentation production of *B. subtilis* XGL resulted in the enzymatic conversion of the original product adenosine to a new product: adenine. To investigate the effect of addition time on adenine yield, we added 13% (v/v) of AdHy crude enzyme solution at 30, 35, and 40 h of *B. subtilis* fermentation, respectively, and the results are shown in [Figure 6](#). When the mixing time was 30, 35, and 40 h, the final adenine yields reached 9.73, 13.68, and 14.90 g/L, respectively. Note that the final yield was not the highest and adenosine did not accumulate. There was a high net increase in biomass after mixing, with a decreasing trend over time. Adenine production was highest when all adenosine present was transformed, but also declined slowly over time and production of *B. subtilis* XGL was found to have been terminated. Analysis showed that adenine production

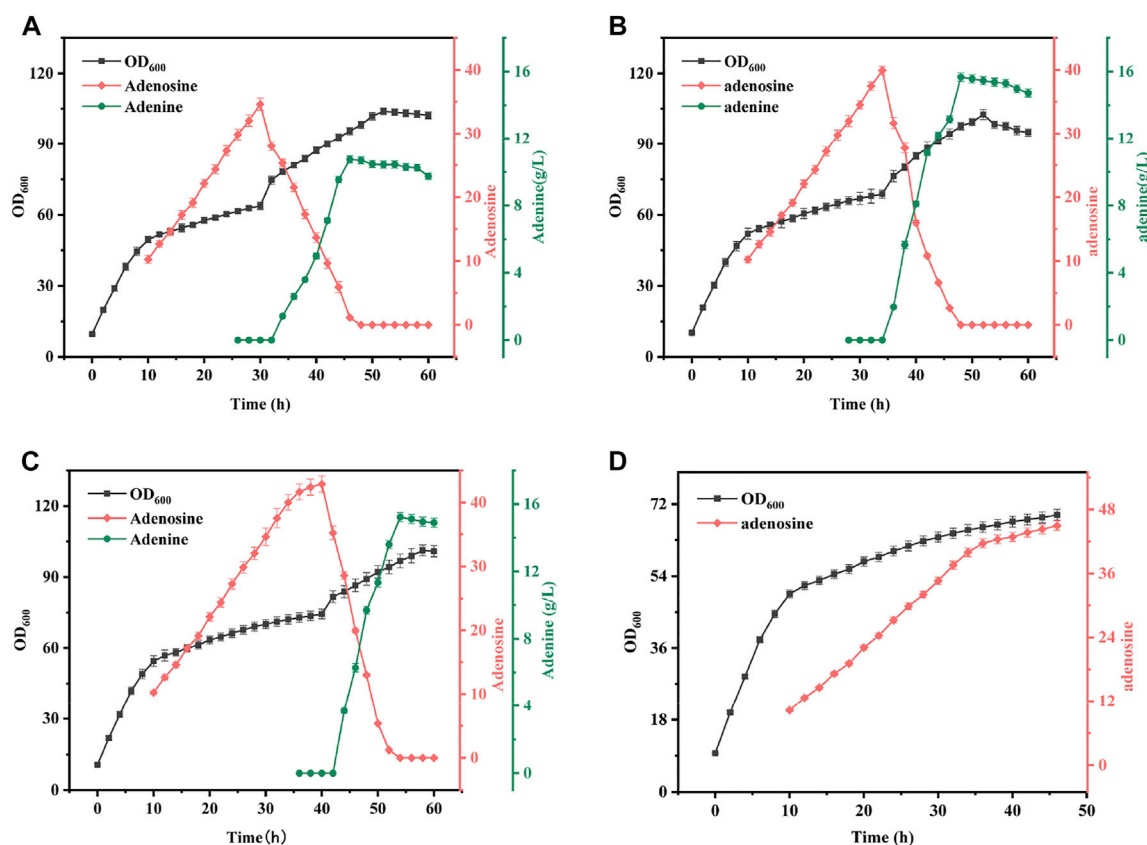


FIGURE 6

Effect of Different Mixing Time on Fermentation Results. Mixed ratio: 13% of *B. subtilis* XGL fermentation system. (A): Changes of biomass, adenosine and adenine production during 30 h mixing operation; (B): Changes of biomass, adenosine and adenine production during 35 h mixing operation; (C): Changes of biomass, adenosine and adenine production during 40 h mixing operation; (D): Changes of biomass and adenosine production during normal fermentation.

increased with increasing mixing time; this was due to the amount of adenosine substrate increasing with increasing fermentation time and therefore adenine production would increase with increased mixing time. The increase in biomass per unit time was further enhanced by the addition of sonicated crude enzyme solution. This is probably due to the fact that *B. subtilis* XGL was in the middle to late stages of growth when bacterial viability and growth rates are significantly reduced (Xu et al., 2021), and that the sonicated crude enzyme solution contains more *E. coli* fragments. Therefore, the crude enzyme solution contained nucleic acids and inorganic salts and sugars, which to some extent can act as high-quality complex nutrients, thus increasing the late growth rate of the bacteria. Eventually, the production of adenine declined slowly and the production of *B. subtilis* XGL stagnated. This is because adenine is involved in the synthesis of DNA and RNA and can therefore be used by bacteria but can only be consumed in small quantities due to the late stage of fermentation. The stalled production of *B. subtilis* XGL is due to feedback inhibition of the entire purine synthesis

pathway by adenine (Smith et al., 1994; Rolfes, 2006) and when adenine reaches high concentrations, the purine synthesis pathway will also cease to function and therefore the bacterium will no longer produce adenosine. For reasons of bacterial growth, adenosine production efficiency and time involved, a 35-h mixed operation was chosen for this study.

Effects of crude enzyme solution addition ratio on synergistic fermentation of bacteria and enzymes

The mixing ratio is another key parameter in the synergistic fermentation of bacteria and enzymes and has a critical role in the conversion of adenosine. To investigate the effect of mixing time on the synergistic fermentation of bacteria and enzymes, in this study, crude enzyme solutions of 6, 13, and 20% were added to *B. subtilis* XGL fermentation after 35 h. The specific experimental results are shown in Figure 7. The conversion rate of adenosine to adenine was rapid as the mixing ratio increased. With the 6% addition, 12 h were required to

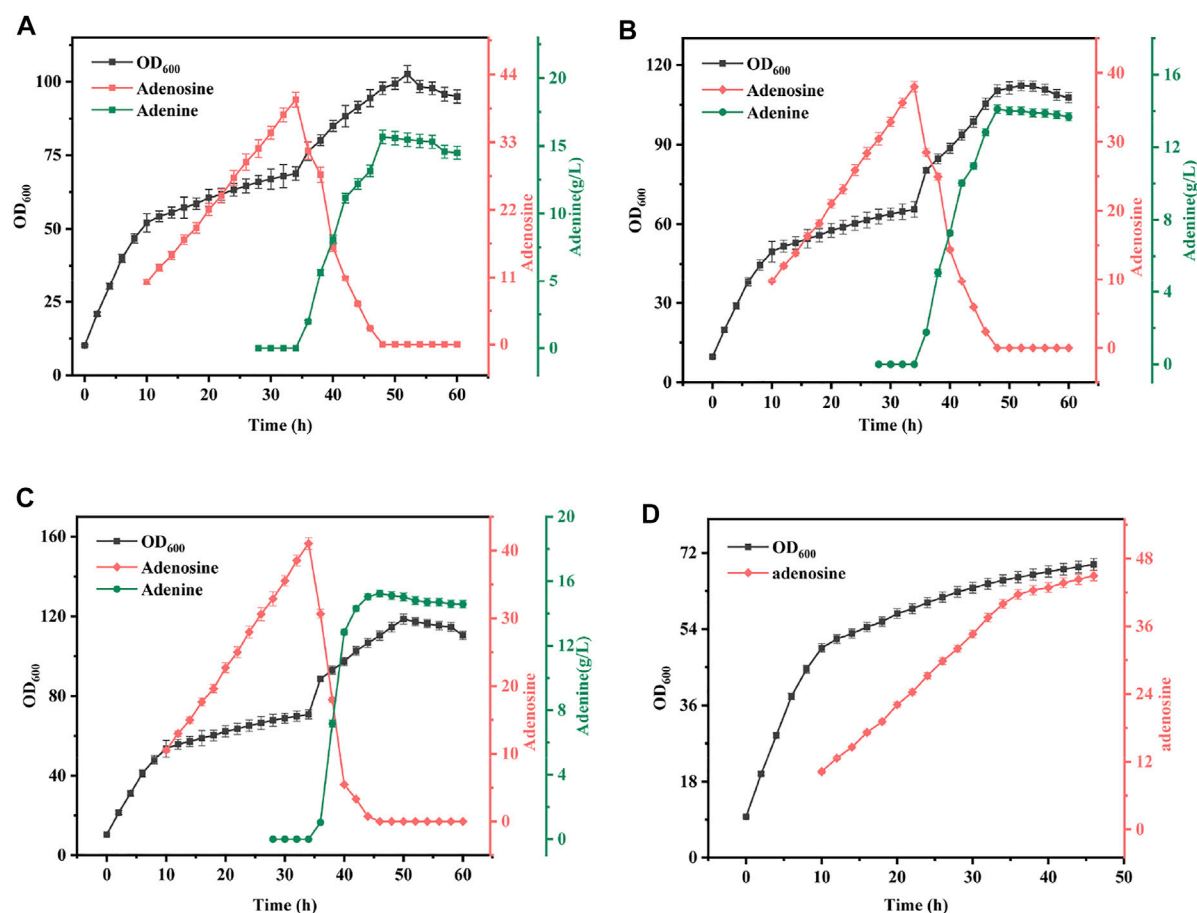


FIGURE 7

Effect of Different Mix Proportion on Fermentation Results. Mixed time: *B. subtilis* XGL fermented to 35 h (A): When the mixed ratio was 6% of *B. subtilis* XGL fermentation system, the changes of biomass, adenosine and adenine production were observed; (B): When the mixed ratio was 13% of *B. subtilis* XGL fermentation system, the changes of biomass, adenosine and adenine production were observed; (C): When the mixed ratio was 20% of *B. subtilis* XGL fermentation system, the changes of biomass, adenosine and adenine production were observed; (D): Changes of biomass and adenosine production during normal fermentation.

complete the conversion of adenosine, but at the 20% mixing ratio, only 8 h were required to complete the conversion of adenosine. The conversion efficiency also increased steadily, from 41% at 6–48% at a 13% mixing ratio. However, when the mixing ratio was further increased, the elevation in terms of conversion efficiency was limited. Analysis showed that with a certain substrate, the amount of enzyme added determined the rate of product production and therefore, When the addition amount increased, the conversion efficiency of adenine was improved. Moreover, as the conversion efficiency was greatly improved, adenine conversion could be completed in a short period of time and the consumption of adenine during the conversion process was reduced and the conversion rate was also augmented. Since there is a linear relationship between conversion efficiency, conversion rate, and mixing ratio, 15% was chosen as the best mixing ratio in subsequent experiments.

Bacterial and enzymatic co-fermentation with coupled ceramic membranes

In order to solve the problems of poor bacterial viability and low productivity in the late fermentation of *B. subtilis* XGL and stagnation of the overall purine metabolic pathway due to inhibition of adenine production in large quantities (Smith et al., 1994), we used a coupled ceramic membrane to dialyze the overall fermentation system with a flow-through of fresh nutrient solution, as shown in Figure 8.

In this experiment, the AdHy crude enzyme solution was added after 35, 65, and 90 h of *B. subtilis* fermentation, with three additions of 15, 15, and 10% of the *B. subtilis* XGL fermentation system. At 45 and 75 h, a coupled ceramic membrane dialysis operation was carried out, followed by refreshment with 60 and 40% of fresh medium. Adenosine production by *B. subtilis* XGL attained 38.72, 24.98, and 10.56 g/L after 35, 65, and 90 h. After

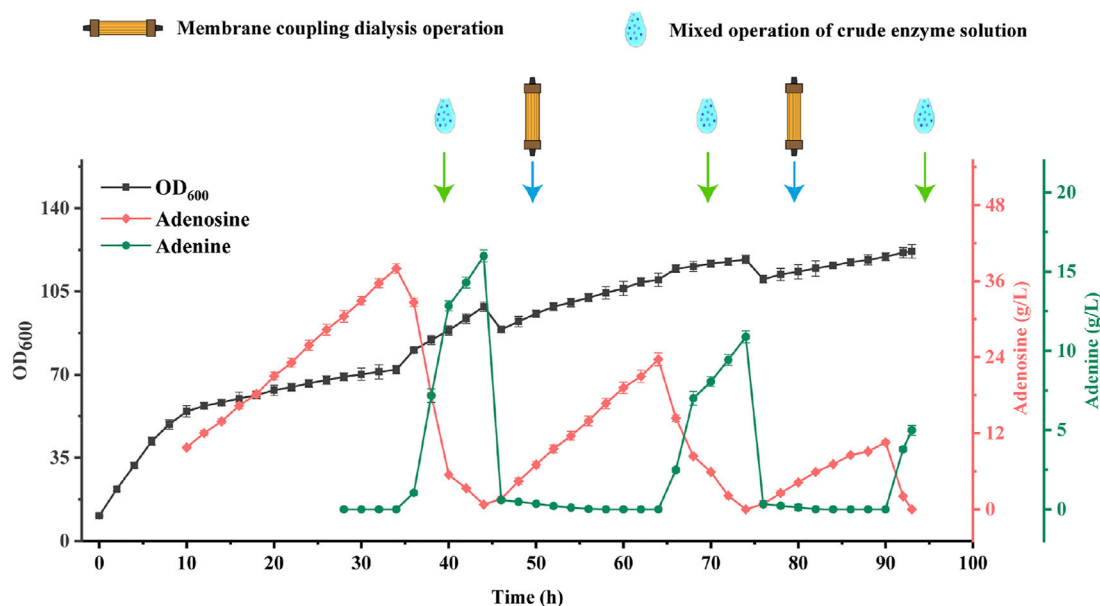


FIGURE 8
Changes of biomass, Adenosine and Adenine Production in Bacterial and Enzyme Mixed Coupling Ceramic Membrane Fermentation.

addition of the crude enzyme solution, there was a stepwise increase in biomass. After coupled ceramic membrane dialysis, there was a stepwise decrease in biomass. The complete conversion of adenosine was completed around 10 h after the coupled ceramic membrane dialysis. This is presumably since membrane-coupled dialysis removes substances that are detrimental to the growth of bacteria in the later stages of fermentation. Inevitably, however, it also eliminates some of the nutrients from the fermentation system, and therefore, a certain percentage of fresh medium needs to be added after the dialysis operation. This helps to “purify” the environment for the bacteria to grow and produce. Furthermore, the ability of *B. subtilis* XGL to produce adenosine was restored after the dialysis operation. This is due to the fact that adenine leaves the fermentation system during membrane-coupled dialysis and, accordingly, inhibition of the purine synthesis pathway by adenine (Smith et al., 1994) is removed and adenosine production is restored. A precipitous drop in biomass volume occurred after each membrane-coupled dialysis operation. This was due to the loss of biomass during the dialysis process, and it is assumed that this may also be the reason for the stepwise decrease in biomass.

Conclusion

The current methods of adenine production mainly include chemical synthesis and enzymatic catalysis. In this study, the enzymatic method was combined with the fermentation method and successfully achieved the conversion of adenine by adding

AdHy crude enzyme solution during the production of fermented adenosine. The overall fermentation system was also permeabilized by coupling the fermentation system to a ceramic membrane. The final total adenine yield was 14 ± 0.25 g/L, the highest yield of adenine fermentation to date. The data shows that the dialysis of the fermentation system resulted in a significant increase in the viability of the bacterium and recovery of the productivity of the bacterium. This indicates that by using a coupled ceramic membrane to dialyze the whole fermentation system, the factors that are detrimental to the growth and production of the bacterium can be effectively removed from the fermentation system, and the growth capacity of the bacterium can be restored to a certain extent.

Data availability statement

The original contributions presented in the study are included in the article/Supplementary Material, further inquiries can be directed to the corresponding author.

Author contributions

QX and PS conceived and designed the study. PS, CL, YG, and JW performed plasmid and strain construction, and fermentation experiments. QX, CL, YG, and JW analyzed data and revised the manuscript. All authors read and approved the final manuscript.

Funding

Baicheng Baiyuan Project—Key Technology of Nutrition and Health and Intelligent Manufacturing (21ZYQCSY00050); Key technologies of green and efficient fermentation of animal essential amino acids (2021ZDSYS10).

Conflict of interest

The authors declare that the research was conducted in the absence of any commercial or financial relationships that could be construed as a potential conflict of interest.

References

- Arivett, B., Farone, M., Masiragani, R., Burden, A., Judge, S., Osinloye, A., et al. (2014). Characterization of inosine-uridine nucleoside hydrolase (RihC) from *Escherichia coli*. *Biochimica Biophysica Acta - Proteins Proteomics* 1844 (3), 656–662. doi:10.1016/j.bbapap.2014.01.010
- Duan, X., Zhou, J., Qiao, S., and Wei, H. (2011). Application of low intensity ultrasound to enhance the activity of anammox microbial consortium for nitrogen removal. *Bioresour. Technol.* 102 (5), 4290–4293. doi:10.1016/j.biortech.2010.12.050
- García-Fraga, B., da Silva, A. F., López-Seijas, J., and Sieiro, C. (2015). Optimized expression conditions for enhancing production of two recombinant chitinolytic enzymes from different prokaryote domains. *Bioprocess Biosyst. Eng.* 38 (12), 2477–2486. doi:10.1007/s00449-015-1485-5
- Gonçalves, I., Silva, C., and Cavaco-Paulo, A. (2015). Ultrasound enhanced laccase applications. *Green Chem.* 17, 1362–1374. doi:10.1039/c4gc02221a
- He, R., Ren, W., Xiang, J., Dabbour, M., Kumah Mintah, B., Li, Y., et al. (2021). Fermentation of *Saccharomyces cerevisiae* in a 7.5L ultrasound-enhanced fermenter: Effect of sonication conditions on ethanol production, intracellular Ca^{2+} concentration and key regulating enzyme activity in glycolysis. *Ultrason. Sonochem.* 76, 105624. doi:10.1016/j.ultrsonch.2021.105624
- Hess, J. R., and Greenwalt, T. J. (2005). *Compositions and methods for the storage of red blood cells*. Cincinnati, US: World Intellectual Property Organization. European Patent NO PCT/US2005/005004.
- Hu, J. H., Wang, F., and Liu, C. Z. (2015). Development of an efficient process intensification strategy for enhancing Pfu DNA polymerase production in recombinant *Escherichia coli*. *Bioprocess Biosyst. Eng.* 38 (4), 651–659. doi:10.1007/s00449-014-1304-4
- Huang, G., Chen, S., Dai, C., Sun, L., Sun, W., Tang, Y., et al. (2017). Effects of ultrasound on microbial growth and enzyme activity. *Ultrason. Sonochem.* 37, 144–149. doi:10.1016/j.ultrsonch.2016.12.018
- Kentish, S., and Ashokkumar, M. (2011). The physical and chemical effects of ultrasound. *Ultrasound Technol. Food Bioprocess* 1, 1–12. doi:10.1007/978-1-4419-7472-3_1
- Ladole, M. R., Mevada, J. S., and Pandit, A. B. (2017). Ultrasonic hyperactivation of cellulase immobilized on magnetic nanoparticles. *Bioresour. Technol.* 239, 117–126. doi:10.1016/j.biortech.2017.04.096
- Li, G., Xu, Q., Xiong, H., Liu, Y., Zhang, Y., Chen, Z., et al. (2021). Improving the L-tyrosine production with application of repeated batch fermentation technology based on a novel centrifuge bioreactor. *Food Bioprod. Process.* 126, 3–11. doi:10.1016/j.fbp.2020.11.001
- Li, Y. S., Yan, Y. Y., Cheng, L. Q., Mao, L. P., and Wang, Y. P. (2016). *A method for the synthesis of adenine*. Beijing, China: China National Intellectual Property Administration. China Patent No CN103709164B.
- Lv, X. Y., and Fu, J. (2008). *Preparation of adenine by catalyst-free hydrolysis of adenosine in high-temperature liquid water*. Beijing, China: China National Intellectual Property Administration. China Patent No CN100537569C.
- Ma, H., Huang, L., Jia, J., He, R., Luo, L., and Zhu, W. (2011). Effect of energy-gathered ultrasound on Alcalase. *Ultrason. Sonochem.* 18 (1), 419–424. doi:10.1016/j.ultrsonch.2010.07.014
- Nadar, S. S., and Rathod, V. K. (2017). Sonochemical effect on activity and conformation of commercial lipases. *Appl. Biochem. Biotechnol.* 181 (4), 1435–1453. doi:10.1007/s12010-016-2294-2
- Neslihan, S., Dilek Kılıç, A., and Ozbek, B. (2006). A modelling study on milk lactose hydrolysis and β -galactosidase stability under sonication. *Process Biochem.* 41 (7), 1493–1500. doi:10.1016/j.procbio.2006.02.008
- O'Donnell, C. P., Tiwari, B. K., Bourke, P., and Cullen, P. J. (2010). Effect of ultrasonic processing on food enzymes of industrial importance. *Trends Food Sci. Technol.* 21 (7), 358–367. doi:10.1016/j.tifs.2010.04.007
- Olaofe, O. A., Burton, S. G., Cowan, D. A., and Harrison, S. T. (2010). Improving the production of a thermostable amidase through optimising IPTG induction in a highly dense culture of recombinant *Escherichia coli*. *Biochem. Eng. J.* 52 (1), 19–24. doi:10.1016/j.bej.2010.06.013
- Paglia, G., Sigurjónsson, Ó. E., Bordbar, A., Rolfsson, O., Magnúsdóttir, M., Pálsson, S., et al. (2016). Metabolic fate of adenine in red blood cells during storage in SAGM solution. *Transfusion* 56 (10), 2538–2547. doi:10.1111/trf.13740
- Petersen, C., and Møller, L. B. (2001). The RihA, RihB, and RihC ribonucleoside hydrolases of *Escherichia coli*. *J. Biol. Chem.* 276 (2), 884–894. doi:10.1074/jbc.M008300200
- Rao, P. R., and Rathod, V. K. (2014). Mapping study of an ultrasonic bath for the extraction of andrographolide from *Andrographis paniculata* using ultrasound. *Industrial Crops Prod.* 66, 312–318. doi:10.1016/j.indcrop.2014.11.046
- Rolfes, R. J. (2006). Regulation of purine nucleotide biosynthesis: In yeast and beyond. *Biochem. Soc. Trans.* 34 (5), 786–790. doi:10.1042/BST0340786
- Smith, J. L., Zaluzec, E. J., Wery, J. P., Niu, L., Switzer, R. L., Zalkin, H., et al. (1994). Structure of the allosteric regulatory enzyme of purine biosynthesis. *Science* 264 (5164), 1427–1433. doi:10.1126/science.8197456
- Takeuchi, I., Kishi, T., Hanya, M., Uno, J., Fujita, K., and Kamei, H. (2015). Effect of adenine on clozapine-induced neutropenia in patients with schizophrenia: A preliminary study. *Clin. Psychopharmacol. Neurosci.* 13 (2), 157–162. doi:10.9758/cpn.2015.13.2.157
- Teitelbaum, J. E., Johnson, C., and St Cyr, J. (2006). The use of D-ribose in chronic fatigue syndrome and fibromyalgia: A pilot study. *J. Altern. Complement. Med.* 12 (9), 857–862. doi:10.1089/acm.2006.12.857
- Wang, Z., Lin, X., Li, P., Zhang, J., Wang, S., and Ma, H. (2012). Effects of low intensity ultrasound on cellulase pretreatment. *Bioresour. Technol.* 117, 222–227. doi:10.1016/j.biortech.2012.04.015
- Xie, X. K., Xu, W., and Wang, B. (2018). *An adenine producing strain and its construction method and application*. Beijing, China: China National Intellectual Property Administration. China Patent No CN108753669A.

Publisher's note

All claims expressed in this article are solely those of the authors and do not necessarily represent those of their affiliated organizations, or those of the publisher, the editors and the reviewers. Any product that may be evaluated in this article, or claim that may be made by its manufacturer, is not guaranteed or endorsed by the publisher.

Supplementary material

The Supplementary Material for this article can be found online at: <https://www.frontiersin.org/articles/10.3389/fbioe.2022.969668/full#supplementary-material>

Xu, H., Tian, Y., Wang, S., Zhu, K., Zhu, L., He, Q., et al. (2021). Batch fermentation kinetics of acetoin produced by *Bacillus subtilis* HB-32. *Prep. Biochem. Biotechnol.* 51 (10), 1004–1007. doi:10.1080/10826068.2021.1885047

You, J. Z., Jiang, S. H., and He, J. S. (2013). *A method for the synthesis of adenine*. Beijing, China: China National Intellectual Property Administration. China Patent No CN102321086B.

Yue, G. Y., Wang, Y., Su, H. Q., and Hao, X. H. (2020). *A method for the preparation of adenine and D-ribose by hydrolysis of adenosine with adenosine*

hydrolase. Beijing, China: China National Intellectual Property Administration. China Patent No CN111378705A.

Zhang, Y., Chen, Z., Sun, P., Xu, Q., and Chen, N. (2021). Effect of low-level ultrasound treatment on the production of L-leucine by *Corynebacterium glutamicum* in fed-batch culture. *Bioengineered* 12 (1), 1078–1090. doi:10.1080/21655979.2021.1906028

Zhao, H. Y., Lau, K. C., Garcia, G. A., Nahon, L., Carniato, S., Poisson, L., et al. (2018). Unveiling the complex vibronic structure of the canonical adenine cation. *Phys. Chem. Chem. Phys.* 20 (32), 20756–20765. doi:10.1039/c8cp02930j



OPEN ACCESS

EDITED BY

Qi Xianghui,
Jiangsu University, China

REVIEWED BY

Yejun Han,
Institute of Process Engineering (CAS),
China
Sujit Jagtap,
University of Illinois at Urbana-
Champaign, United States

*CORRESPONDENCE

Eleftherios T. Papoutsakis,
epaps@udel.edu

SPECIALTY SECTION

This article was submitted
to Industrial Biotechnology,
a section of the journal
Frontiers in Bioengineering and
Biotechnology

RECEIVED 09 June 2022

ACCEPTED 15 July 2022

PUBLISHED 22 August 2022

CITATION

Otten JK, Zou Y and Papoutsakis ET
(2022), The potential of caproate
(hexanoate) production using
Clostridium kluyveri syntrophic
cocultures with *Clostridium*
acetobutylicum or
Clostridium saccharolyticum.
Front. Bioeng. Biotechnol. 10:965614.
doi: 10.3389/fbioe.2022.965614

COPYRIGHT

© 2022 Otten, Zou and Papoutsakis.
This is an open-access article
distributed under the terms of the
Creative Commons Attribution License
(CC BY). The use, distribution or
reproduction in other forums is
permitted, provided the original
author(s) and the copyright owner(s) are
credited and that the original
publication in this journal is cited, in
accordance with accepted academic
practice. No use, distribution or
reproduction is permitted which does
not comply with these terms.

The potential of caproate (hexanoate) production using *Clostridium kluyveri* syntrophic cocultures with *Clostridium acetobutylicum* or *Clostridium saccharolyticum*

Jonathan K. Otten ^{1,2}, Yin Zou¹ and
Eleftherios T. Papoutsakis ^{1,2,3*}

¹Department of Chemical and Biomolecular Engineering, University of Delaware, Newark, DE, United States, ²Delaware Biotechnology Institute, University of Delaware, Newark, DE, United States, ³Department of Biological Sciences, University of Delaware, Newark, DE, United States

Caproate (hexanoate) and other medium-chain fatty acids are valuable platform chemicals produced by processes utilizing petroleum or plant oil. *Clostridium kluyveri*, growing on short chain alcohols (notably ethanol) and carboxylic acids (such as acetate) is noted for its ability to perform chain elongation to produce 4- to 8-carbon carboxylates. *C. kluyveri* has been studied in monoculture and coculture conditions, which lead to relatively modest carboxylate titers after long fermentation times. To assess the biosynthetic potential of *C. kluyveri* for caproate production from sugars through coculture fermentations, in the absence of monoculture data in the literature suitable for our coculture experiments, we first explored *C. kluyveri* monocultures. Some monocultures achieved caproate titers of 150 to over 200 mM in 40–50 h with a production rate of 7.9 mM/h. Based on that data, we then explored two novel, syntrophic coculture partners for producing caproate from sugars: *Clostridium acetobutylicum* and *Clostridium saccharolyticum*. Neither species has been cocultured with *C. kluyveri* before, and both demonstrate promising results. Our experiments of *C. kluyveri* monocultures and *C. kluyveri*–*C. saccharolyticum* cocultures demonstrate exceptionally high caproate titers (145–200 mM), fast production rates (3.25–8.1 mM/h), and short fermentation times (18–45 h). These results represent the most caproate produced by a *C. kluyveri* coculture in the shortest known fermentation time. We also explored the possibility of heterologous cell fusion between the coculture pairs similar to the results seen previously in our group with *C. acetobutylicum* and *Clostridium ljungdahlii*. Fusion events were observed only in the *C. acetobutylicum*–*C. kluyveri* coculture pair, and we offer an explanation for the lack of fusion between *C. saccharolyticum* and *C. kluyveri*. This work supports the promise of coculture biotechnology for sustainable production of caproate and other platform chemicals.

KEYWORDS

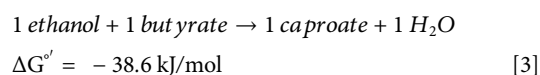
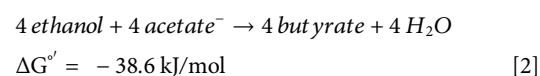
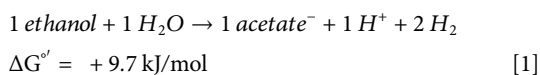
coculture (co-culture), *Clostridium kluyveri*, *Clostridium saccharolyticum*, *Clostridium acetobutylicum* ATCC 824, chain elongation, caproate, hexanoate, *Lacrimispora saccharolytica*

1 Introduction

Caproic (hexanoic) acid, as well as other medium-chain fatty acids (MCFAs), are platform chemicals, fuel precursors, antimicrobial agents, plant growth promoters, lubricant precursors, and flavor additives (Zhang et al., 2019; San-Valero et al., 2020; Ghysels et al., 2021). Currently, they are produced from fossil fuels or through low-yield extractions from coconut or palm kernel oil. As the world gravitates towards more sustainable sources of chemicals, petroleum-based processes will have to be phased out. Palm oil production also carries substantial environmental concerns (Syahril et al., 2019). Biological production of caproic acid and other MCFAs creates a solution to these environmental concerns.

An important organism capable of chain elongation from less-valuable precursors into MCFAs is *Clostridium kluyveri* (*Ckl*), a spore-forming anaerobe that produces caproic (hexanoic) acid (Thauer et al., 1968; Zhang et al., 2019). *Ckl* uses the reverse beta-oxidation pathway to produce MCFAs with ethanol as an electron donor and acetate as an electron acceptor (Richter et al., 2016; San-Valero et al., 2019; Zhang et al., 2019; Ghysels et al., 2021). It also uses other short chain alcohols and carboxylic acids, including propionate to produce pentanoate (valerate) and heptanoate (Candry et al., 2020), and propanol and succinate to produce propionate, butyrate, pentanoate, and caproate (Kenealy & Waselefsky, 1985). *Ckl* grows best with an ethanol:acetate ratio of 3:1 or higher (Bornstein & Barker, 1948; Yin et al., 2017).

Caproate can be slowly converted with a low fractional conversion to the C8 caprylate, and thus trace amounts of caprylate can be formed (Gildemyn et al., 2017). However, due to its low solubility in water (0.0068 g/L), caprylic acid is difficult to measure. Caproate is an essential metabolite to enable the growth of *Ckl* on ethanol and acetate. The energy metabolism of *Ckl* has been extensively studied, and is now well understood (Seedorf et al., 2008). As shown in the following reactions (Seedorf et al., 2008), production of caproate through a coupled reaction network is essential to the energy metabolism of *Ckl*.



The productivity of *Ckl* monocultures growing on ethanol and acetate remains low due to excessive fermentation times. For example, it can produce 83–110 mM of caproate in 38–72 h (Weimer & Stevenson, 2012; Candry et al., 2018; Ghysels et al., 2021). With expanded timescales of 150–200 h, production of 167–181 mM of caproate has been reported (San-Valero et al., 2019; San-Valero et al., 2020). Other strategies such as immobilization (Zhang et al., 2019) or additions of biochar or activated carbon (Ghysels et al., 2021) have improved caproate titers. Table 1 summarizes key literature reports.

Ethanol and acetate are expensive substrates for hexanoate production, so to lower substrate costs, cocultures of *Ckl* have been explored. Potential coculture partners such as *Clostridium acetobutylicum* can utilize a wide variety of sugar feedstocks, including all mono- and oligosaccharides derived from biomass. In nature, microbes live in complex communities, and, thus, it is not surprising that native or synthetic cocultures can improve the efficiency of substrate utilization, improve product yields, and broaden the metabolic space by producing products that cannot be formed by single species alone (Charubin & Papoutsakis, 2019; Cui et al., 2021; Diender et al., 2021). *Ckl* has been studied in coculture with gas-consuming acetogens such as *Clostridium ljungdahlii* (Richter et al., 2016) and the closely-related *C. autoethanogenum* (Diender et al., 2019; Benito-Vaquero et al., 2020), and with Methanogen 166 (Yan & Dong, 2018). *Ckl* has also been studied in the complex environment of anaerobic sludge (Zagrodnik et al., 2020) with mixed substrates of lactose, lactate, ethanol, and acetate; and with ruminal microflora and cellulolytic bacteria (Kenealy et al., 1995; Weimer et al., 2015) with cellulose or cellulosic biomass and supplemental ethanol as substrates. Syntrophic cocultures with *C. ljungdahlii* or *C. autoethanogenum* are noted for their growth on syngas (CO₂/H₂/CO) to transform waste gases into valuable chemicals. However, caproate production from these cocultures reached maximum titers of 7.5–11 mM (Richter et al., 2016; Diender et al., 2019), which are of little practical significance. Hexanol and octanol production, formed in these cocultures by the conversion of a fraction of the corresponding carboxylates, are likewise minimal. Cocultures with methanogens and with ruminal bacteria, or in anaerobic sludge, came closer to matching the product-formation performance of *Ckl* monocultures, but as summarized in Table 2, these cocultures display low caproate productivity: maximum titers of 90 mM and long fermentation times (>6–7 days).

Our goal in this work is to explore new syntrophic coculture partners for *Ckl* that will maximize caproate production with shorter

TABLE 1 Caproate titers and production rates of *Ckl* monocultures.

Max caproate titer (mM)	Max ethanol titer (mM)	Hours	Caproate productivity ^a (mM/h)	pH range	Special conditions	References
219	443	45	4.87	7	One replicate	This work
181	348	192	0.94	6.8	None	San-Valero et al. (2019)
173	485	45	3.84	7	None	This work
167	543	160	1.04	7.5	None	San-Valero et al. (2020)
124		120	1.04	8.1 to 6.1	Recycled biochar	Ghysels et al. (2021)
117	340	18	6.50	6.8	None	This work
110	700	72	1.53	5 to 9	None	Weimer and Stevenson, (2012)
96	343	38	2.53	8.2 to 7.4	None	Candry et al. (2018)
95	315	90	1.06	6.8 to 6.0	Biofilm reuse	Zhang et al. (2019)
94		116	0.81	6.8 to 6.0	Immobilization	Zhang et al. (2019)
91	275	55	1.65	8.1 to 6.6	Activated carbon	Ghysels et al. (2021)
87	265	55	1.58	8.1 to 6.2	Biochar	Ghysels et al. (2021)
83	295	55	1.51	8.1 to 6.2	None	Ghysels et al. (2021)
71		165	0.43	6.8 to 6.0	Ammonia supplementation	Zhang et al. (2019)
65	543	50	1.30	7.5	None	San-Valero et al. (2020)
52	350	42	1.24	5 to 9	None	Weimer and Stevenson, (2012)
35	240	48	0.73	start 6.5	None	Thauer et al. (1968)

^aCalculated as the maximum total caproate titer (mM) divided by the fermentation time needed to reach that maximum (h).

TABLE 2 Caproate titers, production rates, and coculture partners of *Ckl* cocultures.

Max caproate titer (mM)	Max ethanol titer (mM)	Hours	Caproate productivity ^a (mM/h)	pH range	Coculture species	Substrate & (special conditions)	References
161	135	136	1.18	7	<i>C. saccharolyticum</i>	Glucose	This work
120	75	41	2.93	7	<i>C. saccharolyticum</i>	Glucose	This work
65	150	456	0.14	7.5 to 5.5	Clostridia-rich anaerobic digester sludge	Mixed substrate of lactose, lactate, acetate, and ethanol	Zagrodnik et al. (2020)
54	150	168	0.32	7.5 to 5.5	Clostridia-rich anaerobic digester sludge	Mixed substrate of lactose, lactate, acetate, and ethanol	Zagrodnik et al. (2020)
53	225	48	1.09	6.8 to 5.7	Ruminal bacteria	Cellulosic biomass with supplemental ethanol	Weimer et al. (2015)
40	96	112	0.36	6.8	Ruminal bacteria	Cellulose with supplemental ethanol	Kenealy et al. (1995)
31	130	22	1.41	6.2	<i>C. acetobutylicum</i>	Glucose	This work
11	28	300	0.04	6	<i>C. ljungdahlii</i>	Syngas (gas stripping)	Richter et al. (2016)
8	45	168	0.04	6.2	<i>C. autoethanogenum</i>	Carbon monoxide with supplemental ethanol	Diender et al. (2019)

^aCalculated as the maximum total caproate titer (mM) divided by the fermentation time needed to reach that maximum (h).

fermentation times. *C. acetobutylicum* (*Cac*) and *C. saccharolyticum* (*Csh*) were our two species of choice. In the published literature, neither has been reported in coculture with *Ckl*. Both are capable of good ethanol and acetate production to enable good syntrophic coculture productivity. In syntrophy, one organism depends for

survival on the metabolic products of one or multiple organisms (Charubin et al., 2020). Here *Ckl* is the dependent partner fed by an organism (feeder partner) grown on sugars that produces ethanol and acetate to feed *Ckl*. *Cac* is a model organism for acetone-butanol-ethanol fermentation. We have previously reported the engineered

strain *Cac* 824 (pCASAAD), carrying plasmid pCASAAD, produces the highest amount of ethanol observed in a *Cac* fermentation (Sillers et al., 2009). pCASAAD overexpresses the native fusion alcohol/aldehyde dehydrogenase enzyme, which catalyzes both ethanol and butanol formation. It also expresses an antisense RNA molecule, which targets the transcript of the CoA-transferase to result in reduced acetone production. The high ethanol titers (over 300 mM for *Cac*-pCASAAD) and the 3:1 ethanol:acetate ratio of its two metabolic products make *Cac* and *Cac*-pCASAAD good candidates as *Ckl* syntrophic coculture partners.

As *Cac* produces several products (notably butanol, acetone, and butyrate) in addition to ethanol and acetate, we also examined an alternate feeder organism with more favorable profile of metabolites. *Csh*, an ethanologenic anaerobe that produces ethanol, acetate, and lactate (Khan and Murray, 1982), was chosen because of its ability to produce high concentrations of ethanol and acetate in the 3:1 ratio and at neutral pH, both of which are favorable for *Ckl* growth (Richter et al., 2016). *Csh* has been studied in coculture with cellulolytic organisms (Khan and Murray, 1982; Murray, 1986), but not with organisms that produce MCFAs. Its growth at neutral pH indicates good compatibility with *Ckl*.

In designing coculture systems for metabolite production, one needs to understand the capabilities of each organism in terms of substrate utilization (rates and tolerance) and metabolite production (rates, tolerance, and titers) in the medium one intends to utilize for the coculture. As there are no satisfactory such data for *Ckl* in the literature and certainly none for growth media suitable for our cocultures, we first examined the metabolic capabilities of *Ckl* in monocultures: rates of growth, substrate utilization, and metabolite production. This was followed by coculture experiments. We demonstrate the most productive published *Ckl* monocultures. Cocultures of *Ckl* with *Cac* produced more caproate than *C. ljungdahlii* or *C. autoethanogenum* cocultures. Cocultures of *Ckl* with *Csh* demonstrated record-high and record-fast productions of caproate. We also found that heterologous cell fusion between *Ckl* and *Cac* in coculture similar to recently demonstrated fusions between *Cac* and *Clj* (Charubin and Papoutsakis, 2019; Charubin et al., 2020; Charubin et al., 2021). Such fusion events are of interest for further exploration for the development of hybrid cells (Charubin et al., 2020).

2 Materials and methods

2.1 Microorganisms and growth media

C. acetobutylicum (ATCC 824, *Cac*) and *C. kluyveri* (ATCC 8527, *Ckl*) monocultures and cocultures were grown in a growth medium Turbo CGM (Charubin and Papoutsakis, 2019) with the following modifications. Across all culture conditions, the potassium phosphate buffer addition was doubled to 20 mL/L. This buffer

consists of 100 g/L of KH_2PO_4 and 125 g/L of K_2HPO_4 adjusted to a pH of 6.8. *Cac* monocultures were grown in the following medium (termed T-CGM-G): high-buffer Turbo CGM with 80 g/L glucose. *Ckl* monocultures used the following medium (termed T-CGM-NA): high-buffer Turbo CGM with 0 g/L glucose, 8.0 g/L sodium acetate, 15.8 g/L ethanol, 2.5 g/L sodium bicarbonate, and 0.3 g/L L-cysteine HCl. Cocultures of *Cac*-*Ckl* were grown in the following medium (termed T-CGM-CC): high-buffer Turbo CGM with 40–80 g/L glucose, 2.5 g/L sodium bicarbonate, and 0.3 g/L L-cysteine HCl. *C. saccharolyticum* WM1 (ATCC 35040, *Csh*) was grown in monocultures and cocultures in T-CGM-CC with 40 g/L of glucose. To prepare bioreactors for fermentation experiments, they were autoclaved with T-CGM-BR medium, which is T-CGM-CC before the addition of the phosphate buffer, bicarbonate, L-cysteine HCL, glucose, and Wolfe's vitamins (Charubin & Papoutsakis, 2019). Sterile solutions of these chemicals were added after the medium cooled off to form T-CGM-CC.

2.2 Culture of individual microorganisms to prepare inocula for monocultures and cocultures

To begin a *Ckl* culture, a 1.3 ml frozen stock (20% [v/v] glycerol, stored at -80°C) was inoculated in a 100 ml GL-45 media bottle containing 80 ml of T-CGM-NA and grown at 37°C in the incubator of an anaerobic chamber (Thermo Forma 1025) containing an atmosphere of 85% N_2 , 10% CO_2 , and 5% H_2 . The lids of the media bottles were slightly open to allow for gas exchange and the release of excess pressure. After 3 days, once the OD_{600} (Optical Density at 600 nm) reached ~ 0.5 , the initial culture was passaged with a 10% inoculum to fresh T-CGM-NA. This resulting culture can be passaged as needed and cultured under identical conditions to generate additional cells. To prepare inocula for mono- and coculture fermentations, *Ckl* was concentrated with anaerobic centrifugation in multiple 50 ml plastic conical tubes at 4,000 rpm and room temperature for 8 min. The supernatant was then discarded, and the pellets were resuspended in fresh media. 3–5x concentration of cells was employed.

Csh frozen stocks (1.3 ml volume preserved in 20% [v/v] glycerol, stored at -80°C) were inoculated in 100 ml GL-45 media bottles containing 80 ml of T-CGM-CC in the same conditions as the *Ckl* frozen stocks overnight. The next morning, they were suitable for passaging into fresh T-CGM-CC at 10% inoculum to allow for growth to prepare for coculture conditions.

For *Cac*, a streak of a frozen stock (20% [v/v] glycerol, stored at -80°C) was applied onto 2xYTG plates and incubated anaerobically at 37°C for 3–4 days to allow for spore formation. A single colony was used to inoculate 10 ml of T-CGM-G that was heat shocked at 80°C for 10 min. This culture was then incubated at 37°C for 12 h to allow cells to reach mid-exponential phase. The cells could then be passaged at

10% (v/v) into fresh media to generate more cells. 8 h after the start of each passage, sterile 3M NaOH was used to raise the pH of the culture to 5.5–6.5 to prevent cell death and transition the *Cac* to solventogenesis. For 824 (pCASAAD), erythromycin was added to the plates at 40 µg/ml and to the liquid T-CGM-G medium at 100 µg/mL as specified (Sillers et al., 2009).

2.3 Growth of *Ckl* monocultures in serum bottles without pH control

To begin a monoculture fermentation of *Ckl*, cells were concentrated to an initial target OD₆₀₀ of 1. The cells were then resuspended and inoculated in 100 ml GL-45 media bottles containing fresh T-CGM-NA as in Section 2.2.

2.4 Growth of *Cac* monocultures and cocultures in serum bottles without pH control

To begin a monoculture fermentation of *Cac*, a 10% inoculum was used (Section 2.2), which translated to an initial OD₆₀₀ of roughly 0.5. Exponential-phase *Cac*, T-CGM-G, and appropriate antibiotics were utilized. The incubator temperature, gas composition, and 100 ml GL-45 media bottles used for the initial culturing of the organisms were also used to perform chambered mono- and coculture fermentations.

In coculture fermentations, *Ckl* was added after *Cac* acidogenesis was stopped via the addition of 3.0 M NaOH, around 10 h. Because *Ckl* grows more slowly than *Cac*, a ratio of $R \approx 4$ was chosen for inoculation through previous lab experience with *Clostridium* cocultures (Charubin & Papoutsakis, 2019) based on the relative growth rate of the cells. R is defined as the ratios of cell concentration between *Ckl* and *Cac* or *Csh* based on OD₆₀₀. Cocultures used T-CGM-CC and the same unpressurised bottles and chamber conditions as described in Section 2.2.

2.5 Construction and use of 150-ml bioreactors with pH control

For pH-controlled fermentations, small bioreactors were constructed (Supplementary Figure S1). This bioreactor setup uses spinner flasks (Chemglass CLS-1400-100). An active volume of 150 ml was used to cover the pH probe, which was inserted into one of the arms through a rubber grommet (McMaster-Carr 1061T17) into the open aperture of a GL-32 cap. The main reactor lid was solid without a central stirring axle, as a free-spinning stir bar was used instead. The other GL-32 opening held a solvent delivery cap with 4 ¼-28 threaded ports (Cole-Parmer EW-12018-53). These ports were used for sampling, base

injection, gas input, and exhaust output. Each vessel's pH was individually controlled with 1.8 M sterile NaOH by pH controllers (Bluelab pH Controller Connect). Each vessel had individually controlled nitrogen sparging to allow the initial creation of an anaerobic environment, with adjustable flow rates and a pressure of 0.5 psi. All exhaust bubbled through a water-filled bottle to ensure that an anaerobic environment was maintained. 2–3 glass vessels were placed in fiberglass bins set atop individual stir plates, which turned the stir bars in each fermentation vessel. Water was used to fill the bins around the exterior of each vessel, and the water temperature was maintained at 37°C with sous vide circulators.

To ensure sterility, all vessels were autoclaved with 150 ml T-CGM-BR before the addition of the phosphate buffer, L-cysteine HCl, bicarbonate buffer, glucose, or Wolfe's vitamins. After the vessels were removed from the autoclave and cooled, the remaining media supplements were added to create T-CGM-CC in the bioreactors. The pH probes were calibrated and sterilized with ethanol before being added to the vessels, and then nitrogen was sparged through the vessels for several hours as the temperature of the exterior water bins was increased to 37°C. The vessels were then ready for inoculation with syringes of concentrated cells prepared in the anaerobic chamber. For *Ckl* monocultures, cells were added immediately to a target OD₆₀₀ of 1. For *Csh/Ckl* cocultures, *Csh* was added immediately to a target OD₆₀₀ of 0.2. *Ckl* was added an hour later at a target ratio (*Ckl/Csh*) of $R = 4$.

2.6 Metabolite analysis

All cultures were sampled every 6–12 h until fermentation ended. The OD₆₀₀ and pH were recorded, with 1/10 and 1/20 dilutions used for the OD₆₀₀ as applicable so that the spectrophotometer never read a value of over 0.5 to reduce error. The metabolite composition of the media was analyzed with high-performance liquid chromatography as described (Carlson and Papoutsakis, 2017). The OD₆₀₀ of the monocultures of *Ckl* were correlated with the dry weight of the cells by centrifuging 100 ml of cell-containing media at 5,000 rpm for 15 min and then drying the samples in pre-massed weigh boats at 80°C and subtracting the mass of the same volumes of dried cell-free media.

2.7 Fluorescent cell staining for microscopy and flow cytometry analysis

Ckl cells were stained with CellTracker™ Green CMFDA (CTG) (Grego et al., 2013). *Cac*-pCASAAD and *Csh* cells were stained with CellTracker™ Deep Red (CTDR) (Zhou et al., 2016). To prepare these dyes, the CTG is centrifuged then mixed with 80 µL of DMSO, and CTDR is centrifuged and mixed with 20 µL of DMSO. This creates a 1000x solution for staining cell culture

media, which is anaerobically incubated for 30 min before centrifugation in 50 ml conical tubes for 8 min at 4,000 rpm. After a wash and resuspension in the T-CGM-CC, the stained cells are ready for culture.

Stained cells can be analyzed with a BD FACS Aria II flow cytometer immediately or at subsequent timepoints as described (Charubin et al., 2020). To prepare for microscopy, 8-well μ -Slides with ibiTreat (ibidi) were incubated with 200 μ L of 0.1% (w/v) poly-L-lysine overnight. Slides were then washed with sterile water and seeded with 200 μ L of culture media that had been adjusted to an OD₆₀₀ of 0.3. After 30 min of incubation in the anaerobic chamber incubator, wells were washed in three series of three washes with sterile PBS. After the final wash and aspiration, wells were covered with three drops of ProLong Glass (Invitrogen™), which enables long-term storage and protects from photobleaching. The slides were then observed with a Zeiss LSM-900 with Airyscan. Z-stacks were taken of each cell of interest to examine heterologous cell interactions as described (Charubin et al., 2020).

3 Results and discussion

3.1 *C. kluyveri* (*Ckl*) monocultures demonstrate the potential of the organism for efficient and fast caproate production

In order to design the targeted coculture experiments, we first examined the potential and metabolic characteristics of *Ckl* to produce caproate from ethanol and acetate in shorter-duration fermentations in media suitable for subsequent cocultures with *Cac* and *Csh*. We aimed to reduce the fermentation time and to explore a culture pH range that will be compatible with two prospective syntrophic coculture partners. Literature data (Table 1) show that the highest caproate titers are achieved after long fermentation times. Peak caproate titers of 96 mM were reported after 38 h of fermentation in a pH range of 8.2–7.4 (Candry et al., 2018). The highest caproate titers from *Ckl* were reported as 110 mM in 72 h from a bovine-derived strain with 700 mM of ethanol (Weimer and Stevenson, 2012), and 124 mM in 120 h when biochar is added to the fermentation media (Ghysels et al., 2021). As *Ckl* grows slowly, and batch *Ckl* fermentations typically have a maximum OD₆₀₀ below 0.8, to reduce culture time, we hypothesized that a concentrated *Ckl* inoculum might prove beneficial, although there is no assurance that higher starting cell densities will lead to higher rates of metabolite production and titers, as several other factors are known to affect those. Concentrated inocula are routinely used in industrial practice. Thus, we tested the impact of centrifugation (for cell concentration) and passaging on *Ckl* growth. When the same amount of an initial culture of *Ckl* was either directly passaged, centrifuged and passaged, or centrifuged and passaged along with the supernatant, no major differences in OD₆₀₀, pH, or metabolite profiles were observed (data not

shown), so we conclude that the centrifugation process does not harm the *Ckl* cells.

While *Ckl* has most often been cultured in the 7.4–8.2 pH range (Weimer and Stevenson, 2012; Candry et al., 2018), it can also be grown at culture pH between 6 and 7 (Zhang et al., 2019; Ghysels et al., 2021). Thus, we performed a screening experiment at seven different pH values, from 5–6.25, as well as at 7.0, to determine if *Ckl* could grow in a pH range that was compatible with *Cac*. *Ckl* grew to the highest OD₆₀₀ and produced the most caproate at a starting pH of 7; no growth was observed below pH 5.75, and at pH settings lower than 7, less than half as much caproate was produced than at pH 7 (data not shown). Based on these findings, we concluded that the cocultures required at least some periods of growth at pH 7 for caproate production to proceed. Our monoculture experiments employed a concentrated inoculum *via* centrifugation and started at pH 7 aiming to achieve fast caproate production. Figure 1 shows the results of two biological replicates of a *Ckl* monoculture in serum bottles, whereby cells were concentrated by centrifugation and resuspended in fresh T-CGM-NA medium. Culture medium was buffered with both bicarbonate and potassium phosphate, but no base was added during the fermentation. The starting OD₆₀₀ was about 1.2 and rose to 2.2 within 36 h. Based on our found correlation factor of 0.43, this represents 0.51 to 0.94 mgCDW/mL. pH dropped to 6.5 from a starting pH of 6.93. In this set of fermentations, with a starting 3:1 M ratio of ethanol to acetate, *Ckl* produced 115 mM of caproate in less than 20 h at a rate of over 8.1 mM/h or 5.1 mM/h-OD₆₀₀ between hours 0 and 9. Minimal butyrate production with some butyrate uptake was observed. Caproate was the main product, with an almost homo-caproate fermentation. It is possible that caproate production could have continued if ethanol and acetate concentrations were maintained at higher levels, the pH was controlled, or if product inhibition did not occur.

To determine if higher production of caproate was possible, four monoculture fermentations inoculated with concentrated *Ckl* were performed in pH-controlled bioreactors using T-CGM-NA (Figure 2). pH was controlled at 7, and cells grew from their initial OD₆₀₀ of 0.8 to a peak of ~2 before stabilizing at an OD₆₀₀ of ~1.5 (Figure 2A). Ethanol was added twice to maintain its titer above 200 mM (Figure 2C). With acetate added twice as well, the ethanol/acetate ratio remained above 4 (Figure 2D). With these conditions, over 150 mM of caproate was produced in 45 h (Figure 2F), which exceeds the caproate production seen in Figure 1B. One replicate performed even better, producing 219 mM of caproate. This replicate, BR3, consumed the most ethanol and acetate and produced the least butyrate. This caproate titer is the highest ever reported for a *Ckl* monoculture (Table 1), and critically, it was obtained without any *in situ* removal of caproate. Its peak production rates mirrored the rates of the fermentations without pH control (Figure 1B), with 7.9 mM/h or 5.3 mM/h-OD₆₀₀ of caproate

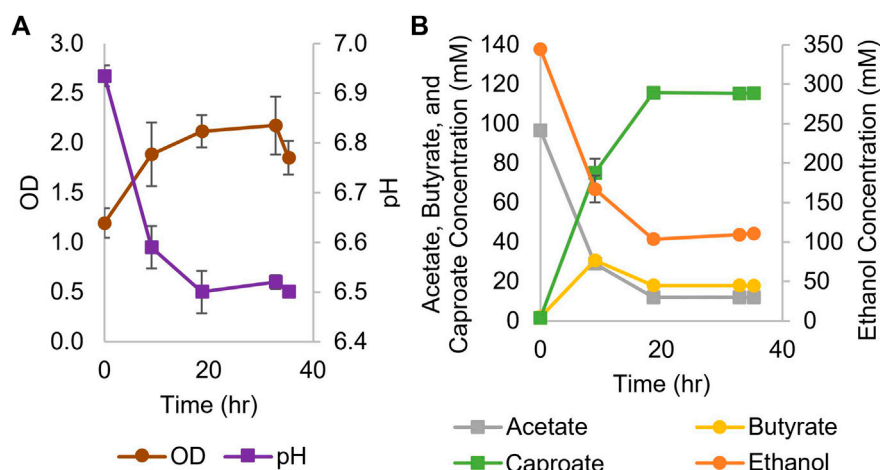


FIGURE 1

Growth and metabolite profiles of *Ckl* cultures for caproate production from ethanol and acetate. (A): OD and pH of cultures in serum bottles ($n = 2$ biological replicates). OD_{600} can be converted to mgCDW/mL by multiplying the OD_{600} by 0.43. (B): Metabolite concentrations. Note the separate axis for ethanol concentration.

produced. We conclude that the presence of high titers of ethanol (over 200 mM) and a neutral pH are beneficial in caproate production. We also note the positive slope to caproate formation in Figure 2F at 48 h, indicative of the continuous capacity of the organism to produce caproate even after significant caproate accumulation, thus demonstrating a good tolerance to caproate toxicity.

We conclude that a concentrated inoculum dramatically decreases fermentation time and improves the caproate production of *Ckl* by enabling a much higher species ratio of the slow-growing *Ckl*. Published data reported fermentation times of 2–3 days to produce over 100 mM of caproate, utilizing either high pH values, twice higher ethanol concentrations, or biochar (Weimer & Stevenson, 2012; Candry et al., 2018; Ghysels et al., 2021). Our data argue for an optimized process using adapted concentrated *Ckl* inocula for fast production of caproate.

3.2 *C. acetobutylicum* (*Cac*) and *Ckl* cocultures demonstrate caproate production from sugars under syntrophic conditions

We first wanted to explore the benefits of a coculture between *Ckl* and *Cac*. *Cac* can utilize a broad spectrum of biomass derived sugars: All 5 and 6-C sugars, oligosaccharides, and xylans (Papoutsakis, 2008; Tracy et al., 2012; Charubin et al., 2018). Thus, it would be beneficial to enable caproate production from such biomass-

derived substrates. There are no literature reports of *Cac* and *Ckl* cocultures. Among other metabolites, *Cac* produces ethanol and acetate that *Ckl* needs for growth (Sillers et al., 2009; Lee et al., 2012). We also hypothesized that *Cac* will be able to reduce the carboxylic acids produced by *Ckl* into their respective alcohols. We tested three biological replicates of batch *Cac* and *Ckl* cocultures to assess their potential for caproate production (Figure 3). Nine hours into a *Cac* fermentation, more glucose and base (for pH control) were added just prior to inoculating the *Cac* culture with concentrated *Ckl* cells. Two more manual additions of sodium hydroxide (for pH control) and glucose were carried out at 15 and 30 h. The glucose additions were to ensure that *Cac* would not exhaust its feedstock. Because of autolysis formation at pH values at and above 6 (Croux et al., 1992), *Cac* began to lyse, and as expected this resulted in decreasing cell densities.

Both caproate (30 mM) and hexanol (5 mM) were produced (Figure 3C), which validates this novel syntrophic coculture. *Ckl* utilizes ethanol and acetate (and possibly butyrate) produced by *Cac*, while *Cac* converts caproate produced by *Ckl* into hexanol, as no hexanol production is possible in *Ckl* monocultures. Notable is the exceptional rate of caproate production (4.2 mM/h or 0.9 mM/h- OD_{600}) between hours 9 and 16. The performance of the coculture in terms of caproate production deteriorates once the ethanol to acetate ratio falls below 2. This identifies the need for improvements. As WT *Cac* does not produce ethanol fast enough, a strain producing ethanol at higher rates will need to be identified or designed. This is pursued in the next two sections.

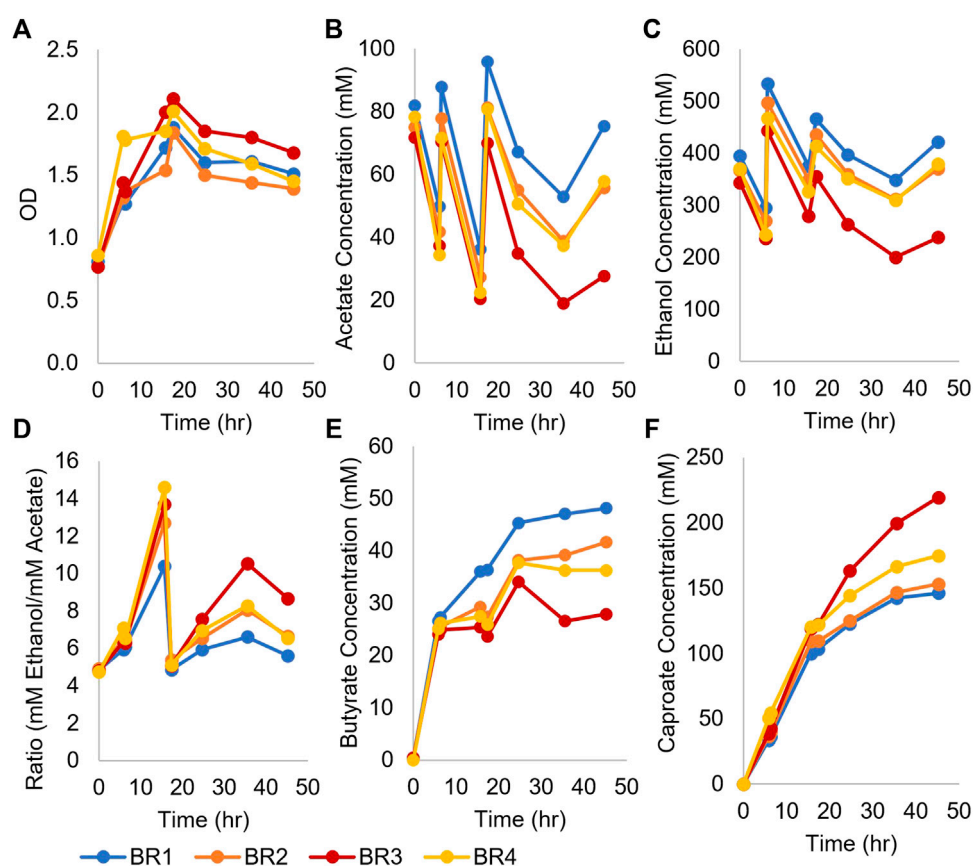


FIGURE 2

Growth and metabolite profiles of four *Ckl* cultures in pH-controlled bioreactors. The OD_{600} values remained high throughout the fermentation. OD_{600} can be converted to mgCDW/mL by multiplying the OD_{600} by 0.43. (A). Ethanol and acetate were added twice at $t = 6$ and $t = 16$ h (B,C). The ethanol/acetate ratio remained >4 throughout the fermentation (D) and butyrate concentrations were far lower than caproate concentrations (E). Note that the culture with the lowest ethanol and butyrate concentrations had the highest caproate titer (F), 219 mM. The positive slopes in (F) indicate continued caproate production.

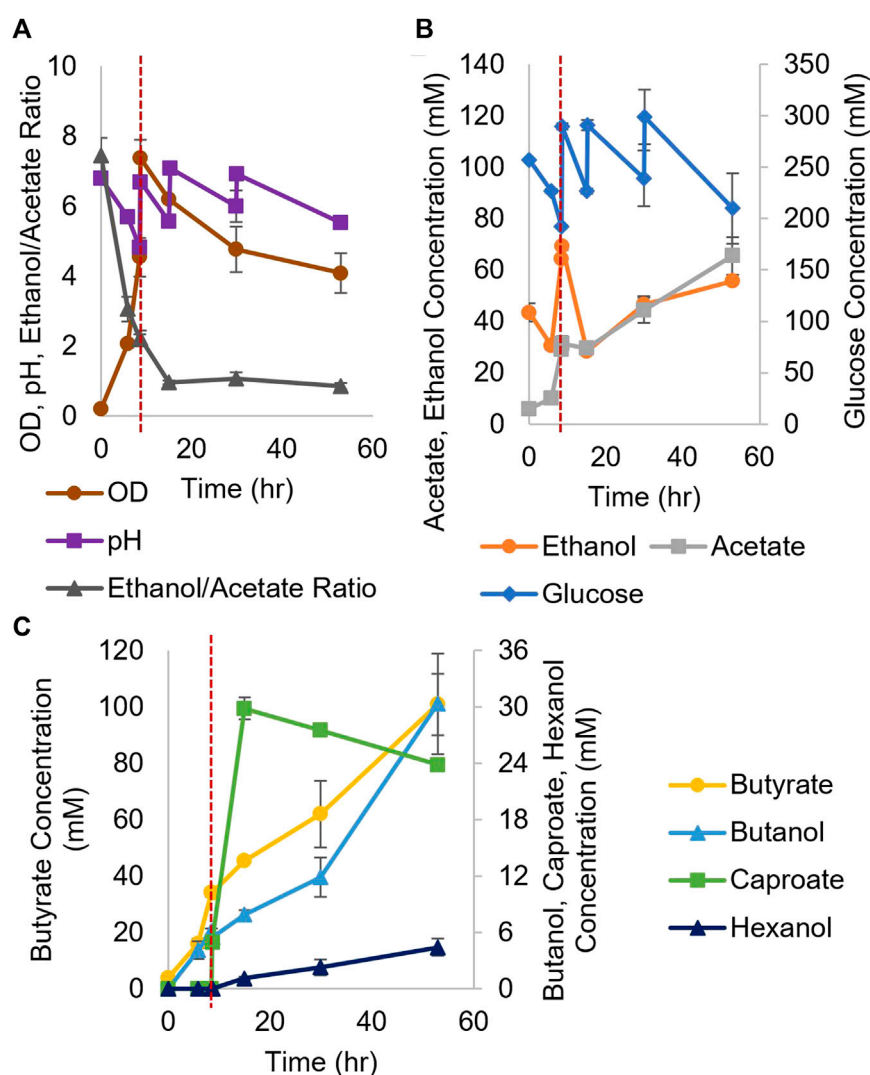
3.3 Exploring the use of *Cac* strain 824 (pCASAAD) for syntrophic cocultures with *Ckl* and the possibility of heterologous cell fusion between *Cac* and *Ckl*

Given the need for higher ethanol concentrations to support the growth of *Ckl*, we explored the use of the 824 (pCASAAD) *Cac* strain (Sillers et al., 2009) which produces much higher levels of ethanol compared to the parent WT *Cac* strain. We first tested the performance of 824 (pCASAAD) monocultures in chambered bottles (Supplementary Figure S2), the chosen setting for the cocultures. An OD_{600} of 9.5 was reached at 22 h, and another 24 h of fermentation further increased metabolite production. pH was adjusted twice with manual additions of base. 160 mM of ethanol was produced in 48 h, which far exceeds ethanol production by WT *Cac*. 50 mM of acetate was produced, which forms a desirable 3:1 ratio with ethanol. Still the major product is

butanol, which reached 220 mM, and this may be an issue with the coculture due to the toxic effect of butanol.

We thus carried out *Ckl* cocultures with 824 (pCASAAD) (Figure 4). After 10 h of 824 (pCASAAD) culture, when the pH dropped below 5 and OD_{600} reached almost 4, the pH was raised to 7.0 and a concentrated *Ckl* inoculum and glucose were added (Figure 4A). The pH was raised to 7.0 three subsequent times, and additional glucose was added at 22 h.

This fermentation produced 30 mM of caproate with a maximum production rate of 4.3 mM/h or 0.9 mM/h- OD_{600} and, notably, 10 mM of hexanol with a maximum production rate of 1 mM/h (Figure 4C). While the ethanol/acetate ratio remains close to 2 (Figure 4B), caproate production ceased by 22 h, although trace amounts of hexanol continued to be produced. The engineered 824 (pCASAAD) doubled the hexanol production relative to the WT *Cac* coculture. The lower ethanol and caproate titers relative to the monocultures

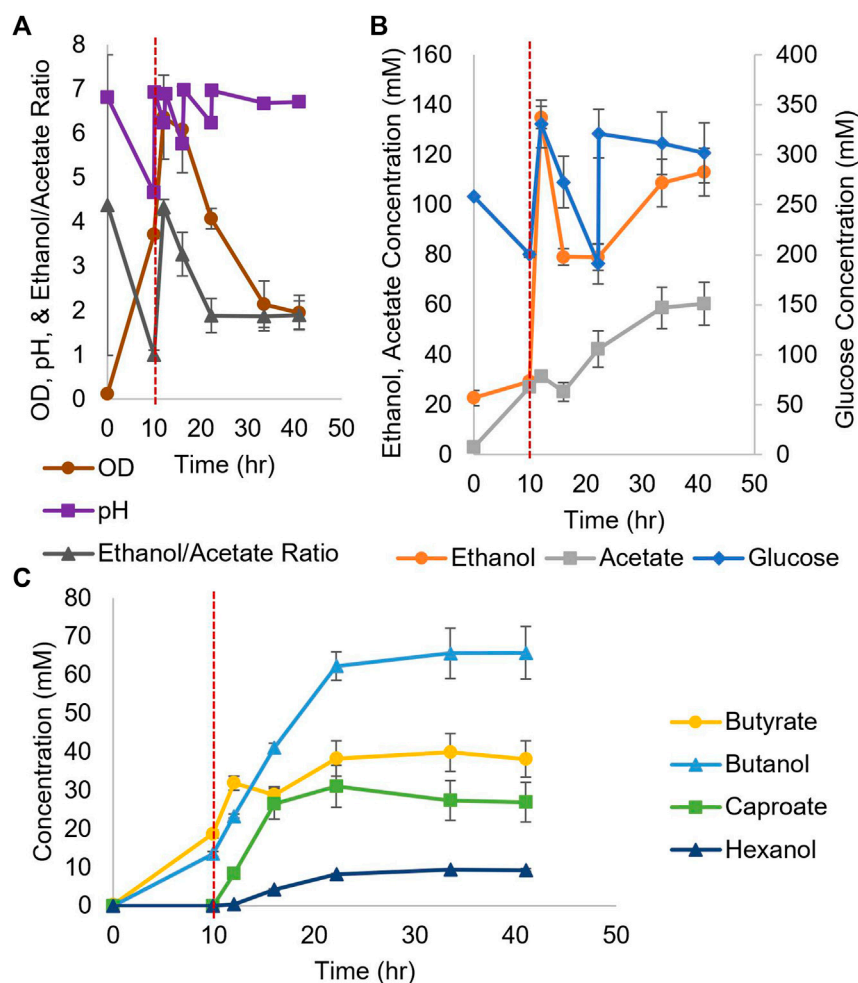
**FIGURE 3**

Growth and metabolite profiles of WT *Cac/Ckl* syntrophic cocultures. The pH was adjusted three times (A) ($n = 3$ biological replicates). In (B), glucose was added three times (note the second axis) and ethanol titers remained low throughout the fermentation. 4- to 6-C product profiles are shown in (C) (note the second axis). Caproate was produced quickly, reaching its maximum titer at 20 h. The red dashed vertical line indicates *Ckl* inoculation.

and the drop in coculture OD (Figure 4A) indicate that the expected pH-mediated *Cac* autolysis release (Croux et al., 1992) continues to impact the viability and productivity of *Cac* cells. While excess ethanol and acetate remained in a ratio greater than 1, which should lead to more caproate production by *Ckl*, the quickly-falling OD lends support to the hypothesis that autolysis formation is impairing the performance of *Ckl* and the coculture at large.

To tune this coculture further and eliminate butanol and hexanol production, the *adhE1* and *adhE2* genes (Yoo et al., 2016) in *Cac* could be knocked out. High butyrate titers are seen in both Figures 3, 4. Butyrate is an intermediate chemical towards

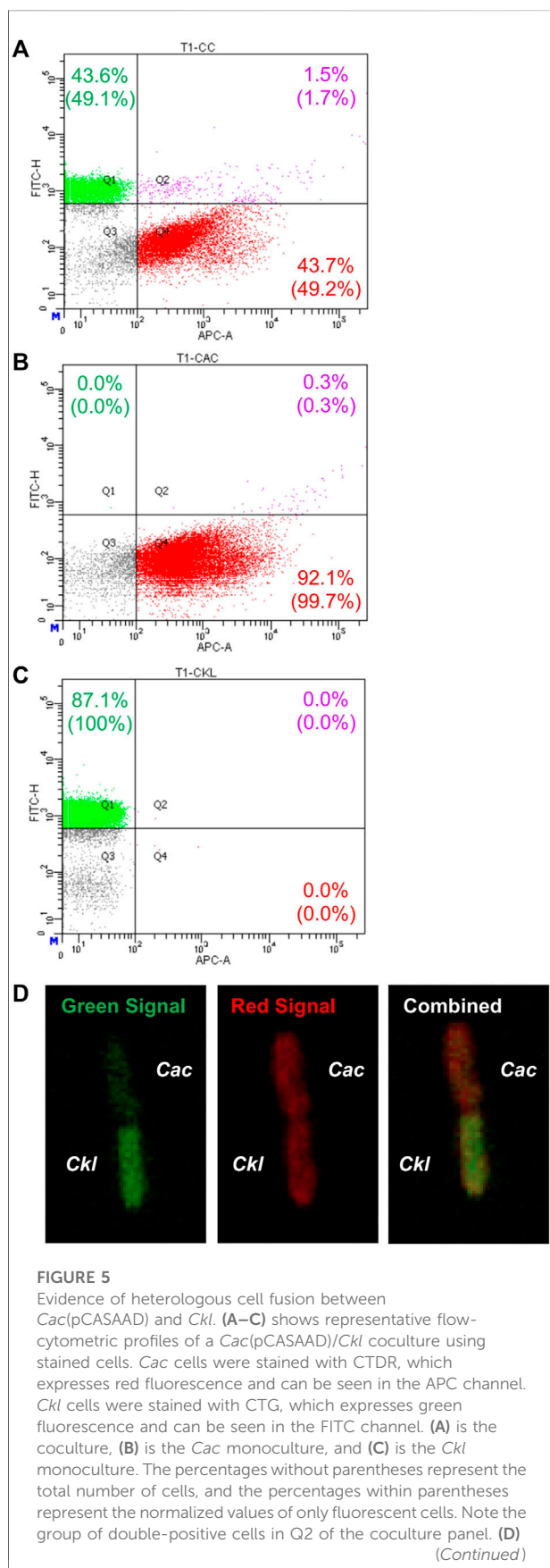
caproate production as is well established (Seedorf et al., 2008). With process optimization, including a strategy to increase ethanol concentrations, butyrate can be converted to caproate based on the kinetics and thermodynamics of well-established reactions (Seedorf et al., 2008), notably reaction [3] above. Ethanol can be sourced either through additions of biologically-produced exogenous ethanol or ethanol produced in coculture. The need for more ethanol and fewer side products led us to consider *Csh* as a coculture partner, which eliminates all butanol production. We believe our ideas and data set the foundation for process development and process optimization to realize an industrial production of caproate from sugars.

**FIGURE 4**

Growth and metabolite profiles of *Cac*(pCASAAD)/*Ckl* cocultures. (A) The profiles of OD₆₀₀, pH, and the ethanol/acetate ratio ($n = 3$ biological replicates). The pH was raised three times to keep it largely over 6, and as a result OD₆₀₀ of the coculture dropped quickly apparently due to autolysis production by *Cac* as discussed in the text. (B) The glucose profile and consumption (glucose was added twice; note the second axis) and the profiles of ethanol and acetate produced by *Cac*. Profiles of 4- and 6-C products are shown in (C). Caproate was produced quickly, reaching its maximum value in about 20 hours. The red dashed vertical line indicates *Ckl* inoculation.

Nevertheless, in view of these data and given that syntrophic WT *Cac-Clj* cocultures led to heterologous cell fusion (Charubin et al., 2020), we examined this possibility for heterologous cell fusion in the *Cac-Ckl* coculture. We used both flow cytometry and fluorescence microscopy (Charubin et al., 2020). *Cac* 824 (pCASAAD) cells were stained with the CTDR dye and *Ckl* cells were stained with the CTG dye and cocultured in T-CGM-CC. Flow cytometry showed that a good population of (CTDR, CTG) double-positive cells at 3.3 h of the coculture (Figure 5A) thus suggesting that the cells are exchanging proteins as a result of heterologous cell fusion. These double cells are not seen in either monoculture (Figures 5B,C). To verify the putative heterologous cell-fusion events, we examined the cells using confocal

microscopy (Figure 5D). Heterologously fusing cells display the same pole-to-pole contact that was observed in the detailed documentation of *Cac-Clj* heterologous cell fusion (Charubin et al., 2020), whereby both cells display both fluorescent signals due to exchange of labeled cellular proteins, but with different intensities: the green fluorescent intensity is higher in the CTG dyed *Ckl* cells and the red fluorescence higher in the CTDR dyed *Cac* cells. We conclude that *Cac* and *Ckl* form heterologous cell fusions similar to the documented *Cac-Clj* fusions. With these data in mind, it is possible to pursue the evolution of these cocultures by subculturing to examine if they may lead to novel stable phenotypes of hybrid cells as reported for the *Cac-Clj* pair (Charubin et al., 2021).

**FIGURE 5**

shows a confocal-microscopy image of a red-dyed *Cac* cell and a green-dyed *Ckl* cell. Both cells exhibit red and green signal, but the combined image on the right shows that the cells maintain their original dyed colors more strongly.

3.4 *C. saccharolyticum* is an effective coculture partner for *Ckl*, dramatically improving coculture-based caproate production from sugars

Our data show that *Cac* and *Ckl* could form successful partners in novel syntrophic cocultures, but their performance was hindered by fundamental pH incompatibilities, suboptimal rates of ethanol and acetate production by *Cac*, and production of *Cac* metabolites, such as butanol, that not only may reduce caproate selectivity, but also likely inhibit *Ckl* growth. *C. saccharolyticum* (*Csh*) (now reclassified as a *Clostridium* class, but genus *Lacrimispora* organism, *Lacrimispora saccharolytica*) (Haas & Blanchard, 2020), which produces mainly ethanol, acetate, and lactate at high titers (Murray et al., 1983), could solve these problems. Compared to 824 (pCASAAD), *Csh* thrives at a neutral pH, does not produce butanol or butyrate, and does not require antibiotics. It also uses an exceptionally broad spectrum of carbohydrate substrates similar to that of *Cac*.

For coculture experiments, *Csh* was inoculated first at an OD₆₀₀ of 0.2 in the small bioreactors filled with anaerobic T-CGM-CC. After 30 min, concentrated *Ckl* cells were added at a 1:5 ratio to account for the lower growth rate of *Ckl*. The pH was maintained at 7 (Figure 6A). The ethanol/acetate ratio started high but was only maintained at around 1 (Figure 6B) due to the consumption of ethanol by *Ckl*. Glucose was added twice. *Ckl* almost immediately started producing caproate at a rate of 3.2 mM/h or 0.9 mM/h-OD₆₀₀ (consistent with the other specific production rates in this work), and, importantly, maintained almost this rate of production for 40 h, producing 120 mM of caproate (Figure 6C). Even as low ethanol titers slowed the production rate to 0.3 mM/h, an average of 161 mM of caproate was produced before 140 h. Critically, these caproate titers are the highest published in any *Ckl* coculture than does not include *in situ* caproate removal.

These caproate production titers show that *Csh* is an exemplary coculture partner for *Ckl*. Since *Ckl* can produce over 200 mM of caproate in 45 h (Figure 2F), even higher coculture performance may be possible. Lowering the species ratio by adding additional *Csh* could have increased the ethanol titers and increased the ethanol to acetate ratio, leading to even faster performance (Figures 2C,D). *Csh* by itself produced ethanol to acetate in a ratio of around 3, but *Ckl* consumed more ethanol than acetate, keeping the ratio low. Nevertheless, the fast ethanol production of *Csh*, as opposed to the much slower ethanol production of *Cac*, led to this coculture's greater

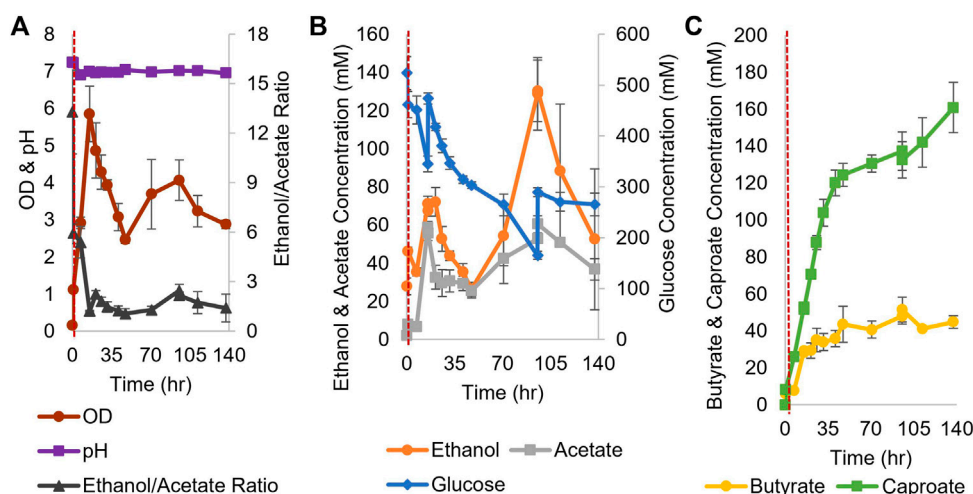


FIGURE 6

Growth and metabolite profiles of *Csh* and *Ckl* cocultures in pH-controlled bioreactors. (A) The OD₆₀₀ and pH. The pH remained at its setpoint of 7 ($n = 3$ biological replicates). (B) shows the glucose profile and consumption (glucose was added twice; note the second axis) and the profiles of ethanol and acetate produced by *Csh*. (C) shows the profiles of the butyrate and caproate produced by *Ckl* in the coculture. Note that most caproate is produced in the initial 35 h, but that production continues until the end of the fermentation with an increase profile slope indicative of continued caproate production. The red dashed vertical line indicates *Ckl* inoculation.

success. While the peak ethanol titers from *Cac*-pCASAAD and *Csh* cocultures are similar, this does not account for all of the ethanol that was elongated into caproate by *Ckl* (in the *Csh* coculture, over 310 mM). Additionally, the compatible pH of *Csh* and *Ckl* led to a coculture without the negative effects of the autolysins and a more stable OD₆₀₀. While no hexanol is produced, genetic modification of *Csh* or introduction of another coculture species could resolve this and further improve this novel coculture. Somewhat surprisingly, our efforts to identify heterologous fusion events in this *Csh*-*Ckl* coculture pair have not proved successful as yet. An essential difference between *Cac* and *Csh* is that they belong to different *Clostridium*-class genera, and that *Csh* is classified as Gram negative versus Gram positive for *Cac*.

4 Conclusion

Ethanologenic clostridia species are effective coculture partners for *Ckl*, and their fast production rates help to make carboxylic acid cocultures industrially viable. *Cac* cocultures outperform other published clostridia cocultures, and *Csh* delivers the highest-observed coculture caproate titers ever. *Cac* could be modified to increase ethanol titers further and to improve its pH tolerance, and *Csh* could be modified to produce even more ethanol or to produce alcohols from its carboxylic acids. *Clj* could also be added to capture lost carbon, and other strategies such as perfusion or biochar addition to

capture the coculture products will increase productivity further.

Data availability statement

The raw data supporting the conclusion of this article will be made available by the authors, without undue reservation.

Author contributions

JO: Conceptualization, Methodology, Validation, Formal analysis, Investigation, Resources, Data Curation, Writing—Original Draft, Writing—Review and Editing, Visualization, Project administration. YZ: Methodology, Investigation. EP: Conceptualization, Writing—Review and Editing, Supervision, Project administration, Funding acquisition.

Funding

This work was supported by the United States Department of Energy under Grant DE-SC0019155. Microscopy access was supported by grants from the NIH-NIGMS (P20 GM103446), the NIH-NIGMS (P20 GM139760), and the State of Delaware.

Acknowledgments

The authors wish to thank Jeffrey Caplan and Sylvain Le Marchand of the Delaware Bioimaging Center for assistance with microscopy and Kamil Charubin and Hannah Streett for assistance with flow cytometry.

Conflict of interest

The authors declare that the research was conducted in the absence of any commercial or financial relationships that could be construed as a potential conflict of interest.

References

- Benito-Vaquerizo, S., Diender, M., Parera Olm, I., Martins Dos Santos, V. A. P., Schaap, P. J., Sousa, D. Z., et al. (2020). Modeling a co-culture of *Clostridium autoethanogenum* and *Clostridium kluyveri* to increase syngas conversion to medium-chain fatty-acids. *Comput. Struct. Biotechnol. J.* 18, 3255–3266. doi:10.1016/j.csbj.2020.10.003
- Bornstein, B. T., and Barker, H. A. (1948). The energy metabolism of *Clostridium kluyveri* and the synthesis of fatty acids. *J. Biol. Chem.* 172 (2), 659–669. doi:10.1016/s0021-9258(19)52752-1
- Candry, P., Ulcar, B., Petrognani, C., Rabaey, K., and Ganigue, R. (2020). Ethanol: propionate ratio drives product selectivity in odd-chain elongation with *Clostridium kluyveri* and mixed communities. *Bioresour. Technol.* 313, 123651. doi:10.1016/j.biortech.2020.123651
- Candry, P., Van Daele, T., Denis, K., Amerlinck, Y., Andersen, S. J., Ganigue, R., et al. (2018). A novel high-throughput method for kinetic characterisation of anaerobic bioproduction strains, applied to *Clostridium kluyveri*. *Sci. Rep.* 8 (1), 9724. doi:10.1038/s41598-018-27594-9
- Carlson, E. D., and Papoutsakis, E. T. (2017). Heterologous expression of the *Clostridium carboxidivorans* CO dehydrogenase alone or together with the acetyl coenzyme A synthase enables both reduction of CO₂ and oxidation of CO by *Clostridium acetobutylicum*. *Appl. Environ. Microbiol.* 83 (16), e00829-17. doi:10.1128/aem.00829-17
- Charubin, K., Bennett, R. K., Fast, A. G., and Papoutsakis, E. T. (2018). Engineering *Clostridium* organisms as microbial cell-factories: Challenges & opportunities. *Metab. Eng.* 50, 173–191. doi:10.1016/j.ymben.2018.07.012
- Charubin, K., Gregory, G. J., and Papoutsakis, E. T. (2021). Novel mechanism of plasmid-DNA transfer mediated by heterologous cell fusion in syntrophic coculture of *Clostridium* organisms. <http://bioRxiv.org/abs/2021.12.15.472834>.
- Charubin, K., Modla, S., Caplan, J. L., and Papoutsakis, E. T. (2020). Interspecies microbial fusion and large-scale exchange of cytoplasmic proteins and RNA in a syntrophic *Clostridium* coculture. *mBio* 11 (5), e02030-20. doi:10.1128/mbio.02030-20
- Charubin, K., and Papoutsakis, E. T. (2019). Direct cell-to-cell exchange of matter in a synthetic *Clostridium* syntrophy enables CO₂ fixation, superior metabolite yields, and an expanded metabolic space. *Metab. Eng.* 52, 9–19. doi:10.1016/j.ymben.2018.10.006
- Croux, C., Canard, C., Goma, G., and Soucaille, P. (1992). Autolysis of *Clostridium acetobutylicum* ATCC 824. *J. Gen. Microbiol.* 138 (5), 861–869. doi:10.1099/00221287-138-5-861
- Cui, Y., Yang, K. L., and Zhou, K. (2021). Using Co-culture to functionalize *Clostridium* fermentation. *Trends Biotechnol.* 39 (9), 914–926. doi:10.1016/j.tibtech.2020.11.016
- Diender, M., Parera Olm, I., Gelderloos, M., Koehorst, J. J., Schaap, P. J., Stams, A. J. M., et al. (2019). Metabolic shift induced by synthetic co-cultivation promotes high yield of chain elongated acids from syngas. *Sci. Rep.* 9 (1), 18081. doi:10.1038/s41598-019-54445-y
- Diender, M., Parera Olm, I., and Sousa, D. Z. (2021). Synthetic co-cultures: Novel avenues for bio-based processes. *Curr. Opin. Biotechnol.* 67, 72–79. doi:10.1016/j.copbio.2021.01.006
- Ghysels, S., Buffel, S., Rabaey, K., Ronsse, F., and Ganigue, R. (2021). Biochar and activated carbon enhance ethanol conversion and selectivity to caproic acid by *Clostridium kluyveri*. *Bioresour. Technol.* 319, 124236. doi:10.1016/j.biortech.2020.124236
- Gildemyn, S., Molitor, B., Usack, J. G., Nguyen, M., Rabaey, K., Angenent, L. T., et al. (2017). Upgrading syngas fermentation effluent using *Clostridium kluyveri* in a continuous fermentation. *Biotechnol. Biofuels* 10, 83. doi:10.1186/s13068-017-0764-6
- Grego, M., Stachowitsch, M., De Troch, M., and Riedel, B. (2013). CellTracker green labelling vs. rose bengal staining: CTG wins by points in distinguishing living from dead anoxia-impacted copepods and nematodes. *Biogeosciences* 10 (7), 4565–4575. doi:10.5194/bg-10-4565-2013
- Haas, K. N., and Blanchard, J. L. (2020). Reclassification of the *Clostridium* cladoformae and *Clostridium* sphenoides clades as *Enterocloster* gen. nov. and *Lacrimispora* gen. nov., including reclassification of 15 taxa. *Int. J. Syst. Evol. Microbiol.* 70, 23–34. doi:10.1099/ijsem.0.003698
- Kenealy, W. R., Cao, Y., and Weimer, P. J. (1995). Production of caproic acid by cocultures of ruminal cellulolytic bacteria and *Clostridium kluyveri* grown on cellulose and ethanol. *Appl. Microbiol. Biotechnol.* 44, 507–513. doi:10.1007/bf00169952
- Kenealy, W. R., and Waselefsky, D. M. (1985). Studies on the substrate range of *Clostridium kluyveri*; the use of propanol and succinate. *Arch. Microbiol.* 141 (3), 187–194. doi:10.1007/bf00408056
- Khan, A. W., and Murray, W. D. (1982). Single step conversion of cellulose to ethanol by a mesophilic coculture. *Biotechnol. Lett.* 4, 177–180. doi:10.1007/bf00144320
- Lee, J., Jang, Y. S., Choi, S. J., Im, J. A., Song, H., Cho, J. H., et al. (2012). Metabolic engineering of *Clostridium acetobutylicum* ATCC 824 for isopropanol-butanol-ethanol fermentation. *Appl. Environ. Microbiol.* 78 (5), 1416–1423. doi:10.1128/aem.06382-11
- Murray, W. D. (1986). Symbiotic relationship of *Bacteroides cellulosolvens* and *Clostridium saccharolyticum* in cellulose fermentation. *Appl. Environ. Microbiol.* 51, 710–714. doi:10.1128/aem.51.4.710-714.1986
- Murray, W. D., Wemyss, K. B., and Khan, A. W. (1983). Increased ethanol production and tolerance by a pyruvate-negative mutant of *Clostridium saccharolyticum*. *Eur. J. Appl. Microbiol. Biotechnol.* 18, 71–74. doi:10.1007/bf00500827
- Papoutsakis, E. T. (2008). Engineering solventogenic clostridia. *Curr. Opin. Biotechnol.* 19 (5), 420–429. doi:10.1016/j.copbio.2008.08.003
- Richter, H., Molitor, B., Diender, M., Sousa, D. Z., and Angenent, L. T. (2016). A narrow pH range supports butanol, hexanol, and octanol production from syngas in a continuous Co-culture of *Clostridium ljungdahlii* and *Clostridium kluyveri* with in-line product extraction. *Front. Microbiol.* 7, 1773. doi:10.3389/fmicb.2016.01773
- San-Valero, P., Abubakar, H. N., Veiga, M. C., and Kennes, C. (2020). Effect of pH, yeast extract and inorganic carbon on chain elongation for hexanoic acid production. *Bioresour. Technol.* 300, 122659. doi:10.1016/j.biortech.2019.122659
- San-Valero, P., Fernandez-Naveira, A., Veiga, M. C., and Kennes, C. (2019). Influence of electron acceptors on hexanoic acid production by *Clostridium kluyveri*. *J. Environ. Manage.* 242, 515–521. doi:10.1016/j.jenvman.2019.04.093
- Seedorf, H., Florian Fricke, W., Veith, B., Bruggemann, H., Liesegang, H., Strittmatter, A., et al. (2008). The genome of *Clostridium kluyveri*, a strict

Publisher's note

All claims expressed in this article are solely those of the authors and do not necessarily represent those of their affiliated organizations, or those of the publisher, the editors and the reviewers. Any product that may be evaluated in this article, or claim that may be made by its manufacturer, is not guaranteed or endorsed by the publisher.

Supplementary material

The Supplementary Material for this article can be found online at: <https://www.frontiersin.org/articles/10.3389/fbioe.2022.965614/full#supplementary-material>

anaerobe with unique metabolic features. *Proc. Natl. Acad. Sci. U. S. A.* 105 (6), 2128–2133. doi:10.1073/pnas.0711093105

Sillers, R., Al-Hinai, M. A., and Papoutsakis, E. T. (2009). Aldehyde-alcohol dehydrogenase and/or thiolase overexpression coupled with CoA transferase downregulation lead to higher alcohol titers and selectivity in *Clostridium acetobutylicum* fermentations. *Biotechnol. Bioeng.* 102 (1), 38–49. doi:10.1002/bit.22058

Syahril, S., Masbar, R., Syahnur, S., Majid, S. A., Zulham, T., Saputra, J., et al. (2019). The effect of global prices of crude palm oil, marketing margins and palm oil plantations on the environmental destruction: An application of johansen cointegration approach. *Int. J. Energy Econ. Policy* 9 (4), 305–312. doi:10.32479/ijep.8010

Tauer, R. K., Jungermann, K., Henninger, H., Wenning, J., and Decker, K. (1968). The energy metabolism of *Clostridium kluyveri*. *Eur. J. Biochem.* 4, 173–180. doi:10.1111/j.1432-1033.1968.tb00189.x

Tracy, B. P., Jones, S. W., Fast, A. G., Indurthi, D. C., and Papoutsakis, E. T. (2012). Clostridia: The importance of their exceptional substrate and metabolite diversity for biofuel and biorefinery applications. *Curr. Opin. Biotechnol.* 23 (3), 364–381. doi:10.1016/j.copbio.2011.10.008

Weimer, P. J., Nerdahl, M., and Brandl, D. J. (2015). Production of medium-chain volatile fatty acids by mixed ruminal microorganisms is enhanced by ethanol in co-culture with *Clostridium kluyveri*. *Bioresour. Technol.* 175, 97–101. doi:10.1016/j.biortech.2014.10.054

Weimer, P. J., and Stevenson, D. M. (2012). Isolation, characterization, and quantification of *Clostridium kluyveri* from the bovine rumen. *Appl. Microbiol. Biotechnol.* 94 (2), 461–466. doi:10.1007/s00253-011-3751-z

Yan, S., and Dong, D. (2018). Improvement of caproic acid production in a *Clostridium kluyveri* H068 and Methanogen 166 co-culture fermentation system. *Amb. Express* 8 (1), 175. doi:10.1186/s13568-018-0705-1

Yin, Y., Zhang, Y., Karakashev, D. B., Wang, J., and Angelidaki, I. (2017). Biological caproate production by *Clostridium kluyveri* from ethanol and acetate as carbon sources. *Bioresour. Technol.* 241, 638–644. doi:10.1016/j.biortech.2017.05.184

Yoo, M., Croux, C., Meynial-Salles, I., and Soucaille, P. (2016). Elucidation of the roles of adhE1 and adhE2 in the primary metabolism of *Clostridium acetobutylicum* by combining in-frame gene deletion and a quantitative system-scale approach. *Biotechnol. Biofuels* 9, 92. doi:10.1186/s13068-016-0507-0

Zagrodnik, R., Duber, A., Lezyk, M., and Oleskowicz-Popiel, P. (2020). Enrichment versus bioaugmentation-microbiological production of caproate from mixed carbon sources by mixed bacterial culture and *Clostridium kluyveri*. *Environ. Sci. Technol.* 54 (9), 5864–5873. doi:10.1021/acs.est.9b07651

Zhang, C., Yang, L., Tsapekos, P., Zhang, Y., and Angelidaki, I. (2019). Immobilization of *Clostridium kluyveri* on wheat straw to alleviate ammonia inhibition during chain elongation for n-caproate production. *Environ. Int.* 127, 134–141. doi:10.1016/j.envint.2019.03.032

Zhou, W., Kang, H. C., O'Grady, M., Chambers, K. M., Dubbels, B., Melquist, P., et al. (2016). CellTrace™ far red & CellTracker™ Deep red. *J. Biol. Methods* 3 (1), e38. doi:10.14440/jbm.2016.113



OPEN ACCESS

EDITED BY

Qi Xianghui,
Jiangsu University, China

REVIEWED BY

Meijuan Xu,
Jiangnan University, China
Jin-Song Gong,
Jiangnan University, China
Hui Ni,
Jimei University, China

*CORRESPONDENCE

Xuetuan Wei,
weixuetuan@mail.hzau.edu.cn

SPECIALTY SECTION

This article was submitted to Industrial Biotechnology, a section of the journal Frontiers in Bioengineering and Biotechnology

RECEIVED 24 June 2022

ACCEPTED 08 August 2022

PUBLISHED 30 August 2022

CITATION

Jiang C, Ye C, Liu Y, Huang K, Jiang X, Zou D, Li L, Han W and Wei X (2022), Genetic engineering for enhanced production of a novel alkaline protease BSP-1 in *Bacillus amyloliquefaciens*. *Front. Bioeng. Biotechnol.* 10:977215. doi: 10.3389/fbioe.2022.977215

COPYRIGHT

© 2022 Jiang, Ye, Liu, Huang, Jiang, Zou, Li, Han and Wei. This is an open-access article distributed under the terms of the [Creative Commons Attribution License \(CC BY\)](https://creativecommons.org/licenses/by/4.0/). The use, distribution or reproduction in other forums is permitted, provided the original author(s) and the copyright owner(s) are credited and that the original publication in this journal is cited, in accordance with accepted academic practice. No use, distribution or reproduction is permitted which does not comply with these terms.

Genetic engineering for enhanced production of a novel alkaline protease BSP-1 in *Bacillus amyloliquefaciens*

Cong Jiang¹, Changwen Ye², Yongfeng Liu³, Kuo Huang², Xuedeng Jiang¹, Dian Zou¹, Lu Li⁴, Wenyuan Han¹ and Xuetuan Wei^{1*}

¹State Key Laboratory of Agricultural Microbiology, Hubei Hongshan Laboratory, Huazhong Agricultural University, Wuhan, China, ²Zhengzhou Tobacco Research Institute of China National Tobacco Corporation, Zhengzhou, China, ³GeneMind Biosciences Company Limited, Shenzhen, China, ⁴Sericultural & Argi-Food Research Institute, Guangdong Academy of Agricultural Sciences/Key Laboratory of Functional Foods, Ministry of Agriculture and Rural Affairs/Guangdong Key Laboratory of Agricultural Products Processing, Guangzhou, China

Alkaline protease has been widely applied in food, medicine, environmental protection and other industrial fields. However, the current activity and yield of alkaline protease cannot meet the demand. Therefore, it is important to identify new alkaline proteases with high activity. In this study, we cloned a potential alkaline protease gene *bsp-1* from a *Bacillus subtilis* strain isolated in our laboratory. BSP-1 shows the highest sequence similarity to subtilisin NAT (S51909) from *B. subtilis* natto. Then, we expressed BSP-1 in *Bacillus amyloliquefaciens* BAX-9 and analyzed the protein expression level under a collection of promoters. The results show that the P43 promoter resulted in the highest transcription level, protein level and enzyme activity. Finally, we obtained a maximum activity of 524.12 U/mL using the P43 promoter after fermentation medium optimization. In conclusion, this study identified an alkaline protease gene *bsp-1* from *B. subtilis* and provided a new method for high-efficiency alkaline protease expression in *B. amyloliquefaciens*.

KEYWORDS

alkaline protease, *bacillus amyloliquefaciens*, promoter screening, recombinant expression, fermentation optimization

1 Introduction

Alkaline protease is found in all living organisms (Gupta et al., 2002). Alkaline protease has a lot of functions and it is widely applied in washing, food, textile, leather, pharmaceutical and other industries (Contesini et al., 2018; Harish and Uppuluri, 2018; Pathak and Rathod, 2018; Tavano et al., 2018; Jahangirian et al., 2019; Sharma et al., 2019; Burchacka et al., 2022). However, in recent years, the yield of alkaline protease fail to satisfy the industrial demand, causing the shortage problem of large-scale industrial enzymes (Barzkar, 2020). Therefore, developing efficient alkaline protease has great industrial prospects.

Many strains produce alkaline protease, *Bacillus* genus are the main producer of the enzyme in industrial production (Cai et al., 2019). *Bacillus* have high secretory capacity and become the main producer of the enzyme in industrial production (Westers et al., 2004). However, the yield and activity of alkaline protease in *Bacillus* is usually low (Zhang et al., 2020; Ouyang et al., 2021; Zhang et al., 2021; Espoui et al., 2022). To achieve high-efficiency expression of target proteins, researchers had reformed expression elements, such as signal peptides, transcription factors, and molecular chaperones (Liu et al., 2019; Suberu et al., 2019; Gong et al., 2020; Neef et al., 2021; Su et al., 2021). For instance, Gang et al. constructed a signal peptide library in *Bacillus subtilis*, and screened out the amylase activity up to 5086 U/mL (Fu et al., 2018). In addition, by combining the transcriptional activator Spo0A with the regulatory region of *Bacillus licheniformis*, Zhou et al. successfully achieved 1.46-fold increase in the yield of alkaline protease AprE (Zhou et al., 2020). In addition, since promoter is one of the most critical factors in gene expression regulation (Kumar and Bansal, 2018; Brázda et al., 2021; Cazier and Blazeck, 2021; Jensen and Galburt, 2021), its engineering also serves as an important strategy to increase microbial gene expression and metabolites production. Su et al. substituted the wild-type -10 box and -35 box of *aprN* promoter, resulting in significantly higher nattokinase production than those previously reported in *B. subtilis* (Wu et al., 2011). Liao et al. (2018) optimized the ribosome-binding site to improve β -Gal activity in *B. amyloliquefaciens*. Together, genetic manipulation of the above elements has been widely applied in the production of industrial enzymes.

B. subtilis has significant attributes, such as fast growth and development, strong metabolic capacity and rich products, *B. subtilis* has been the preferred organisms for industrial production of a variety of products (Gu et al., 2018). *B. amyloliquefaciens* could secrete recombinant proteins using a variety of signal peptides (Cui et al., 2018), thus it had been an efficient platform for producing various proteases (Uyar and Baysal, 2008; Matkawala et al., 2021; Meng et al., 2021). In this study, we identified an alkaline protease gene *bsp-1* from *B. subtilis*, and then expressed it in *B. amyloliquefaciens* BAX-9. Subsequently, we further analyzed the expression level under different promoters. Finally, the highest expression level of alkaline protease was obtained by using the promoter P43 combined with fermentation optimization.

2 Materials and methods

2.1 Chemicals

In this study, the *TransStartFastPfu* DNA polymerase was purchased from TransGen Biotech Co., Ltd. (Beijing, China). Restriction enzymes, dNTPs, T4 ligase and RNase were provided by Takara Biotechnology Co., Ltd. (Dalian, China). We purchased the Total RNA Isolation Kit and PrimeScript RT

Master Mix Kit from Vazyme Biotech Co., Ltd. (Nanjing, China). Standard alkaline protease was purchased from Sigma-Aldrich Co., LLC (St. Louis, United States). All the other chemicals were obtained from Sinopharm Chemical Reagent Co., Ltd. (Shanghai, China).

2.2 Recombinant expression of *bsp-1* gene

To express BSP-1 in *B. amyloliquefaciens* BAX-9, we constructed the recombinant strains following the procedure reported in our previous study (Zou et al., 2020). All strains and plasmids involved were listed in Tables 1, 2, listed all designed primers. For example, a pair of primers were designed to amplify the *bsp-1* gene from *B. subtilis* DNA, Ppqq promoter from *B. amyloliquefaciens* and TamyL terminator from *B. licheniformis* WX-02 respectively, and then Ppqq promoter, TamyL terminator and *bsp-1* gene were fused by Splicing with Overlap Extension PCR (SOE-PCR). The fused fragment and the pHY-300PLK plasmid were digested by restriction enzymes of *Bam*HI and *Xba*I, and then they were ligated to obtain the expression plasmid pHY-Ppqq/BSP-1. The expression plasmid pHY-Ppqq/BSP-1 was electroporated into BAX-9 to obtain the recombinant strain. In this study, the remaining recombinant strains were constructed using the same procedure.

2.3 Skim milk agar medium assay

Skim milk agar medium contain 10 g/L tryptone, 5 g/L yeast extract, 10 g/L NaCl, 1.5% Agar and 2% skim milk. To screen the protease activity, 20 μ L of supernatant of the cultures were added to the wells of milk agar plates made by a hole punch. The radius of transparent circles were measured after the plates were cultured at 37°C for 12 h.

2.4 Protease fermentation

The *B. amyloliquefaciens* cells were inoculated into 5 ml liquid LB medium (10 g/L tryptone, 5 g/L yeast extract, and 10 g/L NaCl), and incubated at 37°C for 12 h with shaking at 180 rpm. Then, a 3% (v/v) inoculum was transferred into the 50 ml alkaline protease fermentation medium (40 g/L tryptone, 20 g/L yeast extract, and 10 g/L NaCl) and cultured at 37°C for 72 h with shaking at 180 rpm.

2.5 SDS-PAGE analysis of the expressed proteins

Protein samples were prepared by 100% trichloroacetic acid (TCA) precipitation (Benabdelkamel et al., 2018).

TABLE 1 Strains and plasmids used in this study.

Strains	Characteristics	Source
BAX-9	<i>B. amyloliquefaciens</i> HZ-12 deficient in <i>epr</i> , <i>nprE</i> , <i>aprE</i> , <i>aprX</i> , <i>mpr</i> , <i>bpf</i> , <i>vpr</i> , <i>htrB</i> , <i>yktc1</i>	Stored in lab
BAX-9/pHY-300	BAX-9 harboring the plasmid pHY300PLK	Stored in lab
BAX-9/pHY-Psra/BSP-1	BAX-9 harboring the plasmid pHY-Psra/BSP-1	This study
BAX-9/pHY-Psrs/BSP-1	BAX-9 harboring the plasmid pHY-Psrs/BSP-1	This study
BAX-9/pHY-PrnpB/BSP-1	BAX-9 harboring the plasmid pHY-PrnpB/BSP-1	This study
BAX-9/pHY-Pffs/BSP-1	BAX-9 harboring the plasmid pHY-Pffs/BSP-1	This study
BAX-9/pHY-Phyp/BSP-1	BAX-9 harboring the plasmid pHY-Phyp/BSP-1	This study
BAX-9/pHY-Ppqq/BSP-1	BAX-9 harboring the plasmid pHY-Ppqq/BSP-1	This study
BAX-9/pHY-Pscp/BSP-1	BAX-9 harboring the plasmid pHY-Pscp/BSP-1	This study
BAX-9/pHY-Pcsp/BSP-1	BAX-9 harboring the plasmid pHY-Pcsp/BSP-1	This study
BAX-9/pHY-P43/BSP-1	BAX-9 harboring the plasmid pHY-P43/BSP-1	This study
BAX-9/pHY-PtrnQ/BSP-1	BAX-9 harboring the plasmid pHY-PtrnQ/BSP-1	This study
BAX-9/pHY-Psrf/BSP-1	BAX-9 harboring the plasmid pHY-Psrf/BSP-1	This study
BAX-9/pHY-Pitu/BSP-1	BAX-9 harboring the plasmid pHY-Pitu/BSP-1	This study
BAX-9/pHY-Pfen/BSP-1	BAX-9 harboring the plasmid pHY-Pfen/BSP-1	This study
BAX-9/pHY-Pbac/BSP-1	BAX-9 harboring the plasmid pHY-Pbac/BSP-1	This study
<i>B. subtilis</i> 168	the strain containing P43 promoter	Stored in lab
<i>B.licheniformis</i> WX-02	CCTCC M208065, wild type	Stored in lab

Plasmid	Characteristics	Source
pHY300PLK	<i>E. coli</i> – <i>Bacillus</i> shuttle vector for gene expression, Apr, Tet	Stored in lab
pHY-PX/BSP-1	pHY300PLK + <i>bsp-1</i> + TamyL	This study
pHY-Psra/BSP-1	pHY300PLK + Psra + <i>bsp-1</i> + TamyL	This study
pHY-Psrs/BSP-1	pHY300PLK + Psrs + <i>bsp-1</i> + TamyL	This study
pHY-PrnpB/BSP-1	pHY300PLK + PrnpB + <i>bsp-1</i> + TamyL	This study
pHY-Pffs/BSP-1	pHY300PLK + Pffs + <i>bsp-1</i> + TamyL	This study
pHY-Phyp/BSP-1	pHY300PLK + Phyp + <i>bsp-1</i> + TamyL	This study
pHY-Ppqq/BSP-1	pHY300PLK + Ppqq + <i>bsp-1</i> + TamyL	This study
pHY-Pscp/BSP-1	pHY300PLK + Pscp + <i>bsp-1</i> + TamyL	This study
pHY-Pcsp/BSP-1	pHY300PLK + Pcsp + <i>bsp-1</i> + TamyL	This study
pHY-P43/BSP-1	pHY300PLK + P43+ <i>bsp-1</i> + TamyL	This study
pHY-PtrnQ/BSP-1	pHY300PLK + PtrnQ + <i>bsp-1</i> + TamyL	This study
pHY-Psrf/BSP-1	pHY300PLK + Psrf + <i>bsp-1</i> + TamyL	This study
pHY-Pitu/BSP-1	pHY300PLK + Pitu + <i>bsp-1</i> + TamyL	This study
pHY-Pfen/BSP-1	pHY300PLK + Pfen + <i>bsp-1</i> + TamyL	This study
pHY-Pbac/BSP-1	pHY300PLK + Pbac + <i>bsp-1</i> + TamyL	This study

Specifically, 0.90 ml of fermentation supernatant was mixed with 0.10 ml of trichloroacetic acid, inverted 10 times to mix and incubated at 4°C for 12 h. Then, the mixture was centrifuged at 6,000 ×g for 10 min. After that, the supernatant was discarded and the pellet was washed with 0.20 ml of absolute ethanol for three times. After dried at 37°C, the pellet was dissolved with 30 µL of loading buffer containing 8 mol/L urea and 2 mol/L thiourea. At last, the samples were analyzed by SDS-PAGE electrophoresis.

2.6 Enzyme activity analysis

1 ml of the sample was transferred to tube A (as blank control) and tube B for activity measurement, respectively. After the samples were heated at 40°C for 2 min, A was supplemented with 2 ml of trichloroacetic acid (64.70 g/L), while B was added with 1 ml of casein solution (10 g/L). Both samples were further heated at 40°C for 10 min. Then, 1 ml casein solution was added into A, and 2 ml trichloroacetic acid

TABLE 2 Primers used in this study.

Primer name	Sequence of primer (5' to 3')
<i>bsp-1</i> -F	CGGGATCCATGAGAAGCAAAAAATTGTGGAT
<i>bsp-1</i> -R	TTATTGTGCAGCTGCTTGTACG
<i>bsp-1</i> (Ppqq)-F	ACAGCTTCATTGCCGAATGAGAAGCAAAAAATTGTGGAT
<i>bsp-1</i> (Tamy)-R	AAGAGCAGAGAGGACTTATTGTGCAGCTGCTTGTACG
TamyL-F	GCAGCTGCACAATAAAAGAGCAGAGAGGACGGATT
TamyL-R	GCTCTAGACGCAATAATGCCGTCGCACT
Psra-F	CGGAATTC AACGAAAAGACGCCAAAAG
Psra-R	CGGGATCCCTTGTTAAGGGTATACGGGAGAT
Psrs-F	CGGAATTCGCAGTTTGTCTTCTTGAAAATCA
Psrs-R	CGGGATCCACAGCAGATTTTGATTTTCAA
PrnpB-F	CGGAATTCGGTCGTATTCGGCGCAT
PrnpB-R	CGGGATCCCAAAATAAATATCAAATTTTGATATG
Pffs-F	CGGAATTCGGATTATGAAACCTTTCATCAAG
Pffs-R	CGGGATCCCTAAGAACACTTGTTCATTATAAAGC
Phyp-F	CGGAATTCCTAAAAATCACACTGACAGCAGAC
Phyp-R	CGGGATCCCTGCCATTGTCTCTCACCTC
Ppqq-F	CGGGATCCGGCAGGAGCTGTCTCTTTAT
Ppqq-R	TTTTTTGCTTCTCATTTCGCAATGAAGCTGTCTTT
P43-F	CGGAATTCCTGATAGGTGGTATGTTTTTCG
P43-R	CGGGATCCGTGTACATTCCTCTCTTACCTATAATG
PtrnQ-F	CGGAATTCGTCGTCTCTTTTCCCATTTT
PtrnQ-R	CGGGATCCATATAGACTGCGTTATGAGAACGTC
Pscp-F	CGGAATTCCTAAAAATAGTGATTTTATCAGG
Pscp-R	CGGGATCCATCTATTCCTCCTTTTCTTTTACTA
Pcsp-F	CGGAATTC AACATGTTATTTGAAAAAAGTTA
Pcsp-R	CGGGATCCGAAATTTCTCTCTAAAGCGAC
Psrf-F	CGGAATTCAGCGCTCTATGTAATAAGAGTGC
Psrf-R	CGGGATCCATGTGTGCGCCTCCCTT
Pitu-F	CGGAATTCCTAATTTCTGACACAATAATGCCAA
Pitu-R	CGGGATCCGAGATTCTCCGATCATATTGAA
Pfen-F	CGGAATTC CAAAAATGGCGGAATTTT
Pfen-R	CGGGATCCAATGGCAGTTTATCCTCCAG
Pbac-F	CGGAATTCATTATTACATCCTCCTTAAGA
Pbac-R	CGGGATCCCTGGATTCCCCGCCTT
pHY300-YF	GTTTATTATCCATACCTTAC
pHY300-YR	CAGATTCGTGATGCTTGTC

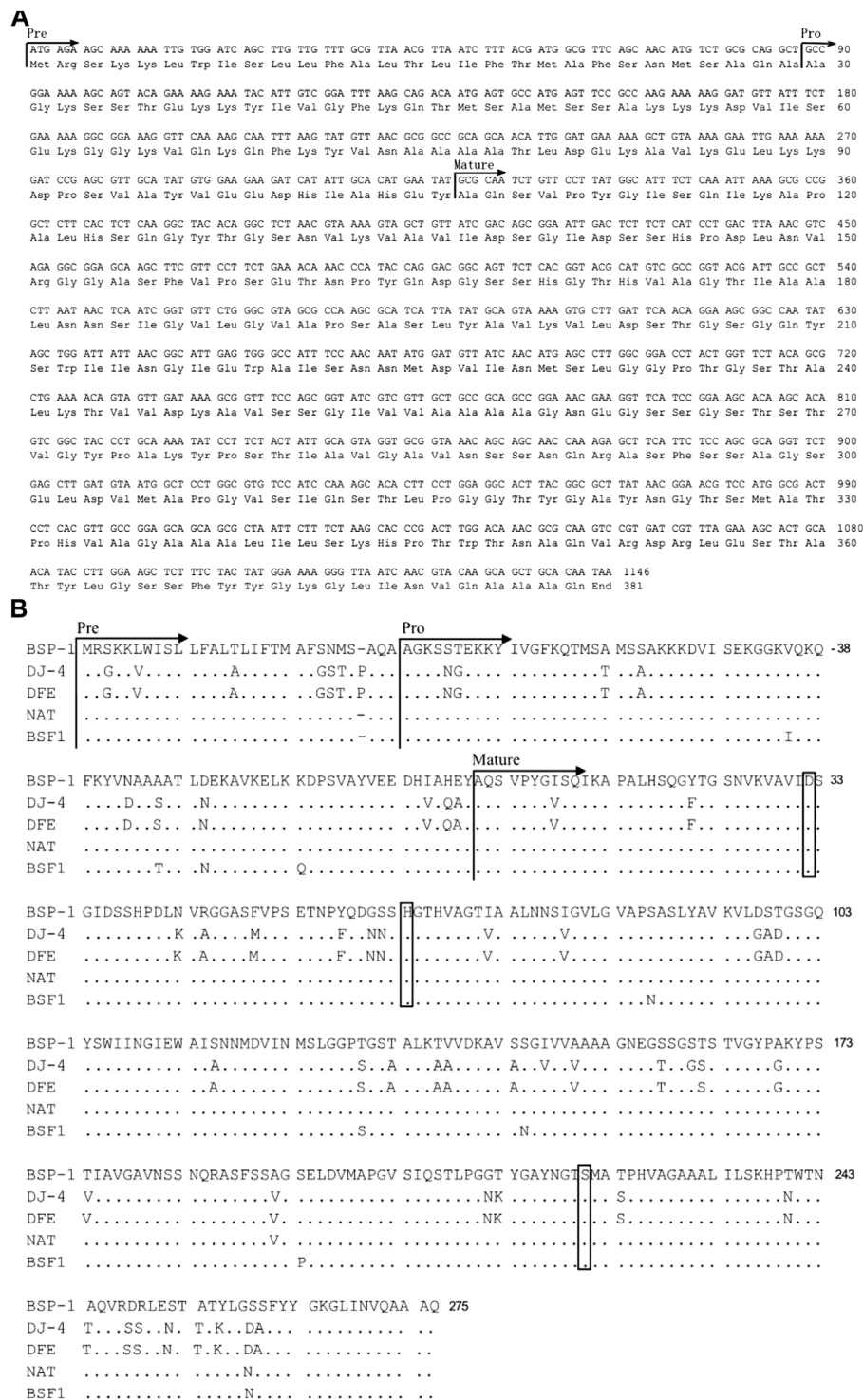
Note: Restriction sites highlight in bold.

was added into B. The mixtures were placed at room temperature for 20 min. Subsequently, A and B were filtered and obtained supernatant, and added 5 ml of sodium carbonate solution and 1 ml of folin phenol reagent to the supernatant, mix well and heat at 40°C for 20 min, and measure the absorbance at 680 nm wavelength. The activity 1) of the dilution of sample was obtained from the standard curve. The enzymatic activity of the sample was calculated as follows:

$$\text{Enzyme activity (U/mL)} = \frac{a \times 4 \times N}{10} \quad (N: \text{Dilution factor of sample})$$

2.7 Transcriptional analysis during the alkaline protease fermentation

The recombinant engineered strains were cultured for 12 h, and then the cells were collected by centrifugation and washed for

**FIGURE 1**

Sequence analysis of *bsp-1* gene and deduced amino acids. **(A)** Nucleotide (upper line) and deduced amino acid (lower line) sequences of the protease BSP-1. The predicted signal peptide, propeptide and mature peptide are marked with arrows. **(B)** Amino acid sequence alignment of the protease BSP-1, with subtilisin (DJ-4, DFE) from *B. amyloliquefaciens* and subtilisin (NAT, BSF1) from *B. subtilis*. The signal peptide, pro-peptide, and mature peptide (mature) were indicated with arrows. "-" indicated the same residue as the first sequence. The catalytic center residues (Asp-32, His-64, and Ser-221) were boxed. The initial amino acid of the mature peptide was numbered as + 1.

transcription analysis, according to the description of Total RNA Isolation Kit and PrimeScript RT Master Mix Kit. DNA removal and RNA reverse transcription were performed simultaneously in one system. The reaction conditions which included EasyScript® RT/RI and gDNA Remover were 25°C for 10 min, 42°C for 15 min, and 85°C for 10 s. RT-PCR amplification was performed using three-steps method. Pre-denaturation: 1 cycle (95°C for 5 min); PCR reaction: 40 cycles (95°C for 30 s, 60°C for 30 s) and dissolution curve (1 min at 95°C, 1 min at 65°C). Relative quantitative analysis was performed with 16 s RNA as the internal reference gene.

2.8 Statistical analysis

Each group of experiments was designed with three independent replicates. SPSS 20.0 was used for statistical analysis, calculating the means and standard deviations, and evaluating the significance. Origin 8.5 was used to process the data and make the graphs.

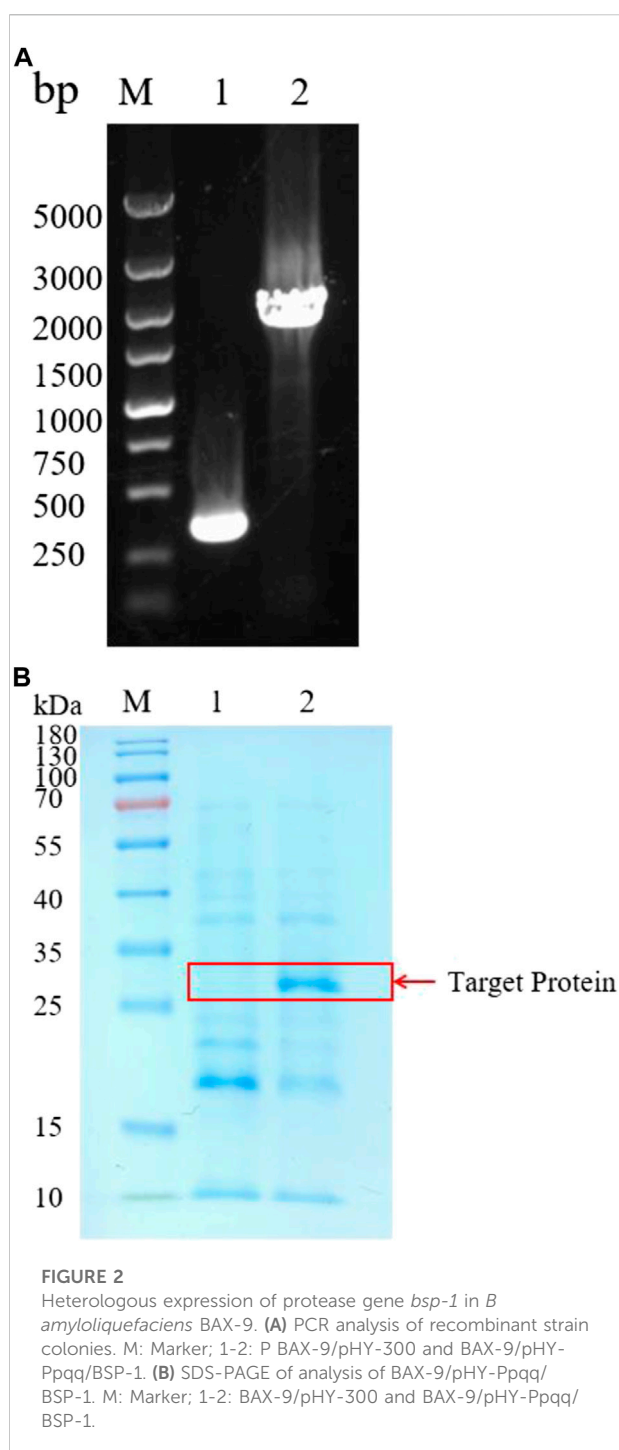
3 Results and discussion

3.1 Identification of an alkaline protease from a new *B. subtilis* strain

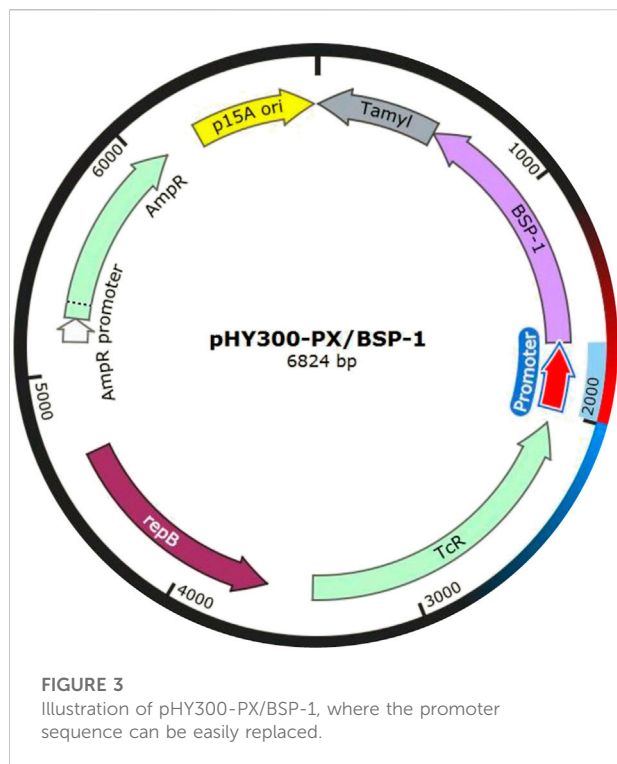
We isolated a *B. subtilis* strain with high protease activity using skim milk plates. Then the new *B. subtilis* strain was named *B. subtilis* D7. In order to identify an alkaline protease from *B. subtilis* D7, we designed a primer set using the gene sequence of subtilisin NAT (S51909) from *B. subtilis*. With the primers, we amplified a gene fragment from *B. subtilis* D7. Sequencing of the gene fragment indicates that it encodes an alkaline protease (BSP-1) containing 381 amino acids (aa) (Figure 1A). Analysis of the protein sequence using SignalP 5.0 indicates a 29-aa predicted signal peptide, while the 30-77 aa and 78-275 aa are the propeptide and mature peptide, respectively (Figure 1A). We aligned the sequence of BSP-1 with four well-characterized proteases (Choi et al., 2004; Yong et al., 2004; Agrebi et al., 2009; Ku et al., 2009), indicating that it has the highest similarity to subtilisin NAT (S51909) and fibrinolytic enzyme BSF1(FJ517584) (>96% similarity) and less similar to subtilisin DJ-4 and subtilisin DFE (Figure 1B). In addition, all the proteases contain the conserved catalytic triad, including Asp-32, His-64, and Ser-221. Together, the data indicates that BSP-1 belong to the subtilisin family of serine proteases (Wei et al., 2011).

3.2 Heterologous expression of BSP-1 in *B. amyloliquefaciens* BAX-9

B. amyloliquefaciens is considered as a safe strain that have been widely used to express industrial enzymes. *B. amyloliquefaciens* is rich in proteases, and can degrade



heterologous proteins. Knockout of the protease genes may solve the problem. Therefore, we expressed BSP-1 in *B. amyloliquefaciens* BAX-9, a strain where many protease genes (*epr*, *nprE*, *aprE*, *aprX*, *mpr*, *bpf*, *vpr*, *htrB*, *yktc1*) have been knocked out (Chen et al., 2022). At first, the promoter of PQQ-binding-like beta-propeller repeat gene (Ppqq) from *B. amyloliquefaciens* was used to express BSP-



1. The constructed expression plasmid, pHY-Ppqq/BSP-1, was electroporated into *B. amyloliquefaciens* BAX-9, generating the strain BAX-9/pHY-Ppqq/BSP-1 (Figure 2A). Subsequently, the fermentation broth of BAX-9/pHY-Ppqq/BSP-1 and the control strain (BAX-9/pHY-300) were used for SDS-PAGE analysis. As shown in Figure 2B, compared to the control strain (BAX-9/pHY-300), the target protein (30 kDa) was found in the fermentation broth of BAX-9/pHY-Ppqq/BSP-1. This result demonstrates that the *bsp-1* gene was significantly expressed in BAX-9. The thickness of the band corresponds to the amount of protein present, the thicker band of the target protein also shows the feasibility and great potential of expressing the heterologous protein in *B. amyloliquefaciens*.

3.3 Promoter screening enhanced BSP-1 expression

To further improve the expression of BSP-1 in *B. amyloliquefaciens*, we screened different promoters driving the expression of BSP-1. The promoters include two reported high-strength promoters (P43 (Wang and Doi, 1984), PtrnQ (Song et al., 2016)) from *B. subtilis* and a promoter collection from *B. amyloliquefaciens* HZ-12. We selected the promoters of potentially highly-expressed genes in HZ-12, including *ssrA* (NC_014551.1: 3271400-3271038), *ssrS* (NC_014551.1:

2609656-2609464), *rnpB* (NC_014551.1: 2202786-2202405), *ffs* (NC_014551.1: 27641-27905), cold-shock protein gene (NC_014551.1: 1029767-1029567), PQQ protein gene (NC_014551.1: 3859752-3858532), spore coat protein gene (NC_014551.1: 1272412-1271912), hypothetical protein gene (NC_014551.1: 1272819-1272505). In addition, since *B. amyloliquefaciens* is highly productive of macromolecular substances such as lipopeptides, the promoters of four gene clusters (Surfactin, Iturin A, Fengycins, Bacillaene) producing lipopeptides, i.e., Psrf, Pitu, Pfen, Pbac, respectively, were also used in the study.

For efficient insertion of the promoters, we constructed a plasmid with replaceable promoter sequence by inserting the fusion fragment of *bsp-1* gene and TamyL terminator into pHY300PLK, resulting in the plasmid pHY300PLK-PX/BSP-1 (Figure 3). Then, the sequences of the promoters were amplified and then inserted into pHY300PLK-PX/BSP-1. The resulting plasmids were transformed into BAX-9 to generate engineered strains for further analysis. Engineered strains containing different promoters (Psra, Psrs, Prnp, Pffs, Ppqq, Pcsp, Pscp, Phyp, Psrf, Pitu, Pfen, Pbac, P43, PtrnQ) and the control strain (BAX-9/pHY-300, BAX-9) were fermented. And the enzyme activities of these strains were preliminarily analyzed by using skim milk agar plates. As shown in Figure 4, the supernatant of the fermentation broth of the engineering strains containing P43, Pitu, Pfen, Ppqq, Psrf, Pcsp, PtrnQ and Pscp produced transparent circles of different radius (7, 7, 7, 6.50, 6, 6, 4, 1.50 mm, respectively), while other promoters (Psra, Psrs, Prnp, Pffs, Phyp, Pbac) did not produce transparent circles. The size of the transparent circle reflects the activity of BSP-1, the size of the transparent circle is positively correlated with the activity.

Accorded to the result of the transparent circle, we selected the Pscp, Pcsp, Ppqq, Psrf, Pitu, Pfen promoters from *B. amyloliquefaciens* and the P43 promoter from *B. subtilis* for further analysis. We analyzed the proteins in the supernatant of BAX-9/pHY-Pscp/BSP-1, BAX-9/pHY-Pcsp/BSP-1, BAX-9/pHY-Ppqq/BSP-1, BAX-9/pHY-Psrf/BSP-1, BAX-9/pHY-Pitu/BSP-1, BAX-9/pHY-Pfen/BSP-1 and BAX-9/pHY-P43/BSP-1 by SDS-PAGE. As shown in Figure 5, BSP-1 was successfully expressed in all recombinant strains, and exhibited the highest level under the promoter P43, Psrf and Pfen, which was consistent with the result of the transparent circle. The data indicates that a high-strength promoter facilitates the protein expression level and thus increase the activity outcome of protein.

3.4 Effects of different promoters on the activity of BSP-1

To further analyze the effect of different promoters on the expression level of protease gene *bsp-1*, we measured the activity

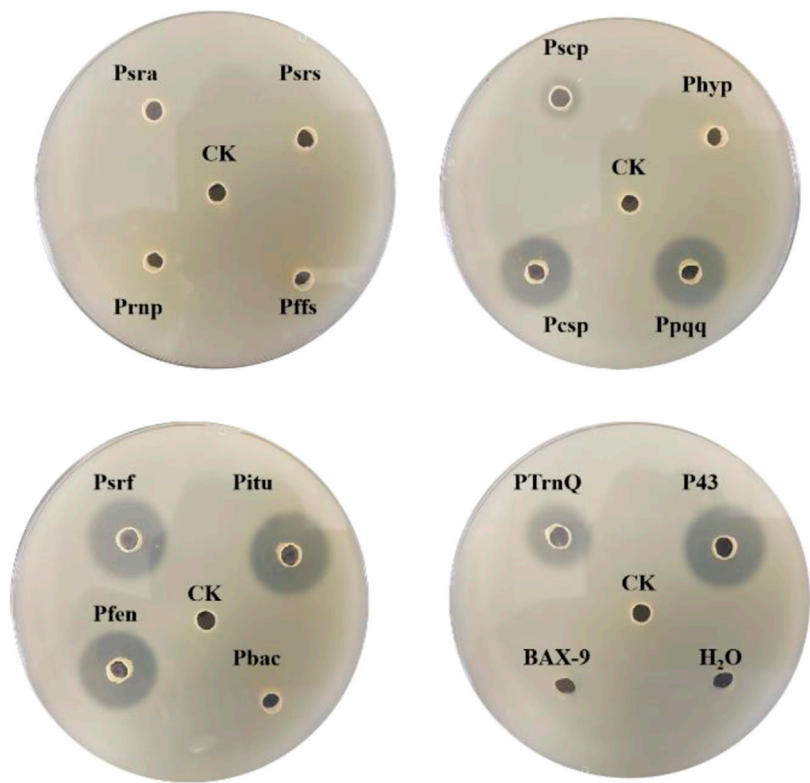


FIGURE 4
Skim milk agar plates of the fermentation supernatant of different strains. CK: BAX-9/pHY-300, Psra: BAX-9/pHY-Psra/BSP-1, Psrs: BAX-9/pHY-Psrs/BSP-1, Prnp: BAX-9/pHY-Prnp/BSP-1, Pffs: BAX-9/pHY-Pffs/BSP-1, Pscp: BAX-9/pHY-Pscp/BSP-1, Ppqq: BAX-9/pHY-Pscp/BSP-1, Pscp: BAX-9/pHY-Pscp/BSP-1, Phyp: BAX-9/pHY-Phyp/BSP-1, Psrf: BAX-9/pHY-Psrf/BSP-1, Pitu: BAX-9/pHY-Pitu/BSP-1, Pfen: BAX-9/pHY-Pfen/BSP-1, Pbac: BAX-9/pHY-Pbac/BSP-1, P43: BAX-9/pHY-P43/BSP-1, PTrnQ: BAX-9/pHY-PTrnQ/BSP-1.

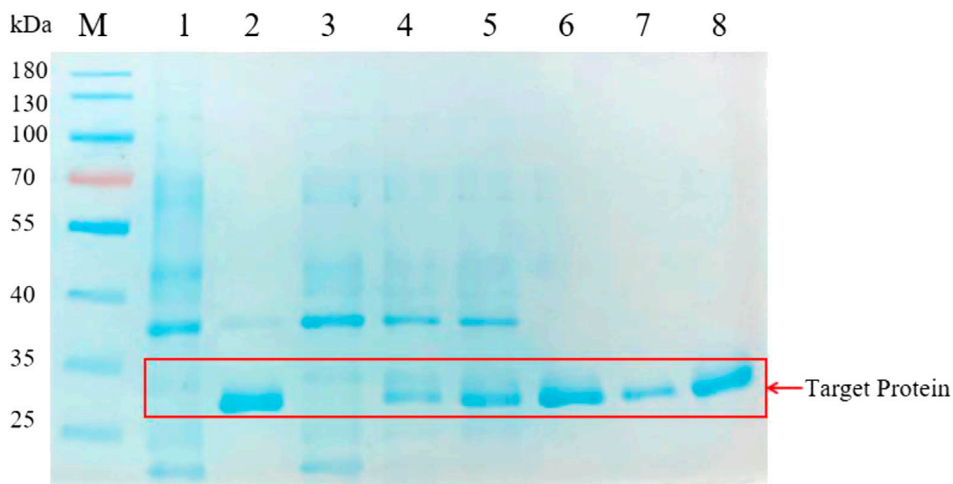


FIGURE 5
SDS-PAGE analysis of the fermentation supernatant of different strains. M: Marker; 1-8: BAX-9/pHY-300, BAX-9/pHY-P43/BSP-1, BAX-9/pHY-Pscp/BSP-1, BAX-9/pHY-Pcsp/BSP-1, BAX-9/pHY-Ppqq/BSP-1, BAX-9/pHY-Psrf/BSP-1, BAX-9/pHY-Pitu/BSP-1, BAX-9/pHY-Pfen/BSP-1.

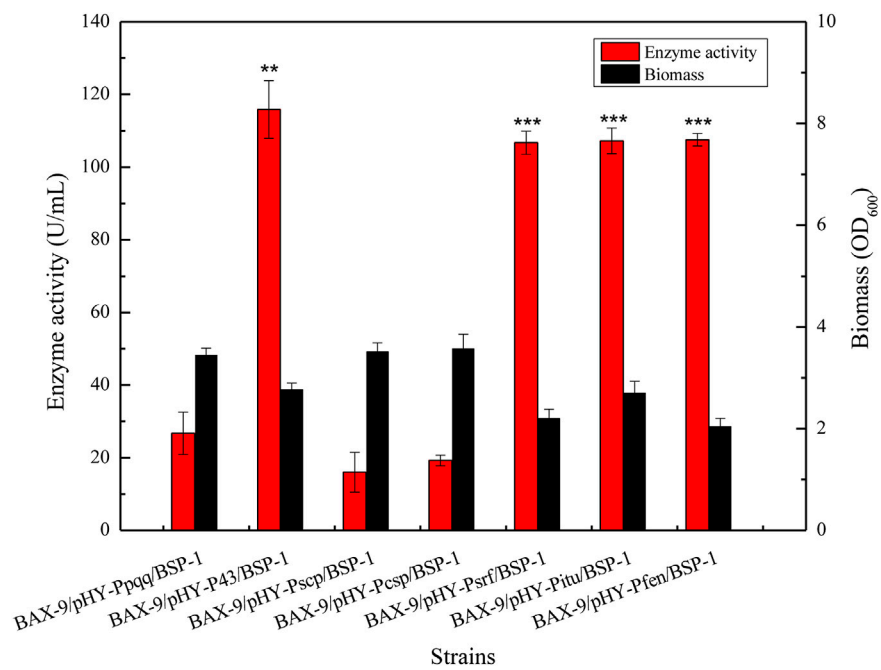


FIGURE 6
Determination of enzyme activity and biomass of recombinant strains. Asterisks show the significant difference ($p < 0.05$) compared with the control.

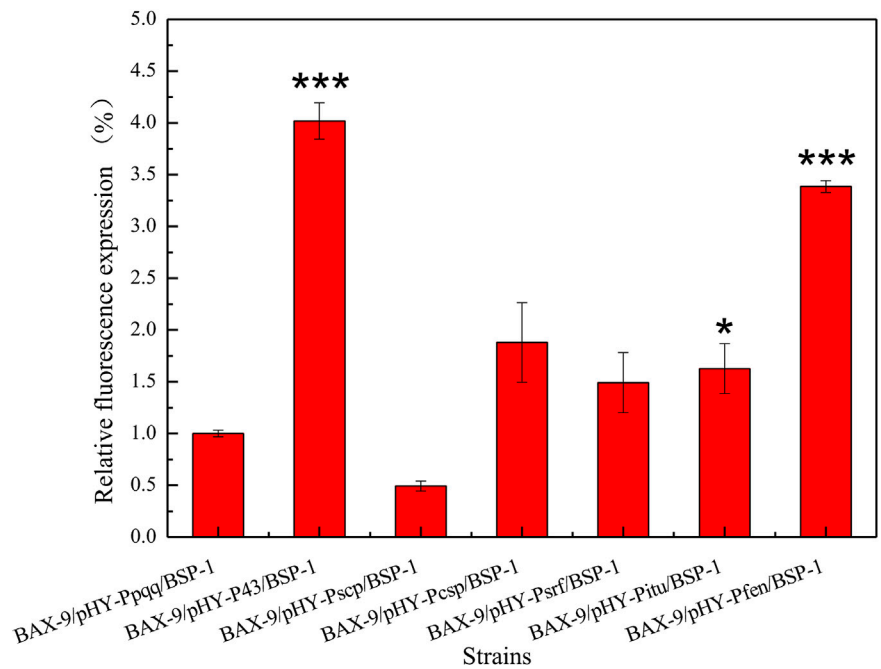


FIGURE 7
RT-PCR results of recombinant strains. Asterisks show the significant difference ($p < 0.05$) compared with the control.

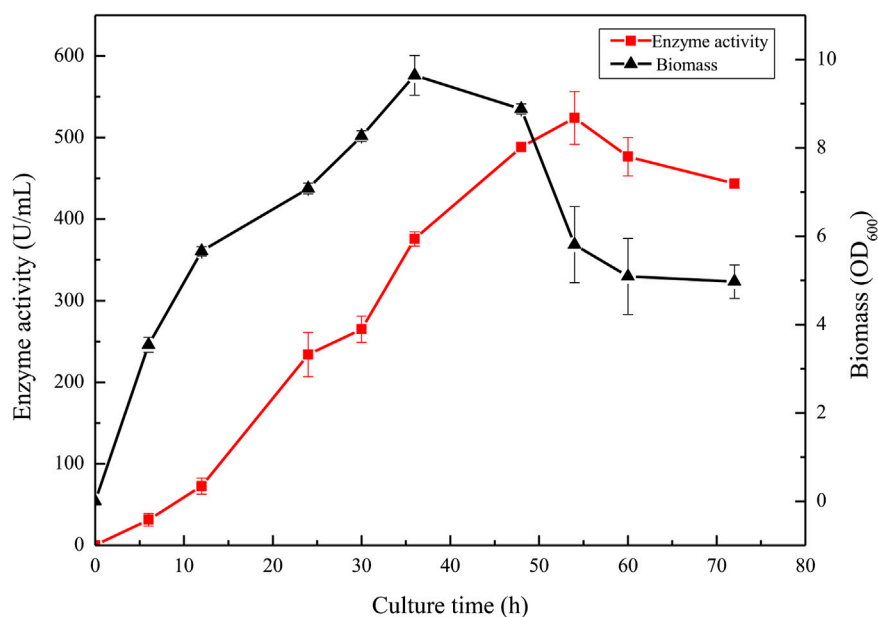


FIGURE 8

Enzyme activity and culture growth of BAX-9/pHY-P43/BSP-1 under fermentation using the optimized fermentation medium.

of BSP-1 and the biomass of the seven cultures at 48 h. As shown in Figure 6, the activity of BSP-1 expressed by the promoter of P43, Psrf, Pitu, and Pfen reached 115.87, 106.71, 107.25, and 107.52 U/mL respectively, improving by 4.3-fold, 4.0-fold, 4.0-fold and 4.0-fold compared to the Ppqq promoter (26.71 U/mL). The data indicated promoter screening efficiently enhanced the activity outcome of BSP-1. In addition, the biomass of Ppqq promoter was significantly higher than that of P43, Psrf, Pitu and Pfen promoter, indicating that the enzyme activity and the biomass are not necessarily positively correlated.

3.5 Verification of the transcription of *bsp-1* driven by different promoters

To verify the effect of promoter on gene transcription level, we established a microbial fermentation model. The total RNA of different recombinant strains was extracted and analyzed. As shown in Figure 7, the transcription levels of *bsp-1* in BAX-9/pHY-P43/BSP-1, BAX-9/pHY-Pscp/BSP-1, BAX-9/pHY-Pcsp/BSP-1, BAX-9/pHY-Psrf/BSP-1, BAX-9/pHY-Pitu/BSP-1, BAX-9/pHY-Pfen/BSP-1 significantly increased compared to that in BAX-9/pHY-Ppqq/BSP-1. Among them, BAX-9/pHY-P43/BSP-1 showed the highest transcription level, 4 folds than that in BAX-9/pHY-Ppqq/BSP-1. The results of RT-PCR were consistent with the results of SDS-PAGE and enzyme activity, revealing that the efficient transcription by P43 generated high protein level and

enzyme activity. The above results provide a reference to select the optimal promoter for protein expression.

3.6 The optimization of fermentation for BSP-1 production in BAX-9/pHY-P43/BSP-1

To further improve the protease yield of the recombinant strain BAX-9/pHY-P43/BSP-1, an optimized medium (40 g/L tryptone, 20 g/L yeast extract, and 10 g/L NaCl) was selected for fermentation (Supplementary Figure S1). During the fermentation process, the activity of BSP-1 protease and the biomass of strains were determined. As shown in Figure 8, in the initial 36 h, the enzyme activity increased as the culture was growing. With the continuation of fermentation, the biomass began to decrease, and the enzyme activity continued to increase until 54 h. The enzyme activity reached a maximum of 524.12 U/mL. Finally, with the continuous decrease of biomass, the enzyme activity declined and tended to be stable. The results indicate that the accumulation of the enzyme was delayed compared to culture growth.

4 Conclusion

In conclusion, the BSP-1 protease gene from *B. subtilis* was identified in this study, and explored possibility of high-efficiency

expression system via *B. amyloliquefaciens*. The enzyme activity and transcription level under the expression of different promoters Ppqq, Pscp, Pcsp, Psrf, Pitu, Pfen and P43 were analyzed, and we found P43 was the optimal promoter for heterologous expression of BSP-1 protease. Nevertheless, Psrf and Pfen show comparable expression strength to P43 and thus can be used as high-strength promoters in future. After fermentation optimization, the highest enzyme activity of the engineering strain BAX-9/pHY-P43/BSP-1 reached 524.12 U/mL. Moreover, monitoring the fermentation process also confirmed no direct correlation between enzyme activity and biomass. This study enriched the originals and hosts for protein expression, and it identified a new resource for the industrialized production of proteases.

Data availability statement

The original contributions presented in the study are included in the article/Supplementary Material, further inquiries can be directed to the corresponding author.

Author contributions

Conceptualization, CJ and WH; Methodology, CJ; Software, CJ and CY; Validation, CJ, CY, and YL; Formal analysis, KH and XJ; Investigation, XW; Resources, XW and WH; Data curation, CJ and YL; Writing—original draft preparation, CJ; Writing—review and editing, CJ, XW, WH, DZ, and LL; Visualization, CY; Supervision, XW; Project administration, XW; Funding acquisition, XW and WH.

References

- Agrebi, R., Haddar, A., Hmidet, N., Jellouli, K., Manni, L., and Nasri, M. (2009). BSF1 fibrinolytic enzyme from a marine bacterium *Bacillus subtilis* A26: Purification, biochemical and molecular characterization. *Process Biochem.* 44 (11), 1252–1259. doi:10.1016/j.procbio.2009.06.024
- Barzkar, N. (2020). Marine microbial alkaline protease: An efficient and essential tool for various industrial applications. *Int. J. Biol. Macromol.* 161, 1216–1229. doi:10.1016/j.ijbiomac.2020.06.072
- Benabdelkamel, H., Masood, A., Alanazi, I. O., and Alfadda, A. A. (2018). Comparison of protein precipitation methods from adipose tissue using difference gel electrophoresis. *Electrophoresis* 39 (14), 1745–1753. doi:10.1002/elps.201800124
- Brázda, V., Bartas, M., and Bowater, R. P. (2021). Evolution of diverse strategies for promoter regulation. *Trends Genet.* 37 (8), 730–744. doi:10.1016/j.tig.2021.04.003
- Burchacka, E., Pięta, P., and Łupicka-Słowik, A. (2022). Recent advances in fungal serine protease inhibitors. *Biomed. Pharmacother.* 146, 112523. doi:10.1016/j.biopha.2021.112523
- Cai, D., Rao, Y., Zhan, Y., Wang, Q., and Chen, S. (2019). Engineering *Bacillus* for efficient production of heterologous protein: Current progress, challenge and prospect. *J. Appl. Microbiol.* 126 (6), 1632–1642. doi:10.1111/jam.14192
- Cazier, A. P., and Blazek, J. (2021). Advances in promoter engineering: Novel applications and predefined transcriptional control. *Biotechnol. J.* 16 (10), 2100239. doi:10.1002/biot.202100239
- Chen, W., Li, L., Ye, C., Zhao, Z., Huang, K., Zou, D., et al. (2022). Efficient production of extracellular alkaline protease in *Bacillus amyloliquefaciens* by host strain construction. *Lwt. Food Sci. Technol.* 163, 113620. doi:10.1016/j.lwt.2022.113620
- Choi, N.-S., Chang, K.-T., Jae Maeng, P., and Kim, S.-H. (2004). Cloning, expression, and fibrin (ogen)olytic properties of a subtilisin DJ-4 gene from *Bacillus* sp. DJ-4. *FEMS Microbiol. Lett.* 236 (2), 325–331. doi:10.1111/j.1574-6968.2004.tb09665.x
- Contesini, F. J., Melo, R. R. d., and Sato, H. H. (2018). An overview of *Bacillus* proteases: From production to application. *Crit. Rev. Biotechnol.* 38 (3), 321–334. doi:10.1080/07388551.2017.1354354
- Cui, W., Han, L., Suo, F., Liu, Z., Zhou, L., and Zhou, Z. (2018). Exploitation of *Bacillus subtilis* as a robust workhorse for production of heterologous proteins and beyond. *World J. Microbiol. Biotechnol.* 34 (10), 145. doi:10.1007/s11274-018-2531-7
- Espou, A. H., Larimi, S. G., and Darzi, G. N. (2022). Optimization of protease production process using bran waste using *Bacillus licheniformis*. *Korean J. Chem. Eng.* 39 (3), 674–683. doi:10.1007/s11814-021-0965-3
- Fu, G., Liu, J., Li, J., Zhu, B., and Zhang, D. (2018). Systematic screening of optimal signal peptides for secretory production of heterologous proteins in *Bacillus subtilis*. *J. Agric. Food Chem.* 66 (50), 13141–13151. doi:10.1021/acs.jafc.8b04183
- Gong, J.-S., Ye, J.-P., Tao, L.-Y., Su, C., Qin, J., Zhang, Y.-Y., et al. (2020). Efficient keratinase expression via promoter engineering strategies for degradation of feather wastes. *Enzyme Microb. Technol.* 137, 109550. doi:10.1016/j.enzmictec.2020.109550

Funding

This study was funded by the National Natural Science Foundation of China (No. 32171423), Key Research and Development Projects of China National Tobacco Corporation (No. 110202102019), and the National Key Research and Development Program of China (No. 2019YFA0906400).

Conflict of interest

YL was employed by GeneMind Biosciences Company Limited. CY and KH were employed by China National Tobacco Corporation.

The remaining authors declare that the research was conducted in the absence of any commercial or financial relationships that could be construed as a potential conflict of interest.

Publisher's note

All claims expressed in this article are solely those of the authors and do not necessarily represent those of their affiliated organizations, or those of the publisher, the editors and the reviewers. Any product that may be evaluated in this article, or claim that may be made by its manufacturer, is not guaranteed or endorsed by the publisher.

Supplementary material

The Supplementary Material for this article can be found online at: <https://www.frontiersin.org/articles/10.3389/fbioe.2022.977215/full#supplementary-material>

- Gu, Y., Xu, X., Wu, Y., Niu, T., Liu, Y., Li, J., et al. (2018). Advances and prospects of *Bacillus subtilis* cellular factories: From rational design to industrial applications. *Metab. Eng.* 50, 109–121. doi:10.1016/j.ymben.2018.05.006
- Gupta, R., Beg, Q., and Lorenz, P. (2002). Bacterial alkaline proteases: Molecular approaches and industrial applications. *Appl. Microbiol. Biotechnol.* 59 (1), 15–32. doi:10.1007/s00253-002-0975-y
- Harish, B., and Uppuluri, K. B. (2018). Microbial serine protease inhibitors and their therapeutic applications. *Int. J. Biol. Macromol.* 107, 1373–1387. doi:10.1016/j.ijbiomac.2017.09.115
- Jahangirian, H., Azizi, S., Rafiee-Moghaddam, R., Baratvand, B., and Webster, T. J. (2019). Status of plant protein-based green scaffolds for regenerative medicine applications. *Biomolecules* 9 (10), 619. doi:10.3390/biom9100619
- Jensen, D., and Galburt, E. A. (2021). The context-dependent influence of promoter sequence motifs on transcription initiation kinetics and regulation. *J. Bacteriol.* 203 (8), e00512–00520. doi:10.1128/JB.00512-20
- Ku, T. W., Tsai, R. L., and Pan, T. M. (2009). A simple and cost-saving approach to optimize the production of subtilisin NAT by submerged cultivation of *Bacillus subtilis* natto. *J. Agric. Food Chem.* 57 (1), 292–296. doi:10.1021/jf8024198
- Kumar, A., Bansal, M., Ghosh, P. K., and Yadav, K. L. (2018). MWCNT/TiO₂ hybrid nano filler toward high-performance epoxy composite. *Ultrason. Sonochem.* 76051, 37–46. doi:10.1016/j.ultrsonch.2017.09.005
- Liao, Y., Wang, B., Ye, Y., and Pan, L. (2018). Determination and optimization of a strong promoter element from *Bacillus amyloliquefaciens* by using a promoter probe vector. *Biotechnol. Lett.* 40 (1), 119–126. doi:10.1007/s10529-017-2449-4
- Liu, Y., Shi, C., Li, D., Chen, X., Li, J., Zhang, Y., et al. (2019). Engineering a highly efficient expression system to produce BcaPRO protease in *Bacillus subtilis* by an optimized promoter and signal peptide. *Int. J. Biol. Macromol.* 138, 903–911. doi:10.1016/j.ijbiomac.2019.07.175
- Matkawala, F., Nighojkar, S., Kumar, A., and Nighojkar, A. (2021). Microbial alkaline serine proteases: Production, properties and applications. *World J. Microbiol. Biotechnol.* 37 (4), 63. doi:10.1007/s11274-021-03036-z
- Meng, Y., Yao, Z., Le, H. G., Lee, S. J., Jeon, H. S., Yoo, J. Y., et al. (2021). Characterization of a salt-resistant fibrinolytic protease of *Bacillus licheniformis* HJ4 isolated from Hwangseokae jeotgal, a traditional Korean fermented seafood. *Folia Microbiol. (Praha)*. 66 (5), 787–795. doi:10.1007/s12223-021-00878-w
- Neef, J., van Dijk, J. M., and Buist, G. (2021). Recombinant protein secretion by *Bacillus subtilis* and *Lactococcus lactis*: Pathways, applications, and innovation potential. *Essays Biochem.* 65 (2), 187–195. doi:10.1042/EBC20200171
- Ouyang, X., Liu, Y., Qu, R., Tian, M., Yang, T., Zhu, R., et al. (2021). Optimizing protein-glutaminase expression in *Bacillus subtilis*. *Curr. Microbiol.* 78 (5), 1752–1762. doi:10.1007/s00284-021-02404-0
- Pathak, A. P., and Rathod, M. G. (2018). A review on alkaline protease producers and their biotechnological perspectives. *Ind. J. Geo-Mar. Sci.* 47 (6), 1113–1119.
- Sharma, M., Gat, Y., Arya, S., Kumar, V., and Kumar, A. (2019). A review on microbial alkaline protease: An essential tool for various industrial approaches. *Ind. Biotechnol. New. Rochelle. N. Y.* 15 (2), 69–78. doi:10.1089/ind.2018.0032
- Song, Y., Nikoloff, J. M., Fu, G., Chen, J., Li, Q., Xie, N., et al. (2016). Promoter screening from *Bacillus subtilis* in various conditions hunting for synthetic biology and industrial applications. *Plos One* 11 (7), e0158447. doi:10.1371/journal.pone.0158447
- Su, L., Li, Y., and Wu, J. (2021). Efficient secretory expression of *Bacillus stearotheophilus* α/β -cyclodextrin glycosyltransferase in *Bacillus subtilis*. *J. Biotechnol.* 331, 74–82. doi:10.1016/j.jbiotec.2021.03.011
- Suberu, Y., Akande, I., Samuel, T., Lawal, A., and Olaniran, A. (2019). Cloning, expression, purification and characterisation of serine alkaline protease from *Bacillus subtilis* RD7. *Biocatal. Agric. Biotechnol.* 20, 101264. doi:10.1016/j.bcab.2019.101264
- Tavano, O. L., Berenguer-urcia, A., Secundo, F., and Fernandez-afuente, R. (2018). Biotechnological applications of proteases in food technology. *Compr. Rev. Food Sci. Food Saf.* 17 (2), 412–436. doi:10.1111/1541-4337.12326
- Uyar, F., and Baysal, Z. (2008). Production and characterization of neutral and alkaline protease from different *Bacillus subtilis* strains. *Chem. Asian. J.* 20 (6), 4523–4530.
- Wang, P.-Z., and Doi, R. H. (1984). Overlapping promoters transcribed by *Bacillus subtilis* sigma 55 and sigma 37 RNA polymerase holoenzymes during growth and stationary phases. *J. Biol. Chem.* 259 (13), 8619–8625. doi:10.1016/S0021-9258(17)39775-2
- Wei, X., Luo, M., Xu, L., Zhang, Y., Lin, X., Kong, P., et al. (2011). Production of fibrinolytic enzyme from *Bacillus amyloliquefaciens* by fermentation of chickpeas, with the evaluation of the anticoagulant and antioxidant properties of chickpeas. *J. Agric. Food Chem.* 59 (8), 3957–3963. doi:10.1021/jf1049535
- Westers, L., Westers, H., and Quax, W. J. (2004). *Bacillus subtilis* as cell factory for pharmaceutical proteins: A biotechnological approach to optimize the host organism. *Biochimica Biophysica Acta - Mol. Cell Res.* 1694 (1-3), 299–310. doi:10.1016/j.bbamcr.2004.02.011
- Wu, S.-M., Feng, C., Zhong, J., and Huan, L.-D. (2011). Enhanced production of recombinant nattokinase in *Bacillus subtilis* by promoter optimization. *World J. Microbiol. Biotechnol.* 27 (1), 99–106. doi:10.1007/s11274-010-0432-5
- Yong, P., Yang, X. J., Lu, X., and Zhang, Y. Z. (2004). Cloning and expression of a fibrinolytic enzyme (subtilisin DFE) gene from *Bacillus amyloliquefaciens* DC-4 in *Bacillus subtilis*. *Res. Microbiol.* 155 (3), 167–173. doi:10.1016/j.resmic.2003.10.004
- Zhang, K., Su, L., and Wu, J. (2020). Recent advances in recombinant protein production by *Bacillus subtilis*. *Annu. Rev. Food Sci. Technol.* 11, 295–318. doi:10.1146/annurev-food-032519-051750
- Zhang, Q., Wu, Y., Gong, M., Zhang, H., Liu, Y., Lv, X., et al. (2021). Production of proteins and commodity chemicals using engineered *Bacillus subtilis* platform strain. *Essays Biochem.* 65 (2), 173–185. doi:10.1042/ebc20210011
- Zhou, C., Zhou, H., Fang, H., Ji, Y., Wang, H., Liu, F., et al. (2020). Spo0A can efficiently enhance the expression of the alkaline protease gene *aprE* in *Bacillus licheniformis* by specifically binding to its regulatory region. *Int. J. Biol. Macromol.* 159, 444–454. doi:10.1016/j.ijbiomac.2020.05.035
- Zou, D., Min, Y., Liu, Y., Wei, X., and Wang, J. (2020). Identification of a spermidine synthase gene from soybean by recombinant expression, transcriptional verification, and sequence analysis. *J. Agric. Food Chem.* 68 (8), 2366–2372. doi:10.1021/acs.jafc.9b07443



OPEN ACCESS

EDITED BY

Qi Xianghui,
Jiangsu University, China

REVIEWED BY

Xuetuan Wei,
Huazhong Agricultural University, China
Pei Xu,
Sun Yat-sen University, China

*CORRESPONDENCE

Xiangjie Zhao,
zhaoxiangjie@hyit.edu.cn

SPECIALTY SECTION

This article was submitted to Industrial Biotechnology, a section of the journal Frontiers in Bioengineering and Biotechnology

RECEIVED 22 September 2022

ACCEPTED 07 November 2022

PUBLISHED 24 November 2022

CITATION

Yang R, Wang Y, Zhao X, Tong Z, Zhu Q, He X, Wang Z, Luo H and Fang F (2022), A facile and efficient synthesis approach of salidroside esters by whole-cell biocatalysts in organic solvents. *Front. Bioeng. Biotechnol.* 10:1051117. doi: 10.3389/fbioe.2022.1051117

COPYRIGHT

© 2022 Yang, Wang, Zhao, Tong, Zhu, He, Wang, Luo and Fang. This is an open-access article distributed under the terms of the [Creative Commons Attribution License \(CC BY\)](#). The use, distribution or reproduction in other forums is permitted, provided the original author(s) and the copyright owner(s) are credited and that the original publication in this journal is cited, in accordance with accepted academic practice. No use, distribution or reproduction is permitted which does not comply with these terms.

A facile and efficient synthesis approach of salidroside esters by whole-cell biocatalysts in organic solvents

Rongling Yang, Yu Wang, Xiangjie Zhao*, Zheng Tong, Qianlin Zhu, Xiaoxi He, Zhaoyu Wang, Hongzhen Luo and Fang Fang

School of Life Science and Food Engineering, Huaiyin Institute of Technology, Huaian, China

Salidroside, the main bioactive compound isolated from the plant source of *Rhodiola rosea* L, possesses broad-spectrum pharmacological activities, but suffers from the low cell membranes permeability and alimentary absorption due to its high polarity. Therefore, a whole-cell catalytic strategy for the synthesis of salidroside esters was explored to improve its lipophilicity. The results showed that *Aspergillus oryzae* demonstrated the highest biocatalytic activity among the microbial strains tested. For the synthesis of salidroside caprylate, the optimum conditions of reaction medium, *Aspergillus oryzae* amount, molar ratio of vinyl caprylate to salidroside and reaction temperature were acetone, 30 mg/ml, 10°C and 40°C, respectively. Under these conditions, the initial reaction rate was 15.36 mM/h, and substrate conversion and regioselectivity all reached 99%. Moreover, the results indicated that although various 6'-monoesters derivatives of salidroside were exclusively obtained with excellent conversions (96%–99%), the reaction rate varied greatly with different chain-length acyl donors. This study details an efficient and cost-effective biocatalytic approach for the synthesis of salidroside esters by using *Aspergillus oryzae* as a catalyst for the first time. Considering the whole cell catalytic efficiency and operational stability, this strategy may provide a new opportunity to develop green industrial processes production for ester derivatives of salidroside and its analogues.

KEYWORDS

salidroside esters, whole-cells, biocatalysis, acyl donor specificity, organic solvents

1 Introduction

Salidroside (4-hydroxyphenethyl- β -D-glucopyranoside) is the main bioactive ingredient isolated from *Rhodiola rosea* L that has been used as a traditional Chinese medicine for a long time (Zhang et al., 2018). Recent studies confirmed that salidroside possesses broad-spectrum pharmacological activities including anti-hypoxic, anti-fatigue, anti-inflammation, anti-cancer, anti-convulsion, as well as protecting the cardiovascular system, exerting neuroprotective effects, improving glucose and lipid metabolism (Hu

et al., 2010; Xing et al., 2018; Wu et al., 2020; Yang L. M. et al., 2020; Qi et al., 2021; Qian et al., 2021; Song et al., 2021; Wu et al., 2021). However, the multiple hydroxyl groups of salidroside make it highly polar, which results in the low cell membranes permeability and alimentary absorption (Liang et al., 2021). Various attempts have been made to improve the bioavailability of phenolic glycosides by modifying their structure to balance their lipophilicity and hydrophilicity. Many studies have found that acylation modification of natural glycosides not only improve their bioavailability but also could increase their pharmacological properties, making them suitable candidates for prodrug development (Chyba et al., 2016; Chen et al., 2019; Yang R. L. et al., 2019; Liu et al., 2020; Hao et al., 2021; Yang et al., 2021; Zhang P. L. et al., 2021). For example, tri-acetylated phloridzin displayed significantly higher anti-proliferative activity against human HepG2 cancer cells than phloridzin, while exhibited moderate to minimal adverse-effects on LO-2 normal hepatic cells (Chen et al., 2019). The intracellular antioxidant activities of acylated cyanidin-3-glucoside were significantly enhanced relative to cyanidin-3-glucoside due to their increased lipophilicity (Zhang X. M. et al., 2021).

Salidroside is a kind of polyhydroxy natural glycosides carrying several hydroxyl groups with similar chemical activity. The biocatalytic acylation of polyhydroxy compounds based on the whole cells and isolated enzymes has become a promising approach due to the mild reaction conditions, high regioselectivity and environmental friendliness (Yu et al., 2008; Chen et al., 2013; Li G. Y. et al., 2018; Sugai et al., 2018; Jeandet et al., 2020; Hao et al., 2021). Salidroside was successfully acylated with aliphatic acids by Novozyme 435, an expensive commercial immobilized lipase (Yu et al., 2008). Compared to purified or immobilized enzymes, employing whole cells biocatalysts can significantly reduce costs by circumventing cell lysis and enzyme purification (Wachtmeister and Rother, 2016). In addition, residual cell wall compounds also have a protective effect on stationary or dead cells, thus enabling them to catalyze reactions in unconventional (non-aqueous) reaction media (Xu et al., 2016; Xin et al., 2017). Hence, the whole cell biocatalysts offered a huge potential in the field of non-aqueous reaction media. Recently, the whole cell biocatalysts displayed similar or better catalytic activity than commercial lipases in the synthesis of glycoside ester derivatives (Yang R. L. et al., 2020; Hao et al., 2021). It is especially critical to identify suitable microbial strains as whole-cell catalysts to catalyze specific natural products, because different microbial cells have different substrate specificities. According to our knowledge, there is no report on the synthesis of salidroside fatty acid ester derivatives catalyzed by the whole cell biocatalysts. Considering the application potential of salidroside esters in pharmaceuticals, the efficient synthesis catalyzed by microbial whole-cells in non-aqueous solvents was firstly investigated. And eight salidroside ester derivatives with different lengths of aliphatic chains were synthesized and structurally identified.

2 Materials and methods

2.1 Materials

Salidroside was obtained from Aladdin (Shanghai, China). The fatty acid vinyl esters as acyl donors were provided by Tokyo Chemical Industry, TCI (Shanghai) Development Co., Ltd. All microbial strains (*Pseudomonas fluorescens*, *Pseudomonas stutzeri*, *Pseudomonas aeruginosa*, *Aspergillus niger*, *Aspergillus oryzae* and *Rhizopus oryzae*) were obtained from Guangdong Institute of Microbiology (Guangzhou, China). Other chemicals were of analytical grade.

2.2 Preparation of whole-cell biocatalysts

Bacterial and fungal strains were cultivated as described previously (Yang L. M. et al., 2020). The bacterial strains were activated in the medium contained 1% sucrose, 1% beef extract, 1% peptone, 0.5% NaCl, 0.5% K_2HPO_4 and 0.02% $MgSO_4 \cdot 7H_2O$. The fungal strains were activated on potato dextrose agar (PDA) medium. Then, the activated bacterial suspension and fungal spore suspension were inoculated into the same fermentation broth respectively, which contained 0.1% soybean oil, 0.2% tryptone, 0.5% $(NH_4)_2SO_4$ and 0.02% $MgSO_4 \cdot 7H_2O$. After cultivation, the cells were collected by filtration or freeze-centrifugation and freeze-dried for 24 h.

2.3 Synthesis of salidroside esters

In a typical experiment, salidroside (20 mM), vinyl caprylate and whole-cell catalyst preparation were added in organic solvents and incubated at 200 rpm. The samples were collected at predetermined time intervals and detected by high-performance liquid chromatography (HPLC). The control experiments without whole-cell catalysts displayed no acylation action. The conversion (C) was measured as the ratio of transformed to initial salidroside. The initial reaction rate (V_0) refers to the substrate consumption per unit time in the initial stage, in which the substrate concentration decreased linearly with the reaction time. The experiments were carried out in triplicates.

2.4 Operational stability of whole-cell biocatalysts

The operational stability of *Aspergillus oryzae* cells during the batch reaction was investigated. The reaction was carried out in anhydrous acetone containing 20 mM salidroside, 200 mM vinyl caprylate, 20 mg/ml whole-cell biocatalysts for 12 h at 40°C and 200 rpm. After each batch synthetic reaction, whole-cell

TABLE 1 Regioselective caproylation of salidroside catalyzed by the whole cells.

Strains	V ₀ (mM/h)	C (%)	Regioselectivity (%)
<i>Rhizopus oryzae</i>	1.86 ± 0.09	20.83 ± 0.17	>99
<i>Aspergillus oryzae</i>	9.30 ± 0.36	95.72 ± 0.51	>99
<i>Pseudomonas aeruginosa</i>	8.92 ± 0.18	93.64 ± 0.35	>99
<i>Pseudomonas fluorescens</i>	1.21 ± 0.10	11.53 ± 0.13	>99
<i>Pseudomonas stutzeri</i>	0.82 ± 0.05	9.47 ± 0.06	>99

Reaction conditions: 0.04 mmol salidroside, 0.4 mmol vinyl caprylate, 0.02 g catalyst preparation, 2 ml anhydrous acetone, 40°C, 200 rpm.

TABLE 2 Effect of organic solvents on caproylation of salidroside catalyzed by *Aspergillus oryzae* cells.

Solvents	Lop	Solubility (mM)	V ₀ (mM/h)	C (%)	Regioselectivity (%)
Acetone	−0.23	164.3 ± 0.70	9.30 ± 0.22	95.72 ± 0.48	>99
Tetrahydrofuran	0.49	110.2 ± 0.61	2.05 ± 0.11	72.35 ± 0.29	>99
2-Methyltetrahydrofuran	1.85	20.6 ± 0.66	8.96 ± 0.15	86.97 ± 0.31	>99
<i>tert</i> -Butanol	0.60	31.5 ± 1.06	1.60 ± 0.08	78.92 ± 0.23	>99
DMSO	−1.3	632.6 ± 2.01	n.d.	n.d.	n.d.
DMF	−1.0	262.9 ± 1.15	n.d.	n.d.	n.d.

Reaction conditions: 0.04 mmol salidroside, 0.4 mmol vinyl caprylate, 0.02 g. *Aspergillus oryzae* cells, 2 ml anhydrous solvent, 40°C, 200 rpm. n.d., not detected.

biocatalysts were separated by filtration, washed with reaction medium and utilized in the next fresh reaction.

2.5 HPLC analysis

All samples were analyzed by RP-HPLC on an Agilent Zorbax Eclipse Plus C18 column (4.6 mm × 250 mm, 5 μm) using Shimadzu LC-200C pump with the DAD detector at 275 nm. The flow rate was 1.0 ml/min. The mobile phase contained a mixture of methanol and water at a 1.0 ml/min flow rate. The volumetric ratio of methanol to water and the retention times for its ester derivatives were 60/40 and 3.018 min (salidroside-6'-acetate), 60/40 and 4.278 min (salidroside-6'-butyrate), 80/20 and 3.265 min (salidroside-6'-hexanoate), 80/20 and 4.355 min (salidroside-6'-caprylate), 80/20 and 6.782 min (salidroside-6'-decanoate), 80/20 and 6.621 min (salidroside-6'-undecenoate), 90/10 and 4.760 min (salidroside-6'-laurate), 90/10 and 6.623 min (salidroside-6'-myristate), 90/10 and 9.981 min (salidroside-6'-palmitate), respectively.

2.6 Structure characterization of the products

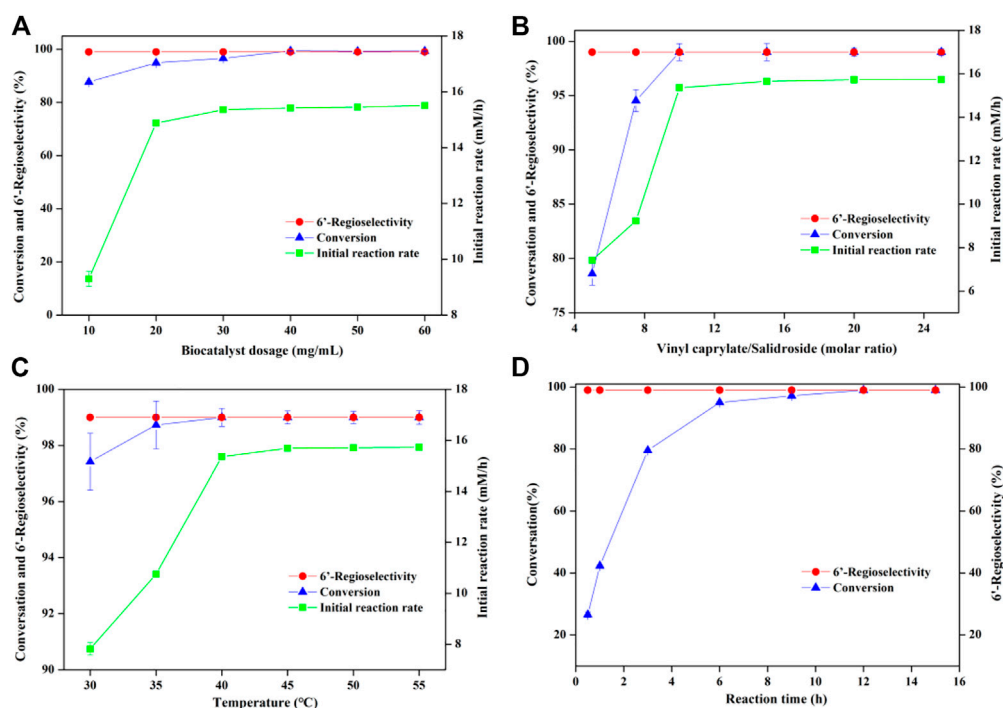
All the synthetic products were purified through flash column chromatography using a mixture of ethyl acetate and

petroleum ether as the mobile phase. The structural identification of the ester derivatives was determined by ¹³C NMR and ¹H NMR (Bruker DRX-400 NMR Spectrometer) at 100 MHz and 400 MHz, respectively, with DMSO-d₆ being the solvent. All the NMR spectroscopic results are shown in the supplementary information.

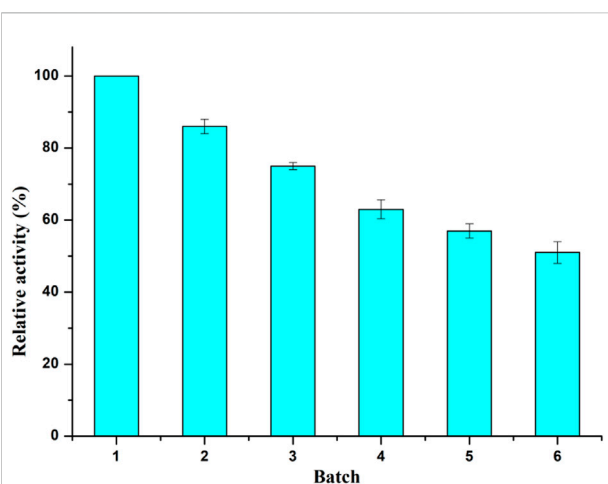
3 Results and discussion

3.1 Strains screening for salidroside ester synthesis

Several lipase-producing strains including bacteria and fungi were screened as the biocatalysts for the synthesis of salidroside caprylate (Table 1). Results revealed that all the tested strains showed different catalytic activities. *Aspergillus oryzae* and *Pseudomonas aeruginosa* demonstrate significant outstanding catalytic activity, affording 95.72% and 93.64% conversion after 24 h, respectively, and both gave substantially superior result to those obtained with the other strains that were tested. The reaction catalyzed by *Rhizopus oryzae*, *Pseudomonas fluorescens* and *Pseudomonas stutzeri* proceeded with 20.83%, 11.53% and 9.47 conversion rate after 24 h, respectively. These results indicated that catalytic properties of different microorganisms in the same induction medium were different, which was consistent with previous studies (Xin et al.,

**FIGURE 1**

Regioselective caproylation of salidoside catalyzed by *Aspergillus oryzae* cells. (A) Effect of biocatalyst dosage [0.04 mmol salidoside, 0.4 mmol vinyl caprylate, 2 ml anhydrous acetone, 40°C, 200 rpm]. (B) Effect of molar ratio [0.04 mmol salidoside, 0.06 g. *Aspergillus oryzae* cells, 2 ml anhydrous acetone, 40°C, 200 rpm]. (C) Effect of temperature [0.04 mmol salidoside, 0.4 mmol vinyl caprylate, 0.06 g. *Aspergillus oryzae* cells, 2 ml anhydrous acetone, 200 rpm]. (D) Effect of reaction time [0.04 mmol salidoside, 0.4 mmol vinyl caprylate, 0.06 g. *Aspergillus oryzae* cells, 2 ml anhydrous acetone, 40°C, 200 rpm].

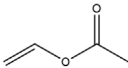
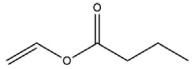
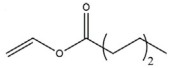
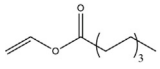
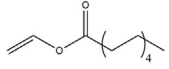
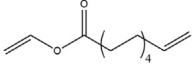
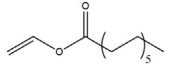
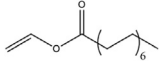
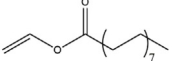
**FIGURE 2**

Operational stability of *Aspergillus oryzae* whole-cell catalyst. Reaction conditions: 0.04 mmol salidoside, 0.4 mmol vinyl caprylate, 0.06 g. *Aspergillus oryzae* cells, 2 ml anhydrous acetone, 40°C, 200 rpm.

2017; Hao et al., 2021). Interestingly, in the regioselective synthesis of helcid aliphatic esters, *Pseudomonas aeruginosa* exhibited excellent catalytic performance, while *Aspergillus oryzae* displayed no catalytic activity (Yang W. et al., 2019). In the synthesis of esculin esters, *Pseudomonas stutzeri* demonstrated the highest catalytic activity (Hao et al., 2021). These results indicated that the whole cell catalysts from different sources have certain substrate specificity. In addition, whole cell catalysts from *Pseudomonas aeruginosa* displayed comparable catalytic activity to an immobilized lipase Novozyme 435 in synthesis of salidoside esters (Yang et al., 2021). From the results in Table 1, it was clear that salidoside was the appropriate substrate for the whole cell catalysts from *Aspergillus oryzae* and *Pseudomonas aeruginosa*.

High regioselectivity is one of the remarkable characteristics of biocatalysts. It is worth mentioning that all microbial whole-cell catalysts tested displayed absolute regioselectivities toward the 6'-hydroxyl of glucose in salidoside, which was comparable to the excellent selectivity of an immobilized lipase Novozyme 435 with salidoside 6'-caprylate being the sole ester product

TABLE 3 Effect of various acyl donors on regioselective acylation of salidroside catalyzed by *Aspergillus oryzae* cells.

Acyl donor	Structural formula of acyl donors	V_0 (mM/h)	Time (h)	C (%)	Regioselectivity (%)
Vinyl acetate		3.37 ± 0.09	24	96.1 ± 0.34	>99
Vinyl butyrate		12.75 ± 0.11	12	97.4 ± 0.36	>99
Vinyl hexanoate		14.76 ± 0.25	12	99.0 ± 0.04	>99
Vinyl caprylate		14.88 ± 0.17	12	99.0 ± 0.04	>99
Vinyl decanoate		15.31 ± 0.20	12	99.0 ± 0.05	>99
Vinyl 10-undecenoate		17.31 ± 0.19	12	99.0 ± 0.03	>99
Vinyl laurate		14.57 ± 0.21	12	98.5 ± 0.33	>99
Vinyl myristate		9.25 ± 0.13	12	97.3 ± 0.26	>99
Vinyl palmitate		8.34 ± 0.12	12	96.5 ± 0.23	>99

Reaction conditions: 0.04 mmol salidroside, 0.4 mmol acyl donor, 0.06 g. *Aspergillus oryzae* cells, 2 ml anhydrous acetone, 40°C, 200 rpm.

(Yang et al., 2021). Similarly, we recently found that *Aspergillus oryzae* whole cells exhibited excellent regioselectivities toward the primary hydroxyl group at allose moiety of helicid, a structural analogue of salidroside (Yang R. L. et al., 2020). The reason may be that the primary hydroxyl group has the less steric hindrance effect than the other hydroxyls. Based on the greater reaction efficiency and regioselectivity, *Aspergillus oryzae* strain was shortlisted for the subsequent investigation.

3.2 Optimization of salidroside ester synthesis

In order to further improve the reaction efficiency, the synthesis of salidroside caprylate was used as a model reaction to investigate the influence of several key variables (reaction medium, molar ratio of substrate, whole-cell dosage) on the reaction. Like enzyme-mediated biotransformation, the nature of reaction medium has a significant effect on the whole-cell biocatalysis, which can impact the biocatalyst

activity and stability. The presence of water may cause the hydrolysis of both the ester products and the acyl donors (vinyl esters), so several traditional organic solvents with different polarities from -0.23 to 1.85 were selected as reaction media (Table 2). Salidroside as a phenolic glycoside has high solubility in strongly polar solvents such as dimethyl sulfoxide (DMSO) and dimethylformamide (DMF) with 77.0 mM and 101.2 mM, respectively, while relatively low solubility in less polar organic solvents (25.3–42.1 mM). As speculated, *Aspergillus oryzae* has no catalytic activity in DMSO and DMF with strong polarity, which may inactivate lipases by destroying the membrane of whole-cell catalysts (Yang R. L. et al., 2019; Yang L. M. et al., 2020; Hao et al., 2021). Among the solvents tested (Figure 2), good conversions were obtained in 2-methyltetrahydrofuran (86.97%), tert-butanol (78.92%) and tetrahydrofuran (72.35%). And the highest conversion efficiency (95.72%) and initial reaction rate (9.30 mM/h) were obtained in acetone. Moreover, there was no significant correlation between the catalytic activity of the cells and the log P of the tested solvents, the commonly used solvent parameter in non-aqueous enzymology. As shown in

Figure 1A, the reaction rate accelerated obviously (9.3 mM/h to 15.36 mM/h) with increasing the whole-cell dosage from 10 to 30 mg/ml, and then no obvious improvements occurred with further increasement of catalyst amount. The molar ratio of vinyl caprylate to salidroside had a great influence on the initial reaction rate and the maximal conversion (Figure 1B), which improved significantly with the increase of vinyl caprylate concentration up to 10 equivalents of salidroside concentration. A high conversion (>99%) and good initial reaction rate (15.36 mM/h) could be acquired with the molar ratio of vinyl caprylate to salidroside as 10. Figure 1C depicted that *Aspergillus oryzae* whole-cells had good biocatalysis performance in the temperature range of 30°C–55°C. Figure 1D showed the reaction process of salidroside acylation with vinyl caprylate under the above-obtained conditions. Salidroside conversion increased sharply at the initial stage of the reaction with 95% at 6 h, and then a slower rise, reaching 99% at 12 h.

Consider the above data comprehensively, the optimum conditions of reaction medium, *Aspergillus oryzae* amount, molar ratio of vinyl caprylate to salidroside and reaction temperature were acetone, 30 mg/ml, 10°C and 40°C, respectively, with initial rate of 15.36 mM/h and the highest substrate conversion of 99%. Additionally, the regioselectivity of the reaction maintained 99% under the above conditions.

3.3 Operational stability of the whole-cell biocatalyst

The reusability of biocatalyst is of great importance to the cost efficiency in industrial production. As shown in Figure 2, the *Aspergillus oryzae* whole cells remained 51% of its original activity after six consecutive batches. And the *Aspergillus oryzae* lost only 25% of its activity after three reaction cycles, which might be that the whole-cell provided a natural protective environment for intracellular enzyme with acylation activity.

3.4 Whole cell-mediated synthesis for aliphatic ester of salidroside

The synthesis of various salidroside aliphatic esters mediated by *Aspergillus oryzae* cells was explored in the above-mentioned optimal reaction conditions, with fatty acid vinyl esters of different chain lengths as acyl donors (Table 3). It is worth mentioning that 6'-monoesters of salidroside were exclusively achieved in all cases by NMR and HPLC analysis, which was similar to that in helicid esters synthesis catalyzed by *Aspergillus oryzae* cells, also affording an excellent selectivity for 6'-OH at allose moiety (Yang R. L. et al., 2020). However, in the synthesis of acetyl ester (a short alkyl acyl group) of salidroside by the commercial lipase Novozyme 435, 6'-O-acetyl salidroside and 3',6'-O-diacetyl salidroside were the main two products, also with a small amount (<5%) of 2',6'-O-

diacryloyl salidroside (Yu et al., 2008). Thus *Aspergillus oryzae* cells exhibited superior regioselectivity to Novozyme 435 in the synthesis for short-chain aliphatic ester of salidroside, which highlighted the excellent regioselectivity of *Aspergillus oryzae* cells.

As shown in Table 3, *Aspergillus oryzae* cells exhibited excellent catalytic activities with 96%–99% conversions in the salidroside acylation with different chain-length acyl donors. Furthermore, the initial reaction rate increased from 3.37 mM/h to 17.31 mM/h with the elongation of chain length of acyl donors from C2 to C11, which indicated that the interaction between medium-chain acyl groups and hydrophobic acyl binding sites of intracellular acylase was stronger than that of short-chain groups. Nevertheless, the initial reaction rate decreased with further extending chain length from C12 to C16, owing to the higher steric hindrance of the longer-chain acyl donors. Previous studies have found that the biocatalysts from different sources showed different catalytic properties for the different acyl donors due to the specific structure of the lipase active site and the acyl (Wang and Zong, 2009; Yang et al., 2013; Li X. F. et al., 2018; Yang W. et al., 2019). For example, the *Pseudomonas aeruginosa* cells were more specific toward the medium-chain acyl donors, as well as *Candida antarctica* lipase B (Novozyme 435) and *Thermomyces lanuginosus* lipase (Lipozyme TLL) (Wang and Zong, 2009; Yang et al., 2013; Yang R. L. et al., 2019), while the whole cells of *Candida parapsilosis* was most efficient for the short chain acyl donor, vinyl propionate. (Li G. Y. et al., 2018).

4 Conclusion

A facile and efficient biocatalytic approach was employed for the synthesis of salidroside esters by using *Aspergillus oryzae* cells, which was a potentially cost-attractive alternative to expensive immobilized enzymes. Various 6'-monoesters derivatives of salidroside were obtained with excellent conversions and high regioselectivities. And the structure of the acyl donors demonstrated an impact on the catalytic characteristic of the *Aspergillus oryzae* whole cells. The results afforded a green and highly efficient strategy for selective structural modification of polyhydroxyl natural products.

Data availability statement

The original contributions presented in the study are included in the article/Supplementary Material, further inquiries can be directed to the corresponding author.

Author contributions

RY and XZ designed the study, analyzed the data and wrote the manuscript. YW, ZT, QZ, and XH performed the experiment

and collected the data. ZW HL, and FF analyzed the data and revised the manuscript.

Funding

We thank the financial support from the National Natural Science Foundation of China (21706088) and the Six Talent Peaks of Jiangsu Province (2018-SWYY-020).

Conflict of interest

The authors declare that the research was conducted in the absence of any commercial or financial relationships that could be construed as a potential conflict of interest.

References

- Chen, Y. S., Liu, J. W., Geng, S., Liu, Y. L., Ma, H. J., Zheng, J., et al. (2019). Lipase-catalyzed synthesis mechanism of tri-acetylated phloridzin and its antiproliferative activity against HepG2 cancer cells. *Food Chem. x* 277, 186–194. doi:10.1016/j.foodchem.2018.10.111
- Chen, Z. G., Zhang, D. N., Cao, L., and Han, Y. B. (2013). Highly efficient and regioselective acylation of pharmacologically interesting cordycepin catalyzed by lipase in the eco-friendly solvent 2-methyltetrahydrofuran. *Bioresour. Technol.* 133, 82–86. doi:10.1016/j.biortech.2013.01.117
- Chyba, A., Mastihubá, V., and Mastihubová, M. (2016). Effective enzymatic caffeoylation of natural glucopyranosides. *Bioorg. Med. Chem. Lett.* 26 (6), 1567–1570. doi:10.1016/j.bmcl.2016.02.010
- Hao, L. S., Zhang, M. M., Li, X. F., Xin, X., Lei, F. L., Lai, X. N., et al. (2021). Highly efficient whole-cell biosynthesis and cytotoxicity of esculin esters. *J. Biotechnol.* 337, 46–56. doi:10.1016/j.jbiotec.2021.06.023
- Hu, X. L., Lin, S. X., Yu, D. H., Qiu, S. F., Zhang, X. Q., and Mei, R. H. (2010). A preliminary study: The anti-proliferation effect of salidroside on different human cancer cell lines. *Cell Biol. Toxicol.* 26 (6), 499–507. doi:10.1007/s10565-010-9159-1
- Jeandet, P., Sobarzo-Sánchez, E., Silva, A. S., Clément, C., Nabavi, S. F., Battino, M., et al. (2020). Whole-cell biocatalytic, enzymatic and green chemistry methods for the production of resveratrol and its derivatives. *Biotechnol. Adv.* 39, 107461. doi:10.1016/j.biotechadv.2019.107461
- Li, G. Y., Wang, J. B., and Reetz, M. T. (2018). Biocatalysts for the pharmaceutical industry created by structure-guided directed evolution of stereoselective enzymes. *Bioorg. Med. Chem.* 26 (7), 1241–1251. doi:10.1016/j.bmc.2017.05.021
- Li, X. F., Xu, H. X., Zhao, G. L., Wu, H., Yu, Y. G., Lai, F. R., et al. (2018). Highly efficient synthesis of arbutin esters catalyzed by whole cells of *Candida parapsilosis*. *RSC Adv.* 8 (18), 10081–10088. doi:10.1039/c8ra00595h
- Liang, C. X., Qi, D. L., Zhang, L. N., Lu, P., and Liu, Z. D. (2021). Preparation and evaluation of a water-in-oil nanoemulsion drug delivery system loaded with salidroside. *Chin. J. Nat. Med.* 19 (3), 231–240. doi:10.1016/s1875-5364(21)60025-0
- Liu, J. N., Zhuang, Y. H., Hu, Y. H., Xue, S., Li, H., Chen, L., et al. (2020). Improving the color stability and antioxidation activity of blueberry anthocyanins by enzymatic acylation with *p*-coumaric acid and caffeic acid. *LWT. Food Sci. Technol.* 130, 109673. doi:10.1016/j.lwt.2020.109673
- Qi, S. S., Shao, L. M., Ze, S., and Zheng, H. X. (2021). Salidroside from *Rhodiola rosea* L. attenuates diabetic nephropathy in STZ induced diabetic rats via

Publisher's note

All claims expressed in this article are solely those of the authors and do not necessarily represent those of their affiliated organizations, or those of the publisher, the editors and the reviewers. Any product that may be evaluated in this article, or claim that may be made by its manufacturer, is not guaranteed or endorsed by the publisher.

Supplementary material

The Supplementary Material for this article can be found online at: <https://www.frontiersin.org/articles/10.3389/fbioe.2022.1051117/full#supplementary-material>

anti-oxidative stress, anti-inflammation, and inhibiting TGF- β 1/Smad pathway. *J. Funct. Foods* 77, 104329. doi:10.1016/j.jff.2020.104329

Qian, J., Wang, X. H., Weng, W. J., Zhou, G. X., Zhu, S. X., and Liu, C. (2021). Salidroside alleviates taurothiocholic acid 3-sulfate-induced AR42J cell injury. *Biomed. Pharmacother.* 142, 112062. doi:10.1016/j.biopha.2021.112062

Song, T. X., Wang, P. L., Li, C. Y., Jia, L., Liang, Q. Q., Cao, Y. L., et al. (2021). Salidroside simultaneously reduces de novo lipogenesis and cholesterol biosynthesis to attenuate atherosclerosis in mice. *Biomed. Pharmacother.* 134, 111137. doi:10.1016/j.biopha.2020.111137

Sugai, T., Higashibayashi, S., and Hanaya, K. (2018). Recent examples of the use of biocatalysts with high accessibility and availability in natural product synthesis. *Tetrahedron* 74 (27), 3469–3487. doi:10.1016/j.tet.2018.05.053

Wachmeister, J., and Rother, D. (2016). Recent advances in whole cell biocatalysis techniques bridging from investigative to industrial scale. *Curr. Opin. Biotechnol.* 42, 169–177. doi:10.1016/j.copbio.2016.05.005

Wang, Z. Y., and Zong, M. H. (2009). Recognition of acyl donors by lipase CAL-B in the acylation of 6-azauridine. *Biotechnol. Prog.* 25 (3), 784–791. doi:10.1002/btpr.237

Wu, Y. F., Wang, Y., Wu, Y. R., Li, T. T., and Wang, W. (2020). Salidroside shows anticonvulsant and neuroprotective effects by activating the Nrf2-ARE pathway in a pentylenetetrazol-kindling epileptic model. *Brain Res. Bull.* 164, 14–20. doi:10.1016/j.brainresbull.2020.08.009

Wu, Y., Ma, Y., Li, J., Zhou, X. L., Li, L., Xu, P. X., et al. (2021). The bioinformatics and metabolomics research on anti-hypoxic molecular mechanisms of Salidroside via regulating the PTEN mediated PI3K/Akt/NF- κ B signaling pathway. *Chin. J. Nat. Med.* 19 (6), 442–453. doi:10.1016/s1875-5364(21)60043-2

Xin, X., Li, X. F., Xiao, X. L., Tang, Y. Q., and Zhao, G. L. (2017). Facile and efficient acylation of bioflavonoids using whole-cell biocatalysts in organic solvents. *ACS Sustain. Chem. Eng.* 5 (11), 10662–10672. doi:10.1021/acssuschemeng.7b02628

Xing, S. S., Li, J., Chen, L., Yang, Y. F., He, P. L., Li, J., et al. (2018). Salidroside attenuates endothelial cellular senescence via decreasing the expression of inflammatory cytokines and increasing the expression of SIRT3. *Mech. Ageing Dev.* 175, 1–6. doi:10.1016/j.mad.2017.12.005

Xu, P., Zheng, G. W., Du, P. X., Zong, M. H., and Lou, W. Y. (2016). Whole-cell biocatalytic processes with ionic liquids. *ACS Sustain. Chem. Eng.* 4 (2), 371–386. doi:10.1021/acssuschemeng.5b00965

- Yang, L. M., Zhou, L., Wang, X. H., Wang, W., and Wang, J. (2020). Inhibition of HMGB1 involved in the protective of salidroside on liver injury in diabetes mice. *Int. Immunopharmacol.* 89, 106987. doi:10.1016/j.intimp.2020.106987
- Yang, R. L., Zhao, X. J., and Liu, X. M. (2013). Novel and highly efficient regioselective route to heligid esters by Lipozyme TLL. *PLOS ONE* 8 (11), e80715. doi:10.1371/journal.pone.0080715
- Yang, R. L., Wu, T. T., Xu, N. N., Zhao, X. J., Wang, Z. Y., Luo, H. Z., et al. (2020). Improving whole-cell biocatalysis for heligid benzylation by the addition of ionic liquids. *Biochem. Eng. J.* 161 (15), 107695. doi:10.1016/j.bej.2020.107695
- Yang, R. L., Zhao, X. J., Wu, T. T., Bilal, M., Wang, Z. Y., Luo, H. Z., et al. (2019). A novel and highly regioselective biocatalytic approach to acetylation of heligid by using whole-cell biocatalysts in organic solvents. *Catal. Commun.* 128, 105707. doi:10.1016/j.catcom.2019.105707
- Yang, W., Kortensniemi, M., Ma, X. Y., Zheng, J., and Yang, B. R. (2019). Enzymatic acylation of blackcurrant (*Ribes nigrum*) anthocyanins and evaluation of lipophilic properties and antioxidant capacity of derivatives. *Food Chem. x.* 281, 189–196. doi:10.1016/j.foodchem.2018.12.111
- Yang, Z. L., Huang, X., Lai, W. F., Tang, Y. H., Liu, J. J., Wang, Y. Z., et al. (2021). Synthesis and identification of a novel derivative of salidroside as a selective, competitive inhibitor of monoamine oxidase B with enhanced neuroprotective properties. *Eur. J. Med. Chem.* 209 (1), 112935. doi:10.1016/j.ejmech.2020.112935
- Yu, H. L., Xu, J. H., Su, J. H., Lu, W. Y., and Lin, G. Q. (2008). Synthesis of novel salidroside esters by lipase-mediated acylation with various functional acyl groups. *J. Biosci. Bioeng.* 106 (1), 65–68. doi:10.1263/jbb.106.65
- Zhang, P. L., Liu, S., Zhao, Z. G., You, L. J., Harrison, M. D., and Zhang, Z. Y. (2021). Enzymatic acylation of cyanidin-3-glucoside with fatty acid methyl esters improves stability and antioxidant activity. *Food Chem. x.* 343 (1), 128482. doi:10.1016/j.foodchem.2020.128482
- Zhang, X. M., Xie, L., Long, J. Y., Xie, Q. X., Zheng, Y., Liu, K., et al. (2021). Salidroside: A review of its recent advances in synthetic pathways and pharmacological properties. *Chem. Biol. Interact.* 339 (25), 109268. doi:10.1016/j.cbi.2020.109268



OPEN ACCESS

EDITED BY

Qi Xianghui,
Jiangsu University, China

REVIEWED BY

Gao-Qiang Liu,
Central South University of Forestry and
Technology, China
Junping Zhou,
Zhejiang University of Technology,
China

*CORRESPONDENCE

An-Dong Gong,
fwjt63298@126.com

SPECIALTY SECTION

This article was submitted to Industrial
Biotechnology,
a section of the journal
Frontiers in Bioengineering and
Biotechnology

RECEIVED 11 October 2022

ACCEPTED 17 November 2022

PUBLISHED 02 December 2022

CITATION

Yang P, Liu W, Chen Y and Gong A-D
(2022), Engineering the glyoxylate cycle
for chemical bioproduction.
Front. Bioeng. Biotechnol. 10:1066651.
doi: 10.3389/fbioe.2022.1066651

COPYRIGHT

© 2022 Yang, Liu, Chen and Gong. This
is an open-access article distributed
under the terms of the [Creative
Commons Attribution License \(CC BY\)](#).
The use, distribution or reproduction in
other forums is permitted, provided the
original author(s) and the copyright
owner(s) are credited and that the
original publication in this journal is
cited, in accordance with accepted
academic practice. No use, distribution
or reproduction is permitted which does
not comply with these terms.

Engineering the glyoxylate cycle for chemical bioproduction

Peng Yang, Wenjing Liu, Yanan Chen and An-Dong Gong*

College of Life Science, Xinyang Normal University, Xinyang, China

With growing concerns about environmental issues and sustainable economy, bioproduction of chemicals utilizing microbial cell factories provides an eco-friendly alternative to current petro-based processes. Creating high-performance strains (with high titer, yield, and productivity) through metabolic engineering strategies is critical for cost-competitive production. Commonly, it is inevitable to fine-tuning or rewire the endogenous or heterologous pathways in such processes. As an important pathway involved in the synthesis of many kinds of chemicals, the potential of the glyoxylate cycle in metabolic engineering has been studied extensively these years. Here, we review the metabolic regulation of the glyoxylate cycle and summarize recent achievements in microbial production of chemicals through tuning of the glyoxylate cycle, with a focus on studies implemented in model microorganisms. Also, future prospects for bioproduction of glyoxylate cycle-related chemicals are discussed.

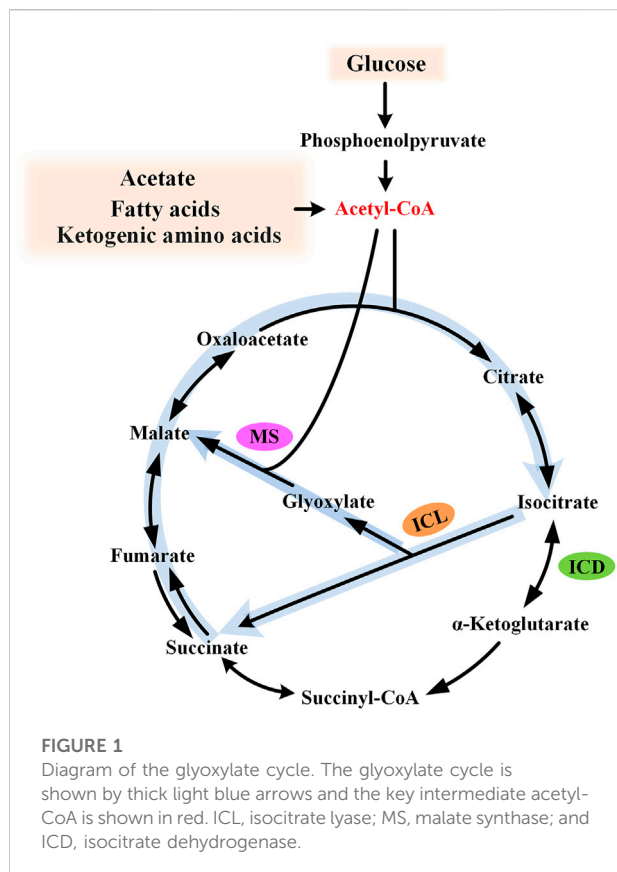
KEYWORDS

glyoxylate cycle, metabolic engineering, biosynthesis, TCA cycle, organic acids, amino acids, fatty acids

Introduction

The glyoxylate cycle, also known as glyoxylate shunt (GS), was identified by Kornberg and Krebs in 1957, explaining how organisms could grow on acetate as the sole carbon source (Kornberg and Krebs, 1957). For substrates degraded exclusively to acetyl moieties (e.g., acetate, fatty acids, and ketogenic amino acids), this pathway provides a simple and efficient strategy for anaplerosis and gluconeogenesis, and, thus, cell growth. The glyoxylate cycle is generally regarded as an ancillary pathway of the TCA cycle, which is widely acknowledged as the central metabolic hub of the cell. This pathway comprises two dedicated enzymes: isocitrate lyase (ICL) and malate synthase (MS). ICL catalyzes the aldol cleavage of isocitrate to succinate and glyoxylate, while MS catalyzes the synthesis of malate from glyoxylate and acetyl-CoA. The overall effect of this pathway is the formation of one malate from two molecules of acetyl-CoA (Figure 1). It bypasses the oxidative

Abbreviations: AFAA, L-aspartate family amino acid; ALA, 5-aminolevulinic acid; GS, glyoxylate shunt; GABA, γ -aminobutyric acid; 4-HIL, 4-hydroxyisoleucine; 3-HP, 3-hydroxypropionate; 4-HB, 4-hydroxybutyric acid; ICL, isocitrate lyase; ICD, isocitrate dehydrogenase; IclR, isocitrate lyase regulator; α -KG, α -ketoglutarate; MS, malate synthase; OAA, oxaloacetate; PEP, phosphoenolpyruvate.



decarboxylation steps of the TCA cycle and conserves carbon skeletons for biomass generation.

In addition to carbon assimilation, the glyoxylate cycle is also implicated in pathogenesis, antibiotic resistance, and oxidative stress tolerance. In view of its significance in metabolism and pathogenicity, the glyoxylate cycle has been extensively studied concerning the enzymology and metabolic regulation, particularly for *Escherichia coli* and the pathogenic bacterium *Mycobacterium tuberculosis* (Dolan and Welch, 2018). Undoubtedly, the gained knowledge lays a foundation for the bioproduction of related chemicals in metabolic engineering.

The glyoxylate cycle is involved in the synthesis of various chemicals. In recent years, studies on biosynthesis of organic acids, amino acids, and fatty acid-related products through GS engineering have been reported. Some of the outstanding results are presented in Table 1. To balance product output, reducing power regeneration, and cell growth, the glyoxylate cycle needs to be reinforced, weakened, fine-tuned, or dynamically controlled in different production cases. When heterologously expressed in some strains lacking this pathway, the GS amplified carbon source spectrum and enabled more metabolic flexibility, thus facilitating bioproduction (Kabisch et al., 2013; Schada von Borzyskowski et al., 2018; Shimizu et al., 2019).

In this review, we will briefly introduce the flux control of glyoxylate cycle in several different bacteria and recent achievements in biosynthesis of related chemicals. In addition, perspective for further study with the GS pathway will be presented.

Regulation of the glyoxylate cycle

The canonical regulation model in *E. coli*

A carbon flux is partitioned between the oxidative TCA branch and GS at the isocitrate node, thereby, maintaining a balance of energy, reducing power, and gluconeogenic precursor production. In addition, glyoxylate is highly reactive or even toxic (due to the aldehyde group). Thus, tight regulation of the glyoxylate cycle is necessary.

In *E. coli*, ICL is a tetramer encoded by *aceA*. Its affinity for isocitrate is much lower than that of the NADP-dependent isocitrate dehydrogenase (ICD, encoded by *icd*). As a result, the control of ICD activity plays an important role in determining the flux of GS (LaPorte et al., 1985). The activity of ICD is primarily controlled by a kinase/phosphatase called AceK (encoded by *aceK*) (Figure 2A). When bacteria are grown on acetate, about 75% of ICD is inactivated by phosphorylation, thus, more isocitrate will be directed through the glyoxylate cycle. The differential kinase/phosphatase activity of AceK is allosterically regulated by several metabolites (e.g., isocitrate, PEP, and ATP), although the precise mechanism is still not fully clear (Ogawa et al., 2007). It is worth noting that PEP also uncompetitively inhibits ICL.

AceK-dependent regulation of the flux through the glyoxylate cycle is a feature associated with only the gram-negative bacteria (this enzyme is absent in nearly all the gram-positive bacteria) (Yates et al., 2011). In addition, ICL is negatively regulated by acetylation in *E. coli* (Castano-Cerezo et al., 2014). On the other hand, MS (encoded by *aceB*) shows high affinities for the substrates glyoxylate and acetyl-CoA, and thus inhibition or activation of MS plays only a minor role in controlling the glyoxylate cycle (Anstrom et al., 2003).

In *E. coli*, the open reading frames (ORFs) of *aceB*, *aceA*, and *aceK* form a tricistronic operon (*aceBAK*), which is positively controlled by a pleiotropic transcriptional regulator Cra and the integration host factor (IHF) and negatively controlled by IclR (isocitrate lyase regulator) (Cozzzone, 1998) (Figure 2A). The expression of the *aceBAK* operon can also be enhanced by Lrp, a transcriptional activator of the upstream *metA* gene (Kroner et al., 2019). Glyoxylate and PEP stabilize the inactive dimeric state of IclR, while pyruvate stabilizes the active tetrameric form (Lorca et al., 2007). Expression of IclR is under self-inhibition and is activated by FadR (which represses β -oxidation and activates biosynthesis of fatty acids) (Gui et al., 1996). The

TABLE 1 Representative studies of chemical biosynthesis through GS engineering.

Strain	Product	Substrate	Production capacity	Reference
<i>E. coli</i> $\Delta adhE \Delta ldhA \Delta ackA \Delta iclR$ /pHL413	Succinate	Glucose	40 g/L in 96 h with a yield of 1.6 mol/mol	Sánchez et al. (2005)
<i>E. coli</i> $\Delta ackA\text{-}pta \Delta poxB \Delta ldhA \Delta adhE \Delta mgsA \Delta pflB \Delta iclR$ P _{L-aceEF} -IpdA/pPYC	Succinate	Glucose	1.69 mol/mol in test-tube; 67.4 g/L in 26 h with a yield of 1.47 mol/mol during high cell density fermentation	Skorokhodova et al. (2015)
<i>E. coli</i> $\Delta sdhAB \Delta iclR \Delta maeB$ /pTrc99a-gltA	Succinate	Acetate	1.73 g/L in 72 h with a yield of 0.46 mol/mol; 7.29 g/L using resting-cells	Li Y et al. (2016)
<i>Methylobacter</i> sp. DH-1 $\Delta sdh aceBA$	Succinate	Methane	195 mg/L with a yield of 0.0789 g/g	Nguyen et al. (2019)
<i>E. coli</i> BL21 (DE3) $\Delta fumB \Delta fumAC \Delta aspA aceBAK::trc ppc::trc$ /pSCppc	Fumarate	Glycerol	41.5 g/L in 82 h with a yield of 0.44 g/g	Li et al. (2014)
<i>E. coli</i> W3110 $\Delta ldhA \Delta poxB \Delta pflB \Delta pta\text{-}ackA \Delta frdBC \Delta fumB \Delta fumAC$ /pETM6R1-(RBS10)/pYJC-EcCS-EcACN _{-(RBS10)} -EcICL-EcSDH-dcuC	Fumarate	Glucose	22.4 g/L in 60 h	Chen et al. (2020)
<i>E. coli</i> B0013 $\Delta adhE \Delta ackA\text{-}pta \Delta ldhA \Delta maeA \Delta maeB \Delta mdh \Delta iclR \Delta arcA$ /PETM7-PGNAB, sgRNA set 2, dCas9	Malate	Glucose	31.8 g/L in 50 h with a yield of 0.74 mol/mol	Gao et al. (2018)
<i>Aspergillus oryzae</i> C4T318 PC MDH ROPYC CS IDH OGD ACN ICL MS Sfc1p LINOX RNAi-cis	Malate	Corn starch	117.2 g/L with a yield of 0.9 g/g and a productivity of 1.17 g/L/h	Liu et al. (2018)
<i>E. coli</i> W $\Delta iclR$ /pCDF _{CAD} , pET _{ACS} , pCOG5	Itaconate	Acetate	3.57 g/L in 88 h with a yield of 0.09 g/g	Noh et al. (2018)
<i>E. coli</i> MG1655 (DE3) $\Delta ldhA \Delta glcB \Delta aceB \Delta aldA$ /pJNU-3, pJNU-4	Glycolate	Glucose	65.5 g/L in 77 h with a yield of 0.765 g/g	Deng et al. (2018)
<i>E. coli</i> $\Delta xylB \Delta glcD \Delta aceB \Delta glcB \Delta gcl$ /pGAX1, pGAX2	Glycolate	Xylose	40 g/L in 80 h with a yield of 0.63 g/g	Pereira et al. (2016)
<i>E. coli</i> $\Delta aceB \Delta gcl \Delta glcDEFG \Delta iclR \Delta edd\text{-}eda \Delta arcA \Delta icd \Delta xylB khkC aldB aldA ghrA aceA galP$	Glycolate	Glucose/xylose	3.73 g/L with a yield of 0.63 g/g	Alkim et al. (2016)
<i>E. coli</i> TWF001 $\Delta iclR \Delta lacI \Delta fadR \Delta fabR \Delta lacA$ P _{aceBA} ::P _{trc} P _{aspC} ::P _{trc} P _{acs} ::P _{tac-trc} P _{aceB} -aceBA P _{fadB} -fadBA P _{tac} -ppnK P _{tac} -thrA ^{BC} -rhtC P _{tac} -aspC P _{tac} -ppc	L-threonine	Glucose	103.89 g/l in 48 h with a yield of 0.72 g/g	Yang et al. (2019)
<i>E. coli</i> $\Delta lacI \Delta gabT \Delta sucA$ /pTA216, pTA1410, pTA1756	GABA	Glucose	4.8 g/L with a yield of 0.492 mol/mol and a productivity of 0.15 g/L/h	Soma et al. (2017)
<i>E. coli</i> $\Delta ldhA \Delta sdhA \Delta iclR$ /pK-hemA, pgrNA-L4, pdcas9-bacteria	5-Aminolevulinate	Glycerol	6.93 g/L in 18 h	Miscevic et al. (2021a)
<i>Corynebacterium glutamicum</i> $\Delta aceB icd^{CTG}$ /pVWEx1-dpkA _{RBS} ^{opt} , pEC-KT99A- <i>xylA_{XC}</i> - <i>xylB_{CG}</i>	Sarcosine	Xylose/acetate	8.7 g/L with a yield of 0.25 g/g	Mindt et al. (2019a)
<i>E. coli</i> JCL16 $\Delta ldhA \Delta adhE \Delta frdBC \Delta pta$ /pCS138, pTO1, pIM8	1-Butanol	Glucose	18.3 g/L in 78 h	Ohtake et al. (2017)
<i>E. coli</i> BL21 (DE3) $\Delta poxB \Delta adhE \Delta ldhA \Delta iclR$	3-Hydroxypropionate	Acetate	7.3 g/L with a yield of 0.26 mol/mol	Lama et al. (2021)
<i>Pseudomonas denitrificans</i> $\Delta 3hpdh \Delta 3hibdhIV \Delta 3hibdhI \Delta pta\text{-}ackA \Delta fabF$ /pUCPK-AM	3-Hydroxypropionate	Acetate	3.64 g/L in 22 h	Zhou et al. (2020)
<i>E. coli</i> $\Delta gabD \Delta yneI \Delta ldhA \Delta adhE \Delta pflB \Delta ptsG$ /p99S4CD, p15PGH	4-Hydroxybutyrate	Glycerol	103.4 g/L with a yield of 0.419 g/g and a productivity of 0.844 g/L/h	Choi S. Y et al. (2016)

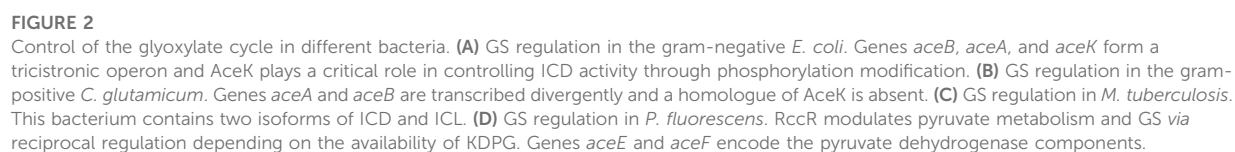
coordination of fatty acid metabolism and the glyoxylate cycle may indicate acetyl-CoA as a signaling molecule.

Control of GS in *Corynebacterium glutamicum*

Unlike the dimeric ICD enzyme from *E. coli*, the homologue (named IDH) is monomeric in *C. glutamicum*. The ORFs of *aceA* and *aceB* are transcribed divergently in *C. glutamicum* and a homologue of AceK is absent (Figure 2B). This organism does not encode an IcdR homologue, while new types of transcription

repressor RamB (regulator of acetate metabolism) and transcription activator RamA were characterized (Gerstmeier et al., 2004; Cramer et al., 2006). In the absence of acetate, RamB represses the expression of *aceA*, *aceB*, and *pta-ack* (encoding phosphotransacetylase and acetate kinase). The induction of glyoxylate cycle genes by acetate occurs independently of the presence or absence of glucose and other carbon source, which is different from *E. coli*.

Kim et al. reported a transcription repressor of *aceB* in *C. glutamicum*, which was designated as GlxR (Kim et al., 2004). The repression occurred in the presence of cAMP (e.g., when glucose medium was used). In addition, GlxR positively regulates



ramA expression independent of the carbon source used (Toyoda et al., 2013) (Figure 2B). The glyoxylate cycle is also regulated through other mechanisms except for the transcriptional level. Maeda et al. found that RNase E/G (encoded by *rneG*) could cleave the *aceA* mRNA at the 3' untranslated region, and the level of *aceA* mRNA was approximately 3-fold higher in the *rneG* mutant than in the wild type (Maeda and Wachi, 2012).

Control of GS in *Mycobacterium tuberculosis* and *Pseudomonas fluorescens*

Bioinformatic studies showed that only microorganisms capable of aerobic metabolism possess the glyoxylate cycle, and the genetic context of related genes were diversified among bacterial genera, indicating more complex regulation (Ahn et al., 2016). For example, a totally different flux rheostat model was characterized in the *Mycobacterium* spp. (Figure 2C) and a reciprocal regulation model was characterized in *P. fluorescens* (Figure 2D). Although application of these strains in metabolic engineering was limited due to the pathogenicity, the mechanisms of GS regulation may be instructive.

M. tuberculosis contains two isoforms of ICD (dimeric Mtb ICD-1 and monomeric Mtb ICD-2), two isoforms of ICL (*E. coli*-like ICL-1 and a less-studied ICL-2), and lacks an AceK homologue (Munoz-Elias and McKinney, 2005). The K_M s of ICL and ICD were comparable, in contrast with the situation in *E. coli* (Murima et al., 2016). The activity of ICD-2 (the primary isoform under physiological conditions) is stimulated by glyoxylate thereby decreasing the flux through GS. In this way, the flux balance between the TCA cycle and GS was achieved via a rheostat model. On glucose, RamB specifically represses the transcription of *icl1* and *ramB* itself (Micklinghoff et al., 2009). PrpR, a transcription factor involved in the methylcitrate pathway, can repress *ramB* expression and activate the expression of *icl1* (Masiewicz et al., 2012). A recent study showed that ICL-2 was markedly activated by acetyl-CoA and propionyl-CoA at high lipid concentrations (Bhusal et al., 2019).

At the posttranslational level, ICL-1 was found to be acetylated on three lysine residues (K322, K331, and K392). Acetylation at position 392 increased ICL activity, whereas acetylation of K322 reduced its activity (Bi et al., 2017). In ICD, residues K30 and K129 are acetylated by Rv2170, and this leads to a 30% reduction in the enzyme activity (Lee et al., 2017).

In *P. fluorescens*, RccR, a homologue of the Entner–Doudoroff pathway regulator HexR, plays the key role in the GS control via reciprocal regulation. In the presence of glucose, RccR binds 2-keto-3-deoxy-6-phosphogluconate (KDPG) and represses the expression of *aceA* and *glcB*. In the

absence of KDPG, it represses the expression of *aceEF* genes. In this way, strain can modulate pyruvate metabolism and GS/gluconeogenesis in response to carbon source availability (Campilongo et al., 2017).

In several studies, unpredictable up/down-regulation of GS was resulted from the fermentation process control or genetic manipulation of the unrelated pathway due to interactional metabolism (Martinez et al., 2010; Wei et al., 2016; Borja et al., 2019). These results provided us new understanding of this pathway, yet were not readily applicable in the targeted metabolic engineering practice. These approaches will not be discussed in the present review.

Production of organic acids

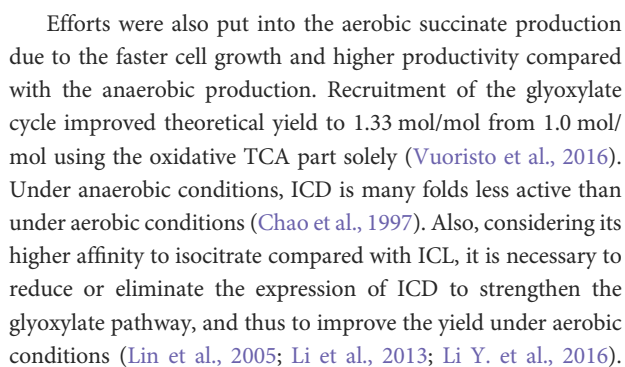
Succinate production

Succinate has been considered as a potential chemical platform with a wide range of applications in food, pharmacy, chemical, and agriculture. Many microorganisms naturally accumulate succinate using the reductive TCA branch:



However, the required NADH is typically generated by glucose heterofermentation, which reduces the theoretical yield to 1 mol/mol glucose (Figure 3). Ailen et al. developed a dual-route succinate production strategy through combining the reductive TCA part and the glyoxylate cycle (Sanchez et al., 2005). The lactate, ethanol, and acetate pathway were blocked to conserve NADH and acetyl-CoA. A heterologous pyruvate carboxylase (*pyc*) was overexpressed then to fix CO₂ and increase the flux into the reductive TCA branch. Most importantly, conserved NADH and acetyl-CoA were channeled into the glyoxylate cycle by deletion of the repressor IclR. The engineered *E. coli* strain produced succinate at a yield of 1.6 mol/mol glucose under anaerobic conditions, which was close to the theoretical maximum (1.7 mol/mol glucose).

To achieve the theoretical maximum, the distribution of metabolic flux between carboxylation of PEP to OAA and decarboxylation of PEP to acetyl-CoA should be 5:2 (Vemuri et al., 2002). Skorokhodova et al. constitutively expressed the NAD⁺-reducing pyruvate dehydrogenase complex (*aceEF-lpdA*) to enhance the flux toward the glyoxylate cycle while supplying additional NADH at the same time (Skorokhodova et al., 2015). In an *E. coli* strain with blocked lactate, acetate, and ethanol pathways, they inactivated the pyruvate formate lyase (*pflB*) to drive acetyl-CoA formation solely by the overexpressed pyruvate dehydrogenase under anaerobic conditions. Further deletion of IclR with a concomitant heterologous pyruvate carboxylase (*pyc*) overexpression enabled a succinate yield of 1.69 mol/mol at tube-scale experiments with NaHCO₃ addition.



The glyoxylate cycle was also engineered in other microbes for succinate production except for *E. coli* (Zhu et al., 2014a; Cui et al., 2017; Babaei et al., 2019; Durall et al., 2021). Specially, Nguyen et al. integrated the GS enzymes from *E. coli* into a methanotroph *Methylomonas* sp. DH-1 (Nguyen et al., 2019). The GS pathway supplied intermediates for biomass synthesis in an *sdh* mutant and activated the serine cycle to provide more acetyl-CoA, which may have improved the cell growth and succinate production. Finally, 195 mg/L succinate,

corresponding to 6.41% of the theoretical yield was produced from methane.

Production of fumarate and malate

Succinate, fumarate, and malate can be interconverted but synthesis of fumarate and malate needs less reducing power compared with succinate under anaerobic conditions. In a study to produce fumarate, *iclR* was deleted to redirect carbon flux into the glyoxylate cycle (Song et al., 2013) (Figure 3). The phosphoenolpyruvate carboxylase (*ppc*) was overexpressed, then *arcA* (encoding a global transcriptional regulator) and *ptsG* (one of the phosphotransferase system genes) were deleted to reinforce the oxidative TCA cycle. Additionally, fumarate consumption was blocked through *fumABC* and *aspA* gene deletion. Finally, glucose uptake was increased by substituting the *galP* promoter. The engineered *E. coli* strain produced 28.2 g/L fumarate in 63 h under aerobic conditions (Song et al., 2013).

In another study, the decreased activity of ICD and activated GS was demonstrated to be effective to reduce acetate accumulation and increase the fumarate production. However, *aceBA* overexpression dramatically slowed cell growth, which demonstrated the importance of flux balance between the GS and oxidative TCA cycle (Li et al., 2014). Chen et al. engineered *E. coli* for fumarate production via the glyoxylate pathway (Chen et al., 2020). They explored the effect of pyruvate carboxylase (*pyc*), citrate synthase (*gltA*), aconitase (*acnB*), isocitrate lyase (*aceA*), and succinate dehydrogenase (*sdh*) overexpression on fumarate production, and found that pyruvate carboxylase and isocitrate lyase played crucial roles. The expression level of these two enzymes varied to balance the glyoxylate cycle and oxidative TCA flux. Through pathway optimization, the fumarate titer was increased from 8.7 g/L to 16.2 g/L.

The glyoxylate pathway was also engineered for malate production in *E. coli* by the same research group (Gao et al., 2018). First, they constructed an *in vitro* malate production system containing five enzymes, which were, pyruvate carboxylase (PC), citrate synthase (CS), aconitase (ACN), isocitrate lyase (ICL), and malate synthase (MS), and explored the optimal level for each enzyme. Then, CRISPRi was employed for enzyme modular coordination *in vivo*. Through the moderate inhibition of PC and CS expression, and fixing the level of ACN: ICL: MS at 4: 5: 4, malate titer was increased by two folds with a yield of 0.85 mol/mol glucose. In addition, *iclR* and *arcA* were inactivated to enhance the flux toward glyoxylate cycle and oxidative TCA cycle.

Trichez et al. engineered an *E. coli* strain for malate production through deletion of the *iclR* and *arcA* genes, block of malate consuming, and overexpression of malate-insensitive PEP carboxylase Ppc^{K620S} and NADH-insensitive citrate synthase GltA^{R164L}. A malate yield of 0.82 mol/mol was obtained. The metabolic flux analysis indicated that the engineered strains had a very high flux over the glyoxylate shunt with almost no flux passing through the isocitrate dehydrogenase reaction (Trichez et al., 2018).

Liu et al. engineered L-malate production in *Aspergillus oryzae* (Liu et al., 2018). First, accumulation of intermediate pyruvate was decreased by overexpressing a pyruvate carboxylase from *Rhizopus oryzae* in the cytosol and mitochondria. Then, malate synthesis via the glyoxylate cycle in the mitochondria was enhanced by overexpression of isocitrate lyase and malate synthase. Interestingly, strengthening the oxidative TCA route diminished spore formation and malate production, while downregulation of the oxidative TCA cycle enhanced the L-malate titer by 10.7%, indicating that the TCA cycle route was not suitable for the malate production in this case. Finally, through the expression of a dicarboxylate carrier and modulation of the NADH/NAD⁺ ratio, 117.2 g/L L-malate was produced, with an L-malate yield of 0.9 g/g corn starch and a productivity of 1.17 g/L/h. Polymalic acid (PMA), a high added-value polyester composed of L-malic acid monomers, can be produced via the glyoxylate cycle naturally by *Aureobasidium pullulans*. A few studies engineered PMA production through enhancement of the glyoxylate cycle (Yang et al., 2018; Zeng et al., 2019).

Production of itaconate

The glyoxylate cycle can also play a positive role in the production of itaconate, an excellent polymeric precursor derived from *cis*-aconitate (Figure 3). Through overexpression of pyruvate carboxylase, citrate synthase, aconitase, and the *cis*-aconitate decarboxylase (AT-CAD, *cad*) from *A. terreus*, flux toward the itaconate production was enhanced. Together with isocitrate dehydrogenase deletion, the titer of itaconate reached to 43 g/L in 32 h from glycerol under high aeration. Elimination of the glyoxylate shunt demonstrated harmful impact on the itaconate production, although this pathway pulled out the carbon flux via the isocitrate node. This may be due to its positive role in regeneration of oxaloacetate, which was important for itaconate synthesis in turn (Chang et al., 2017).

In another study, an acid-tolerant *E. coli* strain was engineered for itaconate production from acetate (Noh et al., 2018). By overexpression of the *cis*-aconitate decarboxylase, only 0.13 g/L itaconic acid was produced because of low acetate uptake. Then, acetate assimilation was enhanced through overexpression of the acetyl-CoA synthetase and activation of the glyoxylate cycle. The high ICL activity was proved to be beneficial for the itaconate production. Together with *gltA* overexpression, 3.57 g/L itaconic acid (16.1% of theoretical maximum yield) was produced from acetate.

Production of glycolate

Glycolate, or glycolic acid (GA) is a small two-carbon α -hydroxy acid used in multiple daily applications (Figure 3). There are no known natural microbial pathways to directly produce GA

from relatively cheap feedstock, yet this chemical can be produced *via* several synthetic pathways including the modified GS pathway (Salusjärvi et al., 2019). In an attempt to produce GA using *E. coli*, flux toward the glyoxylate cycle was enhanced through the overexpression of ICL and deletion of acetate forming pathways, *icd*, *arcA*, and *iclR*. GA synthesis was further enhanced by glyoxylate reductase (*ycdW*) overexpression. Consumption of glyoxylate and GA was blocked through inactivation of MS, glyoxylate carboligase (*gcl*), 2-keto 3-deoxygluconate 6-phosphate aldolase (*eda*), glycolate oxidase (*glcDEFG*) and glycolaldehyde dehydrogenase (*aldA*). To increase the availability of NADPH, which is needed by YcdW, *edd* encoding the 6-phosphogluconate dehydratase was deleted. Finally, 52.2 g/L GA was produced from glucose (Dischert and Soucaille, 2015).

Sometimes complete block of the TCA cycle through *icd* deletion may cause growth retardation. Deng et al. tried to weaken the flux to α -ketoglutarate (α -KG) through overexpression of AceK, which could repress the ICD activity. In this way, the ICD activity was decreased by 83.03%, but poor growth of strain was incurred concomitantly. Then, adaptive evolution was performed to increase the growth rate. Nevertheless, the evolved strain still grew much more slowly than the wild type, which suggested the importance of balance between the TCA cycle and GS reactions. In fed-batch fermentation, the engineered strain produced 56.4 g/L GA (Deng et al., 2015). Subsequently, Deng et al. further improved the producer strain (Deng et al., 2018). Citrate synthase was overexpressed in addition to ICL, YcdW, and AceK. Lactate dehydrogenase (*ldhA*), which competed for the carbon flux to glycolate and AldA involved in GA consumption were deleted. The following optimization of fermentation, 65.5 g/L GA was produced with a yield of 0.765 g/g glucose (90.0% of the theoretical yield).

Pereira et al. engineered an *E. coli* strain to produce GA from xylose, the most abundant pentose (Pereira et al., 2016). Through introduction of the exogenous D-tagatose epimerase, 44.0 g/L GA was produced *via* the D-ribulose-1-phosphate pathway. By combining the D-ribulose-1-phosphate pathway and glyoxylate cycle, the yield was increased from 0.44 to 0.62 g/g xylose (theoretical yield 1 g/g), although the titer did not improve obviously. Cam et al. engineered GA production in *E. coli* from xylose *via* a synthetic xylulose-1 phosphate (X1P) pathway (Cam et al., 2016). In this pathway, D-xylose was converted to glycolaldehyde and DHAP, both of which can be converted to GA with a theoretical yield higher than 20% *via* the glyoxylate shunt alone. Simultaneous operation of the glyoxylate and X1P pathways enabled a yield of 0.63 g/g, when growing on the glucose/xylose mixture (Alkim et al., 2016). It is worth noting that when produced from xylose *via* the Dahms pathway, the yield of GA was only 0.5 g/g xylose (Cabulong et al., 2021).

Li et al. engineered GA production in *E. coli* from acetate *via* the glyoxylate cycle (Li et al., 2019). The glyoxylate bypass was

reinforced by overexpression of ICL and AceK. YcdW was overexpressed to convert glyoxylate to glycolate. MS, glyoxylate carboligase, and glycolate oxidase were inactivated to prevent loss of glyoxylate and glycolate. To strengthen the TCA cycle and acetate utilization, citrate synthase, phosphotransacetylase, and acetate kinase (*ackA*) were co-overexpressed. As a result, the glycolate titer was improved to 2.75 g/L with the pH control in shake flasks. The GA production pathway can be integrated with other metabolic routes to produce value-added chemicals including 3-hydroxy- γ -butyrolactone (3HBL) and GA-containing polymer directly from glucose or/and xylose (Dhamankar et al., 2014; Choi S. Y. et al., 2016; Li Z.-J. et al., 2016; Li Z.-J. et al., 2017). In addition, the glyoxylate cycle was also engineered to produce GA in microbes other than *E. coli*, although the titer was relatively low (Koivistoinen et al., 2013; Zahoor et al., 2014; Lee et al., 2020).

Production of amino acids and derivatives

Production of L-aspartate family amino acids

Several amino acids and their derivatives are synthesized from the GS and TCA cycle intermediates, including OAA, α -KG and succinyl-CoA (Figure 3). L-Aspartate family amino acids (AFAAs) refer to amino acids synthesized from L-aspartate such as L-lysine, L-methionine, L-threonine, and L-isoleucine. Because L-aspartate is directly synthesized from OAA, the OAA supply has been considered as a bottleneck for the production of AFAAs (Li Y. et al., 2017). In one study, the OAA pool was increased to improve L-homoserine production in *E. coli* (Liu et al., 2020). First, *iclR* was deleted to derepress the glyoxylate cycle. Then, citrate synthase (*gltA*) was deleted to conserve OAA. Subsequently, pyruvate kinase (*pykA* and *pykF*) was deleted to drive more anaplerotic flux into OAA. Together with disrupting the competitive and degradative pathways, 35.8 g/L L-homoserine was produced in the fed-batch fermentation. Conversely, simultaneous activation of the glyoxylate cycle and overexpression of *gltA* (rather than weakening its expression) improved AFAAs production in some other studies, which suggested the complexity of metabolism (Flores et al., 2005; Zhu et al., 2019). Sometimes, the glyoxylate cycle could be activated through attenuating the isocitrate dehydrogenase activity, which also resulted in replenishment of OAA (Schwentner et al., 2018).

In another study, L-threonine, which can be synthesized from L-homoserine, was produced in *E. coli* (Zhao et al., 2018). To conserve precursor OAA, the gene *iclR* was deleted, and the native promoter of the *aceBA* operon was replaced by the strong *trc* promoter in the chromosome. Then, the L-threonine

biosynthesis pathway was overexpressed *via* replacing the native promoter of *aspC* (aspartate aminotransferase) by the *trc* promoter in the chromosome and plasmid overexpression of *thrA** (a mutated *thrA*), *thrB*, *thrC*, and *asd* (encoding aspartate kinase I, homoserine kinase, threonine synthase and aspartate semialdehyde dehydrogenase, respectively). The final strain TWF006/pFW01-*thrA*BC*-*asd* produced 15.85 g/l L-threonine with a yield of 0.53 g/g glucose. In a subsequent study, the same group found that increase of the acetyl-CoA pool positively affected L-threonine production (Yang et al., 2019). The acetyl-CoA pool was increased through: deletion of fatty acid degradation/synthesis regulator FadR and FabR; overexpression of acetyl-CoA synthetase (*acs*) to convert acetate into acetyl-CoA; and overexpression of *fadBA* to facilitate fatty acid degradation. The fatty acid degradation and L-threonine biosynthesis pathway were coupled *via* the glyoxylate shunt, and 103.89 g/l L-threonine was produced after 48-h fed-batch fermentation.

Ectoine is a protective agent and stabilizer which can be synthesized from L-Aspartate. Ning et al. introduced the synthesis pathway of ectoine (encoded by the *ectABC* gene cluster from *Halomonas elongata*) into *E. coli* to produce this valuable chemical (Ning et al., 2016). To increase the OAA pool, *iclR* was deleted to enhance the glyoxylate shunt and the expression level of *ppc* (encoding the phosphoenolpyruvate carboxylase) was improved through promoter change. Then, the synthetic pathway of L-lysine and L-threonine was blocked, and a feedback resistant LysC from *C. glutamicum* (encoding the aspartate kinase) was introduced to enhance the flux to ectoine. Together with the overexpression of *ectABC*, 25.1 g/L ectoine was produced by fed-batch fermentation. Increase of the OAA pool *via* deletion of *iclR* was also proved to be effective in a study to produce β -alanine, another AFAA in *E. coli* (Wang et al., 2021). However, further enhancement of GS genes through promoter change did not improve β -alanine production, suggesting the importance of flux balance.

Production of α -ketoglutarate-sourced amino acids

α -KG is the precursor of numerous amino acids, such as L-glutamine, L-glutamate, and L-proline (Figure 3). In a *C. glutamicum* L-glutamate producer strain, glyoxylate pathway was blocked by knocking out *aceA* to conserve the isocitrate pool, and glutamate synthesis was blocked by knocking out *gdh* (encoding glutamate dehydrogenase). As a result, α -KG production was increased by 16-fold to 12.4 g/L in flask culture and 47.5 g/L in 5-L fermentor (Jo et al., 2012). In another study to produce Poly- γ -glutamic acid (γ -PGA) using *Bacillus licheniformis*, the glyoxylate cycle was also reduced to improve the titer (Li et al., 2021). The expression level of *aceBA* was varied through promoter modulation, and with a weak promoter *P_{bacA}*, the activity of ICL was decreased by 41.51%,

which resulted in 23.24% increase in γ -PGA yield. In addition, pyruvate dehydrogenase and citrate synthase were overexpressed to strengthen the flux into the TCA cycle, and pyruvate formate-lyase was deleted to conserve pyruvate. Finally, γ -PGA titer was enhanced to 12.02 g/L.

In biofermentation, it is essential to address the conflict between cell growth and target chemical production, as the overexpressed production pathways often lead to metabolic burden for the cell. In a study to produce γ -aminobutyric acid (GABA), a genetic switch was designed to balance the GABA production and bacterial cell growth (Soma et al., 2017). The cell growth was controlled by conditional interruption of GS and the TCA cycle. In the cell growth mode, α -ketoglutarate decarboxylase (*sucA*) of the TCA cycle and ICL (*aceA*) of the glyoxylate cycle were actively expressed, while turned off in the GABA production mode. On the contrary, pyruvate carboxylase (*pyc*), glutamate dehydrogenase (*gdhA*), glutamate decarboxylase (*gadB*), and the GABA transporter (*gadC*) involved in GABA synthesis were turned on only during the production mode. This strategy balanced the competition for isocitrate and α -KG between cell growth and GABA production, resulting in a 3-fold improvement in the total GABA production titer and yield.

In another study to produce 4-hydroxyisoleucine (4-HIL), a potential medicine for diabetes, the glyoxylate cycle was blocked (by deleting *aceA*) to increase one of the substrates α -KG (Shi et al., 2019). 4-HIL was synthesized from L-isoleucine and α -KG under the activity of L-isoleucine dioxygenase (IDO). The deletion of *aceA* increased the concentration of both α -KG and L-isoleucine, resulting in an 18.9% increase in the titer of 4-HIL. Then, *ido3* (another IDO encoding gene) and *mgo* (encoding malate:quinone oxidoreductase) were coexpressed with *ido* to draw more flux into the Ile and 4-HIL biosynthetic pathways, resulting in another 31.8% increase of the titer. Further expression of the *Vitreoscilla* hemoglobin (*vgb*) and optimization of the fermentation medium led to a final 4-HIL titer of 17.2 g/L.

5-Aminolevulinic acid (ALA) is an α -KG derived non-proteinogenic amino acid with multiple applications in medical, agricultural, and food industries. There are two distinct routes to produce this chemical biologically, the C₅ pathway and the C₄ pathway. In the C₅ pathway, ALA is synthesized from α -KG. To conserve α -KG, the TCA cycle was blocked by deletion of *sucA* (encoding α -ketoglutarate decarboxylase) (Noh et al., 2017). Although the specific ALA production was increased obviously, both ALA titer and cell biomass were reduced probably due to the insufficient production of energy and building blocks. Overexpression of *gltA* encoding citrate synthase only marginally improved cell biomass. Next, the glyoxylate cycle was finely tuned through modulating the promoter of *aceA*. Under the optimal strength, cell biomass and ALA production were increased by 4.45-fold and 2.93-fold, respectively, as compared to the parental strain. After fermentation optimization, high productivity (0.19 g/L/h)

and yield (0.28 g/g) for ALA production from glucose as a sole carbon source was achieved.

In the C_4 pathway, ALA was synthesized from succinyl-CoA and glycine. To reduce the conversion of ALA to downstream tetrapyrrole/porphyrin, Miscevic et al. applied CRISPRi to repress *hemB* expression (Miscevic et al., 2021b). Under microaerobic condition, succinyl-CoA is mainly derived from reductive the TCA cycle and the glyoxylate cycle. The authors inactivated *iclR* to deregulate the glyoxylate shunt while deleting *sdhA* simultaneously to further redirect the carbon flux toward ALA biosynthesis. Finally, 6.93 g/L ALA was produced from 30 g/L glycerol in *E. coli*. In another study, an exogenous glyoxylate transaminase from the human, which enabled autogenous synthesis of glycine from glyoxylate, was introduced into *E. coli* to produce ALA using glucose as the sole carbon source (Ren et al., 2018). The transaminase used alanine as the amino donor, with ATP, PLP, and CoA as cofactors. To increase the supply of glyoxylate, *aceA* was overexpressed. As a proof-of-concept, 521 mg/L 5-ALA was produced in 18 h of fermentation.

Production of tyrosine and *N*-alkylated glyoxylate

Tyrosine is an aromatic amino acid, which can be utilized in many aspects. In a study to engineer tyrosine production from acetate in *E. coli*, precise tuning of the glyoxylate cycle was proved to be vital (Jo et al., 2019). In this case, the two important intermediates for tyrosine synthesis, erythrose-4-phosphate and PEP were both derived from OAA. As acetate was the sole carbon source, it was critical to balance the glyoxylate cycle and TCA cycle, in other words, to balance precursor supply and generation of ATP and NADH. The glyoxylate cycle was precisely controlled by modulating the promoter of *aceA*. As a result, the best engineered strain produced 0.70 g/L tyrosine.

Glyoxylate can be *N*-alkylated by monomethylamine or monoethylamine, forming sarcosine and *N*-ethylglycine, respectively, under the activity of imine reductases DpkA (Mindt et al., 2019b). To increase glyoxylate supply, *aceB* was deleted and the activity of isocitrate dehydrogenase was reduced by changing the preferred translational start codon ATG to GTG. To further activate the glyoxylate cycle, acetate was added into the culture media. Together with other strategies including optimization of carbon source species, the amount and addition time of monomethylamine and acetate, 8.7 g/L sarcosine was produced from xylose and potassium acetate blends using the engineered *C. glutamicum*. Subsequently, DpkA was mutated, which accelerated the production of sarcosine (Mindt et al., 2019a). Using this mutant, production of *N*-ethylglycine from xylose and monoethylamine or from rice straw hydrolysate was demonstrated.

Production of fatty acid-related chemicals and farnesyl diphosphate-derived bioactive compounds

Production of acetyl-CoA derivatives

Synthesis of fatty acids originates from acetyl-CoA in microbial cells. Acetyl-CoA lies at the entrance into the TCA cycle, and is closely related with the glyoxylate cycle. Many polyhydroxyalkanoate monomers and several bioactive compounds can be synthesized from acetyl-CoA, as shown in Figure 3. On the other hand, propionate and 4-hydroxybutyrate (4-HB) can be synthesized from succinyl-CoA, another intermediate strongly linked with GS. Thus, the glyoxylate cycle was engineered to improve production of related chemicals in a few studies.

Nitta et al. engineered an *E. coli* strain to produce 1-butanol, a bulk chemical and promising biofuel (Nitta et al., 2019). All native fermentation pathways were blocked (through deletion of *ldhA*, *adhE*, and *frdBC*) and the strain relied on 1-butanol formation as the sole electron sink to regenerate NAD^+ . 1-Butanol was produced using a heterologous Clostridial CoA-dependent pathway. Then, formate dehydrogenase (*fdh*) from *Candida boidinii* was introduced to supply more NADH. Also, phosphate acetyltransferase (*pta*) was deleted to prevent formation of by-product acetate. In addition, the expression of *AdhE2*, the key enzyme for 1-butanol synthesis was optimized, which resulted in a 1-butanol titer of 18.3 g/L. However, considerable amounts of acetate accumulated (Ohtake et al., 2017). Subsequent metabolome analysis revealed increased accumulation of glyoxylate and acetyl-P with a decrease of α -KG and glutamate in the engineered strain, compared with the base strain. By knocking out *aceA*, acetate production decreased by 72% and the TCA cycle metabolites (including α -KG and glutamate) increased, which resulted in a 10% increase of the cell growth. Finally, 1-butanol production was improved by 39% (Nitta et al., 2019).

In another study, the expression of the glyoxylate cycle was enhanced by knocking out *iclR* to overcome acetate overflow and improve the production of two acetyl-CoA derived chemicals, phloroglucinol (PG) and 3-hydroxypropionate (3-HP) in *E. coli* BL21 (Liu et al., 2017). Acetate accumulation inhibits protein synthesis and depletes the acetyl-CoA pool. Deletion of *iclR* decreased acetate formation and improved the glucose utilization efficiency, which could reduce the production cost. At the same time, the metabolic flux from acetate and PEP to acetyl-CoA was enhanced, resulting in a more than 2-fold increase in the production of PG or 3HP. In a previous study, deletion of *arcA*, the redox regulator known to repress the TCA cycle and glyoxylate cycle, demonstrated similar effects on cell physiology and production of acetyl-CoA derived chemicals (Liu et al., 2016). However, the *arcA* and *iclR* double mutant showed no better results for PG and the 3HP production than *arcA* or *iclR*

single mutant and the mechanisms were unclear. In another study, to produce 3-HP in *E. coli* from acetate, substrate assimilation was enhanced by overexpressing *acs* and the GS was activated by deleting *iclR*. As a result, acetate uptake and cell biomass synthesis were enhanced significantly, and 3-HP production was improved by 2.54-fold (Lee et al., 2018).

To balance the cell growth and 3-HP synthesis, a two-stage strategy was adopted by Lama et al., whereby glucose is used for the cell growth and acetate for 3-HP synthesis (Lama et al., 2021). To increase biomass yield on glucose, pathways for synthesis of by-products lactic acid, ethanol, and acetic acid were removed. Then, the effects of GS and the gluconeogenesis pathways on the cell growth and 3-HP formation during the production stage were studied. As a result, block of gluconeogenesis or GS was detrimental for 3-HP production, while the activation of GS (via deletion of *iclR*) improved the titer of 3-HP. Using fed-batch fermentation, 7.3 g/L 3-HP was produced with a yield of 0.26 mol/mol acetate. Notably, the yield was still low compared with the theoretical maximum of 0.5 mol/mol acetate, which may reflect the operational cost of GS and subsequent gluconeogenesis.

3-HP biosynthesis was also pursued in non-model microorganisms. Using *P. denitrificans* as the producer, activation of GS by deleting *iclR* or enhancement of the oxidative TCA branch by *aceK* deletion did not improve 3-HP significantly, when a similar two-stage production strategy was adopted (Zhou et al., 2020). Lai et al. deleted the fatty acid degradation repressor FadR to enhance acetic acid utilization, which also activated the GS and improved 3-HP production. Using whole-cell biocatalysis, 15.8 g/L and 11.2 g/L of 3-HP was produced from acetate or syngas-derived acetate, respectively (Lai et al., 2021). Sometimes, when a target chemical not so closely-related was produced, the impact of GS would be complicated (Lin et al., 2013; Zhang et al., 2019).

To enhance production of FPP-derived bioactive compounds, the key point was usually the acetyl-CoA level. Citric acid synthase (CIT2 in peroxisome) or malic acid synthase (MLS1 in the cytoplasm) was knocked out in a study to enhance the supply of precursor acetyl-CoA for production of crocetin, a potential drug in *Saccharomyces cerevisiae* (Song et al., 2020). The CIT2 mutant achieved 50% improvement on the total acetyl-CoA content and crocetin production, compared with the parent strain. The MLS1 mutant demonstrated similar effects, but to a lesser degree. Followed by suited fusion expression of key enzymes CrtZ and CCD2 and medium optimization, 12.43 mg/L crocetin was produced in fed-batch fermentation. Deletion of CIT2 and/or MLS1 also proved beneficial to increase the acetyl-CoA level in other studies. In a study to produce α -santalene (an acetyl-CoA derived sesquiterpene) in an engineered yeast strain, deletion of CIT2 or MLS1 improved the titer by 36% and 127%, respectively (Chen et al., 2013). Using CIT2 or MLS1 mutant, the titer of butanol was improved to 14.0 and 16.3 mg/L, respectively in another study (compared with 10.3 mg/L in the parent yeast

strain) (Krivoruchko et al., 2013). However, block of the glyoxylate cycle through deletion of CIT2 or MLS1 compromised cell growth of a PHB-producing yeast strain and resulted in accumulation of acetate and a decrease in PHB content (Kocharin et al., 2012).

Production of succinyl-CoA derivatives

Under the anaerobic condition, succinate was mainly derived from the reductive TCA branch. However, the glyoxylate cycle could play an important role under the aerobic/microaerobic condition. Thus, effects of GS on the succinyl-CoA level were quite DO-dependent. In a study to produce propionate using the sleeping beauty mutase (Sbm) pathway in *E. coli*, the oxidative TCA cycle was blocked via deletion of *sdhA* and the glyoxylate cycle was deregulated by *iclR* deletion to improve the succinyl-CoA level. Through this modification, propionate titer was increased to 3.68 g/L from 1.1 g/L. Finally, 30.9 g/L of propionate was produced with an overall yield of 49.7% under optimized aeration condition using fed-batch fermentation (Miscevic et al., 2020b). Subsequently, 3-hydroxyvalerate was produced through condensation of propionyl-CoA and acetyl-CoA via a heterologous pathway using glycerol as the carbon source (Miscevic et al., 2020a; Miscevic et al., 2020c). The effects of aeration condition on activity of GS, and thus, flux distribution into the Sbm pathway were further demonstrated during production of poly (3-hydroxybutyrate-co-3-hydroxyvalerate) (Miscevic et al., 2021a).

4-HB is another chemical derived from succinyl-CoA that can be converted into various industrial chemicals and polymers. Producer strains of *E. coli* engineered for both aerobic and microaerobic conditions were constructed by Choi et al. based on a genome-scale metabolic model (Choi S. et al., 2016). Under the aerobic condition, the oxidative TCA branch and GS were proved to be essential for the supply of precursor succinate and production of 4-HB. Deletion of *sdhAB* and *iclR* was efficient to increase the titer of 4-HB. However, neither enhancement of GS (via deletion of *iclR*) nor block of GS (via deletion of *aceBA*) were effective in enhancing 4-HB production under the microaerobic condition, and there seemed to exist an optimal expression level of GS. In addition, glycerol was proved to be effective only for the microaerobic producer. Finally, 103.4 g/L of 4-HB was produced by microaerobic fed-batch fermentation from glycerol.

Santala et al. engineered wax esters production in *Acinetobacter baylyi* ADP1 from acetate and gluconate (Santala et al., 2021). By deleting *aceA*, GS was blocked and consumed acetate was dedicated to wax esters biosynthesis. On the other hand, gluconate was used for the synthesis of cofactors and biomass precursors. This design overcame the trade-offs between biomass and product production, an issue frequently

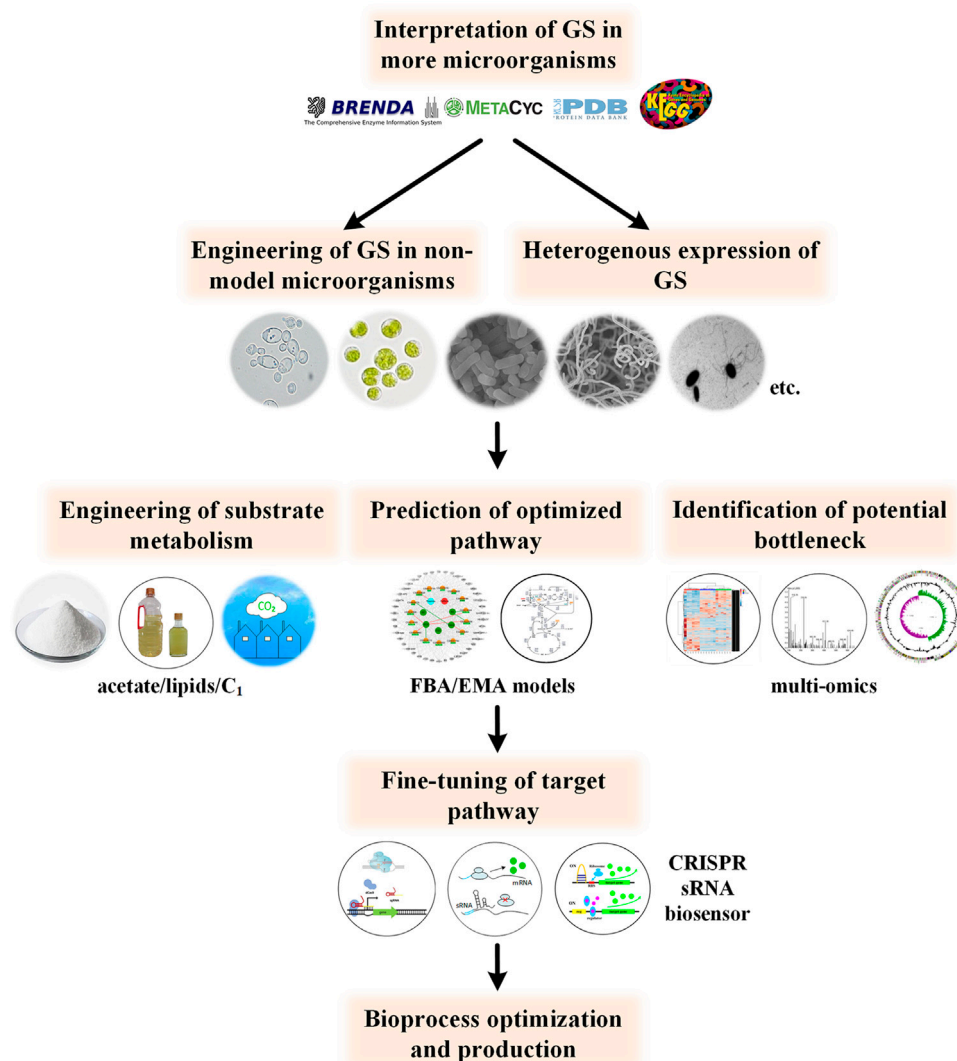


FIGURE 4

Perspective for future studies concerning GS engineering. Further understanding of GS metabolism in more potential producer microorganisms and more precise modulation of related pathways will promote the bioproduction process.

encountered in bioengineering. Through optimization of gluconate feed rate and enhancement of the wax esters pathway, wax esters content, titer and productivity were improved significantly and a yield of 18% C/C-total-substrates was achieved.

Concluding remarks and outlook

As outlined in this review, the biochemistry and regulation of glyoxylate cycle was demonstrated in two industrial microorganisms (*E. coli* and *C. glutamicum*) and two potential pathogenic microorganisms (*M. tuberculosis* and *P. fluorescens*).

Although applications in biosynthesis by *M. tuberculosis* and *P. fluorescens* are limited due to the pathogenicity, the GS control mechanisms may be instructive. Production of target chemicals, divided into several categories, including organic acids, amino acids and fatty acid-related chemicals were also briefly introduced.

Currently, metabolic engineering studies are focused on a small number of model microorganisms, especially *E. coli*. Thus, other potential producer strains with better robust traits, production capacity and feedstock compatibility may have been missed (Zeng, 2019). Considering the deep involvement of glyoxylate cycle in the synthesis of so many chemicals, clear interpretation of the glyoxylate metabolism in other industry

relevant microorganisms will undoubtedly facilitate chemical bioproduction in the future (such as yeast, cyanobacteria, *streptomyces* and *Clostridia* (Chen et al., 2012; Huang et al., 2015; Zhang and Bryant, 2015)). On the other hand, studies on more detailed effects of exogenously introduced the GS pathway on the physiology and production performance of the producers are encouraged (Kabisch et al., 2013; Schada von Borzyskowski et al., 2018; Shimizu et al., 2019). In addition, protein engineering studies of the GS pathway, particularly for biosynthesis purpose are barren to our knowledge.

Metabolism of substrates which could be facilitated by GS are not just limited to acetate, glycerol or fatty acids. Recently, Mainguet et al. constructed a reverse GS which could convert C₄ carboxylates into two molecules of acetyl-CoA without loss of CO₂ (Mainguet et al., 2013). Heterologous enzymes malate thiokinase, malyl-CoA lyase and ATP-citrate lyase were utilized to drive the thermodynamically unfavorable steps, namely the conversion of malate to glyoxylate and acetyl-CoA, and conversion of citrate to OAA and acetyl-CoA at the expense of ATP. When adapted and integrated with central metabolism, conversion of C1 or CO₂ carbon source to acetyl-CoA can be realized (Yu et al., 2018; Yu and Liao, 2018). Although no practical production use of this pathway has been implemented, this non-native route holds the potential for producing various acetyl-CoA derived chemicals, including alcohols, fatty acids, and isoprenoids in the future.

Another challenge is the balance of the cell growth and product biosynthesis. This may be overcome in two steps, that is, accurate prediction of the appropriate GS strength and fine-tuning of its expression level accordingly. Prediction of the optimized metabolic flux can be promoted by multi-omics and more precise genome-scale metabolic models, such as flux balance analysis (FBA)-based models, elementary mode analysis-based ones and kinetic models (Srirangan et al., 2013; Machado and Herrgård, 2015). Then, fine-tuning of the GS pathway could be realized through CRISPRi, CRISPRa, sRNA, or dynamic control (Choi et al., 2019). The outline for future studies is shown in Figure 4. With the development of new techniques and

expansion of the online database, the product portfolio and substrate spectrum can be further expanded in the future.

Author contributions

Conceptualization: PY and A-DG; writing—original draft preparation: PY, WL, and YC; writing—review and editing: PY and A-DG; supervision: A-DG; and funding acquisition: PY and A-DG. All authors read and agreed to the published version of the manuscript.

Funding

This work was funded by grants from the National Natural Science Foundation of China (31800074), Nanhu Scholars Program for Young Scholars of XYNU, Scientific and Technological Project of Henan Province (212102110447), and Natural Science Foundation of Henan (222300420519 and 222301420111).

Conflict of interest

The authors declare that the research was conducted in the absence of any commercial or financial relationships that could be construed as a potential conflict of interest.

Publisher's note

All claims expressed in this article are solely those of the authors and do not necessarily represent those of their affiliated organizations, or those of the publisher, the editors, and the reviewers. Any product that may be evaluated in this article, or claim that may be made by its manufacturer, is not guaranteed or endorsed by the publisher.

References

- Ahn, S., Jung, J., Jang, I. A., Madsen, E. L., and Park, W. (2016). Role of glyoxylate shunt in oxidative stress response. *J. Biol. Chem.* 291 (22), 11928–11938. doi:10.1074/jbc.M115.708149
- Alkim, C., Trichez, D., Cam, Y., Spina, L., François, J. M., and Walther, T. (2016). The synthetic xylulose-1 phosphate pathway increases production of glycolic acid from xylose-rich sugar mixtures. *Biotechnol. Biofuels* 9 (1), 201–211. doi:10.1186/s13068-016-0610-2
- Anstrom, D. M., Kallio, K., and Remington, S. J. (2003). Structure of the *Escherichia coli* malate synthase G: Pyruvate: Acetyl-coenzyme A abortive ternary complex at 1.95 Å resolution. *Protein Sci.* 12 (9), 1822–1832. doi:10.1110/ps.03174303
- Babaei, M., Rueksomtawin Kildegaard, K., Niaei, A., Hosseini, M., Ebrahimi, S., Sudarsan, S., et al. (2019). Engineering oleaginous yeast as the host for fermentative succinic acid production from glucose. *Front. Bioeng. Biotechnol.* 7, 361. doi:10.3389/fbioe.2019.00361
- Bhusal, R. P., Jiao, W., Kwai, B. X., Reynisson, J., Collins, A. J., Sperry, J., et al. (2019). Acetyl-CoA-mediated activation of *Mycobacterium tuberculosis* isocitrate lyase 2. *Nat. Commun.* 10 (1), 4639–4647. doi:10.1038/s41467-019-12614-7
- Bi, J., Wang, Y., Yu, H., Qian, X., Wang, H., Liu, J., et al. (2017). Modulation of central carbon metabolism by acetylation of isocitrate lyase in *Mycobacterium tuberculosis*. *Sci. Rep.* 7 (1), 44826–44911. doi:10.1038/srep44826
- Borja, G. M., Rodriguez, A., Campbell, K., Borodina, I., Chen, Y., and Nielsen, J. (2019). Metabolic engineering and transcriptomic analysis of *Saccharomyces cerevisiae* producing *p*-coumaric acid from xylose. *Microb. Cell Fact.* 18 (1), 191. doi:10.1186/s12934-019-1244-4
- Cabulong, R. B., Bañares, A. B., Nisola, G. M., Lee, W.-K., and Chung, W.-J. (2021). Enhanced glycolic acid yield through xylose and cellobiose utilization by metabolically engineered *Escherichia coli*. *Bioprocess Biosyst. Eng.* 44 (6), 1081–1091. doi:10.1007/s00449-020-02502-6

- Cam, Y., Alkim, C., Trichez, D., Trebosc, V., Vax, A., Bartolo, F., et al. (2016). Engineering of a synthetic metabolic pathway for the assimilation of (D)-xylose into value-added chemicals. *ACS Synth. Biol.* 5 (7), 607–618. doi:10.1021/acssynbio.5b00103
- Campilongo, R., Fung, R. K. Y., Little, R. H., Grenga, L., Trampari, E., Pepe, S., et al. (2017). One ligand, two regulators and three binding sites: How KDPG controls primary carbon metabolism in *Pseudomonas*. *PLoS Genet.* 13 (6), e1006839. doi:10.1371/journal.pgen.1006839
- Castano-Cerezo, S., Bernal, V., Post, H., Fuhrer, T., Cappadona, S., Sanchez-Diaz, N. C., et al. (2014). Protein acetylation affects acetate metabolism, motility and acid stress response in *Escherichia coli*. *Mol. Syst. Biol.* 10, 762. doi:10.15252/msb.20145227
- Chang, P., Chen, G. S., Chu, H.-Y., Lu, K. W., and Shen, C. R. (2017). Engineering efficient production of itaconic acid from diverse substrates in *Escherichia coli*. *J. Biotechnol.* 249, 73–81. doi:10.1016/j.jbiotec.2017.03.026
- Chao, G., Shen, J., Tseng, C. P., Park, S. J., and Gunsalus, R. P. (1997). Aerobic regulation of isocitrate dehydrogenase gene (*icd*) expression in *Escherichia coli* by the *arcA* and *fnr* gene products. *J. Bacteriol.* 179 (13), 4299–4304. doi:10.1128/jb.179.13.4299-4304.1997
- Chen, X., Ma, D., Liu, J., Luo, Q., and Liu, L. (2020). Engineering the transmission efficiency of the noncyclic glyoxylate pathway for fumarate production in *Escherichia coli*. *Biotechnol. Biofuels* 13 (1), 132–210. doi:10.1186/s13068-020-01771-3
- Chen, Y., Daviet, L., Schalk, M., Siewers, V., and Nielsen, J. (2013). Establishing a platform cell factory through engineering of yeast acetyl-CoA metabolism. *Metab. Eng.* 15, 48–54. doi:10.1016/j.ymben.2012.11.002
- Chen, Y., Siewers, V., and Nielsen, J. (2012). Profiling of cytosolic and peroxisomal acetyl-CoA metabolism in *Saccharomyces cerevisiae*. *PLoS ONE* 7 (8), e42475. doi:10.1371/journal.pone.0042475
- Choi, K. R., Jang, W. D., Yang, D., Cho, J. S., Park, D., and Lee, S. Y. (2019). Systems metabolic engineering strategies: Integrating systems and synthetic biology with metabolic engineering. *Trends Biotechnol.* 37 (8), 817–837. doi:10.1016/j.tibtech.2019.01.003
- Choi, S., Kim, H. U., Kim, T. Y., and Lee, S. Y. (2016). Systematic engineering of TCA cycle for optimal production of a four-carbon platform chemical 4-hydroxybutyric acid in *Escherichia coli*. *Metab. Eng.* 38, 264–273. doi:10.1016/j.ymben.2016.09.004
- Choi, S. Y., Park, S. J., Kim, W. J., Yang, J. E., Lee, H., Shin, J., et al. (2016). One-step fermentative production of poly (lactate-co-glycolate) from carbohydrates in *Escherichia coli*. *Nat. Biotechnol.* 34 (4), 435–440. doi:10.1038/nbt.3485
- Cozzzone, A. J. (1998). Regulation of acetate metabolism by protein phosphorylation in enteric bacteria. *Annu. Rev. Microbiol.* 52 (1), 127–164. doi:10.1146/annurev.micro.52.1.127
- Cramer, A., Gerstmeir, R., Schaffer, S., Bott, M., and Eikmanns, B. J. (2006). Identification of *RamA*, a novel LuxR-type transcriptional regulator of genes involved in acetate metabolism of *Corynebacterium glutamicum*. *J. Bacteriol.* 188 (7), 2554–2567. doi:10.1128/JB.188.7.2554-2567.2006
- Cui, Z., Gao, C., Li, J., Hou, J., Lin, C. S. K., and Qi, Q. (2017). Engineering of unconventional yeast *Yarrowia lipolytica* for efficient succinic acid production from glycerol at low pH. *Metab. Eng.* 42, 126–133. doi:10.1016/j.ymben.2017.06.007
- Deng, Y., Ma, N., Zhu, K., Mao, Y., Wei, X., and Zhao, Y. (2018). Balancing the carbon flux distributions between the TCA cycle and glyoxylate shunt to produce glycolate at high yield and titer in *Escherichia coli*. *Metab. Eng.* 46, 28–34. doi:10.1016/j.ymben.2018.02.008
- Deng, Y., Mao, Y., and Zhang, X. (2015). Metabolic engineering of *E. coli* for efficient production of glycolic acid from glucose. *Biochem. Eng. J.* 103, 256–262. doi:10.1016/j.bej.2015.08.008
- Dhamankar, H., Tarasova, Y., Martin, C. H., and Prather, K. L. (2014). Engineering *E. coli* for the biosynthesis of 3-hydroxy- γ -butyrolactone (3HBL) and 3, 4-dihydroxybutyric acid (3, 4-DHBA) as value-added chemicals from glucose as a sole carbon source. *Metab. Eng.* 25, 72–81. doi:10.1016/j.ymben.2014.06.004
- Dischert, W., and Soucaille, P. (2015). *Method for producing high amount of glycolic acid by fermentation*. U.S. Patent No 8,945,888. Washington, DC: U.S. Patent and Trademark Office.
- Dolan, S. K., and Welch, M. (2018). The glyoxylate shunt, 60 years on. *Annu. Rev. Microbiol.* 72, 309–330. doi:10.1146/annurev-micro-090817-062257
- Durall, C., Kukil, K., Hawkes, J. A., Alberghati, A., Lindblad, P., and Lindberg, P. (2021). Production of succinate by engineered strains of *Synechocystis* PCC 6803 overexpressing phosphoenolpyruvate carboxylase and a glyoxylate shunt. *Microb. Cell Fact.* 20 (1), 39–14. doi:10.1186/s12934-021-01529-y
- Flores, N., Flores, S., Escalante, A., de Anda, R., Leal, L., Malpica, R., et al. (2005). Adaptation for fast growth on glucose by differential expression of central carbon metabolism and *gal* regulon genes in an *Escherichia coli* strain lacking the phosphoenolpyruvate: Carbohydrate phosphotransferase system. *Metab. Eng.* 7 (2), 70–87. doi:10.1016/j.ymben.2004.10.002
- Gao, C., Wang, S., Hu, G., Guo, L., Chen, X., Xu, P., et al. (2018). Engineering *Escherichia coli* for malate production by integrating modular pathway characterization with CRISPRi-guided multiplexed metabolic tuning. *Biotechnol. Bioeng.* 115 (3), 661–672. doi:10.1002/bit.26486
- Gerstmeir, R., Cramer, A., Dangel, P., Schaffer, S., and Eikmanns, B. J. (2004). *RamB*, a novel transcriptional regulator of genes involved in acetate metabolism of *Corynebacterium glutamicum*. *J. Bacteriol.* 186 (9), 2798–2809. doi:10.1128/JB.186.9.2798-2809.2004
- Gui, L., Sunnarborg, A., and LaPorte, D. C. (1996). Regulated expression of a repressor protein: FadR activates *iclR*. *J. Bacteriol.* 178 (15), 4704–4709. doi:10.1128/jb.178.15.4704-4709.1996
- Huang, H., Sivapragasam, S., and Grove, A. (2015). The regulatory role of *Streptomyces coelicolor* TamR in central metabolism. *Biochem. J.* 466 (2), 347–358. doi:10.1042/BJ20130838
- Jo, J.-H., Seol, H.-Y., Lee, Y.-B., Kim, M.-H., Hyun, H.-H., and Lee, H.-H. (2012). Disruption of genes for the enhanced biosynthesis of α -ketoglutarate in *Corynebacterium glutamicum*. *Can. J. Microbiol.* 58 (3), 278–286. doi:10.1139/w11-132
- Jo, M., Noh, M. H., Lim, H. G., Kang, C. W., Im, D.-K., Oh, M.-K., et al. (2019). Precise tuning of the glyoxylate cycle in *Escherichia coli* for efficient tyrosine production from acetate. *Microb. Cell Fact.* 18 (1), 57–59. doi:10.1186/s12934-019-1106-0
- Kabisch, J., Pratzka, I., Meyer, H., Albrecht, D., Lalk, M., Ehrenreich, A., et al. (2013). Metabolic engineering of *Bacillus subtilis* for growth on overflow metabolites. *Microb. Cell Fact.* 12 (1), 72–10. doi:10.1186/1475-2859-12-72
- Kim, H. J., Kim, T. H., Kim, Y., and Lee, H. S. (2004). Identification and characterization of *glxR*, a gene involved in regulation of glyoxylate bypass in *Corynebacterium glutamicum*. *J. Bacteriol.* 186 (11), 3453–3460. doi:10.1128/JB.186.11.3453-3460.2004
- Kocharin, K., Chen, Y., Siewers, V., and Nielsen, J. (2012). Engineering of acetyl-CoA metabolism for the improved production of polyhydroxybutyrate in *Saccharomyces cerevisiae*. *Amb. Express* 2 (1), 52–11. doi:10.1186/2191-0855-2-52
- Koivistoinen, O. M., Kuivanen, J., Barth, D., Turkia, H., Pitkänen, J.-P., Penttilä, M., et al. (2013). Glycolic acid production in the engineered yeasts *Saccharomyces cerevisiae* and *Kluyveromyces lactis*. *Microb. Cell Fact.* 12 (1), 82–16. doi:10.1186/1475-2859-12-82
- Kornberg, H. L., and Krebs, H. A. (1957). Synthesis of cell constituents from C₂-units by a modified tricarboxylic acid cycle. *Nature* 179 (4568), 988–991. doi:10.1038/179988a0
- Krivoruchko, A., Serrano-Amatriain, C., Chen, Y., Siewers, V., and Nielsen, J. (2013). Improving biobutanol production in engineered *Saccharomyces cerevisiae* by manipulation of acetyl-CoA metabolism. *J. Ind. Microbiol. Biotechnol.* 40 (9), 1051–1056. doi:10.1007/s10295-013-1296-0
- Kroner, G. M., Wolfe, M. B., and Freddolino, P. L. (2019). *Escherichia coli* Lrp regulates one-third of the genome via direct, cooperative, and indirect routes. *J. Bacteriol.* 201 (3), e00411–e00418. doi:10.1128/JB.00411-18
- Lai, N., Luo, Y., Fei, P., Hu, P., and Wu, H. (2021). One stone two birds: Biosynthesis of 3-hydroxypropionic acid from CO₂ and syngas-derived acetic acid in *Escherichia coli*. *Synthetic Syst. Biotechnol.* 6 (3), 144–152. doi:10.1016/j.synbio.2021.06.003
- Lama, S., Kim, Y., Nguyen, D. T., Im, C. H., Sankaranarayanan, M., and Park, S. (2021). Production of 3-hydroxypropionic acid from acetate using metabolically-engineered and glucose-grown *Escherichia coli*. *Bioresour. Technol.* 320, 124362. doi:10.1016/j.biortech.2020.124362
- LaPorte, D. C., Thorsness, P. E., and Koshland, D. E. (1985). Compensatory phosphorylation of isocitrate dehydrogenase. A mechanism for adaptation to the intracellular environment. *J. Biol. Chem.* 260 (19), 10563–10568. doi:10.1016/S0021-9258(19)85122-0
- Lee, J. H., Cha, S., Kang, C. W., Lee, G. M., Lim, H. G., and Jung, G. Y. (2018). Efficient conversion of acetate to 3-hydroxypropionic acid by engineered *Escherichia coli*. *Catalysts* 8 (11), 525. doi:10.3390/catal8110525
- Lee, S. S., Park, J., Heo, Y. B., and Woo, H. M. (2020). Case study of xylose conversion to glycolate in *Corynebacterium glutamicum*: Current limitation and future perspective of the CRISPR-Cas systems. *Enzyme Microb. Technol.* 132, 109395. doi:10.1016/j.enzmictec.2019.109395
- Lee, W., VanderVen, B. C., Walker, S., and Russell, D. G. (2017). Novel protein acetyltransferase, Rv2170, modulates carbon and energy metabolism in

Mycobacterium tuberculosis. *Sci. Rep.* 7 (1), 72–11. doi:10.1038/s41598-017-00067-1

Li, B., Cai, D., and Chen, S. (2021). Metabolic engineering of central carbon metabolism of *Bacillus licheniformis* for enhanced production of poly- γ -glutamic acid. *Appl. Biochem. Biotechnol.* 193 (11), 3540–3552. doi:10.1007/s12010-021-03619-4

Li, N., Zhang, B., Chen, T., Wang, Z., Tang, Y. J., and Zhao, X. (2013). Directed pathway evolution of the glyoxylate shunt in *Escherichia coli* for improved aerobic succinate production from glycerol. *J. Ind. Microbiol. Biotechnol.* 40 (12), 1461–1475. doi:10.1007/s12029-013-1342-y

Li, N., Zhang, B., Wang, Z., Tang, Y. J., Chen, T., and Zhao, X. (2014). Engineering *Escherichia coli* for fumaric acid production from glycerol. *Bioresour. Technol.* 174, 81–87. doi:10.1016/j.biortech.2014.09.147

Li, W., Chen, J., Liu, C.-X., Yuan, Q.-P., and Li, Z.-J. (2019). Microbial production of glycolate from acetate by metabolically engineered *Escherichia coli*. *J. Biotechnol.* 291, 41–45. doi:10.1016/j.jbiotec.2018.12.012

Li, Y., Huang, B., Wu, H., Li, Z., Ye, Q., and Zhang, Y. P. (2016). Production of succinate from acetate by metabolically engineered *Escherichia coli*. *ACS Synth. Biol.* 5 (11), 1299–1307. doi:10.1021/acssynbio.6b00052

Li, Y., Wei, H., Wang, T., Xu, Q., Zhang, C., Fan, X., et al. (2017). Current status on metabolic engineering for the production of L-aspartate family amino acids and derivatives. *Bioresour. Technol.* 245, 1588–1602. doi:10.1016/j.biortech.2017.05.145

Li, Z.-J., Qiao, K., Che, X.-M., and Stephanopoulos, G. (2017). Metabolic engineering of *Escherichia coli* for the synthesis of the quadripolymer poly (glycolate-co-lactate-co-3-hydroxybutyrate-co-4-hydroxybutyrate) from glucose. *Metab. Eng.* 44, 38–44. doi:10.1016/j.ymben.2017.09.003

Li, Z.-J., Qiao, K., Shi, W., Pereira, B., Zhang, H., Olsen, B. D., et al. (2016). Biosynthesis of poly (glycolate-co-lactate-co-3-hydroxybutyrate) from glucose by metabolically engineered *Escherichia coli*. *Metab. Eng.* 35, 1–8. doi:10.1016/j.ymben.2016.01.004

Lin, F., Chen, Y., Levine, R., Lee, K., Yuan, Y., and Lin, X. N. (2013). Improving fatty acid availability for bio-hydrocarbon production in *Escherichia coli* by metabolic engineering. *PLoS one* 8 (10), e78595. doi:10.1371/journal.pone.0078595

Lin, H., Bennett, G. N., and San, K. Y. (2005). Genetic reconstruction of the aerobic central metabolism in *Escherichia coli* for the absolute aerobic production of succinate. *Biotechnol. Bioeng.* 89 (2), 148–156. doi:10.1002/bit.20298

Liu, J., Li, J., Liu, Y., Shin, H.-d., Ledesma-Amaro, R., Du, G., et al. (2018). Synergistic rewiring of carbon metabolism and redox metabolism in cytoplasm and mitochondria of *Aspergillus oryzae* for increased L-malate production. *ACS Synth. Biol.* 7 (9), 2139–2147. doi:10.1021/acssynbio.8b00130

Liu, M., Ding, Y., Chen, H., Zhao, Z., Liu, H., Xian, M., et al. (2017). Improving the production of acetyl-CoA-derived chemicals in *Escherichia coli* BL21 (DE3) through *iclR* and *arcA* deletion. *BMC Microbiol.* 17 (1), 10–19. doi:10.1186/s12866-016-0913-2

Liu, M., Lou, J., Gu, J., Lyu, X.-M., Wang, F.-Q., and Wei, D.-Z. (2020). Increasing L-homoserine production in *Escherichia coli* by engineering the central metabolic pathways. *J. Biotechnol.* 314, 1–7. doi:10.1016/j.jbiotec.2020.03.010

Liu, M., Yao, L., Xian, M., Ding, Y., Liu, H., and Zhao, G. (2016). Deletion of *arcA* increased the production of acetyl-CoA-derived chemicals in recombinant *Escherichia coli*. *Biotechnol. Lett.* 38 (1), 97–101. doi:10.1007/s10529-015-1953-7

Liu, X., Zhao, G., Sun, S., Fan, C., Feng, X., and Xiong, P. (2022). Biosynthetic pathway and metabolic engineering of succinic acid. *Front. Bioeng. Biotechnol.* 10, 843887. doi:10.3389/fbioe.2022.843887

Lorca, G. L., Ezersky, A., Lunin, V. V., Walker, J. R., Altamentova, S., Evdokimova, E., et al. (2007). Glyoxylate and pyruvate are antagonistic effectors of the *Escherichia coli* *iclR* transcriptional regulator. *J. Biol. Chem.* 282 (22), 16476–16491. doi:10.1074/jbc.M610838200

Machado, D., and Herrgård, M. J. (2015). Co-evolution of strain design methods based on flux balance and elementary mode analysis. *Metab. Eng. Commun.* 2, 85–92. doi:10.1016/j.meten.2015.04.001

Maeda, T., and Wachi, M. (2012). 3' Untranslated region-dependent degradation of the *aceA* mRNA, encoding the glyoxylate cycle enzyme isocitrate lyase, by RNase E/G in *Corynebacterium glutamicum*. *Appl. Environ. Microbiol.* 78 (24), 8753–8761. doi:10.1128/AEM.02304-12

Mainguet, S. E., Gronenberg, L. S., Wong, S. S., and Liao, J. C. (2013). A reverse glyoxylate shunt to build a non-native route from C₄ to C₂ in *Escherichia coli*. *Metab. Eng.* 19, 116–127. doi:10.1016/j.ymben.2013.06.004

Martinez, I., Bennett, G. N., and San, K. Y. (2010). Metabolic impact of the level of aeration during cell growth on anaerobic succinate production by an engineered *Escherichia coli* strain. *Metab. Eng.* 12 (6), 499–509. doi:10.1016/j.ymben.2010.09.002

Masiewicz, P., Brzostek, A., Wolański, M., Dziadek, J., and Zakrzewska-Czerwińska, J. (2012). A novel role of the PrpR as a transcription factor

involved in the regulation of methylcitrate pathway in *Mycobacterium tuberculosis*. *PLoS one* 13 (12), e43651. doi:10.1371/journal.pone.0043651

Micklinghoff, J. C., Breiting, K. J., Schmidt, M., Geffers, R., Eikmanns, B. J., and Bange, F.-C. (2009). Role of the transcriptional regulator RamB (Rv0465c) in the control of the glyoxylate cycle in *Mycobacterium tuberculosis*. *J. Bacteriol.* 191 (23), 7260–7269. doi:10.1128/JB.01009-09

Mindt, M., Hannibal, S., Heuser, M., Risse, J. M., Sasikumar, K., Nampoothiri, K. M., et al. (2019a). Fermentative production of N-alkylated glycine derivatives by recombinant *Corynebacterium glutamicum* using a mutant of imine reductase DpkA from *Pseudomonas putida*. *Front. Bioeng. Biotechnol.* 7, 232. doi:10.3389/fbioe.2019.00232

Mindt, M., Heuser, M., and Wendisch, V. F. (2019b). Xylose as preferred substrate for sarcosine production by recombinant *Corynebacterium glutamicum*. *Bioresour. Technol.* 281, 135–142. doi:10.1016/j.biortech.2019.02.084

Miscevic, D., Mao, J.-Y., Kefale, T., Abedi, D., Huang, C.-C., Moo-Young, M., et al. (2020a). Integrated strain engineering and bioprocessing strategies for high-level bio-based production of 3-hydroxyvalerate in *Escherichia coli*. *Appl. Microbiol. Biotechnol.* 104 (12), 5259–5272. doi:10.1007/s00253-020-10580-5

Miscevic, D., Mao, J.-Y., Mozell, B., Srirangan, K., Abedi, D., Moo-Young, M., et al. (2021a). Bio-based production of poly (3-hydroxybutyrate-co-3-hydroxyvalerate) with modulated monomeric fraction in *Escherichia coli*. *Appl. Microbiol. Biotechnol.* 105 (4), 1435–1446. doi:10.1007/s00253-021-11108-1

Miscevic, D., Mao, J. Y., Kefale, T., Abedi, D., Moo-Young, M., and Perry Chou, C. (2021b). Strain engineering for high-level 5-aminolevulinic acid production in *Escherichia coli*. *Biotechnol. Bioeng.* 118 (1), 30–42. doi:10.1002/bit.27547

Miscevic, D., Mao, J. Y., Moo-Young, M., and Chou, C. H. P. (2020b). High-level heterologous production of propionate in engineered *Escherichia coli*. *Biotechnol. Bioeng.* 117 (5), 1304–1315. doi:10.1002/bit.27276

Miscevic, D., Srirangan, K., Kefale, T., Kilpatrick, S., Chung, D. A., Moo-Young, M., et al. (2020c). Heterologous production of 3-hydroxyvalerate in engineered *Escherichia coli*. *Metab. Eng.* 61, 141–151. doi:10.1016/j.ymben.2019.11.005

Munoz-Elias, E. J., and McKinney, J. D. (2005). *Mycobacterium tuberculosis* isocitrate lyases 1 and 2 are jointly required for *in vivo* growth and virulence. *Nat. Med.* 11 (6), 638–644. doi:10.1038/nm1252

Murima, P., Zimmermann, M., Chopra, T., Pojer, F., Fonti, G., Dal Peraro, M., et al. (2016). A rheostat mechanism governs the bifurcation of carbon flux in mycobacteria. *Nat. Commun.* 7, 12527. doi:10.1038/ncomms12527

Nguyen, D. T. N., Lee, O. K., Hadiyati, S., Affiah, A. N., Kim, M. S., and Lee, E. Y. (2019). Metabolic engineering of the type I methanotroph *Methylobacterium* sp. DH-1 for production of succinate from methane. *Metab. Eng.* 54, 170–179. doi:10.1016/j.ymben.2019.03.013

Ning, Y., Wu, X., Zhang, C., Xu, Q., Chen, N., and Xie, X. (2016). Pathway construction and metabolic engineering for fermentative production of ectoine in *Escherichia coli*. *Metab. Eng.* 36, 10–18. doi:10.1016/j.ymben.2016.02.013

Nitta, K., Laviña, W. A., Pontrelli, S., Liao, J. C., Putri, S. P., and Fukusaki, E. (2019). Metabolome analysis revealed the knockout of glyoxylate shunt as an effective strategy for improvement of 1-butanol production in transgenic *Escherichia coli*. *J. Biosci. Bioeng.* 127 (3), 301–308. doi:10.1016/j.jbiosc.2018.08.013

Noh, M. H., Lim, H. G., Park, S., Seo, S. W., and Jung, G. Y. (2017). Precise flux redistribution to glyoxylate cycle for 5-aminolevulinic acid production in *Escherichia coli*. *Metab. Eng.* 43, 1–8. doi:10.1016/j.ymben.2017.07.006

Noh, M. H., Lim, H. G., Woo, S. H., Song, J., and Jung, G. Y. (2018). Production of itaconic acid from acetate by engineering acid-tolerant *Escherichia coli* W. *Biotechnol. Bioeng.* 115 (3), 729–738. doi:10.1002/bit.26508

Ogawa, T., Murakami, K., Mori, H., Ishii, N., Tomita, M., and Yoshin, M. (2007). Role of phosphoenolpyruvate in the NADP-isocitrate dehydrogenase and isocitrate lyase reaction in *Escherichia coli*. *J. Bacteriol.* 189 (3), 1176–1178. doi:10.1128/JB.01628-06

Ohtake, T., Pontrelli, S., Laviña, W. A., Liao, J. C., Putri, S. P., and Fukusaki, E. (2017). Metabolomics-driven approach to solving a CoA imbalance for improved 1-butanol production in *Escherichia coli*. *Metab. Eng.* 41, 135–143. doi:10.1016/j.ymben.2017.04.003

Pereira, B., Li, Z.-J., De Mey, M., Lim, C. G., Zhang, H., Hoeltgen, C., et al. (2016). Efficient utilization of pentoses for bioproduction of the renewable two-carbon compounds ethylene glycol and glycolate. *Metab. Eng.* 34, 80–87. doi:10.1016/j.ymben.2015.12.004

Ren, J., Zhou, L., Wang, C., Lin, C., Li, Z., and Zeng, A.-P. (2018). An unnatural pathway for efficient 5-aminolevulinic acid biosynthesis with glycine from glyoxylate based on retrobiosynthetic design. *ACS Synth. Biol.* 7 (12), 2750–2757. doi:10.1021/acssynbio.8b00354

Salusjärvi, L., Havukainen, S., Koivistoinen, O., and Toivari, M. (2019). Biotechnological production of glycolic acid and ethylene glycol: Current state

and perspectives. *Appl. Microbiol. Biotechnol.* 103 (6), 2525–2535. doi:10.1007/s00253-019-09640-2

Sanchez, A. M., Bennett, G. N., and San, K. Y. (2005). Novel pathway engineering design of the anaerobic central metabolic pathway in *Escherichia coli* to increase succinate yield and productivity. *Metab. Eng.* 7 (3), 229–239. doi:10.1016/j.ymben.2005.03.001

Santala, S., Santala, V., Liu, N., and Stephanopoulos, G. (2021). Partitioning metabolism between growth and product synthesis for coordinated production of wax esters in *Acinetobacter baylyi* ADP1. *Biotechnol. Bioeng.* 118 (6), 2283–2292. doi:10.1002/bit.27740

Schada von Borzyskowski, L., Sonntag, F., Pöschel, L., Vorholt, J. A., Schrader, J., Erb, T. J., et al. (2018). Replacing the ethylmalonyl-CoA pathway with the glyoxylate shunt provides metabolic flexibility in the central carbon metabolism of *Methylobacterium extorquens* AM1. *ACS Synth. Biol.* 7 (1), 86–97. doi:10.1021/acssynbio.7b00229

Schwentner, A., Feith, A., Münch, E., Busche, T., Rückert, C., Kalinowski, J., et al. (2018). Metabolic engineering to guide evolution—Creating a novel mode for L-valine production with *Corynebacterium glutamicum*. *Metab. Eng.* 47, 31–41. doi:10.1016/j.ymben.2018.02.015

Shi, F., Zhang, S., Li, Y., and Lu, Z. (2019). Enhancement of substrate supply and *Ido* expression to improve 4-hydroxyisoleucine production in recombinant *Corynebacterium glutamicum* ssp. *Appl. Microbiol. Biotechnol.* 103 (10), 4113–4124. doi:10.1007/s00253-019-09791-2

Shimizu, T., Teramoto, H., and Inui, M. (2019). Introduction of glyoxylate bypass increases hydrogen gas yield from acetate and L-glutamate in *Rhodobacter sphaeroides*. *Appl. Environ. Microbiol.* 85 (2), e01873–e01818. doi:10.1128/AEM.01873-18

Skorokhodova, A. Y., Morzhakova, A. A., Gulevich, A. Y., and Debabov, V. G. (2015). Manipulating pyruvate to acetyl-CoA conversion in *Escherichia coli* for anaerobic succinate biosynthesis from glucose with the yield close to the stoichiometric maximum. *J. Biotechnol.* 214, 33–42. doi:10.1016/j.jbiotec.2015.09.003

Soma, Y., Fujiwara, Y., Nakagawa, T., Tsuruno, K., and Hanai, T. (2017). Reconstruction of a metabolic regulatory network in *Escherichia coli* for purposeful switching from cell growth mode to production mode in direct GABA fermentation from glucose. *Metab. Eng.* 43, 54–63. doi:10.1016/j.ymben.2017.08.002

Song, C. W., Kim, D. I., Choi, S., Jang, J. W., and Lee, S. Y. (2013). Metabolic engineering of *Escherichia coli* for the production of fumaric acid. *Biotechnol. Bioeng.* 110 (7), 2025–2034. doi:10.1002/bit.24868

Song, T., Wu, N., Wang, C., Wang, Y., Chai, F., Ding, M., et al. (2020). Crocetin overproduction in engineered *Saccharomyces cerevisiae* via tuning key enzymes coupled with precursor engineering. *Front. Bioeng. Biotechnol.* 8, 578005. doi:10.3389/fbioe.2020.578005

Srirangan, K., Akawi, L., Liu, X., Westbrook, A., Blondeel, E. J., Aucoin, M. G., et al. (2013). Manipulating the sleeping beauty mutase operon for the production of 1-propanol in engineered *Escherichia coli*. *Biotechnol. Biofuels* 6 (1), 139–214. doi:10.1186/1754-6834-6-139

Toyoda, K., Teramoto, H., Gunji, W., Inui, M., and Yukawa, H. (2013). Involvement of regulatory interactions among global regulators GlxR, SugR, and RamA in expression of *ramA* in *Corynebacterium glutamicum*. *J. Bacteriol.* 195 (8), 1718–1726. doi:10.1128/JB.00016-13

Trichez, D., Auriol, C., Baylac, A., Irague, R., Dressaire, C., Carnicer-Heras, M., et al. (2018). Engineering of *Escherichia coli* for Krebs cycle-dependent production of malic acid. *Microb. Cell Fact.* 17 (1), 113–212. doi:10.1186/s12934-018-0959-y

Vemuri, G. N., Eiteman, M. A., and Altman, E. (2002). Effects of growth mode and pyruvate carboxylase on succinic acid production by metabolically engineered strains of *Escherichia coli*. *Appl. Environ. Microbiol.* 68 (4), 1715–1727. doi:10.1128/aem.68.4.1715-1727.2002

Vuoristo, K. S., Mars, A. E., Sanders, J. P. M., Eggink, G., and Weusthuis, R. A. (2016). Metabolic engineering of tca cycle for production of chemicals. *Trends Biotechnol.* 34 (3), 191–197. doi:10.1016/j.tibtech.2015.11.002

Wang, P., Zhou, H.-Y., Li, B., Ding, W.-Q., Liu, Z.-Q., and Zheng, Y.-G. (2021). Multiplex modification of *Escherichia coli* for enhanced β -alanine biosynthesis through metabolic engineering. *Bioresour. Technol.* 342, 126050. doi:10.1016/j.biortech.2021.126050

Wei, L. N., Zhu, L. W., and Tang, Y. J. (2016). Succinate production positively correlates with the affinity of the global transcription factor Cra for its effector FBP in *Escherichia coli*. *Biotechnol. Biofuels* 9, 264. doi:10.1186/s13068-016-0679-7

Yang, J., Fang, Y., Wang, J., Wang, C., Zhao, L., and Wang, X. (2019). Deletion of regulator-encoding genes *fadR*, *fabR* and *iclR* to increase l-threonine production in *Escherichia coli*. *Appl. Microbiol. Biotechnol.* 103 (11), 4549–4564. doi:10.1007/s00253-019-09818-8

Yang, J., Yang, W., Feng, J., Chen, J., Jiang, M., and Zou, X. (2018). Enhanced polymeric acid production from the glyoxylate shunt pathway under exogenous alcohol stress. *J. Biotechnol.* 275, 24–30. doi:10.1016/j.jbiotec.2018.04.001

Yates, S. P., Edwards, T. E., Bryan, C. M., Stein, A. J., Van Voorhis, W. C., Myler, P. J., et al. (2011). Structural basis of the substrate specificity of bifunctional isocitrate dehydrogenase kinase/phosphatase. *Biochemistry* 50 (38), 8103–8106. doi:10.1021/bi200809p

Yu, H., Li, X., Duchoud, F., Chuang, D. S., and Liao, J. C. (2018). Augmenting the Calvin–Benson–Bassham cycle by a synthetic malyl-CoA-glycerate carbon fixation pathway. *Nat. Commun.* 9 (1), 2008–2010. doi:10.1038/s41467-018-04417-z

Yu, H., and Liao, J. C. (2018). A modified serine cycle in *Escherichia coli* converts methanol and CO₂ to two-carbon compounds. *Nat. Commun.* 9 (1), 3992–4010. doi:10.1038/s41467-018-06496-4

Zahoor, A., Otten, A., and Wendisch, V. F. (2014). Metabolic engineering of *Corynebacterium glutamicum* for glycolate production. *J. Biotechnol.* 192, 366–375. doi:10.1016/j.jbiotec.2013.12.020

Zeng, A.-P. (2019). New bioproduction systems for chemicals and fuels: Needs and new development. *Biotechnol. Adv.* 37 (4), 508–518. doi:10.1016/j.biotechadv.2019.01.003

Zeng, W., Zhang, B., Chen, G., Li, M., and Liang, Z. (2019). Efficient production of polymeric acid by a novel isolated *Aureobasidium pullulans* using metabolic intermediates and inhibitors. *Appl. Biochem. Biotechnol.* 187 (2), 612–627. doi:10.1007/s12010-018-2825-0

Zhang, K., Mohsin, A., Dai, Y., Chen, Z., Zhuang, Y., Chu, J., et al. (2019). Combinatorial effect of ARTP mutagenesis and ribosome engineering on an industrial strain of *Streptomyces albus* S12 for enhanced biosynthesis of salinomycin. *Front. Bioeng. Biotechnol.* 7, 212. doi:10.3389/fbioe.2019.00212

Zhang, S., and Bryant, D. A. (2015). Biochemical validation of the glyoxylate cycle in the cyanobacterium *Chlorogloeopsis fritschii* strain PCC 9212. *J. Biol. Chem.* 290 (22), 14019–14030. doi:10.1074/jbc.M115.648170

Zhao, H., Fang, Y., Wang, X., Zhao, L., Wang, J., and Li, Y. (2018). Increasing L-threonine production in *Escherichia coli* by engineering the glyoxylate shunt and the L-threonine biosynthesis pathway. *Appl. Microbiol. Biotechnol.* 102 (13), 5505–5518. doi:10.1007/s00253-018-9024-3

Zhou, S., Lama, S., Jiang, J., Sankaranarayanan, M., and Park, S. (2020). Use of acetate for the production of 3-hydroxypropionic acid by metabolically-engineered *Pseudomonas denitrificans*. *Bioresour. Technol.* 307, 123194. doi:10.1016/j.biortech.2020.123194

Zhu, L., Fang, Y., Ding, Z., Zhang, S., and Wang, X. (2019). Developing an l-threonine-producing strain from wild-type *Escherichia coli* by modifying the glucose uptake, glyoxylate shunt, and l-threonine biosynthetic pathway. *Biotechnol. Appl. Biochem.* 66 (6), 962–976. doi:10.1002/bab.1813

Zhu, N., Xia, H., Yang, J., Zhao, X., and Chen, T. (2014a). Improved succinate production in *Corynebacterium glutamicum* by engineering glyoxylate pathway and succinate export system. *Biotechnol. Lett.* 36 (3), 553–560. doi:10.1007/s10529-013-1376-2



OPEN ACCESS

EDITED BY

Qi Xianghui,
Jiangsu University, China

REVIEWED BY

Mostafa Sobhi,
Alexandria University, Egypt
Feng Wang,
Jiangsu University, China

*CORRESPONDENCE

Yongqian Fu,
✉ bioengineer@163.com

SPECIALTY SECTION

This article was submitted to Industrial Biotechnology, a section of the journal Frontiers in Bioengineering and Biotechnology

RECEIVED 15 December 2022

ACCEPTED 23 December 2022

PUBLISHED 09 January 2023

CITATION

Sun X, Hu J, Wang Y, Luo X, Huang H and Fu Y (2023), One-pot encapsulation of lactate dehydrogenase and Fe₃O₄ nanoparticles into a metal–organic framework: A novel magnetic recyclable biocatalyst for the synthesis of D-phenyllactic acid.
Front. Bioeng. Biotechnol. 10:1124450.
doi: 10.3389/fbioe.2022.1124450

COPYRIGHT

© 2023 Sun, Hu, Wang, Luo, Huang and Fu. This is an open-access article distributed under the terms of the Creative Commons Attribution License (CC BY). The use, distribution or reproduction in other forums is permitted, provided the original author(s) and the copyright owner(s) are credited and that the original publication in this journal is cited, in accordance with accepted academic practice. No use, distribution or reproduction is permitted which does not comply with these terms.

One-pot encapsulation of lactate dehydrogenase and Fe₃O₄ nanoparticles into a metal–organic framework: A novel magnetic recyclable biocatalyst for the synthesis of D-phenyllactic acid

Xiaolong Sun^{1,2}, Jiahuan Hu², Yifeng Wang³, Xi Luo², He Huang^{1,3} and Yongqian Fu^{2*}

¹State Key Laboratory of Material-Oriented Chemical Engineering, School of Pharmaceutical Sciences, Nanjing Tech University, Nanjing, China, ²Taizhou Key Laboratory of Biomass Functional Materials Development and Application, Taizhou University, Taizhou, China, ³School of Food Science and Pharmaceutical Engineering, Nanjing Normal University, Nanjing, China

The main challenges in bio-catalysis of D-phenyllactic acid (D-PLA) are poor tolerance of lactate dehydrogenase (LDH) to harsh environmental conditions and inability to recycle the catalyst. A novel magnetic framework composite was prepared as solid support for the immobilization of enzymes *via* one-pot encapsulation in this study. LDH/MNPs@MAF-7 was synthesized by the one-pot encapsulation of both LDH and magnetic nanoparticles (MNPs) in MAF-7. The LDH/MNPs@MAF-7 showed stable biological activity for the efficient biosynthesis of D-PLA. The structure and morphology of LDH/MNPs@MAF-7 were systematically characterized by SEM, FT-IR, XRD, VSM, XPS, TGA and N₂ sorption. These indicated that LDH/MNPs@MAF-7 was successfully synthesized, exhibiting enhanced resistance to acid and alkali, temperature and organic solvents. Furthermore, the bio-catalyst could be separated easily using a magnet, and the reusability was once considerably expanded with 80% of enzyme activity last after eight rounds of recycling. Therefore, LDH/MNPs@MAF-7 could be used as a potential biocatalyst for the biosynthesis of D-PLA due to its good stability and recovery properties.

KEYWORDS

biocatalyst, d-phenyllactic acid, lactate dehydrogenase, LDH/MNPs@MAF-7, magnetic nanoparticles

1 Introduction

D-phenyllactic acid (D-PLA) has been validated to have inhibitory effects against yeast and a huge variety of molds, together with some mycotoxigenic species (Lavermicocca et al., 2000; Lavermicocca et al., 2003), which gives it great application potential in the food and medicine related fields. Recently, D-PLA has attracted more attention due to the raised food safety awareness (Wu et al., 2021), but the yield of D-PLA that can be obtained through direct microbial fermentation remains low. Nowadays, lactate dehydrogenase (LDH) is expressed in *Escherichia coli* (*E. coli*) to produce D-PLA using phenylpyruvic acid (PPA) as substrate (Luo et al., 2020b). However, enzymes are limited used in industrial applications for various reasons (Torkzadeh-Mahani et al., 2020), including high cost, low substrate or product tolerance, poor stability in harsh environments, and poor reusability, which limit their practical applications

(Sirisha et al., 2016; Du et al., 2022). An effective and common way to extend the tolerance of enzymes is the use of immobilization technology (Chen et al., 2019). In a study by Wang K. et al. (2022), a nascent α -amylase nano-biocatalytic system was constructed using the natural nanostructured mineral montmorillonite, and the prepared immobilized α -amylase exhibited greater stability and higher catalytic activity over a harsh environment. Similarly, Ahmed et al. (2018) successfully fabricated Cellulase@UiO-66-NH₂, which exhibited a significant improvement in tolerance of temperature, pH, reusability and lifetime. Immobilization is an effective tool for enzyme preservation and continuous operation (Siar et al., 2017; Alagoz et al., 2021; Wei et al., 2021).

Metal-organic frameworks (MOFs) have attracted increasing attention as carriers in immobilization systems of enzyme due to their excellent features such as high surface area and favorable biocompatibility, well-defined pore and crystal structure (Du et al., 2022). Nadar and Rathod (2020) encapsulated a lipase inside a ZIF-8 using a biomineralization method. The synthesized immobilized lipase-proline showed a 135% increase in catalytic activity and 4-fold improvement of thermal stability compared to the free enzyme. Wei et al. (2021) first constructed renewable and magnetic MOFs (immobilized β -glucuronidase), and the immobilized enzymes exhibited greater stability over a wide range of temperatures and pH. Liang et al. (2021) noted that immobilized enzymes to hydrophilic ZIF-90 or MAF-7 could maintain enzyme activity, even when exposed to harsh reaction environment. Due to the features mentioned above, encapsulating enzymes in MOFs is an increasingly popular method for enzyme immobilization and protection (Tranchemontagne et al., 2009; Hirai et al., 2014). Especially, zeolitic metal-azolate framework-7 (MAF-7) is one of the most concerned MOFs for enzyme immobilization due to its high stability.

For the sake of simplicity in the downstream separation and recovery operations of enzymatic catalyzed processes, magnetic nanoparticles (MNPs) such as Fe₃O₄, have been co-captured in MOFs together with enzyme. Cao et al. (2022) suggested that the presence of Fe₃O₄ nanoparticles could influence the electron spin state of intermediates and promote enzyme activation through a magnetic induction effect during the reaction process. They immobilized the laccase on magnetic framework composite, and the removal rate of 2,4-dichlorophenol is still more than 80% after nine times of recycling. The prepared magnetic framework composites (MFCs) can be easily recovered by magnet with minimal losses, and the recovered lysozyme or α -amylase/MNP@MOF can often retain stable activity (Li et al., 2020).

To our best knowledge, there are no studies on the biosynthesis of D-PLA using magnetic framework composite, which encapsulated both LDH and MNPs. Therefore, in this work, we attempted to synthesis a novel magnetic framework composite for immobilization of LDH as a biocatalyst to catalyze the synthesis of PLA. On this basis, we tried to characterize the structure and morphology of the MFCs using FTIR, XRD, etc. Meanwhile, in order to evaluate the stability of this magnetic catalyst, the association between reaction environment (temperature, pH, solvent) and enzyme activity was also investigated. This modification method could probably provide viable ideas for the construction and performance optimization of enzyme immobilization composite in the future.

2 Material and methods

2.1 Materials

3-methyl-1,2,4-triazole (Adamas-beta, Hmtz), zinc nitrate hexahydrate (Sinopharm Chemical Reagent Co., Ltd., Zn(NO₃)₂·6H₂O), NH₃·H₂O (25%, Macklin), sodium phenylpyruvate (PPA, Aladdin), Fe₃O₄ (Aladdin), Bradford protein detection kit (TaKaRa). None of the chemicals were further purified before usage.

2.2 Synthesis of LDH/MNPs@MAF-7

The expression and purification of D-LDH (hereinafter referred to as LDH) refer to the previous research methods of our laboratory (Luo et al., 2020a). The LDH expression strain was grown and induced expression in Luria-Bertani (LB) medium containing 50 μ g mL⁻¹ kanamycin. Cells were collected by centrifugation and LDH crude enzyme solution was obtained from lysed cells. The LDH crude enzyme was purified using Ni²⁺-nitrilotriacetic acid column (1.6 cm \times 10 cm, BioRad, United States). And then dialyzed overnight against 20 mM potassium phosphate buffer (pH 8.0) to obtain purified LDH. See support information for specific experimental steps (S 1.1 Expression and purification of D-lactate dehydrogenase).

LDH/MNPs@MAF-7 was synthesized in an aqueous system (total volume was 4 ml) comprising Zn(NO₃)₂·6H₂O (40 mM), Hmtz (120 mM), Fe₃O₄ (20 mM), NH₃·H₂O (10%, 60 μ L) and the indicated concentration of LDH at 25°C under stirring (200 rpm) for 24 h. The obtained material was recovered with magnets, washed thoroughly in distilled water and repeated three times to remove loosely adsorbed LDH.

2.3 Characterization of LDH/MNPs@MAF-7

2.3.1 Scanning electron microscopy (SEM) analysis

The SEM observations of samples were performed on scanning electron microscope (Hitachi S-4800, Japan) with an acceleration voltage set to 30 kV. Before the SEM analysis, the samples are fixed on a stainless-steel frame and sprayed with gold using an ion sprayer. And the elemental composition was also measured by Hitachi S-4800 equipped with energy-disperse spectrometer (EDS) attachment.

2.3.2 FT-IR analysis

The FT-IR spectra of samples were determined by Fourier transform infrared spectrometer (Nicolet 5,700, Thermo Nicolet, United States of America). Each sample was mixed with 200 mg of anhydrous KBr and pressed into pellets, which were scanned and analyzed 16 times on the FT-IR spectroscopy to record the spectra in the frequency range of 400–4,000 cm⁻¹ at a resolution of 4 cm⁻¹.

2.3.3 X-ray diffraction (XRD) analysis

XRD patterns of MAF-7, MNPs@MAF-7, and LDH/MNPs@MAF-7 were recorded using D8 Advance diffractometer (Bruker, Germany) under the following operating conditions: 40 kV and 40 mA with acceptance slot at 0.1 mm and Cu K α radiation at λ = 0.15405 nm. The relative intensity was recorded in the scattering range of 5–80°2 θ at a step of 10°min.

2.3.4 Vibrating-sample magnetometer (VSM) analysis

The magnetic properties of samples were analyzed with a PPMS-9T vibrating sample magnetometer (Quantum Design, United States) at room temperature. The range of varying magnetic field during scanning is from $-20,000$ to $20,000$ Oe. The default sample vibration frequency for the test was 40 Hz.

The VSM curves were measured at room temperature under a varying magnetic field from $-20,000$ to $20,000$ Oe on a PPMS-9T vibrating sample magnetometer (Quantum Design, United States).

2.3.5 X-ray photoelectron spectroscopy (XPS) analysis

The XPS measurement was measured with ESCALAB 250Xi spectrometer (Thermo Scientific, United States of America). The test passing-energy was 50 eV, the step length was 0.05 eV, and the combined Energy standard C 1s = 284.80 eV was used for charge correction.

2.3.6 Thermogravimetric analysis (TGA)

TGA data were collected on a synchronous thermal analyzer (STA) (TGA/DSC, Mettler Toledo, Switzerland). Samples were heated from room temperature to 900°C at a rate of $10^{\circ}\text{C}/\text{min}$. Samples were heated at a constant airflow rate.

2.3.7 Nitrogen adsorption analysis

Nitrogen adsorption and desorption isotherms were recorded on an ASAP-2020-HD88 (Micromeritics, United States) surface characterization analyzer. Approximately 20 mg sample was degassed under dynamic vacuum (12°h , 105°C). After that, the analytical experiments were performed at 277 K.

2.4 Enzyme activity measurement of LDH/MNPs@MAF-7

The enzyme activity was measured by measuring the concentration of D-PLA catalyzed, using PPA (20 mM) and NADH (20 mM) as substrate. HPLC was used for detecting the concentration of D-PLA (Luo et al., 2020a). Specific test conditions refer to the laboratory published literature (Wang Y. et al., 2022). The standard curve of enzyme activity assay is shown in Supplementary Figure S3.

2.5 Stability analysis of LDH/MNPs@MAF-7

2.5.1 Temperature stability

LDH/MNPs@MAF-7 was incubated at 40° – 80°C for 20 min in tris-HCl buffer, and the residual activity was compared with the control incubated at 30°C .

2.5.2 pH stability

LDH/MNPs@MAF-7 has incubated buffers with the indicated pH values (4–10) for 20 min. The treated materials were recovered with magnets and washed thoroughly with distilled water.

2.5.3 Organic solvent stability

LDH/MNPs@MAF-7 was incubated in the presence of different organic solvents, including dimethyl sulfoxide (DMSO), N,

N-dimethylformamide (DMF), and dichloromethane (DCM) for 15 min. The treated materials were collected with magnets and washed thoroughly with distilled water.

2.6 Reusability

LDH/MNPs@MAF-7 was repeated eight times and the residual activity was measured after each use. After each cycle, it was collected with magnets, then added with a new substrate solution (20 mM PPA and NADH) to start a new catalytic reaction.

3 Results and discussion

3.1 One-pot encapsulation strategy for immobilizing LDH

By adopting a one-pot encapsulation strategy, we encapsulated the LDH and MNPs into MAF-7 frame. The performances of the LDH/MNPs@MAF-7 composite were evaluated under various conditions using the preparation of D-PLA as a model reaction (Figure 1).

3.2 SEM analysis

The ultrastructural characteristics of MAF-7 (Figure 2A), MNPs@MAF-7 (Figure 2B), and LDH/MNPs@MAF-7 (Figure 2C) were observed *via* SEM. The MAF-7 particles displayed a typical dodecahedral structure with a diameter of approximately 2–10 μm .

As shown in Figure 2C, LDH/MNPs@MAF-7 exhibited a roughly spherical shape. This may be due to a number of the enzyme is encapsulated and some is exposed. According to the SEM images, the particle sizes of LDH/MNPs@MAF-7 were smaller than those of MAF-7 and MNPs@MAF-7, which might be due to the enzyme immobilization. Ji et al. (2021) observed a similar phenomenon when encapsulating lipase and Fe_3O_4 in ZIF-8. Additionally, elemental mapping (Figures 2D–G) demonstrated that the sample contains nitrogen, zinc, iron, and phosphorus, which is in good agreement with the expected chemical composition of LDH/MNPs@MAF-7.

3.3 FT-IR analysis

The FT-IR bands corresponding to the different functional groups of MAF-7, MNPs@MAF-7, and LDH/MNPs@MAF-7 are indicated in Figure 3. In the FT-IR spectrum of MAF-7, the strong peaks around 424, 1,640 and $2,930\text{ cm}^{-1}$ could correspond to the stretching vibrations of Zn-N, C-N, and imidazole C-H, respectively (Tian et al., 2020; Wang Q. et al., 2022). Several bands were observed in the broad region of $2,500$ – $3,500\text{ cm}^{-1}$, which corresponded to the stretching vibrations of N-H, O-H, and C-H. In the FT-IR spectra of Fe_3O_4 particles, a well-defined band near 600 cm^{-1} indicated the presence of Fe-O bonds. The FT-IR spectrum of MAF-7 was consistent with that of MNPs@MAF-7 and LDH/MNPs@MAF-7, barring the peak around 600 cm^{-1} (Fe-O). Thus, the FT-IR spectra indicated that both LDH and Fe_3O_4 were successfully immobilized in the MAF-7.

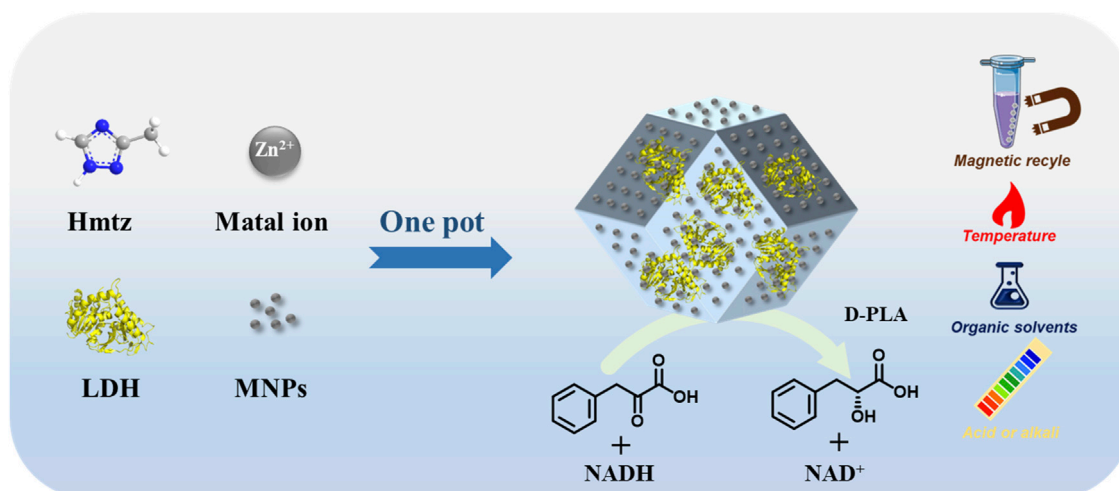


FIGURE 1
The synthesis of the biocatalyst LDH/MNPs@MAF-7 and the catalytic activity evaluation.

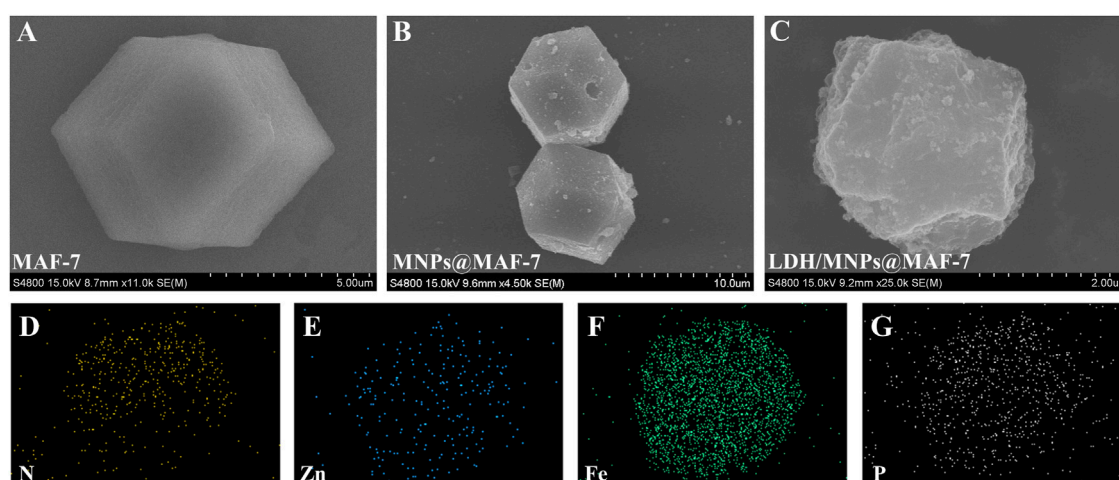


FIGURE 2
SEM spectra of (A) MAF-7 (B) MNPs@MAF-7, and (C) LDH/MNPs@MAF-7; elemental mapping (D–G) of LDH/MNPs@MAF-7.

3.4 XRD analysis

XRD analysis was performed using pure MAF-7, Fe_3O_4 , MNPs@MAF-7, and LDH/MNPs@MAF-7 (Figure 4). Compare to MAF-7, it showed a slightly decreased in the intensity of the characteristic diffraction peaks of LDH/MNPs@MAF-7. It is possibly because that part of MAF-7 sites is occupied by enzyme molecules, which partly disorganized the crystalline structure of the MOF. In addition, the XRD pattern of Fe_3O_4 nanoparticles showed six characteristic peaks at 2θ values of 30.26° , 35.74° , 43.22° , 53.32° , 57.24° and 62.8° , respectively corresponding to planes (220) (311) (400) (422) (511) and (440) of the face-centered cubic spinel Fe_3O_4 structure (Nosike et al., 2020). The XRD patterns collected for LDH/MNPs@MAF-7 indicated that the crystal structure of MAF-7 was not influenced by enzyme and magnetic nanoparticles immobilization.

3.5 Magnetic properties

The VSM with the corresponding field of $-20 \text{ KOe} \sim 20 \text{ KOe}$ was employed to study the magnetic properties of prepared MNPs@MAF-7 and LDH/MNPs@MAF-7 at 300 K. As shown in Figure 5, the appeared magnetism increased with the external magnetic field until the saturation magnetization of the MNPs@MAF-7 and LDH/MNPs@MAF-7 was reached at $M_s = 13.65$ and 8.98 emu/g . This value was much smaller than that of bulk Fe_3O_4 (76.2 emu/g), and the magnetization of Fe_3O_4 was basically consistent with that reported in the literature (81.3 emu/g) (Ge et al., 2020). This indicates that the MAF-7 and LDH shell does not contribute to the magnetization, resulting in a smaller magnetic moment per unit mass. However, a strong response to an external magnetic field was still observed (inset of Figure 5A). After the significant amplification, the coercivity

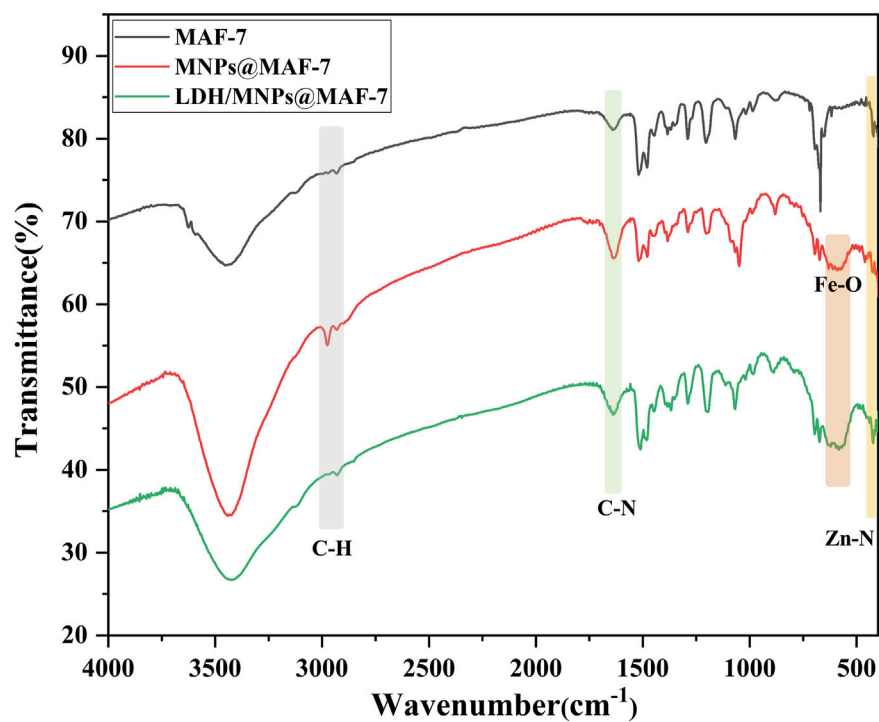


FIGURE 3
FT-IR spectra of MAF-7, MNPs@MAF-7, and LDH/MNPs@MAF-7.

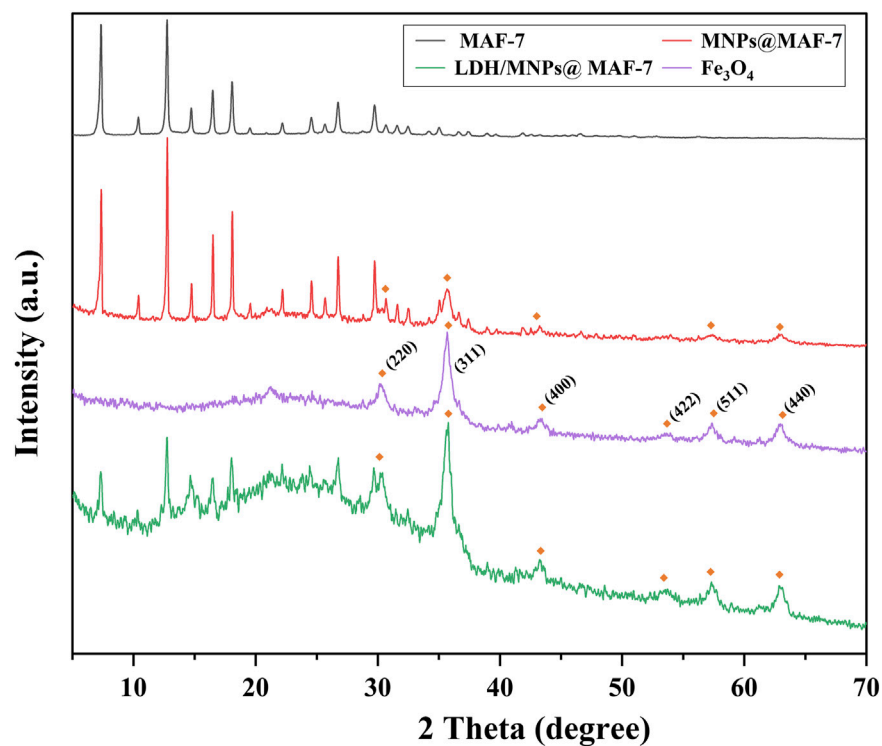


FIGURE 4
XRD patterns of MAF-7, MNPs@MAF-7, and LDH/MNPs@MAF-7.

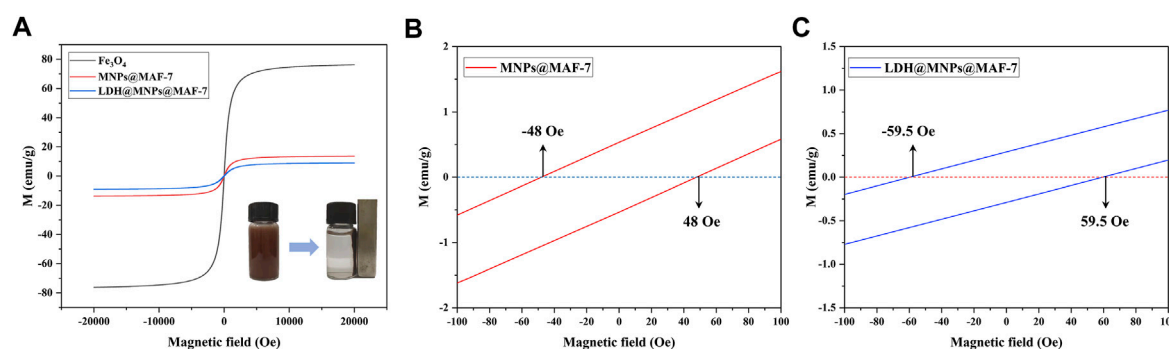


FIGURE 5

(A) Magnetic properties of Fe₃O₄, MNPs@MAF-7 and LDH/MNPs@MAF-7 at 300 K (Right inset: separation of the LDH/MNPs@MAF-7 particles from aqueous solution using an external magnetic field) (B) The magnified curves of MNPs@MAF-7 between -100 and 100 Oe (C) The magnified curves of LDH/MNPs@MAF-7 between -100 and 100 Oe.

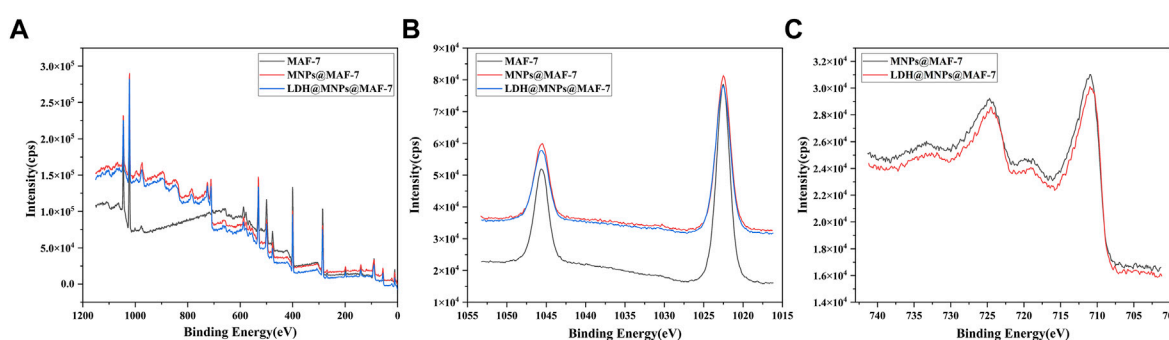


FIGURE 6

(A) XPS spectra of MAF-7, MNPs@MAF-7 and LDH/MNPs@MAF-7 (B) XPS spectra of Zn 2p in MAF-7, MNPs@MAF-7 and LDH/MNPs@MAF-7; and (C) XPS spectra of Fe 2p in MNPs@MAF-7 and LDH/MNPs@MAF-7.

(defined as the field magnitude necessary to obtain $M = 0$) was as low as 48 and 59.5 Oe, respectively, indicating that the microspheres can be easily dispersed in the absence of an external magnetic field. This directly demonstrates that the LDH/MNPs@MAF-7 possess strong magnetic properties. It will be easy and efficient to separate LDH/MNPs@MAF-7 particles from the reaction system.

3.6 XPS analysis

The MAF-7, MNPs@MAF-7 and LDH/MNPs@MAF-7 were analyzed by X-ray photoelectron spectroscopy to investigate the composition as well as the chemical state. In Figure 6A, similar coordination of Zn and N was present in MNPs@MAF-7 and LDH/MNPs@MAF-7 as in MAF-7. The peak at 1,022.48 eV corresponded to Zn 2p peak (Figure 6B), slightly higher than the standard binding energy of Zn²⁺ (1,022 eV), which also indicated that the chemical environment of Zn is dominated by N-coordination (Wang J. et al., 2020). As illustrated in Figure 6C, there are two characteristic peaks at 710.92 and 724.68 eV, which were interpreted as the Fe 2p peaks of Fe₃O₄. As demonstrated in Supplementary Table

S2, we calculated the chemical composition of the elements (C, N, Zn, P, Fe) through the integration of the peak areas. The existence of Fe and P suggested the successful encapsulation of MNP and LDH.

3.7 TGA analysis

The TGA curves exhibited two platforms, meaning two obvious mass loss phases (Figure 7). The initial weight loss phases (start from 30 to 400°C) may corresponded to the removal of water molecules and unreacted materials from the pores (Wang Y. et al., 2022).

The deformation of frame probably accounted for the second mass loss phase (from 400 to 850°C), which was more conspicuous in LDH/MNPs@MAF-7 (Wang L. et al., 2020). After heating to 850°C, the remaining weight of LDH/MNPs@MAF-7 and MNPs@MAF-7 was 32.6 and 45.7%, respectively. This can be explained by the loss of protein, which illustrates that LDH is successfully encapsulated in MAF-7 framework (Shieh et al., 2013; Shieh et al., 2015). According to the results of TGA, the loading efficiency of the enzyme in LDH/MNPs@MAF-7 was 12.1%.

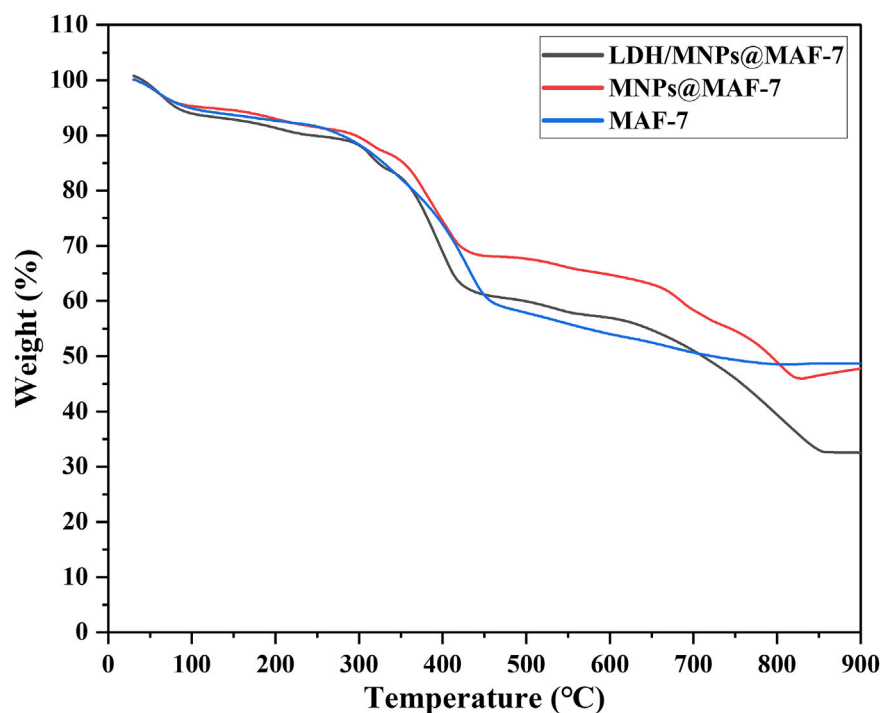


FIGURE 7
Thermogravimetric analysis (TGA) of MAF-7, MNPs@MAF-7 and LDH/MNPs@MAF-7.

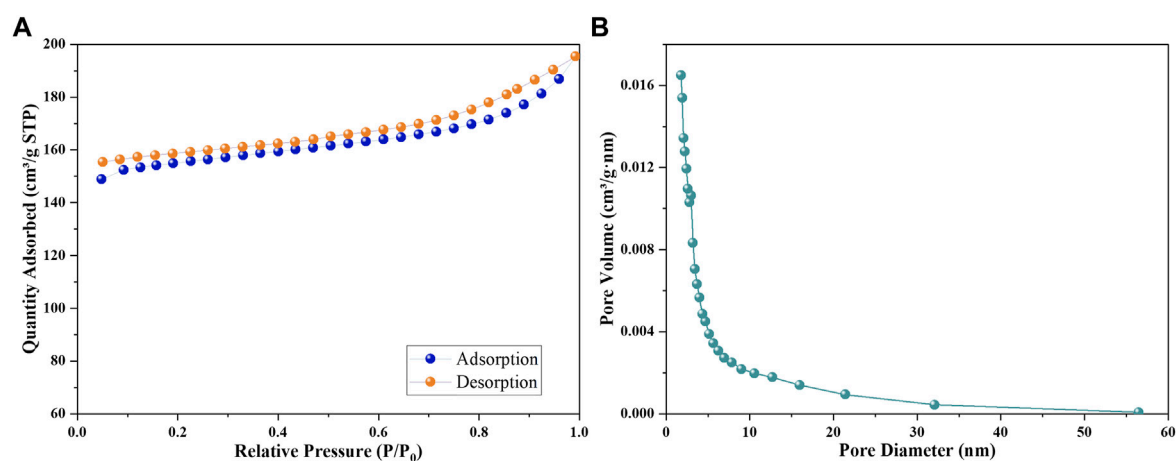


FIGURE 8
(A) N_2 adsorption-desorption isotherms of LDH/MNPs@MAF-7 (B) The pore size distribution of LDH/MNPs@MAF-7.

3.8 Nitrogen adsorption analysis

In order to investigate the BET surface area and pore structure of MAF-7 (Figure 8A), MNPs@MAF-7 (Figure 8B) and LDH/MNPs@MAF-7 (Figure 8C), the N_2 adsorption and desorption experiments were conducted. The isotherms were categorized as a type-II hysteresis loop attributed to the microporous structure of LDH/MNPs@MAF-7, which is similar to the isotherms of MAF-7. The specific surface area of

LDH/MNPs@MAF-7 was $\sim 511 \text{ m}^2/\text{g}$, which was smaller than MNPs@MAF-7 ($\sim 755 \text{ m}^2/\text{g}$) and MAF-7 ($\sim 1,115 \text{ m}^2/\text{g}$), due to the encapsulation of LDH and MNPs (Schejn et al., 2015; Wang L. et al., 2020). Further comparison of the pore diameters of LDH/MNPs@MAF-7, MNPs@MAF-7 and MAF-7 (Figure 8D) suggested that LDH/MNPs@MAF-7 and MNPs@MAF-7 had similar pore structure with MAF-7, illuminating good structural preservation during the encapsulation process.

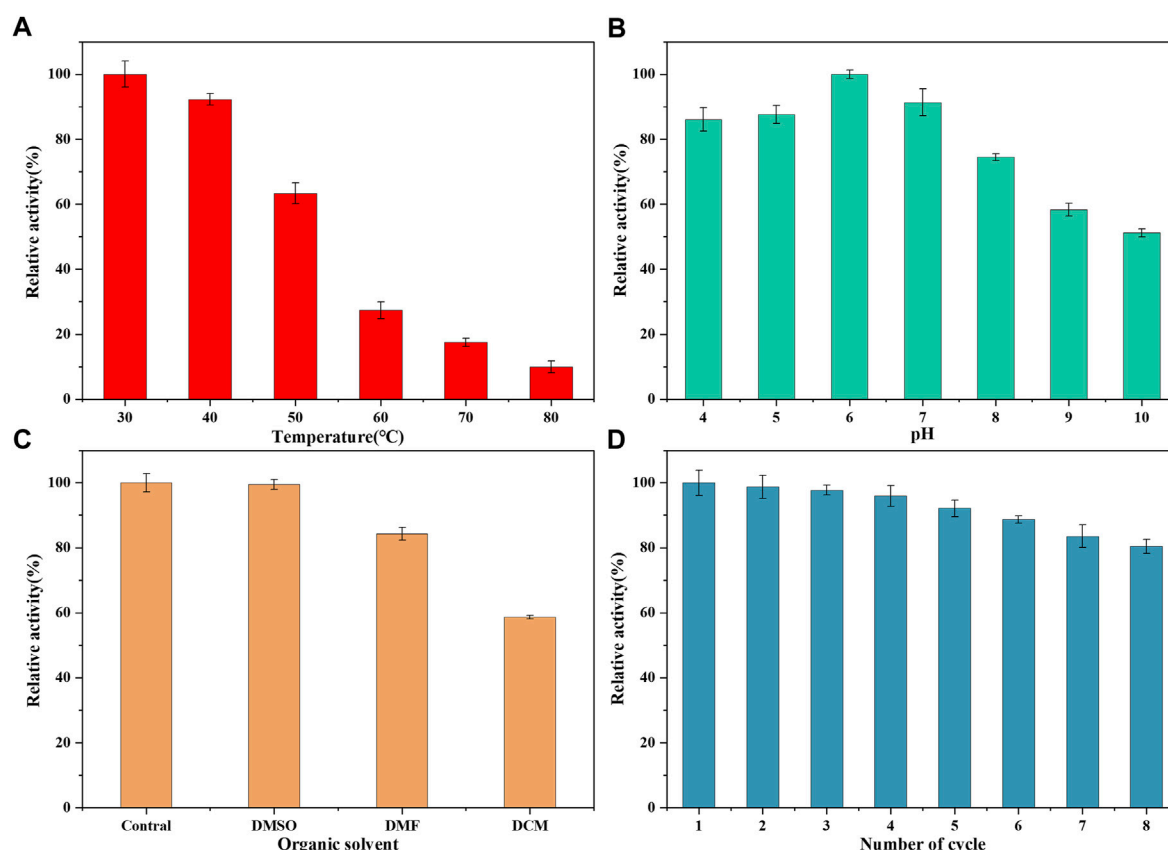


FIGURE 9

(A) Activity of LDH/MNPs@MAF-7 after incubation at the indicated temperatures for 20 min (B) Activity of LDH/MNPs@MAF-7 after incubation at different pH values for 20 min (C) Organic solvent stability of LDH/MNPs@MAF-7 (D) Reusability of LDH/MNPs@MAF-7 up to the 8th reuse cycle.

3.9 Evaluation of stability and recyclability

The enzymatic properties of LDH/MNPs@MAF-7 were investigated using pyruvic acid as the substrate. To evaluate the ability of MAF-7 to protect LDH at high temperatures, LDH/MNPs@MAF-7 was incubated at 30°C–80°C for 20 min. As displayed in Figure 9A, the relative enzyme activity retention rate of LDH/MNPs@MAF-7 decreased with increasing temperature, but the catalyst retained more than 10% of the maximum activity even at 80°C. By contrast, the free LDH was practically completely inactivated at 80°C. The enhanced thermal stability could be illustrated that LDH was protected by the rigid structure of MAF-7. This can minimize the unfolding of the enzyme (Ji et al., 2022).

To evaluate the influence of pH on the catalytic activity of LDH, the catalyst was incubated in tris-HCl buffers with different pH (4–10). As shown in Figure 9B, LDH/MNPs@MAF-7 demonstrated better tolerance under acidic conditions, and the activity reached the maximum at pH 6. This indicates that the three-dimensional structure of MAF-7 provided a microenvironment, thus helping the LDH retain its activity and preventing the subunits dissociation (Li et al., 2018; Ji et al., 2022).

The solubility of PPA is very poor, and it needs to be solubilized with organic solvents. Thus, LDH/MNPs@MAF-7-catalyzed reactions have been assessed in the presence of a variety of organic solvents (DMSO, DMF, DCM) (Figure 9C). LDH/MNPs@MAF-7 showed

excellent tolerance to organic solvents (>58% residual activity). It has been reported that MAF-7 forms a barrier, which effectively reduced exposure to enzymes and organic solvents (Liang et al., 2015; Nadar and Rathod, 2019). The results indicated that the LDH/MNPs@MAF-7 was suitable for the biosynthesis of PLA.

Finally, the reusability of LDH/MNPs@MAF-7 was assessed as an important performance indicator for actual applications. After each cycle, the LDH/MNPs@MAF-7 were recycled and washed completely, then repeated the experiment of enzyme activity assessment. As illustrated in Figure 9D, the residual activity remained above 80% after eight successive cycles. The results demonstrated that LDH/MNPs@MAF-7 had a certain technical dominance in the D-PLA biosynthesis. The decrease of enzyme activity may be attributed to the leakage of enzyme from the supports and denaturation of enzyme during the biocatalytic process over many reuse cycles (Liang et al., 2020).

It is noticed that the intrinsic fragile nature of enzymes makes them prone to denaturation or destabilization in harsh practical conditions, leading to unavoidably shortened lifespan and extremely high cost. Thus, we provided a possible synthesis strategy for application of enzyme immobilization by innovatively magnetic modifications to MAF-7. Herein, LDH/MNPs@MAF-7 exhibited more stable catalytic performances than those of free enzymes, including improved enzyme efficiency, stability and recyclability, due to the protection of enzymes by highly ordered

frameworks. In addition, it exhibited excellent resistance to organic reagents, which makes it suitable for the industrial bioconversion of poorly soluble substrates. To summarize, the considerable universality and expansibility of this synthesis strategy would promise great potential in industrial applications of immobilized enzymes.

4 Conclusion

LDH and MNPs were successfully encapsulated into the MOF material MAF-7 by a one-pot coprecipitation strategy. The consequences of SEM, TGA, FT-IR, XRD, XPS, VSM and N₂ adsorption characterization of LDH/MNPs@MAF-7 showed that LDH and Fe₃O₄ were successfully immobilized into MAF-7. The synthesized LDH/MNPs@MAF-7 particles exhibited stable catalytic activity in thermal stability, resistance to organic solvents and pH stability. What's more, LDH/MNPs@MAF-7 exhibited good reusability, the residual activity remained above 80% after eight successive cycles of reuse. This study demonstrates that LDH/MNPs@MAF-7 could be a potential and magnetically recyclable biocatalyst for the manufactured production of D-PLA.

Data availability statement

The original contributions presented in the study are included in the article/[Supplementary Material](#), further inquiries can be directed to the corresponding author.

Author contributions

Conceptualization, XS, YF and HH; Data curation, XS, YW and JH; Investigation, XS, YF and HH; Validation, XS, XL, JH and YW;

References

- Ahmed, I. N., Yang, X. L., Dubale, A. A., Li, R. F., Ma, Y. M., Wang, L. M., et al. (2018). Hydrolysis of cellulose using cellulase physically immobilized on highly stable zirconium based metal-organic frameworks. *Bioresour. Technol.* 270, 377–382. doi:10.1016/j.biortech.2018.09.077
- Alagoz, D., Toprak, A., Yildirim, D., Tukel, S. S., and Fernandez-Lafuente, R. (2021). Modified silicates and carbon nanotubes for immobilization of lipase from *Rhizomucor miehei*: Effect of support and immobilization technique on the catalytic performance of the immobilized biocatalysts. *Enzyme Microb. Technol.* 144, 109739. doi:10.1016/j.enzmictec.2020.109739
- Cao, M., Yu, J., Zhang, X., Lin, Y., and Huang, H. (2022). Laccase-functionalized magnetic framework composite enabled chlorophenols degradation, a potential remediation for fungicides residues in leather. *J. Leather Sci. Eng.* 4 (21), 21. doi:10.1186/s42825-022-00094-3
- Chen, G., Huang, S., Kou, X., Wei, S., Huang, S., Jiang, S., et al. (2019). A convenient and versatile amino-acid-BoostedBiomimeticStrategy for the NondestructiveEncapsulation of biomacromolecules within metal-organic frameworks. *Angew. Chem. Int. Ed.* 58, 1463–1467. doi:10.1002/anie.201813060
- Du, Y., Jia, X., Zhong, L., Jiao, Y., Zhang, Z., Wang, Z., et al. (2022). Metal-organic frameworks with different dimensionalities: An ideal host platform for enzyme@MOF composites. *Coord. Chem. Rev.* 454, 214327. doi:10.1016/j.ccr.2021.214327
- Ge, J., Liu, L., Cui, Y., Li, R., Meng, F., and Wang, F. (2020). Optimizing the electromagnetic wave absorption performances of designed Fe₃O₄@SiO₂@MnO₂ hybrids. *Ceram. Int.* 46 (10), 15325–15332. doi:10.1016/j.ceramint.2020.03.074
- Hirai, K., Reboul, J., Morone, N., Heuser, J. E., Furukawa, S., and Kitagawa, S. (2014). Diffusion-coupled molecular assembly: Structuring of coordination polymers across multiple length scales. *J. Am. Chem. Soc.* 136 (42), 14966–14973. doi:10.1021/ja507971r
- Ji, Y., Gao, W., Zhang, S., Li, B., Huang, H., and Zhang, X. (2022). Confining natural/mimetic enzyme cascade in an amorphous metal-organic framework for the construction

Writing—original draft, XS, XL and JH; Writing—review and editing, XS, YW and JH. All authors have read and agreed to the published version of the manuscript.

Funding

This research was funded by the Zhejiang Provincial Natural Science Foundation of China (Grant No. LGG20B060001), the Key Research & Development plan of Zhejiang Province (2020C02049).

Conflict of interest

The authors declare that the research was conducted in the absence of any commercial or financial relationships that could be construed as a potential conflict of interest.

Publisher's note

All claims expressed in this article are solely those of the authors and do not necessarily represent those of their affiliated organizations, or those of the publisher, the editors and the reviewers. Any product that may be evaluated in this article, or claim that may be made by its manufacturer, is not guaranteed or endorsed by the publisher.

Supplementary material

The Supplementary Material for this article can be found online at: <https://www.frontiersin.org/articles/10.3389/fbioe.2022.1124450/full#supplementary-material>

of recyclable biomaterials with catalytic activity. *Langmuir* 38 (3), 927–936. doi:10.1021/acs.langmuir.1c02093

Ji, Y., Wu, Z., Zhang, P., Qiao, M., Hu, Y., Shen, B., et al. (2021). Enzyme-functionalized magnetic framework composite fabricated by one-pot encapsulation of lipase and Fe₃O₄ nanoparticle into metal-organic framework. *Biochem. Eng. J.* 169, 107962. doi:10.1016/j.bej.2021.107962

Lavermicocca, P., Valerio, F., Evidente, A., Lazzaroni, S., Corsetti, A., and Gobetti, M. (2000). Purification and characterization of novel antifungal compounds from the sourdough *Lactobacillus plantarum* strain 21B. *Appl. Environ. Microbiol.* 66 (9), 4084–4090. doi:10.1128/aem.66.9.4084-4090.2000

Lavermicocca, P., Valerio, F., and Visconti, A. (2003). Antifungal activity of phenyllactic acid against molds isolated from bakery products. *Appl. Environ. Microbiol.* 69 (1), 634–640. doi:10.1128/AEM.69.1.634-640.2003

Li, P., Chen, Q., Wang, T. C., Vermeulen, N. A., Mehdi, B. L., Dohnalkova, A., et al. (2018). Hierarchically engineered mesoporous MetalOrganic frameworks toward cell-free immobilized enzyme systems. *Chem* 4, 1022–1034. doi:10.1016/j.chempr.2018.03.001

Li, Q., Pan, Y., Li, H., Alhalhooly, L., Li, Y., Chen, B., et al. (2020). Size-tunable Metal–Organic framework-coated magnetic nanoparticles for enzyme encapsulation and large-substrate biocatalysis. *ACS Appl. Mater. Interfaces* 12, 41794–41801. doi:10.1021/acsami.0c13148

Liang, K., Ricco, R., Doherty, C. M., Styles, M. J., Bell, S., Kirby, N., et al. (2015). Biomimetic mineralization of metal-organic frameworks as protective coatings for biomacromolecules. *Nat. Commun.* 6, 7240. doi:10.1038/ncomms8240

Liang, S., Wu, X.-L., Xiong, J., Zong, M.-H., and Lou, W.-Y. (2020). Metal-organic frameworks as novel matrices for efficient enzyme immobilization: An update review. *Coord. Chem. Rev.* 406, 213149. doi:10.1016/j.ccr.2019.213149

Liang, W., Wied, P., Carraro, F., Sumby, C. J., Nidetzky, B., Tsung, C. K., et al. (2021). Metal-organic framework-based enzyme biocomposites. *Chem. Rev.* 121 (3), 1077–1129. doi:10.1021/acs.chemrev.0c01029

- Luo, X., Zhang, Y., Yin, F., Hu, G., Jia, Q., Yao, C., et al. (2020a). Enzymological characterization of a novel D-lactate dehydrogenase from *Lactobacillus rossiae* and its application in D-phenyllactic acid synthesis. *3 Biotech.* 10 (3), 101. doi:10.1007/s13205-020-2098-5
- Luo, X., Zhang, Y., Yin, L., Zheng, W., and Fu, Y. (2020b). Efficient synthesis of D-phenyllactic acid by a whole-cell biocatalyst co-expressing glucose dehydrogenase and a novel D-lactate dehydrogenase from *Lactobacillus rossiae*. *3 Biotech.* 10 (1), 14. doi:10.1007/s13205-019-2003-2
- Nadar, S. S., and Rathod, V. K. (2020). Immobilization of proline activated lipase within metal organic framework (MOF). *Int. J. Biol. Macromol.* 152, 1108–1112. doi:10.1016/j.ijbiomac.2019.10.199
- Nadar, S. S., and Rathod, V. K. (2019). One pot synthesis of α -amylase metal organic framework (MOF)-sponge via dip-coating technique. *Int. J. Biol. Macromol.* 138, 1035–1043. doi:10.1016/j.ijbiomac.2019.07.099
- Nosike, E. I., Jiang, Z., Miao, L., Akakuru, O. U., Yuan, B., Wu, S., et al. (2020). A novel hybrid nano-adsorbent for effective Hg^{2+} adsorption based on zeolitic imidazolate framework (ZIF-90) assembled onto poly acrylic acid capped Fe_3O_4 nanoparticles and cysteine. *J. Hazard. Mater.* 392, 122288. doi:10.1016/j.jhazmat.2020.122288
- Schejn, A., Mazet, T., Falk, V., Balan, L., Aranda, L., Medjahdi, G., et al. (2015). Fe_3O_4 @ZIF-8: Magnetically recoverable catalysts by loading Fe_3O_4 nanoparticles inside a zinc imidazolate framework. *Dalton Trans.* 44, 10136–10140. doi:10.1039/c5dt01191d
- Shieh, F.-K., Wang, S.-C., Leo, S.-Y., and Wu, K. C. (2013). Water-Based synthesis of zeolitic imidazolate framework-90 (ZIF-90) with a controllable particle size. *Chem.* 19, 11139–11142. doi:10.1002/chem.201301560
- Shieh, F.-K., Wang, S.-C., Yen, C.-I., Wu, C.-C., Dutta, S., Chou, L.-Y., et al. (2015). Imparting functionality to biocatalysts via embedding enzymes into nanoporous materials by a de Novo approach: Size-selective sheltering of catalase in Metal–Organic framework microcrystals. *J. Am. Chem. Soc.* 137, 4276–4279. doi:10.1021/ja513058h
- Siar, E.-H., Zaak, H., Kornecki, J. F., Zidoune, M. N., Barbosa, O., and Fernandez-Lafuente, R. (2017). Stabilization of ficin extract by immobilization on glyoxyl agarose. Preliminary characterization of the biocatalyst performance in hydrolysis of proteins. *Process Biochem.* 58, 98–104. doi:10.1016/j.procbio.2017.04.009
- Sirisha, V. L., Jain, A., and Jain, A. (2016). Enzyme immobilization: An overview on methods, support material, and applications of immobilized enzymes. *Adv. Food Nutr. Res.* 79, 179–211. doi:10.1016/bs.afnr.2016.07.004
- Tian, Y., Zhou, Y., Zong, Y., Li, J., Yang, N., Zhang, M., et al. (2020). Construction of functionally compartmental inorganic photocatalyst-enzyme system via imitating chloroplast for efficient photoreduction of CO_2 to formic acid. *ACS Appl. Mater. Interfaces* 12 (31), 34795–34805. doi:10.1021/acsami.0c06684
- Torkzadeh-Mahani, M., Zaboli, M., Barani, M., and Torkzadeh-Mahani, M. (2020). A combined theoretical and experimental study to improve the thermal stability of recombinant D-lactate dehydrogenase immobilized on a novel superparamagnetic Fe_3O_4 NPs@ metal-organic framework. *Appl. Organomet. Chem.* 34, e5581. doi:10.1002/aoc.5581
- Tranchemontagne, D. J., Mendoza-Cortes, J. L., O’Keeffe, M., and Yaghi, O. M. (2009). Secondary building units, nets and bonding in the chemistry of metal-organic frameworks. *Chem. Soc. Rev.* 38 (5), 1257–1283. doi:10.1039/b817735j
- Wang, J., Zang, W., Xi, S., Kosari, M., Pennycook, S. J., and Zeng, H. C. (2020). Trimetal atoms confined in openly accessible nitrogen-doped carbon constructs for an efficient ORR. *J. Mater. Chem. A* 8 (33), 17266–17275. doi:10.1039/d0ta05984f
- Wang, K., Lv, R., Sun, S., Dong, F., Liu, M., Liu, J., et al. (2022). Nanobiocatalyst consisting of immobilized α -amylase on montmorillonite exhibiting enhanced enzymatic performance based on the allosteric effect. *Colloids Surfaces B Biointerfaces* 211, 112290. doi:10.1016/j.colsurfb.2021.112290
- Wang, L., Liu, G., Ren, Y., Feng, Y., Zhao, X., Zhu, Y., et al. (2020). Integrating target-triggered aptamer-capped HRP@Metal-Organic frameworks with a colorimeter readout for on-site sensitive detection of antibiotics. *Anal. Chem.* 92 (20), 14259–14266. doi:10.1021/acs.analchem.0c03723
- Wang, Q., Ji, Y., Zhang, X., He, H., Wang, G., Xu, C., et al. (2022). Boosting the quantum yield of oxygen-doped $g-C_3N_4$ via a metal-azolate framework-enhanced electron-donating strategy for highly sensitive sulfadimethoxine tracing. *Anal. Chem.* 94 (14), 5682–5689. doi:10.1021/acs.analchem.2c00423
- Wang, Y., Luo, X., Sun, X., Hu, J., Guo, Q., Shen, B., et al. (2022). Lactate dehydrogenase encapsulated in a metal-organic framework: A novel stable and reusable biocatalyst for the synthesis of D-phenyllactic acid. *Colloids Surf. B Biointerfaces* 216, 112604. doi:10.1016/j.colsurfb.2022.112604
- Wei, B., Xu, H., Cheng, L., Yuan, Q., Liu, C., Gao, H., et al. (2021). Highly selective entrapment of his-tagged enzymes on superparamagnetic zirconium-based MOFs with robust renewability to enhance pH and thermal stability. *ACS Biomaterials Sci. Eng.* 7 (8), 3727–3736. doi:10.1021/acsbiomaterials.1c00780
- Wu, H., Guang, C., Zhang, W., and Mu, W. (2021). Recent development of phenyllactic acid: Physicochemical properties, biotechnological production strategies and applications. *Crit. Rev. Biotechnol.* 1–16. doi:10.1080/07388551.2021.2010645



OPEN ACCESS

EDITED BY

Hossain M. Zayed,
Jiangsu University, China

REVIEWED BY

Hongzhen Luo,
Huaiyin Institute of Technology, China
Tanim Jabid Hossain,
University of Chittagong, Bangladesh

*CORRESPONDENCE

Ivan Mijakovic,
✉ ivmi@biosustain.dtu.dk

†PRESENT ADDRESS

Aida Kalantari,
Synlogic, Inc., Cambridge, Massachusetts,
United States

SPECIALTY SECTION

This article was submitted to Industrial
Biotechnology,
a section of the journal
Frontiers in Bioengineering and
Biotechnology

RECEIVED 17 November 2022

ACCEPTED 04 January 2023

PUBLISHED 16 January 2023

CITATION

Garg A, Jers C, Hwang HJ, Kalantari A,
Ventina I and Mijakovic I (2023),
Engineering *Bacillus subtilis* for production
of 3-hydroxypropanoic acid.
Front. Bioeng. Biotechnol. 11:1101232.
doi: 10.3389/fbioe.2023.1101232

COPYRIGHT

© 2023 Garg, Jers, Hwang, Kalantari,
Ventina and Mijakovic. This is an open-
access article distributed under the terms
of the [Creative Commons Attribution
License \(CC BY\)](#). The use, distribution or
reproduction in other forums is permitted,
provided the original author(s) and the
copyright owner(s) are credited and that
the original publication in this journal is
cited, in accordance with accepted
academic practice. No use, distribution or
reproduction is permitted which does not
comply with these terms.

Engineering *Bacillus subtilis* for production of 3-hydroxypropanoic acid

Abhroop Garg¹, Carsten Jers¹, Hee Jin Hwang^{2,3}, Aida Kalantari^{2†},
Ildze Ventina¹ and Ivan Mijakovic^{1,2*}

¹Novo Nordisk Foundation Center for Biosustainability, Technical University of Denmark, Kgs Lyngby, Denmark, ²Systems and Synthetic Biology Division, Department of Biology and Biological Engineering, Chalmers University of Technology, Gothenburg, Sweden, ³Department of Molecular Science and Technology, Ajou University, World cup-ro, Yeongtong-gu, Suwon-si, South Korea

3-Hydroxypropionic acid (3-HP) is a valuable platform chemical that is used as a precursor for several higher value-added chemical products. There is an increased interest in development of cell factories as a means for the synthesis of 3-HP and various other platform chemicals. For more than a decade, concentrated effort has been invested by the scientific community towards developing bio-based approaches for the production of 3-HP using primarily *Escherichia coli* and *Klebsiella pneumoniae* as production hosts. These hosts however might not be optimal for applications in e.g., food industry due primarily to endotoxin production and the pathogenic origin of particularly the *K. pneumoniae*. We have previously demonstrated that the generally recognized as safe organism *Bacillus subtilis* can be engineered to produce 3-HP using glycerol, an abundant by-product of the biodiesel industry, as substrate. For commercial exploitation, there is a need to substantially increase the titer. In the present study, we optimized the bioprocess conditions and further engineered the *B. subtilis* 3-HP production strain. Thereby, using glycerol as substrate, we were able to improve 3-HP production in a 1-L bioreactor to a final titer of 22.9 g/L 3-HP.

KEYWORDS

3-hydroxypropanoic acid, glycerol, biosynthesis, cell factory, synthetic biology, metabolic engineering

1 Introduction

3-Hydroxypropionic acid, also called 3-hydroxypropionate (3-HP) is a valuable platform chemical used as a precursor in the chemical industry (Andreeßen and Steinbüchel 2010; Jiang et al., 2021). 3-HP is used as a precursor for the industrial synthesis of several higher value-added chemical products, including acrylic acid, acrylamide, methyl acrylate, acrylonitrile (ACN), ethyl 3-HP, 1,3-propanediol, 3-hydroxypropionaldehyde, propiolactone, and malonic acid, as well as biodegradable materials, especially poly(3-hydroxypropionate) (P3HP) based homopolymers and heteropolymers (Andreeßen and Steinbüchel 2010; Jers et al., 2019; Jiang et al., 2021). These platform chemicals are essential for the synthesis of numerous products, such as solvents, cleaning agents, adhesives, paints and coatings, plastics and plastic packaging, resin-based floor polishes, fibers, absorbent diapers, and disinfectants for sterilizing tissue grafts (Andreeßen and Steinbüchel 2010; Matsakas et al., 2018).

The chemical synthesis of 3-HP in petroleum oil refineries is very costly and generates toxic intermediates with serious environmental effects (Matsakas et al., 2018). There are diminishing global crude oil reserves and increasing environmental deterioration due to notorious chemical pollutants from petroleum and petrochemical industries. These

circumstances have necessitated the accelerated growth of biorefinery as an alternative source for the synthesis of various platform chemicals (Li et al., 2016). Biorefinery is the optimized biomass usage for the production of biomaterials, biochemicals, and biofuels for chemical and energy applications with substantial benefits of lower costs and reduced environmental impacts (Hingsamer and Jungmeier 2019). In the production of biodiesel, crude glycerol is the most abundant byproduct. For every 10 tons of biodiesel produced *via* transesterification of vegetable oils or animal fats, 1 ton of crude glycerol is recovered (Andreeßen et al., 2010). This in turn has led to a growing interest in crude glycerol as a renewable substrate for the production of 3-HP and other chemicals (Jiang et al., 2018). The bioconversion of crude glycerol to 3-HP occurs *via* microbial-mediated fermentation processes. To date, a wide repertoire of bacteria with diverse biochemical abilities to naturally produce 3-HP from crude glycerol have been identified (Jers et al., 2019). Genetic engineering has been widely employed for the development of improved 3-HP production strains (Li et al., 2016; Jers et al., 2019). Engineering strategies include screening for better production pathway enzymes, developing expression systems for efficiently producing 3-HP and re-allocation of cellular resources to accumulate 3-HP (Zhao and Tian 2021). With respect to engineering, particularly the Gram-negative bacteria *K. pneumoniae* and *E. coli* have been considered. The highest 3-HP titer, 102.6 g/L, was obtained using *K. pneumoniae* (Zhao et al., 2019). In *E. coli*, the highest titer reported is 76.2 g/L (Kim et al., 2020). However, its pathogenic nature is a deterrent for its use as a cell factory (Zhao and Tian 2021; Zaved et al., 2022). Other hosts, such as *Lactobacillus reuteri*, *Pseudomonas denitrificans*, *Corynebacterium glutamicum* and *B. subtilis* have also been applied for 3-HP production generally with lower resulting titers (Zhou et al., 2013; Ramakrishnan et al., 2015; Chen et al., 2017; Kalantari et al., 2017).

As mentioned, the main body of work has been done using the Gram-negative bacteria *K. pneumoniae* and *E. coli*. Considering that 3-HP can find application in diverse fields including food and pharma sector, these hosts can potentially be problematic. Firstly, due to the production of endotoxin that is observed for most Gram-negative bacteria, and secondly, due to the pathogenic origin of the strains (Li and Tian 2015; Zaved et al., 2022). Consequently, it should be desirably to explore and/or engineer new hosts for 3-HP production. We previously demonstrated a potential of the Gram-positive bacterium *B. subtilis* as a host for heterologous expression of the 3-HP synthetic pathway (Kalantari et al., 2017) and this bacterium is generally recognized as safe (GRAS). The 3-HP biosynthetic pathway from *K. pneumoniae* was successfully introduced in *B. subtilis* to redirect its glycerol metabolism towards 3-HP allowing a titer of 10 g/L in shake flask fermentations (Kalantari et al., 2017). This titer is not high enough for commercial exploitation and a combination of strain and process engineering would be needed to substantially improve titers. Several challenges can be targeted such as preventing buildup of the toxic intermediate 3-hydroxypropanal (3-HPA) as well as byproducts, NAD⁺ co-factor requirement of the aldehyde dehydrogenase, and tolerance to substrate and product (Liang et al., 2022; Zaved et al., 2022). Optimization of the production conditions is key to attain the full potential of production strains. To this end, various fermentation conditions such as growth medium, pH, and dissolved oxygen content have been optimized. For

instance, in *K. pneumoniae* and *L. reuteri* optimization of the medium composition led to an increase of 80% and 70% in 3-HP production, respectively (Li et al., 2016; Couvreur et al., 2017). Dissolved oxygen could have different effects on 3-HP production where on one hand aerobic conditions are needed for efficient regeneration of the cofactor NAD⁺ but on the other hand the enzyme glycerol dehydratase is sensitive to oxygen (Jers et al., 2019). Using metabolically engineered *E. coli*, the authors were able to improve the production of 3-HP to 76.2 g/L using fed-batch fermentation by controlling the dissolved oxygen levels at 10% (Kim et al., 2020).

In the present study, the *B. subtilis* strain previously engineered to produce 3-HP from glycerol (Kalantari et al., 2017) was utilized with the aim to improve its 3-HP production capacity. Process conditions for 3-HP production in a bioreactor were optimized and the strain was engineered in order to address NAD⁺ co-factor regeneration, and transport of substrates and product. Collectively, this allowed the production of 23.0 g/L 3-HP using an engineered strain in a 1-L bioreactor.

2 Materials and methods

2.1 Chemicals

3-HP used as a standard was purchased from TCI Europe N.V. (Zwijndrecht, Belgium). All other chemicals were purchased from Sigma-Aldrich (Steinheim, Germany).

2.2 Strains and DNA manipulations

All strains used in this study are listed in Table 1. *E. coli* NM522 was used for plasmid propagation. For marker-free disruptions of the genes *spoIIAC* and *lutP* in *B. subtilis*, the plasmid pMAD carrying a thermosensitive replicon was used (Arnaud et al., 2004). Regions up- and downstream from the target gene were PCR-amplified using relevant primers (Supplementary Figure S1; Table 1) and inserted in the pMAD plasmid. The *spoIIAC* mutation was introduced in the *B. subtilis* strain h-syn-KpDhaB-PuuC-ΔglpK-ii to generate the strain PS (production strain). In the PS, the gene *lutP* was disrupted to yield PSΔ*lutP*. The pMAD plasmid was also used to integrate the gene *udhA* from *E. coli* under the control of P43 promoter into the *thrC* gene in the PS. The P43 promoter fragment was amplified from the *B. subtilis* genomic DNA while the terminator fragment was amplified from pBS1C plasmid (Radeck et al., 2013).

Additionally, the pMAD plasmid was used to replace the native promoter of *ndh* in the PS with the P43 promoter. For replacing the native promoters of the genes *glpF*, *yvrC* and *lctP* with P43 promoter, a CRISPR-Cas9-based method was used (Altenbuchner 2016). The 20 bp spacer sequence oligos were annealed and inserted in the plasmid pJOE8999 between the *BsaI* restriction sites. The repair template (P43 promoter sequence, and up- and downstream regions) was inserted between the *SfiI* restriction sites. The pJOE8999 plasmid with the spacer and the repair template was used to transform the PS as described earlier (Yasbin et al., 1975). The resulting strains were analyzed by sequencing to confirm the correct insertion.

TABLE 1 Strains used in this study.

Strains	Description	References
h-syn-KpDhaB-PuuC-Δglpk-ii	<i>Bacillus subtilis</i> recombinant strain	Kalantari et al. (2017)
PS	h-syn-KpDhaB-PuuC-Δglpk-ii + ΔspoIIAC	This study
PS(<i>udhA</i>) ^{ox}	PS + Δ <i>thrC</i> ::P43- <i>udhA</i>	This study
PS(<i>ndh</i>) ^{ox}	PS + P43- <i>ndh</i>	This study
PSΔ <i>lutP</i>	PS + Δ <i>lutP</i>	This study
PSΔ <i>lutP</i> (<i>yvrC</i>) ^{ox}	PSΔ <i>lutP</i> + P43- <i>yvrC</i>	This study
PSΔ <i>lutP</i> (<i>glpF</i>) ^{ox}	PSΔ <i>lutP</i> + P43- <i>glpF</i>	This study
PSΔ <i>lutP</i> (<i>lctP</i>) ^{ox}	PSΔ <i>lutP</i> + P43- <i>lctP</i>	This study
PS4mut	PSΔ <i>lutP</i> + P43- <i>yvrC</i> + P43- <i>glpF</i> + P43- <i>lctP</i>	This study

2.3 Media and growth conditions

E. coli and *B. subtilis* were routinely cultured in LB medium (10 g/L tryptone, 5 g/L yeast extract, and 5 g/L NaCl) at 37°C. For experiments to test production of 3-HP, two different media were used; a modified M9 (MM9) medium and a fed-batch fermentation (FBF) medium essentially as reported previously by Wang and co-workers (Wang et al., 2011). The growth medium components of MM9 medium are as follows (in g/L): MM9 seed medium: KH₂PO₄ 3.0, Na₂HPO₄·2H₂O 8.5, NaCl 0.5, NH₄Cl 1.0, MgSO₄·7H₂O 0.0246, citric acid·H₂O 0.0021, MnCl₂·4H₂O 0.001, CoCl₂·6H₂O 0.0006, NaMoO₄·2H₂O 0.0006, ZnCl₂ 0.0017, CuCl₂·2H₂O 0.00043, FeCl₃·6H₂O 0.00135, CaCl₂·2H₂O 0.00147, yeast extract 1.0, glucose 10.0; MM9 initial medium: KH₂PO₄ 6.0, Na₂HPO₄·2H₂O 17.0, NaCl 1.0, NH₄Cl 2.0, MgSO₄·7H₂O 0.0492, citric acid·H₂O 0.0042, MnCl₂·4H₂O 0.002, CoCl₂·6H₂O 0.0012, NaMoO₄·2H₂O 0.0012, ZnCl₂ 0.0034, CuCl₂·2H₂O 0.00086, FeCl₃·6H₂O 0.0027, CaCl₂·2H₂O 0.00294, yeast extract 5.0, glucose 10.0, glycerol 10.0; MM9 feed medium is same as MM9 initial medium except: glucose 400.0, glycerol 50.0.

The growth medium components of FBF medium are as follows (in g/L): FBF seed medium: KH₂PO₄ 1.0, K₂HPO₄ 1.65, NaNO₃ 10.0, NH₄NO₃ 5.0, MgSO₄·7H₂O 1.5, MnCl₂·4H₂O 0.04, ZnCl₂ 0.0189, FeCl₂·4H₂O 0.047, citric acid 0.019, yeast extract 5.0, glucose 20.0; FBF initial medium: KH₂PO₄ 4.0, K₂HPO₄ 7.5, NaNO₃ 10.0, NH₄NO₃ 5.0, MgSO₄·7H₂O 3.0, MnCl₂·4H₂O 0.02, ZnCl₂ 0.00945, FeCl₂·4H₂O 0.031, citric acid 0.019, yeast extract 5.0, glucose 20.0, glycerol 10.0; FBF feed medium: KH₂PO₄ 5.0, K₂HPO₄ 5.0, NaNO₃ 10.0, MgSO₄·7H₂O 2.0, yeast extract 10.0, glucose 650.0, glycerol 50.0.

For shake flask fermentation experiments, a single colony was inoculated in 10 mL FBF seed medium and incubated with shaking at 37°C overnight. This culture was then used to inoculate 50 mL FBF initial medium supplemented with 10 μM isopropyl β-D-1-thiogalactopyranoside (IPTG) and 15 μM coenzyme B₁₂, to obtain a final OD₆₀₀ of 0.05. Shake flask cultures were incubated at 37°C, shaking at 200 rpm for either 30 h or 40 h. For measuring cell density (OD₆₀₀) and the concentration of various metabolites, 1 mL culture broth was taken out at the following time-points (h): 0, 6, 24 and 30 (for 30 h experiments) or 0, 16, 24 and 40 (for 40 h experiments). For the latter, the samples were centrifuged (11,000 g for 3 min) and the supernatant stored at −20°C for the HPLC analysis.

Repeated fed-batch fermentation experiments were carried out at 37°C (unless otherwise stated) in a 1-L Sartorius bioreactor. The pH was maintained at 7.0 by adding 2 M KOH automatically. The stirrer speed was set to be minimum 500 rpm and maximum 1200 rpm, and air flow between 0.15 L/min and 1.5 L/min. These two parameters were controlled automatically in order to maintain the desired dissolved oxygen content. To inoculate the fermentor, a single colony was inoculated in 10 mL seed medium (MM9 or FBF as relevant) and incubated 37°C overnight. The next morning, 30 mL seed medium in a 250 mL shake flask was inoculated with the overnight culture to an OD₆₀₀ of 0.05. The culture was grown until it reached an OD₆₀₀ of approximately 3.0. The seed culture was then used to inoculate 400 mL of initial medium in the 1-L bioreactor to an OD₆₀₀ of 0.1. The initial medium was supplemented with 1 mM IPTG, 20 μM Coenzyme B₁₂, and seven drops of Antifoam 204 (Sigma-Aldrich). The Prima BT Bench Top Process Gas Analysis Mass Spectrometer (Thermo Fisher Scientific) was used to monitor the carbon dioxide concentration in the off-gas. Feed medium supplemented with 1 mM IPTG and 20 μM Coenzyme B₁₂, was successively added to the bioreactor when glucose was depleted, which was indicated by the decline in carbon dioxide concentration in the off-gas. Glucose depletion in the fermentation broth was also verified using the Glucose MQuant™ (Merck Millipore) glucose strips. A volume of feed medium was added so that the final glucose concentration of was 10 or 20 g/L (as in the corresponding initial medium). Before adding the feed media, 2 mL culture broth was taken out for measuring the cell density and the concentration of select metabolites. Again, the samples were centrifuged (11,000 g for 3 min) and the supernatant stored at −20°C before subsequent HPLC analysis. Experiments were carried out for up to 45 h. In pilot experiments, we did not see any substantial productivity increases after 40 h (data not shown).

2.4 HPLC analysis

The concentration of glycerol, 3-HP, glucose, and lactic acid in the growth medium was quantified using HPLC. Samples were centrifuged and filtered through a 0.2 μm sterile filter before the HPLC analysis. 20 μL of sample was run on Aminex HPX-87H ion exclusion column for 45 min. The mobile phase was 0.5 mM H₂SO₄.

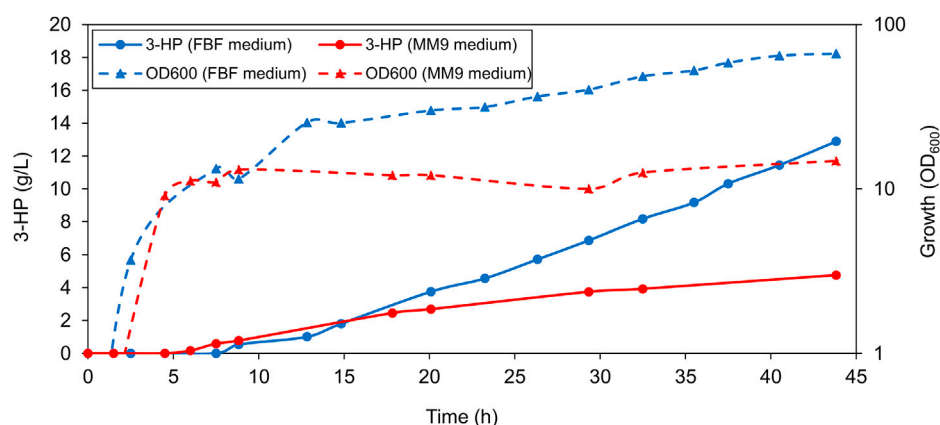


FIGURE 1

Production of 3-HP in a 1-L bioreactor. Representative graph depicting the concentration of 3-HP and cell density (OD_{600}) values of PS grown in fermentation medium compared to the modified 2x M9 medium throughout the 44-h growth period. Cells grown in the fermentation medium exhibited a higher maximum optical density (OD_{600}) as well as a higher 3-HP titer.

at the flowrate of 0.5 mL/min. The column temperature was set to 65°C, and the refractive index was measured at 35°C. The Shodex RH-101 refractive index detector was used to detect 3-HP, glucose and glycerol. The analytes were identified and quantified by comparing the chromatogram with the respective standards (glycerol, 3-HP, glucose, and lactic acid). The primary rationale for including lactic acid, was its similarity with our target product 3-HP. Based on the standards, we could confirm that the method allowed separating the two compounds. Lactic acid was not detected in any of the samples.

2.5 Statistical analysis

Shake flasks experiments were performed in biological replicates. One-way analysis of variance and Tukey's post-hoc test ($\alpha = 0.05$) was performed to infer statistically significant differences between the tested strains with respect to 3-HP production. For the repeated fed-batch experiments, the experiments were repeated twice and a representative experiment is shown.

3 Results and discussion

Before conducting bioreactor experiments, we made a non-sporulating variant of the 3-HP producing strain we previously generated (Kalantari et al., 2017). This was done by inactivating *spoIIAC* which renders *B. subtilis* incapable of sporulation (Kim and Kim 2001). This strain is referred to as the *B. subtilis* production strain (annotated in the text as PS) henceforth. The PS was tested for growth and 3-HP production in a 1-L bioreactor in the MM9 medium. The PS exhibited a maximum cell density with an OD_{600} of 14.8, and 3-HP titer of 4.8 g/L in the MM9 medium (Figure 1). Because of surprisingly low values of cell density and 3-HP production, we then proceeded to test the PS for growth and 3-HP production in the FBF medium that was previously used successfully for riboflavin production in *B. subtilis*. The PS grew better in the FBF medium where it exhibited a higher maximum cell density with an

OD_{600} of 66.6, and a higher 3-HP concentration of approximately 12.9 g/L (Figure 1). As the FBF medium enabled both, a higher cell density and 3-HP titer, we selected the FBF medium for all further analyses of the strain.

3.1 Optimization of bioconversion process conditions

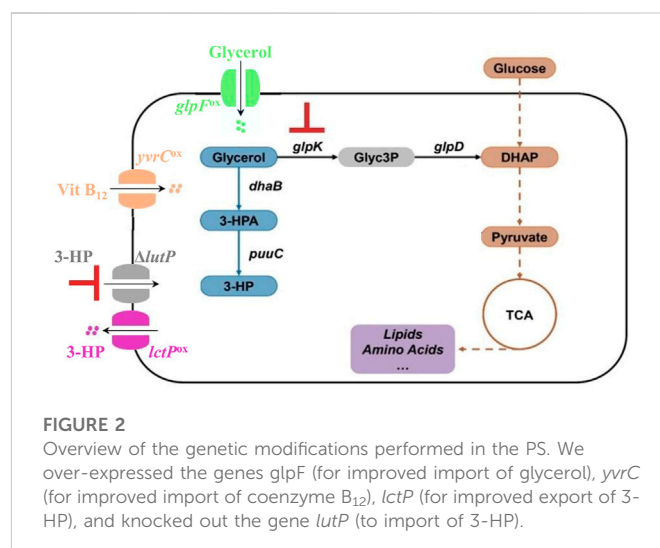
Having selected a growth medium, we subsequently tested the effect of modifying various fermentation conditions on 3-HP production capacity of the PS in a 1-L bioreactor. For different *B. subtilis* strains, generally optimum temperatures between 30°C and 37°C for growth and/or fermentation activity have been reported (Hoffmann and Bremer 2011; Ju et al., 2019). We thus wanted to probe the temperature-dependence of the process. At 30°C, both the growth (Supplementary Figure S1) and the 3-HP production capacity (4.3 g/L 3-HP) of the PS were significantly reduced as compared to the control (12.9 g/L 3-HP) grown at 37°C (Supplementary Figure S1). This finding indicated that the 3-HP production activity of the PS is temperature-sensitive. The PS needed a favorable temperature of 37°C for optimal growth as previously reported for *B. subtilis* strain 168 (Hoffmann and Bremer 2011).

Next, we tested the effect of IPTG concentration on the 3-HP production capacity of PS. It is well-known that the IPTG concentration can affect the gene expression of IPTG-inducible promoters and consequently target protein concentration. Balancing the expression of the production pathway enzymes could be key in alleviating stresses imposed by e.g., heterologous protein expression and product toxicity due to intracellular accumulation. We tested different concentrations of IPTG (1 μ M, 10 μ M, 100 μ M and 1 mM) in shake flasks for induction of the 3-HP operon, and found that 3-HP production was highest at 10 μ M IPTG (Supplementary Figure S2). While the shake flask experiment indicated a potential for improving 3-HP production *via* modulating heterologous gene expression, it did not translate into the same effect in the bioreactor. In the bioreactor setup, the application of 10 μ M IPTG led to a reduced production of 3-HP

(9.5 g/L 3-HP) (Supplementary Figure S1) as compared to using 1 mM IPTG (12.9 g/L 3-HP).

A potential problem could reside in the stability of production pathway enzymes. The enzyme glycerol dehydratase is prone to being inactivated due to error in regenerating the coenzyme B₁₂ cofactor. Glycerol dehydratase reactivase can reactivate the enzyme with help of ATP and intact coenzyme B₁₂ (Jers et al., 2019). Thus, the amount of coenzyme B₁₂ present can be critical for the continuity of the first step of 3-HP production. We therefore tested the effect of doubling the amount of coenzyme B₁₂ on 3-HP production level in a 1-L bioreactor. This led to a slight reduction in 3-HP production (9.2 g/L 3-HP) (Supplementary Figure S1) as compared to the control (12.9 g/L 3-HP) indicating that sufficient coenzyme B₁₂ was supplied. Considering that the substrate might be limiting, we also tested if doubling the amount of glycerol (2%) would lead to an improved 3-HP production in the PS. This, however, led to a reduced 3-HP titer (7.4 g/L 3-HP) (Supplementary Figure S1) as compared to the control (12.9 g/L 3-HP).

Finally, we evaluated the 3-HP production capability of the PS under different levels of dissolved oxygen. Oxygen could potentially influence the 3-HP bioprocess by affecting production pathway enzyme stability and co-factor regeneration. A high level of oxygen could lead to inactivation of the oxygen-sensitive enzyme glycerol dehydratase that catalyzes the first step in the 3-HP biosynthetic pathway (glycerol to 3-HPA). On the other hand, the second step of the pathway requires nicotinamide adenine dinucleotide (NAD⁺) as a co-factor, wherein NAD⁺ is reduced to NADH. In an aerobic process, the regeneration of NAD⁺ involves donation of electrons from NADH with oxygen being the final electron acceptor in the electron transport chain. Thus, lowering oxygen level might impact the availability of NAD⁺, thereby affecting the second enzymatic step. Additionally, being a facultative anaerobe, *B. subtilis* generally grows better under aerobic conditions (Hoffmann et al., 1995). Thus, we tested 3-HP production capability of the PS in a 1-L bioreactor under reduced oxygen environment (growth at dissolved oxygen levels of 40%, 20%, 10%, and 1%), but not under anaerobic environment. Surprisingly, no remarkable differences were observed in neither 3-HP production, nor in the growth profile of the cells (Supplementary Figure S3) when grown under different dissolved oxygen conditions. The 3-HP titers were 10.1, 10.4 and 14.2 g/L at dissolved oxygen levels of 20, 10% and 1%, respectively, compared to 12.9 g/L with 40% DO. These findings suggest that either only a minimal amount of oxygen is needed for the regeneration of NAD⁺ from NADH, or other alternative processes are being utilized for regeneration of NAD⁺, especially under near-anaerobic conditions. During anaerobic regeneration of NAD⁺, organic molecules can be used to regenerate NAD⁺ from NADH. For instance, NADH can aid the conversion of pyruvate into lactic acid, and is oxidized to NAD⁺ in the process (Ramos et al., 2000). During alcohol fermentation, alcohol dehydrogenase can oxidize NADH to NAD⁺ while reducing acetaldehyde to ethanol. In the present study, the ability of the PS to regenerate NAD⁺ from NADH under reduced dissolved oxygen growth conditions suggests that oxygen is not critical for this process. Indeed, *B. subtilis* can grow under anaerobic conditions due to their ability to utilize nitrate ammonification and various fermentation processes (Marino et al., 2001). Since the different levels of dissolved oxygen seemed to have almost no effect on the 3-HP production or biomass growth, all subsequent 1-L bioreactor runs were performed under 1% DO.



3.2 Genetic modification of *Bacillus subtilis* leads to an improved 3-HP production

Having performed an optimization of the production conditions, we next wanted to assess the possibility of improving 3-HP production via genetic engineering of the production strain. Initially we considered the possibility that an increase in NAD⁺/NADH ratio would improve 3-HP production. Consequently, we used different approaches to modulate this ratio. The native NADH dehydrogenase encoded by *ndh*, which can oxidize NADH to NAD⁺ was over-expressed (Marreiros et al., 2016). This was done by placing it under the control of P43 promoter. Additionally, we introduced the enzyme pyridine nucleotide transhydrogenase (UdhA) from *E. coli*, which increases the transfer of reducing equivalents between NAD⁺ and NADP⁺ (Boonstra et al., 1999). Unfortunately, none of these introduced gene components substantially increased 3-HP production in the PS (Supplementary Figure S4). These experiments, in addition to fermentation experiments with different oxygen levels, indicated that the balance of NAD⁺/NADH was not a bottleneck in the 3-HP production in our experiments. Other studies have reported various means, including aeration control, electro-fermentation and enzymatic approaches, to control the redox balance leading to improved 3-HP production (Li et al., 2013; Kim et al., 2017; Kim et al., 2020). While NAD⁺/NADH in our current strain did not appear to be a bottleneck, further improvement in 3-HP production and derived NAD⁺-drain could make it a relevant parameter in a later stage.

As described above, increasing the amount of coenzyme B₁₂ and glycerol also did not lead to an increase in 3-HP production. We hypothesized that this could be because of limitations in their uptake by the bacterial cell. Therefore, we made a series of genetic modifications in the PS targeting transporters to increase substrate import (GlpF), product export (LctP), and import of the glycerol dehydratase coenzyme B₁₂ (YvrC) as well as preventing import of the product molecule 3-HP (LutP). The genetic modifications performed in the PS are depicted in the Figure 2. *B. subtilis* does not have dedicated 3-HP transporters but due to the structural similarity we hypothesized that the native lactate transporters facilitated the transport of 3-HP. To assure that 3-HP is efficiently secreted, we

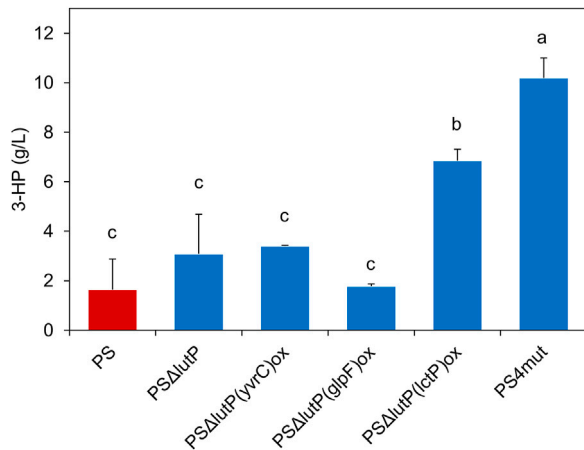


FIGURE 3
3-HP production in the genetically modified strains PSΔlutP, PSΔlutP(lctP)^{ox}, PSΔlutP(glpF)^{ox}, PSΔlutP(yvrC)^{ox} and PS4mut compared to the PS grown in shake flasks after 30 h. The “*” represents statistical significance with $p < 0.05$. The error bars represent standard deviation ($n = 2$). Different roman letters show significantly different means as determined by Tukey’s post-hoc test.

over-expressed the permease LctP that is responsible for the export of lactate (Ramos et al., 2000; Chai et al., 2009), and hence potentially of 3-HP as well. As 3-HP concentration increases in the fermentation broth, re-uptake of 3-HP could potentially be decreasing the productivity, and with the same rationale, we therefore targeted the main permease for lactate uptake LutP (Chai et al., 2009). To address these transport processes, we inactivated the *lutP* gene to yield the strain PSΔlutP. In this strain, we further over-expressed *lctP* by placing it under the control of the strong promoter P43, thereby obtaining the strain PSΔlutP(lctP)^{ox}. The influx of the substrate glycerol could also be a potential bottleneck. We therefore overexpressed the glycerol transporter GlpF (Stroud et al., 2003) by placing *glpF* under control of the P43 promoter to yield the strain PSΔlutP(glpF)^{ox}. Our 3-HP synthesis pathway is dependent on the cofactor coenzyme B₁₂. However, in presence of coenzyme B₁₂, the uptake is negatively regulated via a riboswitch regulating expression of *yvrC* encoding

an ABC transporter protein (Nahvi et al., 2004). To improve coenzyme B₁₂ uptake, we therefore placed *yvrC* under control of the P43 promoter to obtain PSΔlutP(yvrC)^{ox}. Finally, we also constructed a strain in which all the four mutations were introduced simultaneously. This strain, PSΔlutP(yvrC)^{ox}(glpF)^{ox}(lctP)^{ox}, is referred to as PS4mut in this manuscript.

These five engineered strains, i.e., PSΔlutP, PSΔlutP(glpF)^{ox}, PSΔlutP(yvrC)^{ox}, PSΔlutP(lctP)^{ox} and PS4mut, along with PS (as a reference) were evaluated in shake flasks to determine the effect of these genetic modifications on 3-HP production (Figure 3). The PS produced about 1.6 ± 1.2 g/L 3-HP while the single mutant strain PSΔlutP produced 3.1 ± 1.6. Neither of the double mutants strains PSΔlutP(glpF)^{ox}, or PSΔlutP(yvrC)^{ox} exhibited a significant increase in the 3-HP titer compared to the PS. In the strain PSΔlutP(lctP)^{ox} where the aim is to improve export and decrease re-import of 3-HP we observed a significant increase in 3-HP titer (6.9 ± 0.5 g/L). We previously observed no apparent growth defect of *B. subtilis* in presence of ~9 g/L 3-HP (Kalantari et al., 2017), which could indicate that the primary effect is exerted via the improved secretion of 3-HP. Similar benefits, albeit in connection with higher overall 3-HP titers, has been observed in *E. coli* where upregulation of transporter YohJK leads to improved 3-HP tolerance and increased 3-HP production (Nguyen-Vo et al., 2019; Nguyen-Vo et al., 2020). Combining all four mutations led to further significant improvement in 3-HP titer (10.2 ± 0.8 g/L) as compared to the PSΔlutP(lctP)^{ox}. It is worth noting that the genetic modifications led to altered growth behavior for all strains. For all five mutant strains, we observed a reduced final cell density in the shake flask cultures compared to the PS strain (OD₆₀₀ of 11.2–13.2 vs. 17.7, respectively) (Supplementary Figure S5).

The shake flask experiments, indicated a potential of the PS4mut strain for the production of 3-HP. Next, we wanted to test the performance of this strain in our 1-L bioreactor setup. Anticipating a higher 3-HP production in the quadruple mutant as compared to the PS, we doubled the amount of input glycerol (2% glycerol) in order for it to not be a limiting factor. As expected, an improved 3-HP production with a titer of about 22.9 g/L was observed in this strain (Figure 4), thus highlighting the importance of optimizing the transport processes in the production strain. By a combination of metabolic engineering of *B. subtilis* and optimization of the

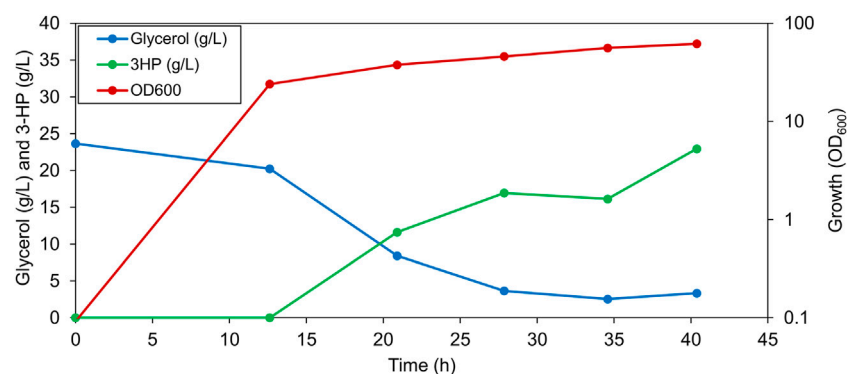


FIGURE 4
Representative graph depicting 3-HP production, residual glycerol in the broth and the OD₆₀₀ value of PS4mut in a 1-L bioreactor cultured under 1% dissolved oxygen and 2% glycerol.

bioprocess conditions, we were able to increase 3-HP production by 4.8-fold (from 4.8 g/L in the PS to 22.9 g/L in PS4mut) in a 1-L bioreactor.

4 Conclusion and perspectives

The potential of *B. subtilis* as a cell factory has been established earlier (Kalantari et al., 2017). By optimization of the bioprocess conditions and genetic engineering, we have further improved the 3-HP production capacity of *B. subtilis* by 4.8-fold to a maximum titer of 22.9 g/L. This titer is still not high enough for commercial exploitation. Further improvements in 3-HP production could potentially be achieved by improving the resistance of the production strain towards 3-HP and glycerol by adaptive laboratory evolution (ALE). For instance, ALE was used to develop a 3-HP tolerant *E. coli* strain which produced more 3-HP as compared to the reference strain (Nguyen-Vo et al., 2019). In another study, the glycerol assimilating capability of *Cupriavidus necator* was improved by ALE (González-Villanueva et al., 2019). Employment of highly active and specific glycerol dehydratases and alcohol dehydrogenases could be a venue for further improving the 3-HP production. Importance need also be given to the optimization of the bioprocess conditions. Such a combinatorial approach would be needed in order to reach industrially relevant 3-HP titer, yield and productivity.

Data availability statement

The original contributions presented in the study are included in the article/Supplementary Material, further inquiries can be directed to the corresponding author.

Author contributions

AG, CJ, and IM designed experiments; AG, CJ, HJH, and IV performed the experiments; AG, CJ, HJH, AK, IV, and IM performed

the data analysis; AG drafted the manuscript; All authors revised the manuscript and approved the final version.

Funding

This work was supported by grants from the Novo Nordisk Foundation (Grant no. NNF16OC0021474 and NNF10CC1016517) to IM.

Acknowledgments

The HPLC runs and the fed-batch fermentation runs were carried out at the DTU Biosustain analytics section and pre-pilot plant, respectively.

Conflict of interest

The authors declare that the research was conducted in the absence of any commercial or financial relationships that could be construed as a potential conflict of interest.

Publisher's note

All claims expressed in this article are solely those of the authors and do not necessarily represent those of their affiliated organizations, or those of the publisher, the editors and the reviewers. Any product that may be evaluated in this article, or claim that may be made by its manufacturer, is not guaranteed or endorsed by the publisher.

Supplementary material

The Supplementary Material for this article can be found online at: <https://www.frontiersin.org/articles/10.3389/fbioe.2023.1101232/full#supplementary-material>

References

- Altenbuchner, J. (2016). Editing of the *Bacillus subtilis* genome by the CRISPR-cas9 system. *Appl. Env. Microbiol.* 82, 5421–5427. doi:10.1128/AEM.01453-16
- Andreeßen, B., Lange, A. B., Robenek, H., and Steinbüchel, A. (2010). Conversion of glycerol to poly(3-hydroxypropionate) in recombinant *Escherichia coli*. *Appl. Env. Microbiol.* 76, 622–626. doi:10.1128/AEM.02097-09
- Andreeßen, B., and Steinbüchel, A. (2010). Biosynthesis and biodegradation of 3-hydroxypropionate-containing polyesters. *Appl. Env. Microbiol.* 76, 4919–4925. doi:10.1128/AEM.01015-10
- Arnaud, M., Chastanet, A., and Débarbouillé, M. (2004). New vector for efficient allelic replacement in naturally nontransformable, low-GC-content, gram-positive bacteria. *Appl. Env. Microbiol.* 70, 6887–6891. doi:10.1128/AEM.70.11.6887-6891.2004
- Boonstra, B., French, C. E., Wainwright, I., and Bruce, N. C. (1999). The *udhA* gene of *Escherichia coli* encodes a soluble pyridine nucleotide transhydrogenase. *J. Bacteriol.* 181, 1030–1034. doi:10.1128/JB.181.3.1030-1034.1999
- Chai, Y., Kolter, R., and Losick, R. (2009). A widely conserved gene cluster required for lactate utilization in *Bacillus subtilis* and its involvement in biofilm formation. *J. Bacteriol.* 191, 2423–2430. doi:10.1128/JB.01464-08
- Chen, Z., Huang, J., Wu, Y., Wu, W., Zhang, Y., and Liu, D. (2017). Metabolic engineering of *Corynebacterium glutamicum* for the production of 3-hydroxypropionic acid from glucose and xylose. *Metab. Eng.* 39, 151–158. doi:10.1016/j.ymben.2016.11.009
- Couvreur, J., Teixeira, A., Allais, F., Spinnler, H.-E., Saulou-Bérion, C., and Clément, T. (2017). Wheat and sugar beet coproducts for the bioproduction of 3-hydroxypropionic acid by *Lactobacillus reuteri* DSM17938. *Fermentation* 3, 32. doi:10.3390/fermentation3030032
- González-Villanueva, M., Galaiya, H., Staniland, P., Staniland, J., Savill, I., Wong, T. S., et al. (2019). Adaptive laboratory evolution of *Cupriavidus necator* H16 for carbon Co-utilization with glycerol. *Int. J. Mol. Sci.* 20, 5737. doi:10.3390/ijms20225737
- Hingsamer, M., and Jungmeier, G. (2019). "Biorefineries," in *The role of bioenergy in the bioeconomy*. Editors C. Lago, N. Caldes, and Y. Lechón (Netherlands: Elsevier), 179.
- Hoffmann, T., and Bremer, E. (2011). Protection of *Bacillus subtilis* against cold stress via compatible-solute acquisition. *J. Bacteriol.* 193, 1552–1562. doi:10.1128/JB.01319-10
- Hoffmann, T., Troup, B., Szabo, A., Hungerer, C., and Jahn, D. (1995). The anaerobic life of *Bacillus subtilis*: Cloning of the genes encoding the respiratory nitrate reductase system. *FEMS Microbiol. Lett.* 131, 219–225. doi:10.1111/j.1574-6968.1995.tb07780.x
- Jers, C., Kalantari, A., Garg, A., and Mijakovic, I. (2019). Production of 3-hydroxypropionic acid from glycerol by metabolically engineered bacteria. *Front. Bioeng. Biotechnol.* 7, 124. doi:10.3389/fbioe.2019.00124
- Jiang, J., Huang, B., Wu, H., Li, Z., and Ye, Q. (2018). Efficient 3-hydroxypropionic acid production from glycerol by metabolically engineered *Klebsiella pneumoniae*. *Bioresour. Bioprocess.* 5, 34. doi:10.1186/s40643-018-0218-4

- Jiang, X.-R., Yan, X., Yu, L.-P., Liu, X.-Y., and Chen, G.-Q. (2021). Hyperproduction of 3-hydroxypropionate by *Halomonas bluephagenesis*. *Nat. Commun.* 12, 1513. doi:10.1038/s41467-021-21632-3
- Ju, S., Cao, Z., Wong, C., Liu, Y., Foda, M. F., Zhang, Z., et al. (2019). Isolation and optimal fermentation condition of the *Bacillus subtilis* subsp. natto strain WTC016 for nattokinase production. *Fermentation* 5, 92. doi:10.3390/fermentation5040092
- Kalantari, A., Chen, T., Ji, B., Stancik, I. A., Ravikumar, V., Franjevic, D., et al. (2017). Conversion of glycerol to 3-hydroxypropanoic acid by genetically engineered *Bacillus subtilis*. *Front. Microbiol.* 8, 638. doi:10.3389/fmicb.2017.00638
- Kim, C., Kim, M. Y., Michie, I., Jeon, B. H., Premier, G. C., Park, S., et al. (2017). Anodic electro-fermentation of 3-hydroxypropionic acid from glycerol by recombinant *Klebsiella pneumoniae* L17 in a bioelectrochemical system. *Biotechnol. Biofuels* 10, 199. doi:10.1186/s13068-017-0886-x
- Kim, J. H., and Kim, B. G. (2001). Construction of spore mutants of *Bacillus subtilis* for the development as a host for foreign protein production. *Biotechnol. Lett.* 23, 999–1004. doi:10.1023/A:1010515632509
- Kim, J. W., Ko, Y.-S., Un Chae, T. U., and Lee, S. Y. (2020). High-level production of 3-hydroxypropionic acid from glycerol as a sole carbon source using metabolically engineered *Escherichia coli*. *Biotechnol. Bioeng.* 117, 2139–2152. doi:10.1002/bit.27344
- Li, Y., Su, M., Ge, X., and Tian, P. (2013). Enhanced aldehyde dehydrogenase activity by regenerating NAD⁺ in *Klebsiella pneumoniae* and implications for the glycerol dissimilation pathways. *Biotechnol. Lett.* 35, 1609–1615. doi:10.1007/s10529-013-1243-1
- Li, Y., and Tian, P. (2015). Contemplating 3-hydroxypropionic acid biosynthesis in *Klebsiella pneumoniae*. *Indian J. Microbiol.* 55, 131–139. doi:10.1007/s12088-015-0513-0
- Li, Y., Wang, X., Ge, X., and Tian, P. (2016). High production of 3-hydroxypropionic acid in *Klebsiella pneumoniae* by systematic optimization of glycerol metabolism. *Sci. Rep.* 6, 26932. doi:10.1038/srep26932
- Liang, B., Sun, G., Zhang, X., Nie, Q., Zhao, Y., and Yang, J. (2022). Recent advances, challenges and metabolic engineering strategies in the biosynthesis of 3-hydroxypropionic acid. *Biotechnol. Bioeng.* 119, 2639–2668. doi:10.1002/bit.28170
- Marino, M., Ramos, H., Hoffmann, T., Philippe, G., and Jahn, D. (2001). Modulation of anaerobic energy metabolism of *Bacillus subtilis* by *arfM* (*ywiD*). *J. Bacteriol.* 183, 6815–6821. doi:10.1128/JB.183.23.6815-6821.2001
- Marreiros, B. C., Sena, F. V., Sousa, F. M., Batista, A. P., and Pereira, M. M. (2016). Type II NADH:quinone oxidoreductase family: Phylogenetic distribution, structural diversity and evolutionary divergences. *Environ. Microbiol.* 18, 4697–4709. doi:10.1111/1462-2920.13352
- Matsakas, L., Hruzová, K., Rova, U., and Christakopoulos, P. (2018). Biological production of 3-hydroxypropionic acid: An update on the current status. *Fermentation* 4, 13. doi:10.3390/fermentation4010013
- Nahvi, A., Barrick, J. E., and Breaker, R. R. (2004). Coenzyme B12 riboswitches are widespread genetic control elements in prokaryotes. *Nucleic. acids. Res.* 32, 143–150. doi:10.1093/nar/gkh167
- Nguyen-Vo, T. P., Ko, S., Ryu, H., Kim, J. R., Kim, D., and Park, S. (2020). Systems evaluation reveals novel transporter YohJK renders 3-hydroxypropionate tolerance in *Escherichia coli*. *Sci. Rep.* 10, 19064. doi:10.1038/s41598-020-76120-3
- Nguyen-Vo, T. P., Liang, Y., Sankaranarayanan, M., Seol, E., Chun, A. Y., Ashok, S., et al. (2019). Development of 3-hydroxypropionic-acid-tolerant strain of *Escherichia coli* W and role of minor global regulator *yieP*. *Metab. Eng.* 53, 48–58. doi:10.1016/j.ymben.2019.02.001
- Radeck, J., Kraft, K., Bartels, J., Cikovic, T., Dürr, F., Emenegger, J., et al. (2013). The *Bacillus* BioBrick box: Generation and evaluation of essential genetic building blocks for standardized work with *Bacillus subtilis*. *J. Biol. Eng.* 7, 29. doi:10.1186/1754-1611-7-29
- Ramakrishnan, G. G., Nehru, G., Suppuram, P., Balasubramaniam, S., Gulab, B. R., and Subramanian, R. (2015). Bio-transformation of glycerol to 3-hydroxypropionic acid using resting cells of *Lactobacillus reuteri*. *Curr. Microbiol.* 71, 517–523. doi:10.1007/s00284-015-0878-7
- Ramos, H. C., Hoffmann, H. T., Marino, M., Nedjari, H., Presecan-Siedel, E., Dreesen, O., et al. (2000). Fermentative metabolism of *Bacillus subtilis*: Physiology and regulation of gene expression. *J. Bacteriol.* 182, 3072–3080. doi:10.1128/jb.182.11.3072-3080.2000
- Stroud, R. M., Nollert, P., and Miercke, L. (2003). The glycerol facilitator GlpF its aquaporin family of channels, and their selectivity. *Adv. Protein. Chem.* 63, 291–316. doi:10.1016/s0065-3233(03)63011-1
- Wang, Z., Chen, Y., Ma, X., Shen, Z., and Zhao, X. (2011). Enhancement of riboflavin production with *Bacillus subtilis* by expression and site-directed mutagenesis of *zwf* and *gnd* gene from *Corynebacterium glutamicum*. *Bioresour. Technol.* 102, 3934–3940. doi:10.1016/j.biortech.2010.11.120
- Yasbin, R. E., Wilson, G. A., and Young, F. E. (1975). Transformation and transfection in lysogenic strains of *Bacillus subtilis*: Evidence for selective induction of prophage in competent cells. *J. Bacteriol.* 121, 296–304. doi:10.1128/jb.121.1.296-304.1975
- Zabed, H. M., Akter, S., Rupani, P. F., Akor, J., Zhang, Y., Zhao, M., et al. (2022). Biocatalytic gateway to convert glycerol into 3-hydroxypropionic acid in waste-based biorefineries: Fundamentals, limitations, and potential research strategies. *Biotechnol. Adv.* 62, 108075. doi:10.1016/j.biotechadv.2022.108075
- Zhao, P., Ma, C., Xu, L., and Tian, P. (2019). Exploiting tandem repetitive promoters for high-level production of 3-hydroxypropionic acid. *Appl. Microbiol. Biotechnol.* 103, 4017–4031. doi:10.1007/s00253-019-09772-5
- Zhao, P., and Tian, P. (2021). Biosynthesis pathways and strategies for improving 3-hydroxypropionic acid production in bacteria. *World J. Microbiol. Biotechnol.* 37, 117. doi:10.1007/s11274-021-03091-6
- Zhou, S., Catherine, C., Rathnasingh, C., Somasundar, A., and Park, S. (2013). Production of 3-hydroxypropionic acid from glycerol by recombinant *Pseudomonas denitrificans*. *Biotechnol. Bioeng.* 110, 3177–3187. doi:10.1002/bit.24980



OPEN ACCESS

EDITED BY

Qi Xianghui,
Jiangsu University, China

REVIEWED BY

Hu Jin,
Institute of Hydrobiology (CAS), China
Shuo Han,
University of Missouri–Kansas City,
United States

*CORRESPONDENCE

Qi Li,
✉ liqi@jiangnan.edu.cn

SPECIALTY SECTION

This article was submitted to Industrial Biotechnology, a section of the journal Frontiers in Bioengineering and Biotechnology

RECEIVED 30 November 2022

ACCEPTED 09 January 2023

PUBLISHED 20 January 2023

CITATION

Liang K, Luo H and Li Q (2023), Enhancing and stabilizing monoclonal antibody production by Chinese hamster ovary (CHO) cells with optimized perfusion culture strategies.
Front. Bioeng. Biotechnol. 11:1112349.
doi: 10.3389/fbioe.2023.1112349

COPYRIGHT

© 2023 Liang, Luo and Li. This is an open-access article distributed under the terms of the [Creative Commons Attribution License \(CC BY\)](https://creativecommons.org/licenses/by/4.0/). The use, distribution or reproduction in other forums is permitted, provided the original author(s) and the copyright owner(s) are credited and that the original publication in this journal is cited, in accordance with accepted academic practice. No use, distribution or reproduction is permitted which does not comply with these terms.

Enhancing and stabilizing monoclonal antibody production by Chinese hamster ovary (CHO) cells with optimized perfusion culture strategies

Kexue Liang¹, Hongzhen Luo^{1,2} and Qi Li^{1*}

¹Key Laboratory of Industrial Biotechnology, Ministry of Education, School of Biotechnology, Jiangnan University, Wuxi, China, ²School of Life Science and Food Engineering, Huaiyin Institute of Technology, Huaian, China

The perfusion medium is critical in maintaining high cell concentration in cultures for the production of monoclonal antibody by Chinese hamster ovary cells. In this study, the effects of perfusion culture strategies when using different media on the process stability, product titer, and product quality were investigated in 3-L bioreactor. The results indicated that continuous perfusion could maintain higher levels of cell density, product titer, and quality in comparison with those of the intermittent perfusion culture. Next, the perfusion culture conditions with different perfusion rates and temperature reduction methods were further optimized. When combining the high perfusion rates and delayed reduction of culture temperature at day 6, the product titer reached a higher level of 16.19 g/L with the monomer relative abundant of 97.6%. In this case, the main peak of the product reached 56.3% and the total N-glycans ratio was 95.2%. To verify the effectiveness of the optimized perfusion culture in a larger scale, a 200-L bioreactor was used to perform and the final product titer reached the highest level of 16.79 g/L at day 16. Meanwhile, the product quality (monomer abundant of 97.6%, main peak of 56.3%, and N-glycans ratio of 96.5%) could also be well maintained. This study provided some guidance for the high-efficient production of monoclonal antibody by CHO cells via optimized perfusion culture strategy.

KEYWORDS

perfusion culture, process optimization, Chinese hamster ovary cells, monoclonal antibody, product quality

1 Introduction

Recently, monoclonal antibodies (mAbs) and recombinant biopharmaceutical proteins (rBPs) have revolutionized the pharmaceutical industry (Dahodwala and Lee 2019; Zhang et al., 2021). Since 2016, about 70% of all rBPs and mAbs were produced from Chinese hamster ovary (CHO) cell lines, which are attributed to their robust growth and potential to produce non-immunogenic antibodies with similar glycosylation patterns to those of human antibodies (Lalonde and Durocher 2017; Dahodwala and Lee 2019; MacDonald et al., 2021). Meanwhile, at the current approval rate of four new products a year, more than 70 mAbs were on the market by 2020, and the world-wide sales will reach \$125 billion (Ecker et al., 2015; Bhatti and Salama 2018). Compared with most of the small molecular drugs, mAbs feature with some advantages such as reduced off-target effects, greater surface area for binding, etc. (Shepard et al., 2017; Ha et al., 2022). In order to improve the competitiveness of one mAb

product, the mAb titer needs to be improved to elevate the economic effectiveness (Ha et al., 2022). Therefore, it is essential to develop advanced technology by process engineering, optimization, and control strategies.

Nowadays, fed-batch and perfusion cell cultures are the two current processes of the large-scale industrial production of mAbs and rBPs (Zhuang et al., 2017; Zheng et al., 2018; Schulze et al., 2022). Generally, scaling of the fed-batch process needs larger and more rigid layouts which limits its application (Karst et al., 2016; MacDonald et al., 2021). The membrane-based alternating tangential flow filtration (ATF) technology is the most commonly used cell retention method in perfusion cultures to increase cells density and mAbs productivity (Genzel et al., 2014; Gräniche et al., 2020). It has been reported that for the production of unstable therapeutic proteins, such as recombinant enzymes and blood coagulation factors, the perfusion process possesses more advantages (Bettinardi et al., 2020; MacDonald et al., 2021). In the perfusion mode, culture broth contained products and waste is perfused through the bioreactor under the perfusion controller, while the cells/products are retained or recycled back into the bioreactor (Ahn et al., 2008; MacDonald et al., 2021; MacDonald et al., 2022). Consequently, a consistent and steady culture condition with metabolized by-product rapidly removal results in a stable and uniform product of high quality under perfusion culture process (Schwarz et al., 2020; Yin et al., 2021). In general, culture environmental parameters including temperature, osmolality, levels of dissolved oxygen (DO), CO₂ partial pressure (pCO₂), and perfusion rate could affect the performance of recombinant protein production in CHO cells (Sou et al., 2017; Wang Q. et al., 2018b; Hippach et al., 2018; Madabhushi et al., 2021). Some studies found that the specific productivity of recombinant CHO cell lines and the product quality can be improved by lowering the culture temperature (Tait et al., 2013; Wang K. et al., 2018a). Due to the various quality attributes and types of proteins, the culture temperature and other environmental factors still should be optimized to improve the process stability and product quality when exploring a specified mAb.

Besides the improvement of product titer, consistently good product quality is also a considerable factor (Ha et al., 2022). The product quality is the suitability of a drug product for its intended use. Based on the current good manufacturing practices (cGMP) of the Food and Drug Administration (FDA) of U.S., the critical quality attributes include aggregation, charge variation, and glycosylation (Bonaccorso et al., 2021; Ha et al., 2022). In addition, scaling up the production process in a larger bioreactor for verifying the effectiveness of process strategy is the crucial step for the commercial category (Xing et al., 2009; Vodopivec et al., 2019).

Based on the above analysis, the objective of this study was to optimize the production process under perfusion culture strategy of the CHO cell line producing one anti-PD-1 mAb. Firstly, the effects of different media on the perfusion culture and product quality were investigated to reduce the raw material costs. Subsequently, the perfusion culture conditions, including perfusion rates and culture temperature, were further optimized for improving the product titer and quality. Finally, the effectiveness of the optimized perfusion culture strategy was successfully verified in a 200-L bioreactor. The obtained results could provide some guidance for the mAb production *via* process optimization and control methods.

2 Materials and methods

2.1 Cell line and culture media

The CHO cell line, which could produce anti-PD-1 mAb, was used in this work. Here, several media were chosen for CHO cells culture. The chemical composition of basic medium I (BM-I) was 24.30 g/kg Dynamics serum-free medium (Thermo Fisher, NH, United States), 15.49 g/kg hypoxanthine monosodium, 3.80 mg/kg thymidine, 0.57 g/kg glutamine, 0.70 g/kg cell boost 5 (HyClone™), and 1.00 g/kg poloxamer 188 (HyClone™). The feed medium I (FM-I) consists of 79.60 g/kg CD efficient feed C AGT nutrient supplement (Life Technologies Corporation, United States), 15.00 g/kg sheff-CHO plus PF ACF (Kerry Biofunctional Ingredients Inc., United States), and 13.30 g/kg 10 N NaOH solution. The feed medium II (FM-II) consists of 4.75 g/kg L-tyrosine, and 7.95 g/kg L-cystine. The chemical composition of basic medium II (BM-II) was 24.30 g/kg CD CHO AGT (Thermo Fisher, NH, United States), 0.58 g/kg glutamine, 15.81 mg/kg hypoxanthine monosodium, and 3.88 mg/kg thymidine. The basic medium III (BM-III) consists of 22.23 g/kg Eden B600S, 0.58 g/kg glutamine, 15.49 mg/kg hypoxanthine monosodium, 3.80 mg/kg thymidine, and 2.13 g/kg NaHCO₃. The feed medium III (FM-III) consists of 177.05 g/kg Eden F600aS. The feed medium IV (FM-IV) consists of 71.84 g/kg Eden F600bS and 25.70 g/kg NaOH. The basic medium IV (BM-IV) consists of 22.31 g/kg Eden B501S, 0.58 g/kg glutamine, 15.49 mg/kg hypoxanthine monosodium, 3.80 mg/kg thymidine, and 2.18 g/kg NaHCO₃. The feed medium V (FM-V) consists of 179.69 g/kg Eden F500aS. The feed medium VI (FM-VI) consists of 77.47 g/kg Eden F200bS and 29.05 g/kg NaOH. The feed medium VII (FM-VII) consists of 20.01 g/kg Eden B600S, 0.52 g/kg glutamine, 13.49 mg/kg hypoxanthine monosodium, 3.42 mg/kg thymidine, 1.92 g/kg NaHCO₃, and 17.71 g/kg Eden F600aS. The commercial media including Eden B600S, Eden F600aS, F600bS, Eden B501S, Eden F500aS, Eden F200bS, and Eden B501S were purchased from Bio-Engine Co., Ltd., Shanghai, China.

2.2 Culture conditions

In this study, eight runs (#1-#8) were performed by using 3-L bioreactor (Applikon, Schiedam, Netherlands) for the optimization of perfusion culture strategy to produce anti-PD-1 mAb. Furthermore, run #9 was performed by using a 200-L bioreactor (Applikon, Schiedam, Netherlands) for verifying the effectiveness of perfusion culture for mAb production with a larger scale. The alternating tangential flow filtration (ATF) technology was used to develop a concentration culture by using the hollow fiber membranes (50 kDa). The schematic diagram of the CHO perfusion culture for the production of anti-PD-1 mAb was shown in Figure 1. In the perfusion cultures of runs #1-#8, 2 L of CHO cells with the density of 1.5×10^6 cells/mL were inoculated in the 3-L bioreactor. For the run #9, 180 L of CHO cells with the density of 1.5×10^6 cells/mL were inoculated in the 200-L bioreactor. The culture pH was automatically controlled at 6.80–6.90 by adding either NaHCO₃ or CO₂. The agitation speed was kept constant at 250 rpm during the whole culture process. The dissolved oxygen (DO) concentration was maintained at $40 \pm 15\%$ of air saturation. The initial culture temperature was controlled at 36.5°C during the growth stage and then decreased to 31.0°C at day 5 (runs #1-#4, run #5, and run #7) or day 6 (run #6 and runs #8-#9). The cultures were ended at day 14 or day 16. The perfusion rates (L/L/day, VVD) and

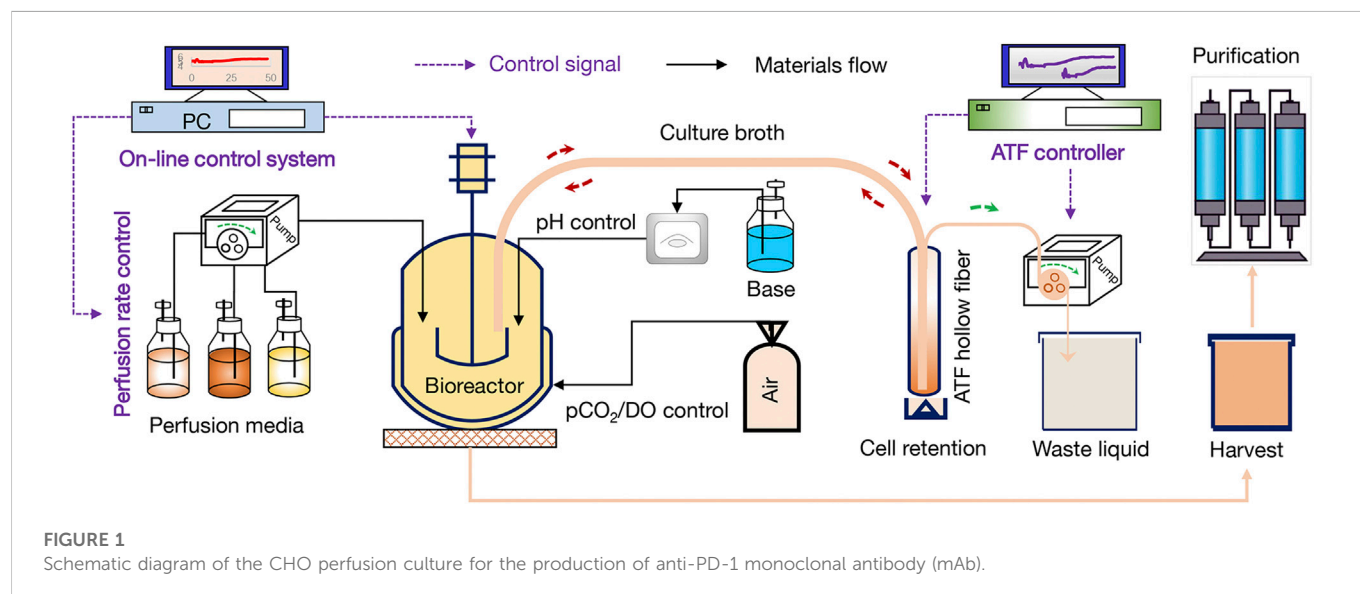


TABLE 1 The perfusion rates (VVD) of perfusion media in runs #1-#4 by using 3-L bioreactor.

Culture time (day)	Run #1 (continuous perfusion)			Run #2 (continuous perfusion)			Run #3 (intermittent perfusion)			Run #4 (continuous perfusion)		
	BM-I	FM-I	FM-II	BM-II	FM-III	FM-IV	BM-II	FM-III	FM-IV	BM-IV	FM-V	FM-VI
D2	0.400	0.000	0.005	0.400	0.000	0.005	N/A	N/A	N/A	0.400	0.000	0.005
D3	0.450	0.050	0.005	0.450	0.050	0.005	0.500	0.050	0.005	0.450	0.050	0.005
D4	0.595	0.105	0.005	0.595	0.105	0.005	N/A	N/A	N/A	0.595	0.105	0.005
D5	0.680	0.120	0.005	0.680	0.120	0.005	0.500	0.050	0.005	0.680	0.120	0.005
D6	0.680	0.120	0.005	0.680	0.120	0.005	N/A	N/A	N/A	0.680	0.120	0.005
D7, D9, D11, D13	0.900	0.100	0.005	0.900	0.100	0.005	0.500	0.050	0.005	0.900	0.100	0.005
D8, D10, D12	0.900	0.100	0.005	0.900	0.100	0.005	N/A	N/A	N/A	0.900	0.100	0.005

Note: The culture temperature of runs #1-#4 was reduced at day 5.

TABLE 2 The optimization of perfusion culture in runs #5-#8 by using 3-L bioreactor.

Culture time (day)	Run #5			Run #6			Run #7			Run #8		
	BM-II	FM-III	FM-IV	BM-II	FM-III	FM-IV	BM-II	FM-III	FM-IV	BM-II	FM-III	FM-IV
D2	0.400	0.000	0.005	0.400	0.000	0.005	0.450	0.050	0.005	0.300	0.300	0.005
D3	0.450	0.050	0.005	0.450	0.050	0.005	0.450	0.050	0.005	0.585	0.065	0.005
D4	0.595	0.105	0.005	0.595	0.105	0.005	0.675	0.075	0.005	1.000	0.100	0.005
D5	0.680	0.120	0.005	0.680	0.120	0.005	0.675	0.075	0.005	1.000	0.100	0.005
D6	0.680	0.120	0.005	0.680	0.120	0.005	0.675	0.075	0.005	1.000	0.100	0.005
D7-D12	0.900	0.100	0.005	0.900	0.100	0.005	0.900	0.100	0.005	1.000	0.100	0.005
D13-D15	0.900	0.100	0.005	0.900	0.100	0.005	0.900	0.100	0.005	1.300	0.140	0.005

Note: The culture temperature of run #5 and run #7 was reduced at day 5. Run #5 refers to the perfusion culture with N-2/N-1 adaption by using BM-II as the basic medium. Run #6 refers to the perfusion culture with the same perfusion rates, while the temperature was reduced at day 6. Run #7 refers to the perfusion culture with different perfusion rates of run #5-#6. Run #8 refers to the perfusion culture with higher perfusion rates and the temperature was reduced at day 6.

culture conditions of runs #1–#8 were set as shown in Tables 1, 2. For the continuous perfusions (runs #1–#2, runs #4–#9), the ATF controller was started at day 2 and cells were pumped in and out of the hollow fiber with a setting rate by using different feeding media (Tables 1, 2). For the intermittent perfusion of run #3, the ATF controller was started at day 3 for running 24 h and then stopped for 24 h (the detailed perfusion rates were shown in Table 1). It should be noted that the run #5 was the perfusion culture with N-2/N-1 adaption by using BM-II as the basic medium. In addition, the perfusion rates and culture conditions of run #9 were the same as the run #8. A 50-mL sample was collected daily to determine viable cell density (VCD), viability, and the supernatant obtained after centrifugation was kept at -80°C for the further analysis of glucose concentration and lactate concentration.

2.3 Analytical methods

CHO cells were sampled from bioreactor every day, and the cell density and viability were then measured with an automatic cell counter (Vi-Cell XR, Beckman Coulter Inc., United States). The mAb titer was measured by a POROSTM A20 column (2.1 mm \times 30 mm, Thermo Fisher Scientific) with an HPLC system (Agilent 1260 Infinity II). Antibody purity and aggregation analysis were performed by the analytical size-exclusive chromatography (SEC-HPLC, Agilent 1260, United States) with the column of TSKgel G3000SWXL (7.8 mm \times 250 mm \times 5 μm , Tosoh, Tokyo, Japan) (Zhuang et al., 2017). The charge variation of the anti-PD-1 mAb was determined by cation-exchange chromatography (CEX-HPLC). Antibody charge variants were separated on a column of ProPac WCX-10 (4 mm \times 250 mm \times 10 μm , Thermo Fisher Scientific, Sunnyvale, CA, United States) using an Agilent 1260 HPLC system at a flow rate of 1.0 mL/min (Zhuang et al., 2017).

The oligosaccharide profiles were ascertained for the quantitative assessment of the mAb products by an HPLC-based method (Zheng et al., 2018). For simplicity, the four dominant glycoforms are written as G0F, G1F, G2F, and Man-5, in which the letter “G” indicates glycans, the number signifies how many terminal galactose molecules are attached to the two arms of the glycan, and the letter “F” indicates a fucosylated N-linked glycan in the immunoglobulin G (IgG) Fc domain.

2.4 Statistical analysis

In this study, to ensure the data accuracy and reproducibility, all analytical methods used were validated prior to the measurements. The data are represented as mean \pm SD of three biological independent experiments. Significant differences between perfusion cultures were confirmed by a two-tailed Student's *t*-test using Microsoft Excel 2016. The statistical significance was considered as $p < 0.05$.

3 Results and discussion

3.1 Production performance of mAb under CHO cell perfusion cultures using different media in 3-L bioreactor

For the production of mAb using CHO cells, the raw materials cost (mainly the cost of culture medium) generally occupies high ratio over the total production cost. Therefore, several cultures using relative low-

price medium to replace the high-price and commercial media (BM-I, FM-I, and FM-II used in run #1 as the control) were performed in a 3-L bioreactor to improve the overall economics. In this study, some culture media purchased from Bio-Engine Co., Ltd. (Shanghai, China) with low-prices were selected as the perfusion culture media for evaluation of the production performance of anti-PD-1 mAb. The perfusion culture conditions for runs #1–#4 were summarized in Table 1. The changing patterns of VCD, viability, glucose concentration, lactate concentration, osmolality (Osmo), and pCO_2 during perfusion cultures by using different media in 3-L bioreactor were shown in Figure 2. The VCD during the first 3 days in runs #1–#4 stayed at the similar levels of 1.5×10^6 – 17×10^6 cells/mL although using different media for perfusion culture (Figure 2A). When using BM-I, FM-I, and FM-II as the media for continuous perfusion (run #1), the highest VCD reached 63.0×10^6 cells/mL at day 6, while it then gradually decreased to a final level of 53.7×10^6 cells/mL at day 14. In run #2, the alternative media of BM-II, FM-III, and FM-IV were used for continuous perfusion after day 2 and the VCD during day 5–14 was kept at 50.1×10^6 – 65.6×10^6 cells/mL (Figure 2A). In addition, the intermittent perfusion culture when using BM-II, FM-III, and FM-IV was also performed (run #3). The VCD data of run #3 showed that intermittent perfusion could not elevate the cells density, which is mainly attributed to the nutrient shortage (Pérez-Rodríguez et al., 2020; MacDonald et al., 2021). The results indicated that continuous perfusion could maintain higher VCD levels (Figure 2A). As shown in Figure 2B, the viability of CHO cells during culture from day 0 to day 8 in four runs was maintained at $> 95\%$, and it still kept at the similar levels in runs #2–#3 which used BM-II, FM-III, and FM-IV during the perfusion culture. In run #1 and run #4, the final viability of CHO cells was decreased to $\sim 85\%$. The above results of VCD and viability of CHO cells in the four runs revealed that BM-II, FM-III, and FM-IV were the better media for perfusion culture.

Besides CHO cells growth, the key metabolites including glucose and lactate in culture broth were also analyzed. The glucose concentration during the period of day 6–14 in run #1 ranged 3.73–4.53 g/L, which was lower than that of runs #2–#4 (Figure 2C). As shown in Figure 2D, the lactate concentration in run #3 under intermittent perfusion culture kept at the higher levels of 0.57–1.60 g/L after day 4. In addition, the lactate concentration in culture broth (runs #1, #2, and #4) was relative lower with a final accumulation of 0.2–0.3 g/L. It was reported that lactate accumulation during cell culture could cause negative effects on CHO cells growth and mAb production (Konakovsky et al., 2016; Graham et al., 2019), which could also be reflected by the VCD changing patterns in run #3. For the anti-CD52 rCHO cell perfusion cultures, it was found that the initial osmolality of 180 mOsm/kg in early stage of perfusion cultures could inhibit the viable cell density, but the stable osmolality finally achieves higher mAb production (Qin et al., 2019). As shown in Figure 2E, the osmolality changings in four runs revealed that the range of 300–400 mOsm/kg could not significantly inhibit the CHO cells growth. Furthermore, the pCO_2 levels were shown in Figure 2F with no significant difference among different perfusion cultures.

The profiles of mAb titer, monomer and aggregate relative abundance, variant contents, and percentages of N-glycans under perfusion cultures of run #1–#4 were displayed in Figure 3. Obviously, under the intermittent perfusion culture strategy, the mAb production in run #3 was only 4.39 g/L at day 14, while the titer still reached to higher levels of 8.73–9.83 g/L in other three runs under continuous perfusion cultures (Figure 3A). The balance between light chains and heavy chains of immunoglobulins could change the

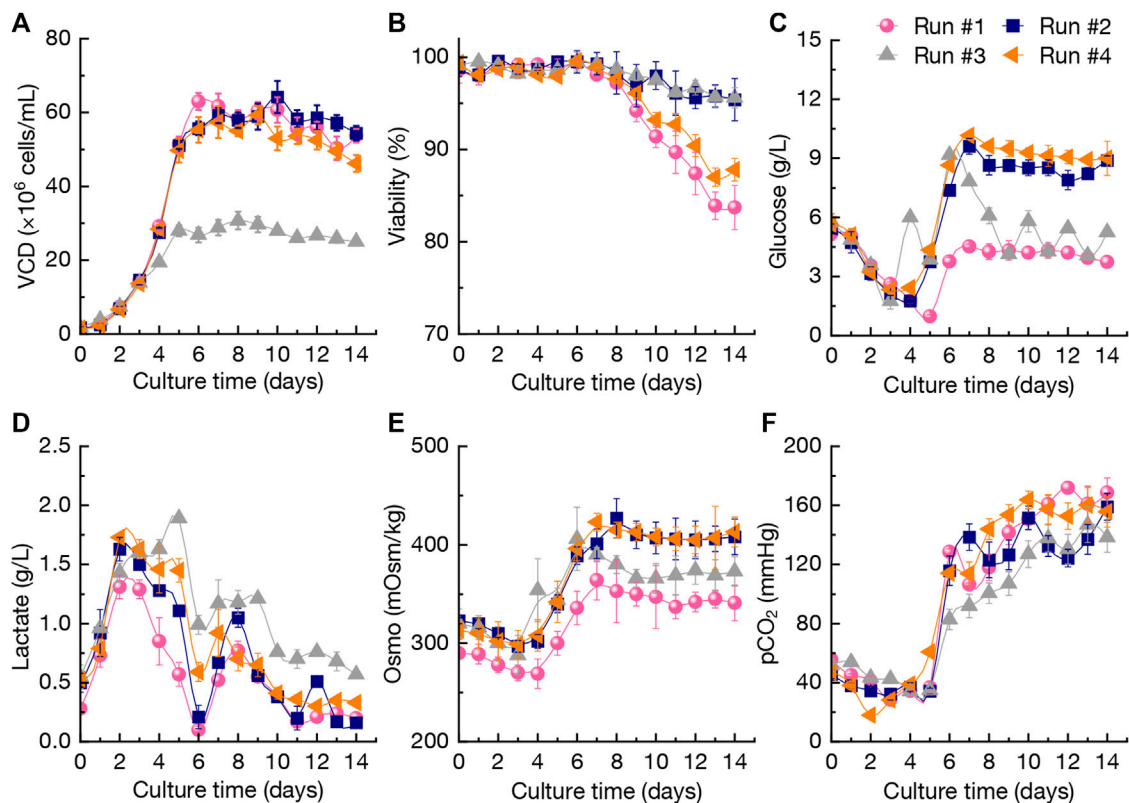


FIGURE 2 Changing profiles of viable cell density (VCD) (A), viability (B), glucose concentration (C), lactate concentration (D), osmolality (Osmo) (E), and pCO_2 (F) during perfusion cultures using different media in 3-L bioreactor. The error bars indicate the standard deviations (SD) of three independent experiments. Continuous perfusion: run #1, #2, and #4; intermittent perfusion: run #3. The perfusion rates and conditions in the four runs were shown in Table 1.

aggregation of mAbs which is a crucial key in the mAb production process (van der Kant et al., 2017). As shown in Figure 3B, the monomer relative abundance in different runs was comparable which ranged from 96.5% to 97.9%. The aggregate relative abundance in mAbs obtained from intermittent perfusion culture (run #3) reached the highest level of 3.5% (vs. 2.1%–2.2% under continuous perfusion cultures of runs #1–#2). The results revealed that intermittent perfusion strategy could not only affect the CHO cells growth (Figure 2A), but also improve the aggregate relative abundance (Figure 3B) because of the varied growth conditions (Kim et al., 2008; Bettinardi et al., 2020). Due to the potential effects on the stability and biological potency, the charge heterogeneity is considered as the critical quality index during the mAb production processes (Hintersteiner et al., 2016; Qin et al., 2019). As shown in Figure 3C, the main peak contents of 55.4% in run #2 were significantly higher than those of run #1 (49.5%) and run #4 (49.5%). In addition, the acidic variant content in run #4 when using BM-IV, FM-V, and FM-VI as the perfusion media reached 27.5% with significant differences between other cases ($p < 0.05$, Figure 3C). The basic variant content in run #1 by using BM-I, FM-I, and FM-II as the perfusion media was 28.4% which would decrease the mAb quality. The N-linked oligosaccharides (i.e., N-glycans) profiles were shown in Figure 3D and four dominant glycoforms (G0F, G1F, G2F, and Man-5) were exhibited. There is no statistically significant difference for all glycoforms except for G1F and G2F. The Man-5 ratio in mAbs produced from different cultures was maintained 0.5%–0.7% which could meet the specified requirement for mAbs quality commercially

(lower than 5.0%, Figure 3D). In summary, based on the above results including process parameters, anti-PD-1 mAb titer, and mAb quality, the continuous perfusion culture by using BM-II, FM-III, and FM-IV as the media (run #2) could replace the commercial media used in run #1 for mAb production.

3.2 Optimized CHO perfusion cultures for enhancing and stabilizing mAb production in 3-L bioreactor

In order to improve the overall performance of mAb production, several cultures of runs #5–#8 were further performed, and the culture conditions/perfusion rates were summarized in Table 2. In run #5, BM-II was used for the adaption of N-2/N-1 CHO cells for cultivation. In addition, the culture temperature was reduced at day 5 in runs #5 and #7, while it reduced at day 6 in runs #6 and #8. The perfusion rates were systematically optimized for evaluation of the effects on process parameters, mAb titers, and product quality.

As shown in Figure 4A, the VCD of CHO cells during perfusion culture under N-2/N-1 adaption (run #5) reached 57.9×10^6 cells/mL at day 7 and final VCD was 45.6×10^6 cells/mL at day 16. In contrast, when reducing the culture temperature to 31.0°C from day 5 to day 6 (run #6), the VCD of CHO cells was higher than that of run #5 during the period of day 8–16. It was found that adjustment of the perfusion rates in day 2–6 (run #7) could not increase the VCD of CHO cells compared with runs

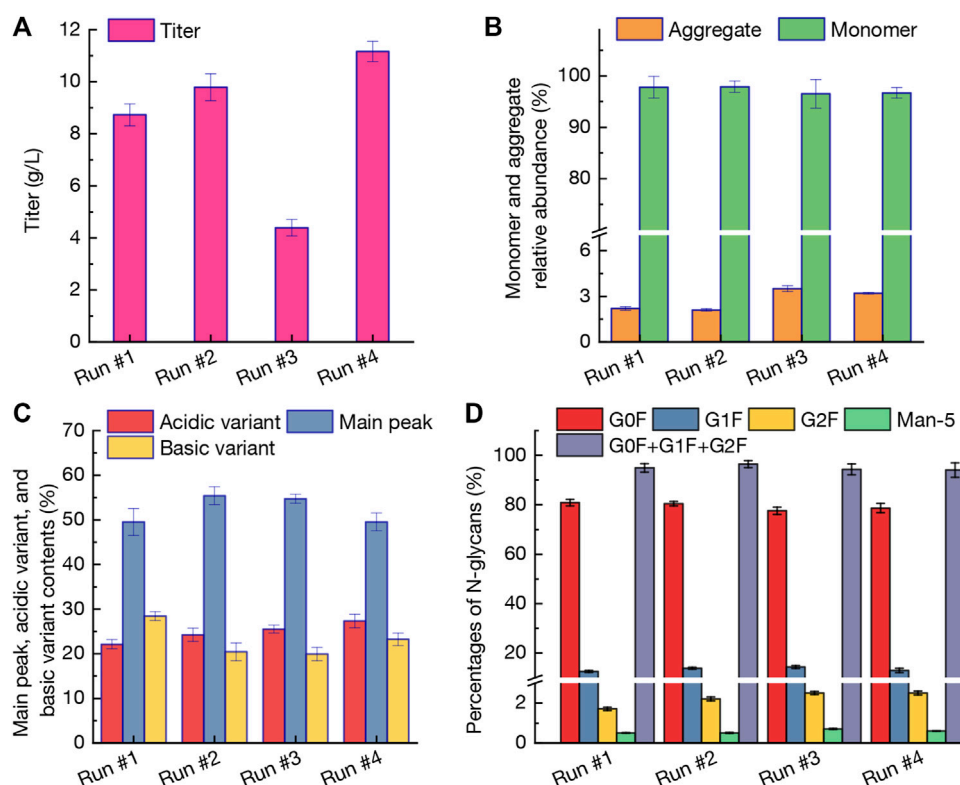


FIGURE 3

Profiles of mAb titer (A), monomer and aggregate relative abundance (B), variant contents (C), and percentages of N-glycans (D) under perfusion cultures of run #1-#4. The error bars indicate the SD of three independent experiments.

#5-#6 (Figure 4A). In addition, increasing the perfusion rates (run #8) resulted in the highest VCD levels of 76.1×10^6 – 80.5×10^6 cells/mL at day 7–11. At the culture end at day 16, the final VCD still kept at a higher level of 63.6×10^6 cells/mL. The viability of CHO cells in run #5 was the lowest level among the cultures after day 7, which indicated that N-2/N-1 adaption by BM-II could not improve the robustness of CHO cells growth. The viability of CHO cells in runs #5-#8 maintained at more than 95% without significant differences ($p > 0.05$, Figure 4B). The changing patterns of glucose concentration and lactate concentration in runs #5-#8 revealed that those two process parameters were not significantly influenced by different perfusion culture strategies, although the VCD and viability of CHO cells showed various trends (Figures 4C, D). Compared with run #5, the osmotic pressure in run #8 during day 6–16 with high perfusion rates kept relative lower levels (Figure 4E). Furthermore, the pCO_2 in run #8 was also lower than that of run #5 (Figure 4F). Zhu et al. (2005) reported that elevating pCO_2 from 50 mmHg to 150 mmHg under controlled osmolality leads to a 9% reduction in CHO cells growth rate with fed-batch culture, and a 60% reduction in cells growth was achieved when increasing the osmotic pressure from 316 mOsm/kg to 450 mOsm/kg (Zhu et al., 2005). The results obtained from the perfusion culture strategies (Figure 4) were consistent with the above conclusions.

The mAb production obtained from runs #5-#8 was shown in Figure 5A. At day 11, the titer reached 4.46 g/L in run #5, 6.61 g/L in run #6, 5.65 g/L in run #7, and 8.33 g/L in run #8, respectively. It is concluded that N-2/N-1 adaption method could restrict the CHO cells growth (Figure 4) and mAb production during culture process. The

lower VCD and viability of CHO cells in run #5 (Figures 4A, B) resulted in the lowest titer. Furthermore, when using the high perfusion rate strategy (run #8), the titer at day 14 reached 12.93 g/L and final titer was up to a higher level of 16.19 g/L at day 16 (Figure 5A). In this case, the mAb production rate was 1.572 g/L/day which was significantly higher than other three runs (1.195 g/L/day for run #5, 1.278 g/L/day for run #6, and 1.210 g/L/day for run #7). Due to the vital role in therapeutic protein products, the aggregation of mAbs should be carefully investigated and analyzed (Wang 2005; Ha et al., 2022). Interestingly, as shown in Figure 5B, the relative abundance of monomer and aggregate maintained at similar levels of 2.3%–2.5% and 97.5%–97.7% in runs #5-#8 with no statistically significant difference ($p > 0.05$). The results revealed that the selected perfusion media (BM-II, FM-III, and FM-IV) could not affect the aggregation relative abundance significantly. The contents of main peak, along with the acidic and basic variants produced from the four perfusion runs were shown in Figure 5C. Since the variant of acidic and basic in mAbs are the heterologous structures formed under some modifications in the main peak (Ha et al., 2022). When adaption of CHO cells with BM-II before inoculation in bioreactor, the acidic variant and basic variant ratios were 23.6% and 22.6%. When reduction of the culture temperature at day 6, the corresponding indexes still kept similar levels of 23.4% and 21.7% ($p > 0.05$). When increasing the perfusion rate in run #8, the acidic variant also maintained 23.8% with $p > 0.05$, while the basic variant was reduced to a lower level of 19.9% ($p < 0.05$). Compared with the main peak in run #5 (53.8%), the contents of main peak was 54.9% in

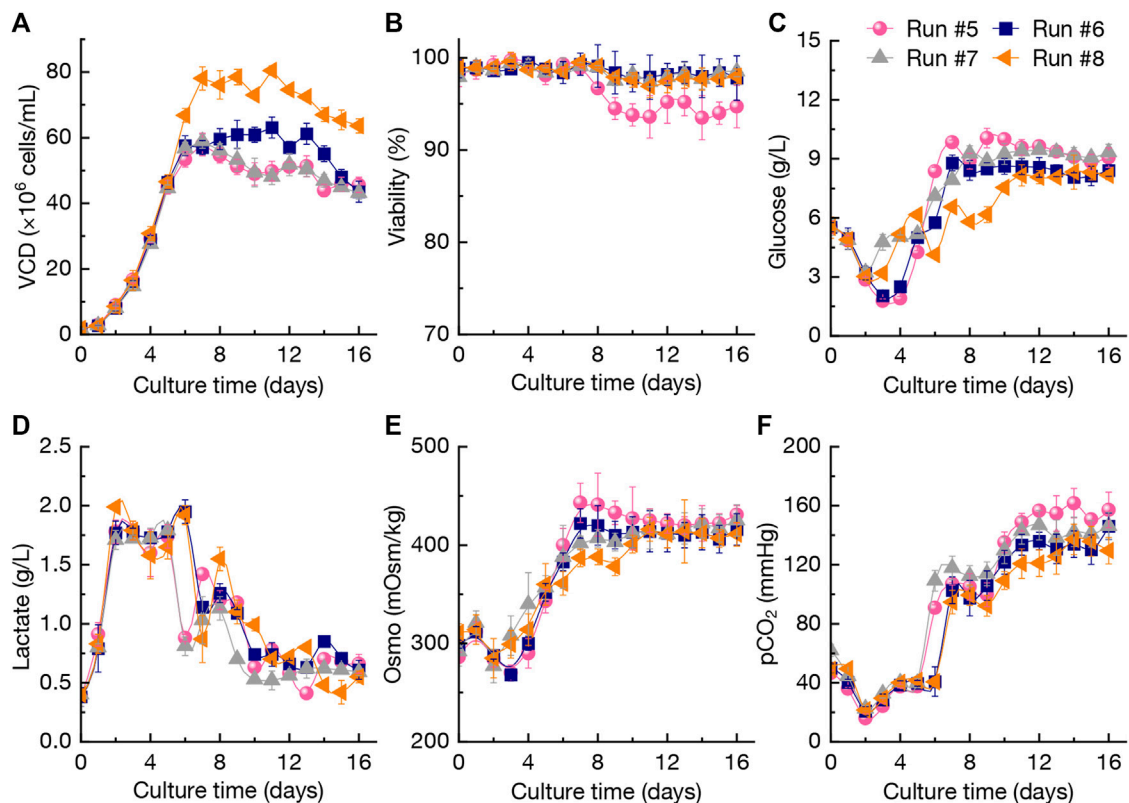


FIGURE 4

Changing profiles of VCD (A), viability (B), glucose concentration (C), lactate concentration (D), Osmo (E), and pCO₂ (F) during different perfusion cultures in 3-L bioreactor. The error bars indicate the SD of three independent experiments.

run #6 ($p > 0.05$), 55.1% in run #7 ($p > 0.05$), and 56.3% in run #8 ($p < 0.05$), respectively. Furthermore, the biological and physiological properties of proteins could be affected by N-glycans. As shown in Figure 5D, the percentage of G0F, G1F, and G2F in run #5 was 80.6%, 12.4%, and 2.1%, with a total N-glycans of 95.1%. Although the perfusion culture strategies varied in runs #6–#8, the N-glycans percentage was not significantly changed (95.2% for run #6, 95.5% for run #7, and 95.2% for run #8). In addition, the Man-5 ratio in the four perfusion cultures varied in a range of 0.3%–0.4% (Figure 5D). In summary, based on the results of mAb quality including titer, monomer and aggregate relative abundance, main peak and variants, and N-glycans percentages, it could be concluded that the culture strategy with higher perfusion rates (run #8) could achieve an excellent production of mAb with relative higher quality.

3.3 The mAb production performance under the optimized perfusion culture in 200-L bioreactor

Generally, it is considered that large-scale bioproduction is the key to a successful biopharmaceutical manufacturing. However, the mAb production performance under large-scale bioreactor was not desirable due to the lower cell viability and productivity (Gao et al., 2016; Vodopivec et al., 2019). Here, the effectiveness of the optimized perfusion culture strategy proposed in 3-L bioreactor (run #8) on the

anti-PD-1 mAb production performance was further verified in the 200-L bioreactor (run #9).

As shown in Figure 6A, under the perfusion culture strategy, the VCD of CHO cells reached 55.5×10^6 cells/mL at day 5 rapidly and then the cells growth rate was reduced gradually. The highest VCD reached 73.0×10^6 cells/mL at day 7, which was lower than that of run #8 (80.5×10^6 cells/mL at day 11, Figure 4A). The results indicated that larger bioreactor could affect the CHO cells growth mainly due to the various mixing environments. During the perfusion culture stage, the viability in run #9 maintained at higher levels of 96.5%–100%. The glucose concentration in culture broth was gradually increased from 3.25 g/L (day 0) to 9.08 g/L (day 10), and then it was reduced to a final concentration of 6.28 g/L at day 16 (Figure 6B). In this case, the glucose concentration during day 14–16 was lower than run #8 (Figure 4C). In addition, the lactate concentration maintained at lower levels of 0.20–0.27 g/L during day 10–14, which indicated that the assimilation of lactate by CHO cells was efficient. Afterwards, the accumulation of lactate was increased to a higher concentration of 0.96 g/L (Figure 6B). It has reported that pCO₂ could accumulate to the higher levels in large-scale bioreactors when the formed CO₂ from CHO cells was not removed efficiently (Zhu et al., 2005). As exhibited in Figure 6C, the pCO₂ reached up to ~175 mmHg after day 10 which was significantly higher than the culture performed in 3-L bioreactor (run #8, $p < 0.05$). It was mainly attributed to the higher lactate accumulation (Figure 6B). In addition, the osmolality under the perfusion culture strategy was kept at appropriate level

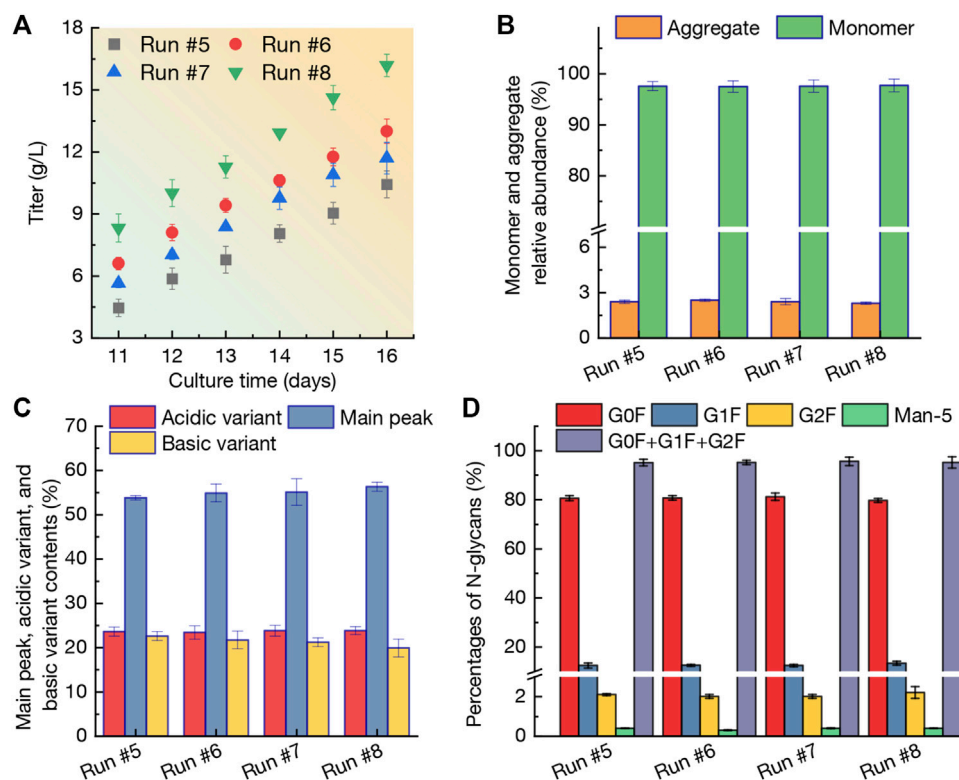


FIGURE 5

Profiles of mAb titer (A), monomer and aggregate relative abundance (B), variant contents (C), and percentages of N-glycans (D) during perfusion cultures of run #5-#8. The error bars indicate the SD of three independent experiments.

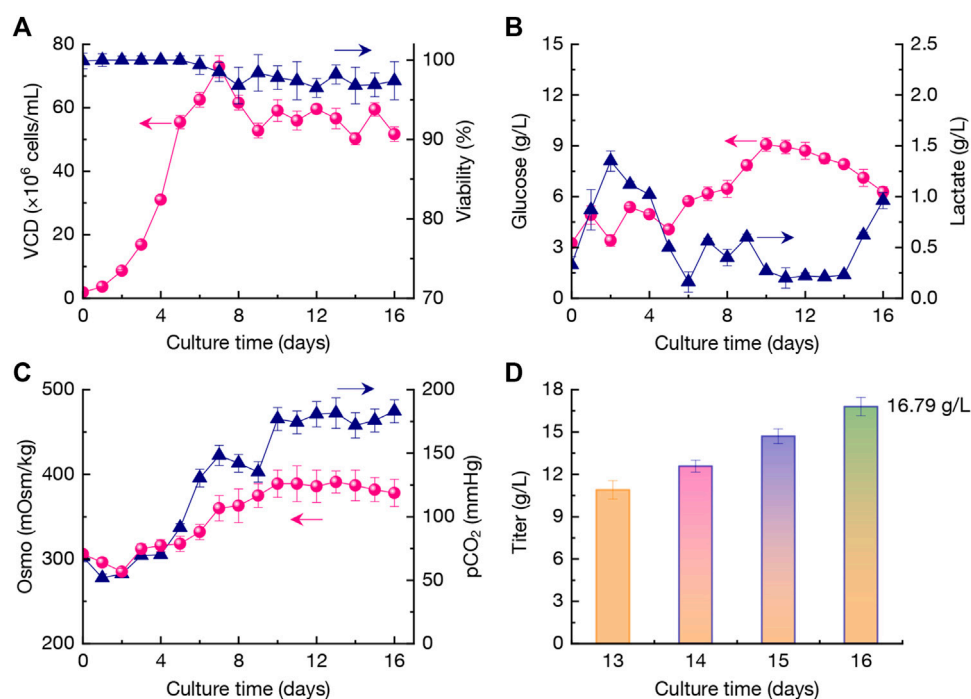


FIGURE 6

Changing profiles of VCD and viability (A), glucose and lactate concentration (B), Osmo and pCO₂ (C), and titer (D) during the optimized perfusion culture in a 200-L bioreactor. The error bars indicate the SD of three independent experiments.

TABLE 3 Protein titers and relative abundant, mAb charge variant content, and percentages of N-glycans under different perfusion strategies.

Culture runs with perfusion strategies		Run #1 (3 L reactor) ^a	Run #2 (3 L reactor) ^a	Run #8 (3 L reactor) ^b	Run #9 (200 L reactor) ^b
Titer (g/L)	Day 14	8.73 ± 0.42	9.79 ± 0.52	12.93 ± 0.12	12.57 ± 0.42
	Day 16	N/A	N/A	16.19 ± 0.54	16.79 ± 0.65
Relative abundant (%)	Aggregate	2.2 ± 0.11	2.1 ± 0.08	2.3 ± 0.07	2.3 ± 0.11
	Monomer	97.8 ± 2.10	97.9 ± 1.10	97.6 ± 1.24	97.6 ± 0.89
Content (%)	Acidic variant	22.1 ± 0.97	24.2 ± 1.50	23.8 ± 0.90	23.5 ± 0.89
	Main peak	49.5 ± 2.90	55.4 ± 1.90	56.3 ± 1.00	56.3 ± 2.13
	Basic variant	28.4 ± 0.96	20.4 ± 1.96	19.9 ± 1.98	20.2 ± 1.20
N-glycans (%)	G0F	80.8 ± 1.30	80.4 ± 0.90	79.7 ± 0.80	80.8 ± 0.90
	G1F	12.5 ± 0.38	13.8 ± 0.40	13.3 ± 0.80	13.6 ± 0.32
	G2F	1.7 ± 0.08	2.2 ± 0.10	2.2 ± 0.29	2.1 ± 0.08
	G0F + G1F + G2F	94.9 ± 1.76	96.4 ± 1.40	95.2 ± 2.31	96.5 ± 1.30
	Man-5	0.5 ± 0.01	0.5 ± 0.02	0.4 ± 0.01	0.4 ± 0.01

N/A, not applicable for Run #1 and Run #2.

^aThe parameters including relative abundant, content, and N-glycans were determined by the Day 14 samples in Run #1 and Run #2.

^bThe parameters including relative abundant, content, and N-glycans were determined by the Day 16 samples in Run #8 and Run #9.

of <390 mOsm/kg (Figure 6C), which might be beneficial for high-efficient mAb production.

The mAb production profiles were displayed in Figure 6D. At day 13, the titer was 10.89 g/L. The average productivity of mAb during day 13–16 reached 1.97 g/L/day with the higher final titer of 16.79 g/L. The titer was kept with comparable level with run #8 (16.19 g/L, $p > 0.05$). Furthermore, the overall production performances of different cultures including run #1, #2, #8, and #9 were summarized in Table 3. The relative abundant of aggregate in run #9 was 2.3% and the monomer ratio reached 97.6%. In this case, the contents of main peak, acidic variant, and basic variant were 56.3%, 23.5%, and 20.2%, respectively (Table 3). In addition, the total N-glycans of 96.5% was also obtained with 80.8% of G0F, 13.6% of G1F, and 2.1% of G2F, and the content of Man-5 was kept at a low level of 0.4%.

Perfusion culture processes have been widely used for enhancing the production performance by CHO or human cell lines. A CHO cell line expressing a humanized anti-CD52 mAb was cultivated in perfusion mode, which results in a higher productivity and stabilized product quality. In the perfusion process, the maximal volumetric productivity reached up to 0.55 g/L/day, which was 2.2-fold higher than that of the fed-batch culture (Zhuang et al., 2017). Recently, Schwarz et al. (2020) reported that the higher cell density of $\sim 80 \times 10^6$ cells/mL could be achieved with perfusion cultivations and the recombinant human Erythropoietin (rhEPO) was stabilized expressed with a volumetric productivity of 0.6 g/L/day (Schwarz et al., 2020). Additionally, the recent advances of perfusion culture of CHO cells used in the biopharmaceutical industry with the demands for Industry 4.0 were also systematically reviewed in 2021 (MacDonald et al., 2021). In summary, the results obtained in present study revealed that the optimized perfusion culture strategy could high-efficient and stabilized produce anti-PD-1 mAb by CHO cells with a low raw materials cost, high titer/productivity, and stabilized quality (Table 3). It should be

emphasized that, the effectiveness of the optimized perfusion culture strategy for other mAbs and rBPs production will be further investigated for process intensification.

4 Conclusion

In this study, the continuous perfusion culture was verified as an optimized method for mAb production by CHO cells with low-priced perfusion media. Then, the perfusion culture rates and culture temperature were also optimized for evaluation of mAb titer and quality in 3-L bioreactor. The results indicated that the product titer reached a higher level of 16.19 g/L when combining the high perfusion rates and delayed reduction of culture temperature at day 6. In addition, the effectiveness of the proposed perfusion culture strategy was successfully verified in a 200-L bioreactor, which produced 16.79 g/L mAb at day 16 and the product quality was also maintained. This study provides some guidance for the mAb production by CHO cells with process engineering methods.

Data availability statement

The original contributions presented in the study are included in the article/Supplementary Material, further inquiries can be directed to the corresponding author.

Author contributions

KL: Investigation, conceptualization, methodology, writing—original draft; HL: Visualization, writing—reviewing and

editing; and QL: Supervision, conceptualization, writing—reviewing and editing.

Conflict of interest

The authors declare that the research was conducted in the absence of any commercial or financial relationships that could be construed as a potential conflict of interest.

References

- Ahn, W. S., Jeon, J.-J., Jeong, Y.-R., Lee, S. J., and Yoon, S. K. (2008). Effect of culture temperature on erythropoietin production and glycosylation in a perfusion culture of recombinant CHO cells. *Biotechnol. Bioeng.* 101, 1234–1244. doi:10.1002/bit.22006
- Bettinardi, I. W., Castan, A., Medronho, R. A., and Castilho, L. R. (2020). Hydrocyclones as cell retention device for CHO perfusion processes in single-use bioreactors. *Biotechnol. Bioeng.* 117, 1915–1928. doi:10.1002/bit.27335
- Bhatti, M. T., and Salama, A. K. S. (2018). Neuro-ophthalmic side effects of molecularly targeted cancer drugs. *Eye* 32, 287–301. doi:10.1038/eye.2017.222
- Bonaccorso, A., Russo, G., Pappalardo, F., Carbone, C., Puglisi, G., Pignatello, R., et al. (2021). Quality by design tools reducing the gap from bench to bedside for nanomedicine. *Eur. J. Pharm. Biopharm.* 169, 144–155. doi:10.1016/j.ejpb.2021.10.005
- Dahodwala, H., and Lee, K. H. (2019). The fickle CHO: A review of the causes, implications, and potential alleviation of the CHO cell line instability problem. *Curr. Opin. Biotechnol.* 60, 128–137. doi:10.1016/j.copbio.2019.01.011
- Ecker, D. M., Jones, S. D., and Levine, H. L. (2015). The therapeutic monoclonal antibody market. *mAbs* 7, 9–14. doi:10.4161/19420862.2015.989042
- Gao, Y., Ray, S., Dai, S., Ivanov, A. R., Abu-Absi, N. R., Lewis, A. M., et al. (2016). Combined metabolomics and proteomics reveals hypoxia as a cause of lower productivity on scale-up to a 5000-liter CHO bioprocess. *Biotechnol. J.* 11, 1190–1200. doi:10.1002/biot.201600030
- Genzel, Y., Vogel, T., Buck, J., Behrendt, I., Ramirez, D. V., Schiedner, G., et al. (2014). High cell density cultivations by alternating tangential flow (ATF) perfusion for influenza A virus production using suspension cells. *Vaccine* 32, 2770–2781. doi:10.1016/j.vaccine.2014.02.016
- Graham, R. J., Bhatia, H., and Yoon, S. (2019). Consequences of trace metal variability and supplementation on Chinese hamster ovary (CHO) cell culture performance: A review of key mechanisms and considerations. *Biotechnol. Bioeng.* 116, 3446–3456. doi:10.1002/bit.27140
- Gränicher, G., Coronel, J., Trampler, F., Jordan, I., Genzel, Y., and Reichl, U. (2020). Performance of an acoustic settler versus a hollow fiber-based ATF technology for influenza virus production in perfusion. *Appl. Microbiol. Biotechnol.* 104, 4877–4888. doi:10.1007/s00253-020-10596-x
- Ha, T. K., Kim, D., Kim, C. L., Grav, L. M., and Lee, G. M. (2022). Factors affecting the quality of therapeutic proteins in recombinant Chinese hamster ovary cell culture. *Biotechnol. Adv.* 54, 107831. doi:10.1016/j.biotechadv.2021.107831
- Hintersteiner, B., Lingg, N., Zhang, P., Woen, S., Hoi, K. M., Stranner, S., et al. (2016). Charge heterogeneity: Basic antibody charge variants with increased binding to Fc receptors. *mAbs* 8, 1548–1560. doi:10.1080/19420862.2016.1225642
- Hippach, M. B., Schwartz, I., Pei, J., Huynh, J., Kawai, Y., and Zhu, M. M. (2018). Fluctuations in dissolved oxygen concentration during a CHO cell culture process affects monoclonal antibody productivity and the sulfhydryl-drug conjugation process. *Biotechnol. Prog.* 34, 1427–1437. doi:10.1002/btpr.2697
- Karst, D. J., Serra, E., Villiger, T. K., Soos, M., and Morbidelli, M. (2016). Characterization and comparison of ATF and TFF in stirred bioreactors for continuous mammalian cell culture processes. *Biochem. Eng. J.* 110, 17–26. doi:10.1016/j.bej.2016.02.003
- Kim, B. J., Oh, D. J., and Chang, H. N. (2008). Limited use of centrifuge lab II centrifuge in perfusion culture of rCHO cells for the production of recombinant antibody. *Biotechnol. Prog.* 24, 166–174. doi:10.1021/bp070235f
- Konakovskiy, V., Clemens, C., Müller, M. M., Bechmann, J., Berger, M., Schlatter, S., et al. (2016). Metabolic control in mammalian fed-batch cell cultures for reduced lactic acid accumulation and improved process robustness. *Bioengineering* 3, 5. doi:10.3390/bioengineering3010005
- Lalonde, M.-E., and Durocher, Y. (2017). Therapeutic glycoprotein production in mammalian cells. *J. Biotechnol.* 251, 128–140. doi:10.1016/j.jbiotec.2017.04.028
- MacDonald, M. A., Nöbel, M., Martínez, V. S., Baker, K., Shave, E., Gray, P. P., et al. (2022). Engineering death resistance in CHO cells for improved perfusion culture. *mAbs* 14, 2083465. doi:10.1080/19420862.2022.2083465
- MacDonald, M. A., Nöbel, M., Roche Recinos, D., Martínez, V. S., Schulz, B. L., Howard, C. B., et al. (2021). Perfusion culture of Chinese Hamster Ovary cells for bioprocessing applications. *Crit. Rev. Biotechnol.* 42, 1099–1115. doi:10.1080/07388551.2021.1998821
- Madabhushi, S. R., Podtelezhnikov, A. A., Murgolo, N., Xu, S., and Lin, H. (2021). Understanding the effect of increased cell specific productivity on galactosylation of monoclonal antibodies produced using Chinese hamster ovary cells. *J. Biotechnol.* 329, 92–103. doi:10.1016/j.jbiotec.2021.01.023
- Pérez-Rodríguez, S., Ramírez-Lira, M. d. J., Trujillo-Roldán, M. A., and Valdez-Cruz, N. A. (2020). Nutrient supplementation strategy improves cell concentration and longevity, monoclonal antibody production and lactate metabolism of Chinese hamster ovary cells. *Bioengineered* 11, 463–471. doi:10.1080/21655979.2020.1744266
- Qin, J., Wu, X., Xia, Z., Huang, Z., Zhang, Y., Wang, Y., et al. (2019). The effect of hyperosmolality application time on production, quality, and biopotency of monoclonal antibodies produced in CHO cell fed-batch and perfusion cultures. *Appl. Microbiol. Biotechnol.* 103, 1217–1229. doi:10.1007/s00253-018-9555-7
- Schulze, M., Kumar, Y., Rattay, M., Niemann, J., Wijffels, R. H., and Martens, D. E. (2022). Transcriptomic analysis reveals mode of action of butyric acid supplementation in an intensified CHO cell fed-batch process. *Biotechnol. Bioeng.* 119, 2359–2373. doi:10.1002/bit.28150
- Schwarz, H., Zhang, Y., Zhan, C., Malm, M., Field, R., Turner, R., et al. (2020). Small-scale bioreactor supports high density HEK293 cell perfusion culture for the production of recombinant Erythropoietin. *J. Biotechnol.* 309, 44–52. doi:10.1016/j.jbiotec.2019.12.017
- Shepard, H. M., Phillips, G. L., Thanos, C. D., and Feldmann, M. (2017). Developments in therapy with monoclonal antibodies and related proteins. *Clin. Med.* 17, 220–232. doi:10.7861/clinmedicine.17-3-220
- Sou, S. N., Jedrzejewski, P. M., Lee, K., Sellick, C., Polizzi, K. M., and Kontoravdi, C. (2017). Model-based investigation of intracellular processes determining antibody Fc-glycosylation under mild hypothermia. *Biotechnol. Bioeng.* 114, 1570–1582. doi:10.1002/bit.26225
- Tait, A. S., Tarrant, R. D. R., Velez-Suberbie, M. L., Spencer, D. I. R., and Bracewell, D. G. (2013). Differential response in downstream processing of CHO cells grown under mild hypothermic conditions. *Biotechnol. Prog.* 29, 688–696. doi:10.1002/btpr.1726
- van der Kant, R., Karow-Zwick, A. R., Van Durme, J., Blech, M., Gallardo, R., Seeliger, D., et al. (2017). Prediction and reduction of the aggregation of monoclonal antibodies. *J. Mol. Biol.* 429, 1244–1261. doi:10.1016/j.jmb.2017.03.014
- Vodopivec, M., Lah, L., Narat, M., and Curk, T. (2019). Metabolomic profiling of CHO fed-batch growth phases at 10, 100 and 1,000 L. *Biotechnol. Bioeng.* 116, 2720–2729. doi:10.1002/bit.27087
- Wang, K., Zhang, T., Chen, J., Liu, C., Tang, J., and Xie, Q. (2018a). The effect of culture temperature on the aggregation of recombinant TNFR-Fc is regulated by the PERK-eIF2a pathway in CHO cells. *Protein Pept. Lett.* 25, 570–579. doi:10.2174/0929866525666180530121317
- Wang, Q., Chung, C. Y., Chough, S., and Betenbaugh, M. J. (2018b). Antibody glycoengineering strategies in mammalian cells. *Biotechnol. Bioeng.* 115, 1378–1393. doi:10.1002/bit.26567
- Wang, W. (2005). Protein aggregation and its inhibition in biopharmaceutics. *Int. J. Pharm.* 289, 1–30. doi:10.1016/j.ijpharm.2004.11.014
- Xing, Z., Kenty, B. M., Li, Z. J., and Lee, S. S. (2009). Scale-up analysis for a CHO cell culture process in large-scale bioreactors. *Biotechnol. Bioeng.* 103, 733–746. doi:10.1002/bit.22287
- Yin, L., Au, W. Y., Yu, C. C., Kwon, T., Lai, Z., Shang, M., et al. (2021). Miniature auto-perfusion bioreactor system with spiral microfluidic cell retention device. *Biotechnol. Bioeng.* 118, 1951–1961. doi:10.1002/bit.27709
- Zhang, L., Schwarz, H., Wang, M., Castan, A., Hjalmarsson, H., and Chotteau, V. (2021). Control of IgG glycosylation in CHO cell perfusion cultures by GReBA mathematical model supported by a novel targeted feed, TAFE. *Metab. Eng.* 65, 135–145. doi:10.1016/j.ymben.2020.11.004
- Zheng, C., Zhuang, C., Chen, Y., Fu, Q., Qian, H., Wang, Y., et al. (2018). Improved process robustness, product quality and biological efficacy of an anti-CD52 monoclonal antibody upon pH shift in Chinese hamster ovary cell perfusion culture. *Process Biochem.* 65, 123–129. doi:10.1016/j.procbio.2017.11.013
- Zhu, M. M., Goyal, A., Rank, D. L., Gupta, S. K., Boom, T. V., and Lee, S. S. (2005). Effects of elevated pCO₂ and osmolality on growth of CHO cells and production of antibody-fusion protein B1: A case study. *Biotechnol. Prog.* 21, 70–77. doi:10.1021/bp049815s
- Zhuang, C., Zheng, C., Chen, Y., Huang, Z., Wang, Y., Fu, Q., et al. (2017). Different fermentation processes produced variants of an anti-CD52 monoclonal antibody that have divergent *in vitro* and *in vivo* characteristics. *Appl. Microbiol. Biotechnol.* 101, 5997–6006. doi:10.1007/s00253-017-8312-7

Publisher's note

All claims expressed in this article are solely those of the authors and do not necessarily represent those of their affiliated organizations, or those of the publisher, the editors and the reviewers. Any product that may be evaluated in this article, or claim that may be made by its manufacturer, is not guaranteed or endorsed by the publisher.



OPEN ACCESS

EDITED BY

Hossain M. Zayed,
Jiangsu University, China

REVIEWED BY

Yuvaraj Ravikumar,
Jiangsu University, China
Feng Wang,
Jiangsu University, China

*CORRESPONDENCE

Juan Nogales,
✉ j.nogales@csic.es

RECEIVED 28 February 2023

ACCEPTED 06 April 2023

PUBLISHED 20 April 2023

CITATION

Carranza-Saavedra D, Torres-Bacete J,
Blázquez B, Sánchez Henao CP,
Zapata Montoya JE and Nogales J (2023),
System metabolic engineering of
Escherichia coli W for the production of
2-ketoisovalerate using
unconventional feedstock.
Front. Bioeng. Biotechnol. 11:1176445.
doi: 10.3389/fbioe.2023.1176445

COPYRIGHT

© 2023 Carranza-Saavedra, Torres-Bacete, Blázquez, Sánchez Henao, Zapata Montoya and Nogales. This is an open-access article distributed under the terms of the [Creative Commons Attribution License \(CC BY\)](https://creativecommons.org/licenses/by/4.0/). The use, distribution or reproduction in other forums is permitted, provided the original author(s) and the copyright owner(s) are credited and that the original publication in this journal is cited, in accordance with accepted academic practice. No use, distribution or reproduction is permitted which does not comply with these terms.

System metabolic engineering of *Escherichia coli* W for the production of 2-ketoisovalerate using unconventional feedstock

Darwin Carranza-Saavedra^{1,2,3}, Jesús Torres-Bacete²,
Blas Blázquez^{2,3}, Claudia Patricia Sánchez Henao¹,
José Edgar Zapata Montoya¹ and Juan Nogales^{2,3*}

¹Faculty of Pharmaceutical and Food Sciences, Nutrition and Food Technology Group, University of Antioquia, Medellín, Colombia, ²Department of Systems Biology, National Centre for Biotechnology (CSIC), Systems Biotechnology Group, Madrid, Spain, ³Interdisciplinary Platform for Sustainable Plastics Towards a Circular Economy-Spanish National Research Council (SusPlast-CSIC), Madrid, Spain

Replacing traditional substrates in industrial bioprocesses to advance the sustainable production of chemicals is an urgent need in the context of the circular economy. However, since the limited degradability of non-conventional carbon sources often returns lower yields, effective exploitation of such substrates requires a multi-layer optimization which includes not only the provision of a suitable feedstock but the use of highly robust and metabolically versatile microbial biocatalysts. We tackled this challenge by means of systems metabolic engineering and validated *Escherichia coli* W as a promising cell factory for the production of the key building block chemical 2-ketoisovalerate (2-KIV) using whey as carbon source, a widely available and low-cost agro-industrial waste. First, we assessed the growth performance of *Escherichia coli* W on mono and disaccharides and demonstrated that using whey as carbon source enhances it significantly. Second, we searched the available literature and used metabolic modeling approaches to scrutinize the metabolic space of *E. coli* and explore its potential for overproduction of 2-KIV identifying as basic strategies the block of pyruvate depletion and the modulation of NAD/NADP ratio. We then used our model predictions to construct a suitable microbial chassis capable of overproducing 2-KIV with minimal genetic perturbations, i.e., deleting the pyruvate dehydrogenase and malate dehydrogenase. Finally, we used modular cloning to construct a synthetic 2-KIV pathway that was not sensitive to negative feedback, which effectively resulted in a rerouting of pyruvate towards 2-KIV. The resulting strain shows titers of up to 3.22 ± 0.07 g/L of 2-KIV and 1.40 ± 0.04 g/L of L-valine in 24 h using whey in batch cultures. Additionally, we obtained yields of up to 0.81 g 2-KIV/g substrate. The optimal microbial chassis we present here has minimal genetic modifications and is free of nutritional autotrophies to deliver high 2-KIV production rates using whey as a non-conventional substrate.

KEYWORDS

dairy by-products, L-valine, bioeconomy, feedback inhibition, non-conventional microbial factories, systems biotechnology

1 Introduction

Success in the implementation of a fully circular economy demands sustainable alternatives to substrates traditionally used in fermentative processes to avoid competition with human and animal food, e.g., glucose. Fulfilling this simple and yet very ambitious goal is the challenge driving interest in the use of agricultural and agro-industrial waste as feedstock for large-scale fermentation processes. However, non-conventional carbon sources often deliver lower yields due to their limited degradability and the presence of toxic byproducts (Ren et al., 2011; Lopes et al., 2019). Overcoming these challenges therefore requires multi-layer optimization to deliver suitable alternative feedstocks and non-conventional, highly robust and metabolically versatile microbial biocatalysts.

In recent years, much research has been conducted into the use of whey as a fermentation medium to produce lipids, organic acids and alcohols (Cao et al., 2020; Mano et al., 2020; Novak et al., 2020). The physicochemical composition of whey is behind this growing interest, as it typically contains around 88% lactose, 4% protein, 1.4% (w/w) lipids and trace minerals in powder product (Carranza-Saavedra, Sánchez Henao and Zapata Montoya, 2021). While it is usually more expensive to grow bacteria on pure lactose than on glucose, using whey as a source of lactose significantly reduces the cost (Silva et al., 2015; Amado et al., 2016), thus making whey a promising non-conventional feedstock for microbial biotechnology.

Searching for a new non-conventional bacterial chassis able to deal with such a novel feedstock while providing additional metabolic and/or genetic advantages is also a challenge. Strains free from catabolic repression phenomena, among other features, would be the ideal candidates (Calero and Nikel, 2019). The *Escherichia coli* W strain has been used previously to produce natural metabolites and it brings potential improvements over *E. coli* K-12 strains: 1) it is able to use a broader range of carbon sources, at high concentration, 2) it is the only safe *E. coli* strain that uses sucrose as a carbon source (Archer et al., 2011; Felpeto-Santero et al., 2015; Erian et al., 2018), 3) it releases smaller amounts of acetate during fermentation while generating more biomass in batch culture (Archer et al., 2011), and 4) it tolerates increased stress conditions, such as high ethanol concentrations, acidic pH, high temperature and osmotic stress (Shiloach and Bauer, 1975; Gleiser and Bauer, 1981; Alterthum and Ingram, 1989; Nagata, 2001).

On the other hand, despite the long history of success using traditional metabolic engineering strategies, successful integration of modern biotechnology into the circular economy requires the development of new holistic approaches and tackling the complexity of living organisms from a systems-level perspective. The combination of computational methods based on metabolic models and cutting-edge synthetic biology has so far delivered a high degree of success in metabolic engineering endeavors. Indeed, it has paved the way for systematic exploration of the metabolic solution spaces required to produce target metabolites (Wu et al., 2016; Gudmundsson and Nogales, 2021). Design-Build-Test-Learn (DBTL) iterative cycles stand up as popular examples of such multidisciplinary approaches to the

production of a plethora of chemical compounds (Gurdo et al., 2022). DBTL cycles are iterative designs combining the advances in systems and synthetic biology to deliver rational genetic modifications and high-throughput phenotyping of strains. DBTL-driven research leads to the establishment of sound conclusions from experimental results, knowledge building and the generation of new hypotheses. Hence, it contributes to unlocking novel biotechnological processes supporting the circular economy.

In this context, an interesting idea is to apply multidisciplinary approaches to optimize biotechnological platforms towards the cost-effective production of key building blocks, which in turn are the precursors of a variety of value-added compounds. 2-ketoisovalerate (2-KIV) is one of these key building blocks and it has been the focus of significant attention (Gu et al., 2017). 2-KIV is an important precursor in the biosynthesis of branched chain amino acids (BCAAs) such as L-valine, cofactors such as pantothenate, coenzyme A and other biologically active compounds such as glucosinolates (Felnagle et al., 2012; Lee et al., 2019; Zhao et al., 2022). In microorganisms and plants, synthesis of 2-KIV requires two pyruvate molecules via three consecutive reactions included in the BCAAs pathway which are catalyzed by acetolactate synthase (AHAS), ketol-acid reductoisomerase (KARA) and dihydroxy-acid dehydratase (DHAD) (Figure 1). Production of 2-KIV has been addressed using *Klebsiella pneumoniae* (Gu et al., 2017), *Corynebacterium glutamicum* (Buchholz et al., 2013), *Pseudomonas putida* (Batianis et al., 2022) and, more recently, *E. coli* (Zhou et al., 2022). 2-KIV production with *E. coli* has also been addressed extensively in the context of L-valine and isobutanol production (Blombach et al., 2007; 2011; Park et al., 2007; Atsumi et al., 2008; Holátko et al., 2009; Krause et al., 2010; Park et al., 2011a; Bartek et al., 2011; Park et al., 2011b; Li et al., 2011; Hou et al., 2012; Lee et al., 2012; Buchholz et al., 2013; Hasegawa et al., 2013; Chen et al., 2015; Gu et al., 2017; Liang et al., 2018; Schwentner et al., 2018; Westbrook et al., 2018; Noda et al., 2019; Hao et al., 2020; Jung et al., 2020). However, such studies used conventional feedstocks and highly engineered strains harboring multiple autotrophies, thus requiring complex and expensive production media to support the bioprocess.

In this study, we used systems and synthetic biology to produce 2-KIV in a microbial factory fueled by whey and driven by the non-conventional and promising *E. coli* W strain. The strain's design featured minimal genetic intervention in order to preserve its growth performance in minimal medium without the addition of expensive nutritional supplements. 24 h batch culture assays returned a 3.22 ± 0.07 g/L titer for 2-KIV and 1.40 ± 0.04 g/L for L-valine. We also obtained yields (Yp/s) of up to 0.8 g/g for 2-KIV.

2 Materials and methods

2.1 Strains, plasmids, primers and DNA parts

Bacterial strains and plasmids used in this work are listed in Table 1. Additional biological material including primers, DNA parts (expression systems, promoters, RBSs, CDSs, terminators and host plasmids) can be found in Supplementary Tables S1–S3.

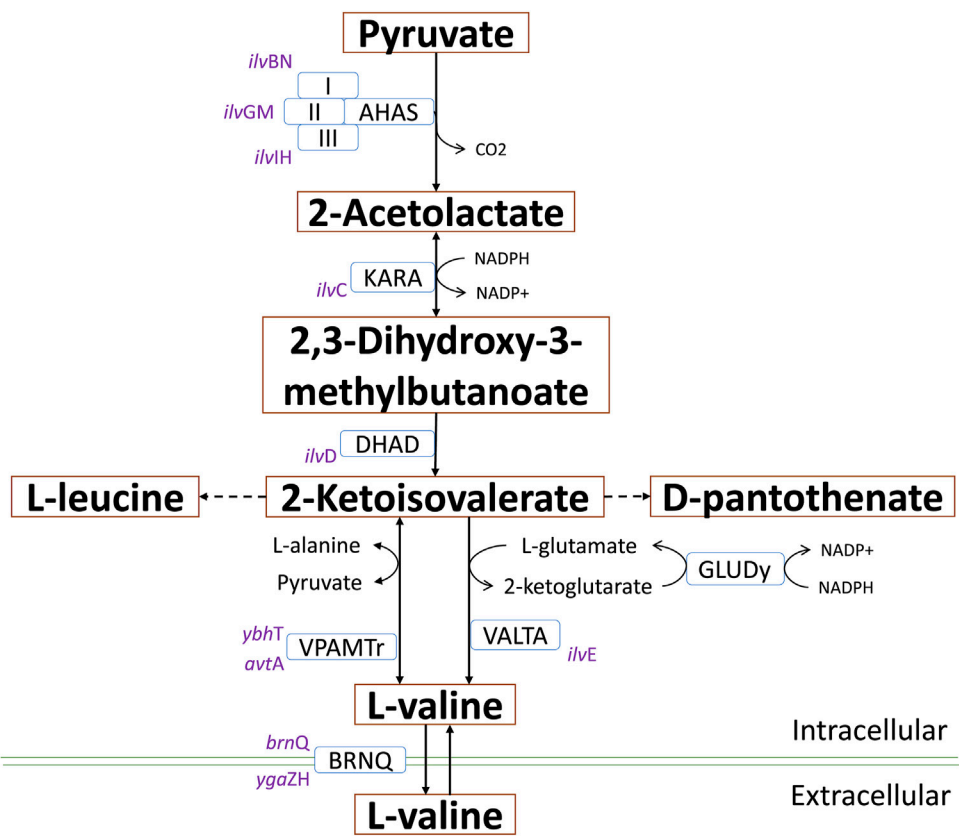


FIGURE 1
L-valine biosynthesis in *E. coli* via 2-KIV. Acetohydroxyacid synthase (AHAS), ketol-acid reductoisomerase (AHAIR), dihydroxyacid dehydratase (DHAD), valine transaminase (VALTA), valine-pyruvate aminotransferase (VPAMTr), branched-chain amino acid transport system 2 carrier protein (BRNQ). Gene names are shown in purple.

TABLE 1 Strain, plasmids and DNA used in this study.

Strain	Genotype	Source
<i>E. coli</i> DH5α	fluA2 Δ(argF-lacZ)U169 phoA glnV44 Φ80 Δ(lacZ)M15 gyrA96 recA1 relA1 endA1 thi-1 hsdR17	New England BioLabs (NEB)
<i>E. coli</i> W	Wild Type (ATCC 9637) (WT)	www.atcc.org
WT Δmdh-aceF	<i>E. coli</i> W, Δmdh-ΔaceF	This study
<i>E. coli</i> W1288	<i>E. coli</i> W, Δmdh-ΔaceF, pSEVA681	This study
<i>E. coli</i> W1294	<i>E. coli</i> W, pSEVA681-kiv	This study
<i>E. coli</i> W1262	<i>E. coli</i> W, Δmdh-ΔaceF, pSEVA681-kiv	This study
Plasmid	Description	Source
pSLTS	ori SC101(Ts) Apr; ParaB for λ-Red; PtetR for I-SceI Gama, beta, exo	Kim et al. (2014)
pSEVA182	Amp ^r , pUC ori, cargo: lacZα-pUC19	Martínez-García et al. (2022)
pSBG422	I-SceI site and a kanamycin resistance gene with SacI/BamHI sites and SacI/BamHI pUC ori Km and Ap	
pSEVA681	Gm ^r , pUC ori (cloning vector of high copy number), cargo: MCS-default	
pKIV	Gm ^r , pUC ori, CDS: XylS/Pm- <i>alsS-ilvD-ilvC</i> , RBS-ST, BBa_B1006 terminator and linkers	This study

2.2 Reagents and culture media

Spray-dried, food grade whey powder containing $88.08\% \pm 1.93\%$ lactose, $4.16\% \pm 0.12\%$ protein and $1.46\% \pm 0.25\%$ fat (w/w) was purchased from Cimpa S.A.S. (Bogotá, Colombia). Other reactive agents used were analytical grade. *E. coli* strains grown in Luria-Bertani (LB) medium and Minimal medium M9 (pH 7.2) (Landor et al., 2023) with carbon source concentrations set at 2 g/L. Under production conditions, M9 was supplemented with 1 g/L of yeast extract and 10 g/L of carbon source. We prepared a stock solution for whey-based fermentation media mixing 10 g of whey powder in 100 mL of distilled water. All culture media and work solutions were sterilized at 121°C for 15 min and their initial pH adjusted to 7.0 before use.

2.3 DNA manipulation

We used *E. coli* DH5 α as the cloning host for plasmid and cassette construction and *E. coli* W as the starting strain for genomic manipulations. We purchased DNA polymerases and other DNA-modifying enzymes from New England Biolabs (Ipswich, United States) and oligonucleotides from Sigma-Aldrich (Madrid, Spain). We sourced DNA purification kits from Nyztech (Lisbon, Portugal). We ran PCRs on a Mastercycler Nexus Gradient thermal cycler (Eppendorf, Germany) and analyzed PCR products with 0.7 or 1.5% agarose gel-electrophoresis using a 1X Tris-acetate buffer. Antibiotics, i.e., ampicillin (100 μ g/mL), kanamycin (50 μ g/mL) and gentamicin (10 μ g/mL) were added to culture media and agar plates according to assay requirements.

aceF and *mdh* genes were deleted by using scarless genome editing as described by Kim et al. (2014) with slight modifications. 300 DNA-base pair plasmids corresponding to homologous regions of the *E. coli* W genome were designed and pSEVA182_aceF_Arm1y2 and pSEVA182_mdh_Arm1y2 cassettes delivered by means of digestion with type II restriction enzymes and ligation with T4 ligases (Supplementary Figures S1, S2; cassette sequences in Supplementary Table S3). Further details are available in Supplementary MD1. Supplementary Figure S3 shows PCR and gel electrophoresis verification of mutations.

We assembled a synthetic expression system using a modular cloning technique based on Golden Standard (Blázquez et al., 2022; Martínez-García et al., 2022). Simultaneous design of overexpression systems supported combinatorial, multi-part assembly of standardized genetic elements to deliver genetic circuits. We designed the pKIV plasmid using the 3-methylbenzoate (3 MB)-activated XylS/Pm expression system (Gawin et al., 2017). Detailed descriptions of synthetic pathway construction are available in Supplementary MD2.

2.4 Production in shake flasks

We inoculated strains in 25 mL LB medium (seed culture) in 250 mL shake flasks and incubated overnight at 37°C in a MaxQ 4000 incubator shaker (Thermo Scientific, United States) at 250 rpm. Seed cultures were centrifuged (5,200 g), washed with NaCl (0.85% w/v) and inoculated in 25 mL of growth medium

(preinoculum) at 37°C and 250 rpm for 24 h. Preinocula were washed with NaCl and transferred to a 250 mL shake flask containing 20 mL of fermentation medium for 24 h-cultivation at 37°C, 250 rpm shaking and initial optical density (OD_{600nm}) set to 1.0. 0.5 mM 3 MB inductor was added to the fermentation medium. We analyzed the cellular toxicity due 2-KIV and did not observe negative effect on growth at concentration ranging from 0 to 5 mM (data not shown).

2.5 System-level analysis of sugar metabolism

To assess growth kinetics, cells were cultivated at 37°C for 13 h in a growth medium containing a mixture of glucose, lactose, galactose, sucrose, fructose and maltose at a concentration of 2 g/L as carbon source. Initial OD_{600nm} was 0.1 and shaking was set to 250 rpm. Besides, each of the sugars was mixed with glucose at a 50:50 glucose:target sugar ratio (concentration in the mix was 2 g/L). Whenever we used sucrose, *E. coli* W was grown twice in M9 supplemented with sucrose before running growth kinetics assays.

2.6 Analytical techniques

We measured OD_{600nm} with a Genesys 10S UV-Vis spectrophotometer (Thermo Scientific, U.S.A) to quantify biomass. OD_{600nm} readings were correlated with dry cell weight per liter (g DCW/L) using the equation: g DCW/L = OD_{600nm}*0.452 (Erian et al., 2018).

Sugar concentrations (glucose and lactose) were quantified by spectrophotometric techniques using the DNS method (Carranza-Saavedra et al., 2021). We measured sample absorbance at 540 nm wavelength in a Genesys 10S UV-Vis spectrophotometer (Thermo Scientific, U.S.A). We then used glucose and lactose concentrations ranging between 0.5 and 8 g/L to plot calibration curves for both sugars.

We used HPLC to measure organic acid and L-valine concentrations. All samples were carefully filtered using a 0.2 μ m cellulose nitrate syringe filter before being injected into the HPLC. Analyses were carried out using a Thermo Ultimate 3000 HPLC system (Thermo Fisher Scientific, United States) equipped with a quaternary pump, an automatic injector, a column thermostat set and a diode arrangement detector with UV detection. Following the method described by Kerem et al. (Kerem et al., 2004), a Zorbax Bonus-RP Column 4.6 \times 250 mm (Agilent, U.S.A), particle size 5 μ m, was used to quantify 2-KIV. We used two solvents as eluents for gradient elution: solvent A was trifluoroacetic acid (0.2% in water, pH 1.96) and solvent B was acetonitrile. Injection volume was 20 μ L and 10 min equilibration intervals (solvent A) were required between injections. Elution started at 0.8 mL/min with an isocratic step of solvent A (15 min), then a solvent B linear gradient (0%–50%) for the next 5 min and, finally, 5 min with 80% solvent B. Column temperature was set to 30°C and detection wavelength to 210 nm. We used organic acid concentrations from 3 to 30 mM to plot a calibration curve (external standard).

Amino acids (L-valine) were separated in a Zorbax Eclipse AAA-C18 column 4.6 \times 75 mm (Agilent, United States), particle

size 3.5 μm , with a Zorbax Eclipse AAA pre-column 4.6 \times 12.5 mm (Agilent, United States), particle size 5 μm and quantification following the procedure described by Cigić, et al. (Cigić et al., 2008). The column thermostat was set to 40°C and detection wavelength to 338 nm to quantify primary amino acids. We pre-derivatized *in situ* with ortho-phthalaldehyde and 3-marcaptopropionic acid (OPA/3-MPA). An amino acids standard curve (0.5, 1.0, 1.5 and 2.0 $\mu\text{mol/mL}$) was used for quantification (external standard).

2.7 Kinetic parameters

We calculated maximum specific growth rate (μ_{max}) by linear regression of the natural logarithm of g DCW/L over time (Eq. 1) during the exponential phase. Substrate yields in biomass (Eq. 2), substrate in product (Eq. 3) and biomass in product (Eq. 4) were calculated using the relationship between the concentration of resulting dry biomass, the concentration of consumed glucose and total product concentrations, respectively.

$$\mu_{\text{max}} = \frac{dX}{Xdt} \quad (1)$$

$$Y_{X/S} = \frac{dX}{dS} \quad (2)$$

$$Y_{P/S} = \frac{dP}{dS} \quad (3)$$

$$Y_{P/X} = \frac{dP}{dX} \quad (4)$$

2.8 Constraints-based analysis

The *E. coli* W iCA_1273 metabolic model was download from the BioModels Database (MODEL1507180010) (<https://www.ebi.ac.uk/biomodels/>). iCA_1273 is a manually curated and validated metabolic model (Archer et al., 2011) including 2,477 reactions and 1,111 metabolites encoded by 1,273 genes. Our analyses required adding the ability to secrete 2-KIV to the model, which resulted in a new model featuring 2,480 reactions. We used flux balance analysis (FBA) (Heirendt et al., 2019) to interrogate the model and characterized flux distribution through the network of reactions with Eq. 5.

$$S \cdot v = 0 \quad (5)$$

Where S is the dimension of the stoichiometric matrix given by m (number of metabolites in the reaction network) and n (number of reactions). v indicates the flow rate through each of the reactions.

In silico analysis was performed with MATLAB R2018a, the COBRA Toolbox v.3.0 and Gurobi solver (version 9.5.1). We used Monte Carlo sampling to register frequency and flux variability along pathways showing potential increases in pyruvate, 2-KIV and L-valine production. Samples were collected from 35,000 points over 4 h (previous test) (Heirendt et al., 2019). Reactions assessed using Monte Carlo sampling are listed in Supplementary Table S4.

2.9 Statistical analysis

All shake flask experiments were performed in duplicate and data obtained were expressed as mean \pm standard error. Kinetic parameters obtained from experiments were analyzed against each other using Duncan's multiple comparison (Duncan, 1955) with a confidence level of 95%. Our aim was to establish potential significant differences in performance and relate them to the carbon sources used in growth media.

3 Results and discussion

3.1 Systems-level analysis of complex sugar metabolism in *E. coli* W

It is well-known that *E. coli* W has a complex sugar metabolism and is able to use several types of carbohydrate as sole carbon and energy sources (Wang et al., 2019). To assess the metabolic performance of *E. coli* W growing on such compounds, we monitored the growth kinetics of cultures feeding on a variety of monosaccharides (glucose, fructose and galactose), disaccharides (lactose, sucrose and maltose) and a mixture of them all. Glucose and fructose were rapidly assimilated (Figure 2), so they turned out to support the shortest lag phase. They were followed by lactose and sucrose, while galactose and maltose displayed the longest lag phases. Despite their longer latency periods, disaccharides provided the highest growth rates (lactose > sucrose > maltose) and final OD₆₀₀ (sucrose > lactose > maltose). Interestingly, we observed the shortest latency period, highest growth rate and greatest final biomass with the sugar mix, which strongly suggests a synergistic and complementary metabolism supporting fast nutrient consumption and growth. The absence of diauxic growth curves strongly argues in favor of a limited effect of catabolic repression in the metabolism of mixture of sugars in this strain. These results show not just that *E. coli* W is able to use a variety of carbohydrates as single carbon and energy sources efficiently, but more critically that the availability of a carbohydrate mix has a positive impact on its growth performance. In addition, negligible catabolic repression (CCR) is an advantage over other conventional *E. coli* strains like *E. coli* K12, which suffered from the negative impacts of CCR in experiments using glucose and non-PTS sugars as carbon source (Luo et al., 2014).

We implemented a series of growth experiments using glucose at different ratios as an additional carbon source to further assess the role of CCR in *E. coli* W and verify whether its growth performance improves when using carbohydrate mixes instead of single carbon sources (Figure 3). Although there is no evidence of a marked diauxic behavior in our kinetics assessment, μ_{max} analysis for each of the different substrates (Supplementary Table S5) shows a slight affectation when using glucose with galactose and maltose (Figures 3B, E). However, there are no significant differences ($p < 0.05$) in μ_{max} between other glucose-containing mixes. Significant differences between glucose-lactose mixes and other mixes, particularly when they contained glucose, show that the former favor growth. Overall, our results suggest that sugar-mix-powered *E. coli* W microbial cell factories are very promising, not just because they are virtually free of CCR but because their growth performance is improved when multiple sugars are simultaneously available.

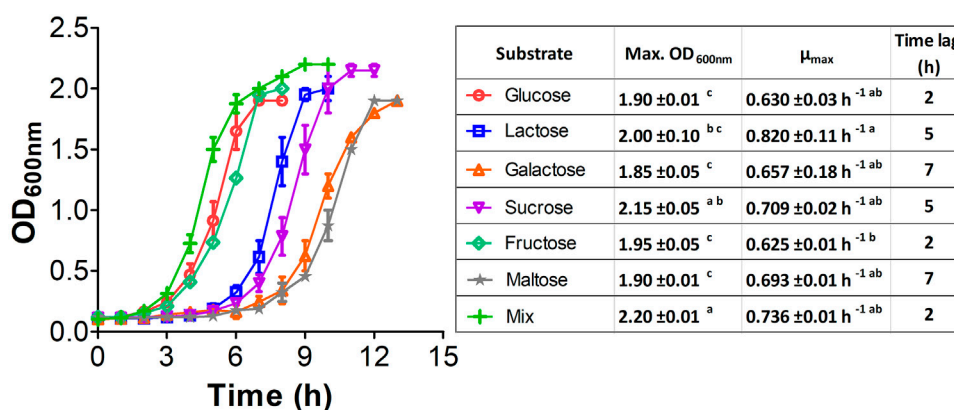


FIGURE 2

Growth kinetic of *E. coli* W using a variety of mono and disaccharides as sole carbon and energy source. 2 g/L of each single carbon source were used while for the mixture, a total of 0.33 g/L of each compound were used. Vertical bars, \pm represent standard deviation and lines are a guide for the eye. Similar lowercase letters per column indicate no statistical difference between treatments ($p < 0.05$).

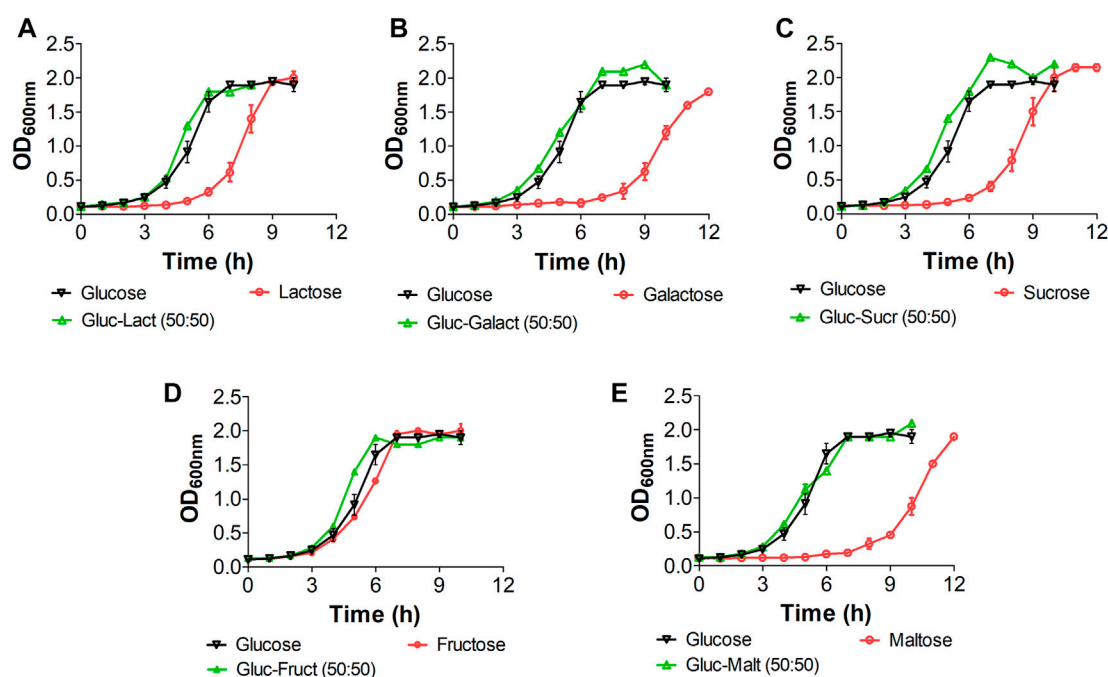


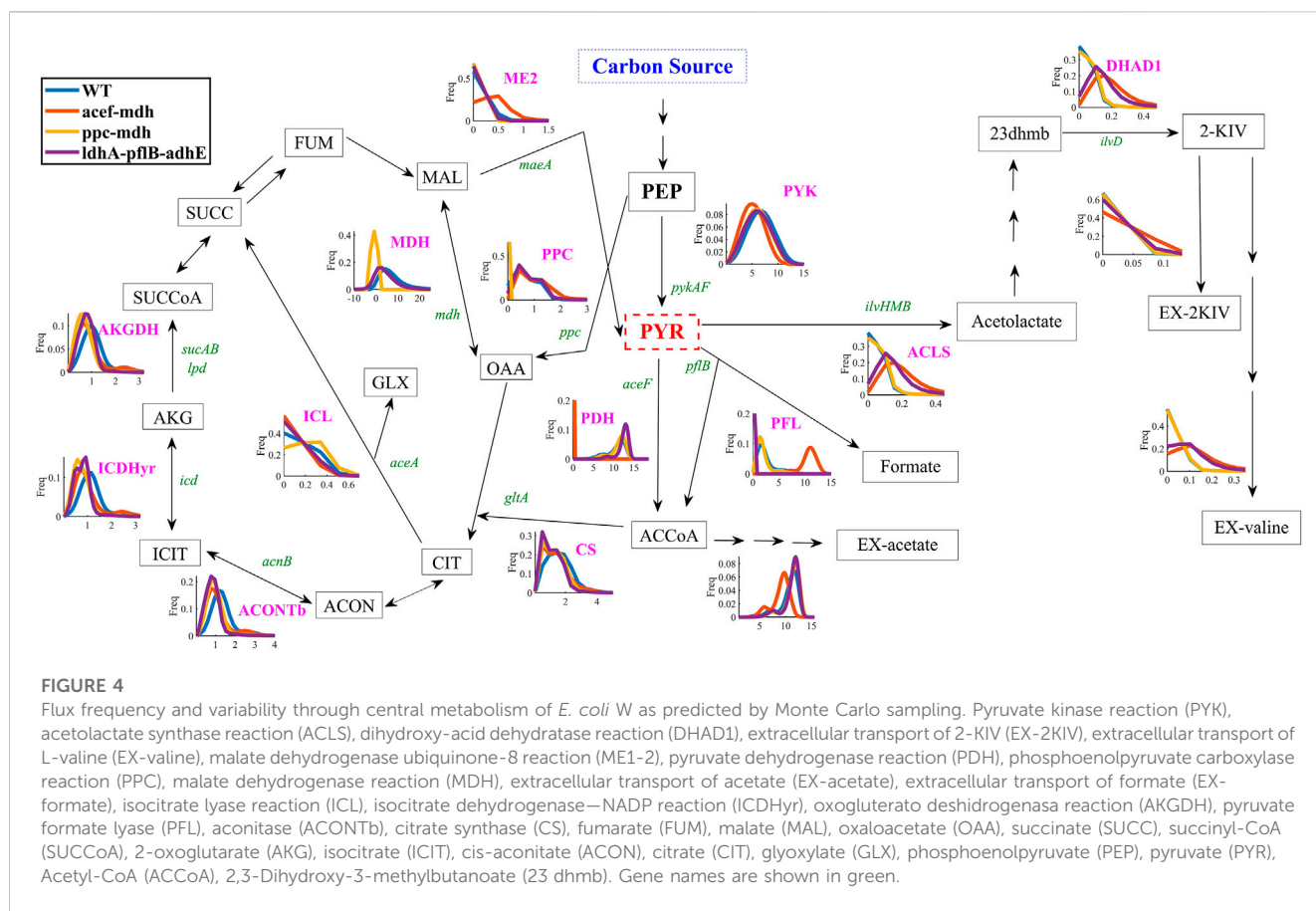
FIGURE 3

Growth kinetic of *E. coli* W in mix sugars with glucose for studying diauxic growth. All mix and pure carbon source were used at of 2 g/L. Vertical bars represent standard deviation and lines are a guide for the eye. (A): Kinetic with lactose, (B): kinetic with galactose, (C): kinetic with sucrose, (D): kinetic with fructose, (E): kinetic with maltose.

3.2 Legacy and model-based design of a set of 2-KIV overproducer *E. coli* W strains

E. coli W's efficient carbohydrate metabolism ensures a large carbon flux around pyruvate, a key metabolic hub in sugar catabolism and the main precursor of 2-KIV. However, cost-effective production of pyruvate-derived metabolites such as 2-KIV requires additional flux rerouting (Gu et al., 2017; Noda

et al., 2019). Nowadays, redirection of carbon flux towards pyruvate has been unlocked in a large variety of microorganisms (Buchholz et al., 2013; Gu et al., 2017; Novak et al., 2020), although most studies have focused on disabling pyruvate consumption along competing pathways (Noda et al., 2019; Novak et al., 2020). For instance, detailed analysis of studies dealing with overproduction of 2-KIV from glucose (Supplementary Figure S4; Supplementary Table S6) revealed



three main knockout strategies. The first is the preferred choice and it avoids consumption of pyruvate as a precursor of: 1) acetyl-CoA via the pyruvate dehydrogenase complex (PDH, *aceEF*) or pyruvate formate lyase (PFL, *pflABCD*), 2) acetate via pyruvate oxidase (PO, *poxB*), 3) lactate via lactate dehydrogenase (LDH, *ldhA*), 4) L-alanine via glutamate-pyruvate aminotransferase (GPA, *yfdZQ*) and 5) L-valine via branched-chain amino acid aminotransferases (*ilvE*) (Wang et al., 2018). Deletion of PDH seems to be of critical importance and is thus the most widely deleted competing pathway to increase levels of pyruvate in the cell (Supplementary Figure S4) (Blombach et al., 2007; 2011; Park et al., 2007; Park et al., 2011a; Bartek et al., 2011; Buchholz et al., 2013; Chen et al., 2015; Nitschel et al., 2020). Alternatively, deleting anaplerotic reactions such as phosphoenolpyruvate carboxylase (PPC, *ppc*) reduces gluconeogenesis from pyruvate and therefore delivers higher levels of 2-KIV (Buchholz et al., 2013; Hasegawa et al., 2013; Schwentner et al., 2018). Beyond blocking pyruvate-consuming pathways, the second strategy is aimed at unbalancing the NAD/NADP ratio via deletion of malate dehydrogenase (MDH, *mdh*) (Park et al., 2007; Park et al., 2011b) or redirecting the flux towards PPP via deletion of phosphate glucose isomerase (PGI, *pgi*). This has been often used to increase the carbon flux through the branched chain amino acid (BCAA) pathway (Park et al., 2007; Park et al., 2011a; Bartek et al., 2011; Noda et al., 2019). Finally, deleting metabolite-specific competing reactions in order to streamline

the optimized pathway is also a recurrent strategy resulting in improved titers (Supplementary Figure S4). For instance, efficient production of L-valine required blocking the biosynthesis of alternative 2-KIV derivatives, such as L-leucine and/or pantothenate (Radmacher et al., 2002; Park et al., 2007; Holátko et al., 2009; Park et al., 2011b; Westbrook et al., 2018). However, these deletions resulted in auxotroph strains requiring complex culture media to grow, thus increasing the operational cost of the bioprocess.

It seems reasonable to minimize the number of knockouts while maintaining high production in minimal medium to deliver a cost-effective 2-KIV production bioprocess. Therefore, we assessed 2-KIV production *in silico* to measure the performance of a set of knockout scenarios harboring minimal deletions. These included the removal of pyruvate-consuming pathways and generation of cofactor imbalances. Specifically, we used Monte Carlo Sampling to explore the metabolic space of three *in silico* mutant strains, i.e., *aceF-mdh*, *ppc-mdh* and *ldhA-pflB-adhE* (Figure 4). Selection of this set of reactions was based on the outcomes of previous studies (Supplementary Table S6; Supplementary Figure S4) using caution to avoid auxotrophies in the final chassis.

Quantitative analysis of flux frequency shows that, of all tested mutants, the double *aceF-mdh* *in silico* strain exhibited the highest flux through the ACLS, DHAD and Ex-2KIV reactions (Figure 4). These results strongly suggest an increased flux through the BCAA pathway, which is in agreement with results from previous studies dealing with L-valine production (Park et al., 2007). Similarly, the

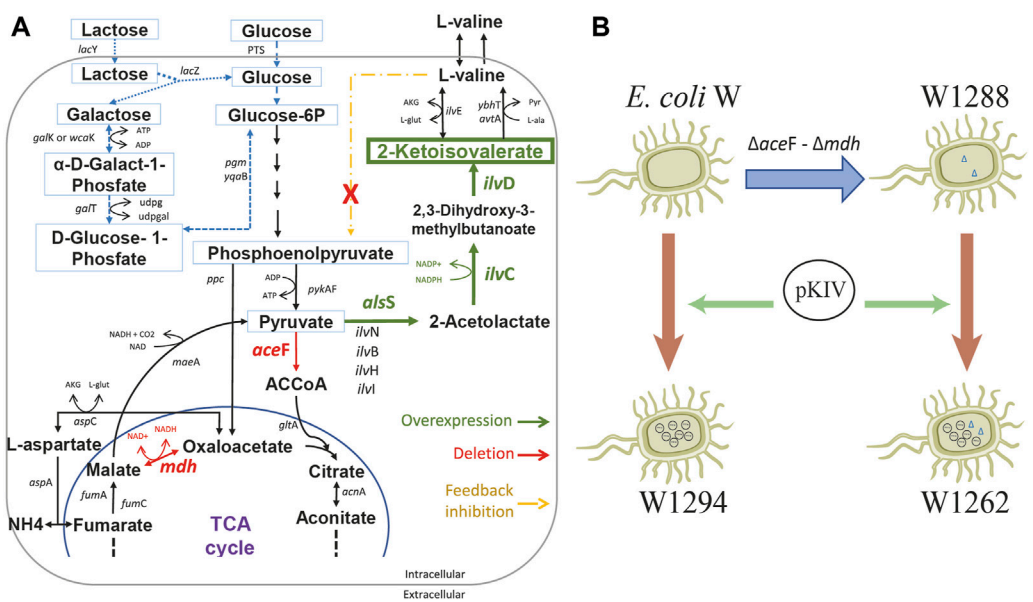


FIGURE 5 Schematic diagram of *E. coli* W engineering for 2-ketoisovalerate (2-KIV) overproduction. (A): Main genetic interventions addressed to construct a 2-KIV overproducer *E. coli* W strain, (B): Engineering *E. coli* W strains. Phosphotransferase system (PTS), Glucose-6-phosphate (Glucose-6P), acetylcoenzyme A (ACCoA), Tricarboxylic Acid Cycle (TCA cycle). Gene names are shown in italic.

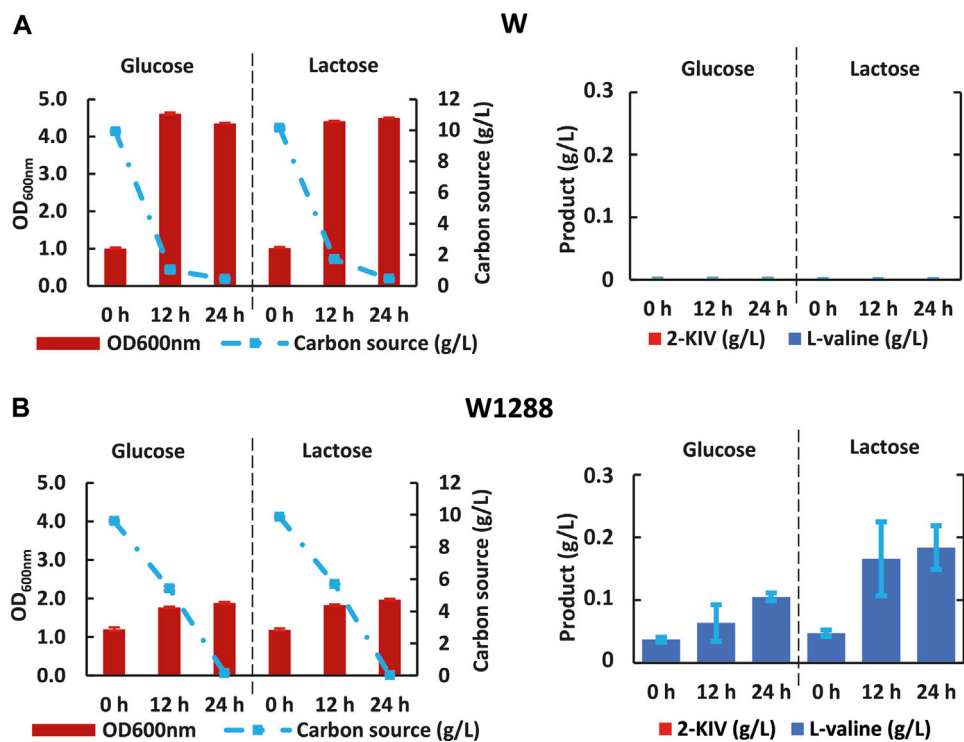


FIGURE 6 Kinetic of growth, substrate uptake and 2-ketoisovalerate and L-valine production of *E. coli* W (A) and *E. coli* W1288 (B) in shake flask experiments using glucose and lactose. Error bars indicate the difference between replicate cultures.

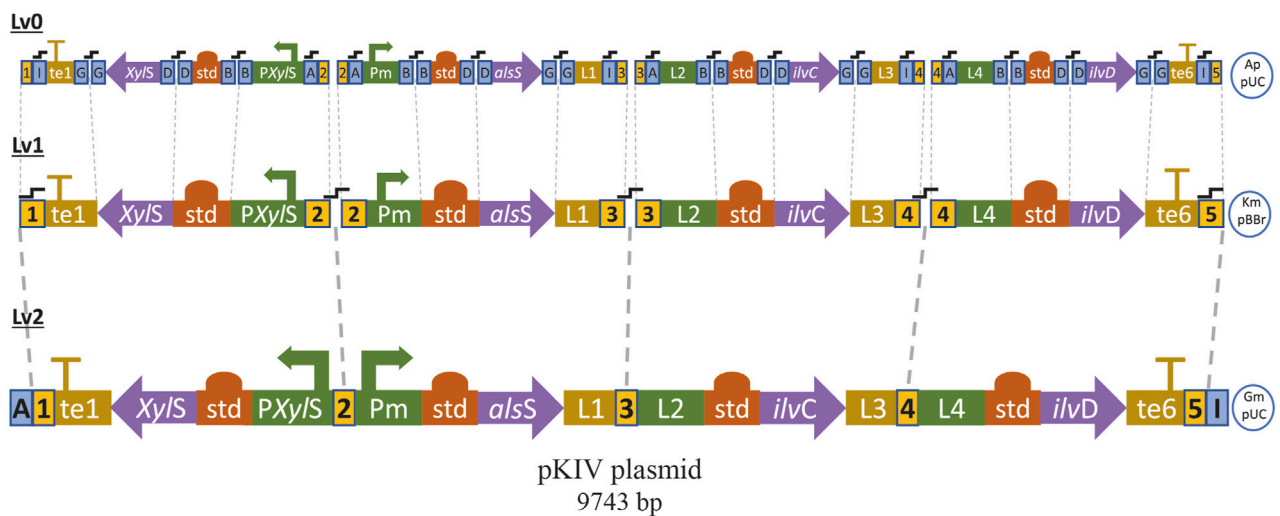


FIGURE 7

Sequential modular assembly of pKIV plasmid from basic DNA parts by using Golden Standard (See method). te1: T1 Terminator, L1, L2, L3 and L4: linker terminals and promoters, te6: BBa B1006 Terminator, std: consensus RBS, Ap: ampicillin resistance, Km: kanamycin resistance, Gm: gentamycin resistance, \blacktriangleleft fusion sites of BsaI (blue square) and BpiI (yellow square) enzymes.

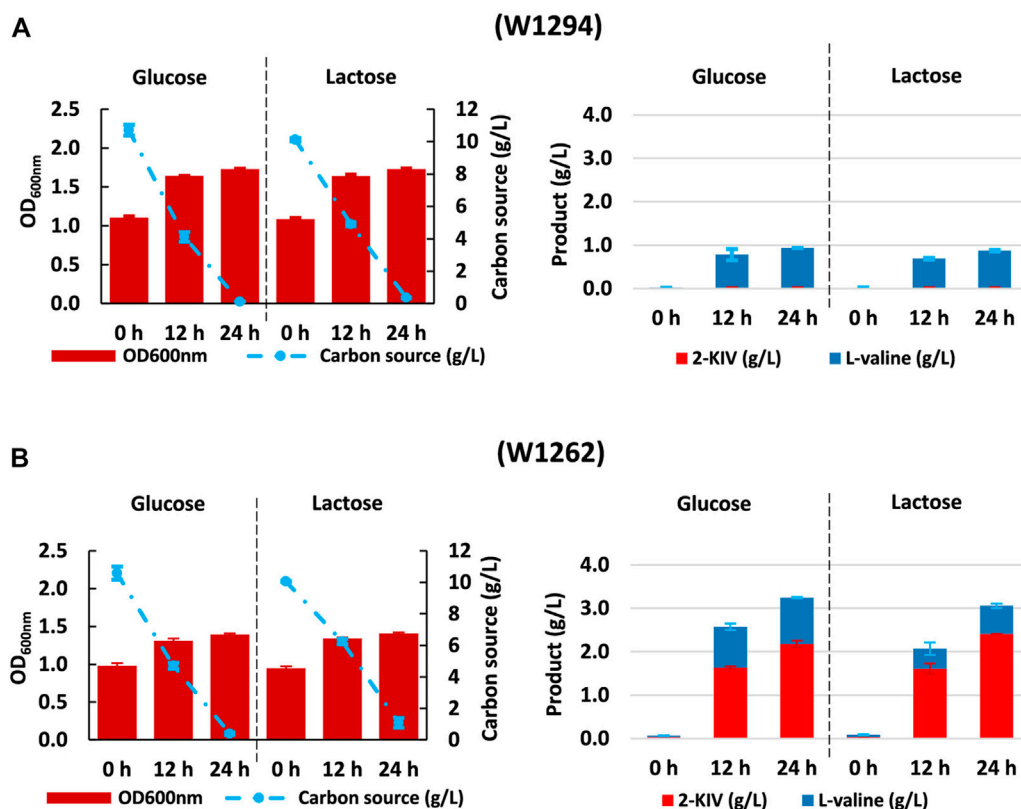
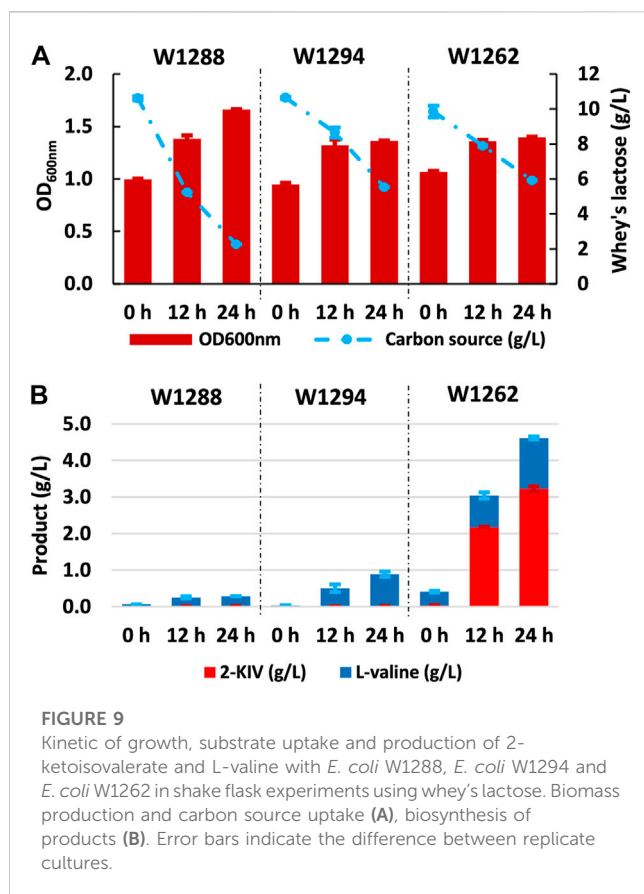


FIGURE 8

Kinetic of Growth, substrate uptake and 2-ketoisovalerate and L-valine production of *E. coli* W1294 (A) and *E. coli* W1292 (B) in shake flask experiments using glucose and lactose. Error bars indicate the difference between replicate cultures.

aceF-mdh double mutant has a higher frequency and metabolic flux through the ME2 reaction. This should significantly contribute not only to providing additional levels of NADPH to the KARA reaction

(Figure 1), but also to increasing pyruvate levels (Noronha et al., 2000), thus resulting in higher levels of 2-KIV. Finally, the double *aceF-mdh* mutant also exhibited a significantly lower acetate



secretion compared to the other mutants, which greatly enhances this strain's potential. Overall, we found that the double *aceF-mdh* was the most promising.

3.3 Carbon flux rerouting towards pyruvate promotes L-valine production in *E. coli* W

We constructed a 2-KIV biotechnological platform comprising three major stages: 1) deletion of the *aceF* and *mdh* genes to re-route the carbon flux, 2) overexpression of the 2-KIV biosynthesis pathway and 3) removal of L-valine negative feedback (Figure 5).

First we rerouted carbon flux towards pyruvate using scarless genome editing (Kim et al., 2014) to sequentially delete *aceF* and *mdh*. We then monitored growth performance of the resulting *E. coli* W1288 strain using glucose and lactose as sole carbon sources and compared it with the parental strain. We found significant differences in the engineered strain's growth performance irrespective of the carbon source used in shake flask assays (Figure 6). For instance, *E. coli* W1288 exhibited lower substrate consumption and biomass production using glucose and lactose. As predicted *in silico*, deletion of *aceF* and *mdh* putatively resulted in lower levels of Acetyl-CoA in this phenotype and, therefore, TCA blockage thus explaining the growth performance observed. We registered significantly higher amounts of L-valine in cultures of *E. coli* W1288 using lactose as carbon source (up to 0.2 g/L) (Figure 6). This behavior was in line with *in silico* predictions and it strongly suggested that the double deletion increased flux through the BCAA pathway.

3.4 Engineering a 2-KIV *E. coli* W overproducer strain

We assembled a synthetic pathway to express genes *alsS*, *ilvC* and *ilvD* under heterologous expression driven by the *XylS/Pm* system (Figure 7). *ilvC* and *ilvD* encode the ketol-acid reductoisomerase and dihydroxy-acid dehydratase, which are responsible for synthesizing 2-KIV from acetolactate, while *alsS* from *Bacillus subtilis* encodes a L-valine-insensitive acetolactate synthase broadly used for L-valine production (Felpeto-Santero et al., 2015; Hao et al., 2020). The synthetic pathway was constructed using Golden Standard technology (Blázquez et al., 2022) in conjunction with a high-copy-number host vector (Figure 7). The resulting plasmid, pKIV, was further expressed in wild-type *E. coli* W and *E. coli* W1288, thus yielding the *E. coli* W1294 and *E. coli* W1262 strains, respectively (Figure 5).

Despite no toxicity due 2-KIV has been previously reported (Zhou et al., 2022), we found that irrespective of the carbon source, expression of pKIV placed a metabolic burden on carrier strains that appeared to be greater in the wild-type genetic background of *E. coli* W1294 (Figure 8). Under production conditions, final biomass of W1294 was halved, while only a slight reduction was observed with the W1262 strain (Figures 6, 8). Beyond the potential metabolic burden induced by the replication and maintenance of pKIV (Fakruddin et al., 2013), we noticed a significant reduction in W1294s substrate consumption compared to the wild-type strain which contributed to its poor growth performance. Production of L-valine in large amounts (around 1 g/L) is likely the reason behind W1294s poorer growth performance and it suggests the absence of feedback inhibition of AHAS by L-valine using *alsS* from *B. subtilis*.

Regarding the W1262 strain, we observed significant levels of L-valine production with minimal changes in growth and substrate consumption (Figure 8). Interestingly, the combination of carbon rerouting towards pyruvate, overexpression of the 2-KIV pathway and removal of feedback inhibition concurring in strain W1262 resulted in large titers of 2-KIV (2.2 ± 0.08 with glucose and 2.4 ± 0.00 g/L with lactose) (Figure 8C). In addition, we did not found side compounds such as acetate, formate and alcohols in the supernatants. The absence of byproducts suggests that 1) all the pyruvate available was funneled to 2-KIV and L-valine and 2) genetic modifications triggered no evident metabolic overflows, which is in agreement with *in silico* predictions.

3.5 Production of 2-KIV from non-conventional feedstock using non-conventional microbial cell factories

The main aim of our work was to produce 2-KIV efficiently using whey (specifically the lactose contained in whey - see Materials and methods) as a non-conventional feedstock. To this end, we assessed the growth performance and 2-KIV production potential of strains W1288, W1294 and W1262 using whey lactose as sole carbon and energy source. Overall, we observed minor changes in terms of growth and L-valine production compared with the previous experiments performed with glucose and lactose. It was also noteworthy that the lactose in the whey was not fully consumed, especially not by strains harboring the pKIV plasmid,

TABLE 2 Production of 2-KIV by different strains.

Strain	Operation mode	Medium	Time (h)	Total substrate uptake	2-KIV (g/L)	Y _{x/s} (g/g)	Y _{p/s} (g/g)	Y _{p/x} (g/g)	References
<i>Corynebacterium glutamicum</i>	Fed-batch bioreactor	CGXII	56	82 g/L glucose approx.; 24 g/L potassium acetate approx	25.56	0.20	0.31	1.58	Krause et al. (2010)
		20 g/L ammonium sulfate; 1 g/L yeast extract; 5 g/L urea; 0.2 mg/L biotin							
<i>Corynebacterium glutamicum</i>	Fed-batch bioreactor	CGXII	44	82 g/L glucose approx.; 5 g/L potassium acetate approx	35.00	0.14	0.18	1.34	Buchholz et al. (2013)
		10 g/L yeast extract; 10 mM L-valine, L-isoleucine and L-leucine							
<i>Klebsiella pneumoniae</i>	Batch bioreactor	5 g/L yeast Extract; 4 g/L corn steep liquor; 5 g/L (NH ₄) ₂ SO ₄ ; 0.4 g/L KCl and 0.1 g/L MgSO ₄	26	81 g/L glucose approx	17.40	0.05	0.21	4.68	Gu et al. (2017)
<i>Pseudomona putida</i>	Batch shake flask	M9	24	12 g/L glucose approx.; 0.12 g/L acetate approx	0.81	0.07 approx	0.40	0.95 approx	Batianis et al. (2022)
<i>E. coli</i> B0016	Fed-batch bioreactor	M9	26	130 g/L glucose approx	55.8	0.15 approx	0.55	2.93 approx	Zhou et al. (2022)
		5 g/L yeast extract; fed with 90 g/L yeast extract and 15 g/L peptone							
<i>E. coli</i> W1262	Batch shake flask	M9	24	10.2 g/L glucose	2.18	0.04	0.21	5.17	This study
		1 g/L yeast extract							
<i>E. coli</i> W1262	Batch shake flask	M9	24	9.0 g/L lactose	2.41	0.05	0.27	5.15	This study
		1 g/L yeast extract							
<i>E. coli</i> W1262	Batch shake flask	M9	24	3.9 g/L whey's lactose	3.22	0.08	0.81	9.71	This study
		1 g/L yeast extract							

i.e., W1294 and W1262 (Figure 9). In what seems to be the corroboration of the suitability of whey lactose as an optimal carbon source for *E. coli* W, we found that strain W1262 delivered the greatest titers (3.22 ± 0.07 g/L 2-KIV and 1.40 ± 0.04 g/L L-valine) with whey lactose as carbon source, it is worth mentioning that, in all cases, a pH reduction in the medium between 6–6.5 was observed, which suggests that using a buffered medium with greater ionic strength would help to maintain a stable pH. Overall, we obtained up to 4.62 g/L of products with 3.9 g/L of whey lactose (Figure 8). These high yields are probably related to the presence of additional nutrients in the whey, i.e., up to 0.06% protein and 0.02% fat (Carranza-Saavedra et al., 2021; Tsermoula et al., 2021). Altogether, these results highlight the potential of whey lactose as feedstock for value-added compounds derived from pyruvate, such as 2-KIV and L-valine.

Finally, we compared our results with previously published works where authors had used alternative microbial cell factories and feedstocks (Table 2). Although a direct comparison is challenging due to differing methodologies and operation modes, we found that product yields per unit of biomass using *E. coli* W1262 exceeds yields reported for *K. pneumoniae*, *C. glutamicum* and *E. coli* B0016 irrespective of the carbon source, i.e., glucose,

lactose and whey lactose (Table 2). Despite recording lower substrate-to-product conversion yields (Y_{p/s}) with glucose and pure lactose than in recent studies with *P. putida* and *E. coli* B0016 (Batianis et al., 2022; Zhou et al., 2022), in the presence of whey lactose we achieved the highest Y_{p/s} reported so far. This strongly highlights the potential of whey, a non-conventional feedstock, as a promising carbon source with the necessary potential to reduce production costs in microbial fermentation processes.

4 Conclusion

In this study we implemented an iterative approach to the production of valuable building blocks such as 2-KIV using non-conventional feedstocks and cell factories, i.e., whey lactose and the non-model *E. coli* W strain, and we demonstrated the latter's suitability to deal with complex mixes of mono and disaccharides. In order to reduce the operational costs of the bioprocess, we designed a microbial chassis free of autotrophies and rich media requirements for growth and we rerouted the carbon flux towards pyruvate. Finally, we applied cutting-edge synthetic biology to

the construction of a recombinant *E. coli* W strain capable of overproducing large titers of 2-KIV at the highest Yp/s reported so far. In what is a perfect fit for the demands of the circular economy, our approach and the W1262 strain pave the way for cost-effective production of key building blocks using recalcitrant feedstocks.

Data availability statement

The original contributions presented in the study are included in the article/[Supplementary Material](#), further inquiries can be directed to the corresponding author.

Author contributions

Experiments and analysis of data: DC-S; Sample analysis: DC-S; Construction of knockout mutants: DC-S and JT-B; Construction of synthetic expression systems: DC-S, JT-B, and BB; *In silico* modeling: DC-S; Manuscript draft preparation: DC-S and JN; Data interpretation: DC-S, CH, JM, and JN; Manuscript review: JT-B, BB, CH, JM, and JN; Project supervision: JM and JN All authors revised and approved manuscript.

Funding

This work was supported by the European Union's Horizon 2020 Research and Innovation Programme under Grant agreements no. 814650 (SynBio4Flav). Funding was likewise provided by the Spanish Ministry of Science and Innovation under "Severo Ochoa" Programme for Centers of Excellence in R&D, grant SEV-2017-0712 (AEI/10.13039/501100011033) and the RobExplode project: PID 2019-108458RB-I00 (AEI/10.13039/501100011033). JN, DC-S, and BB acknowledge the financial support of CSIC's

Interdisciplinary Platform for Sustainable Plastics towards a Circular Economy + (PTI-SusPlast+). DC-S was funded by the Ministerio de Ciencia Tecnología e Innovación (MINCIENCIAS) of Colombia [Contract number: FP44842-397].

Acknowledgments

The authors thank Sebastian Gaviria, Nutrition and Food Technology Group of the University of Antioquia (Colombia), for his support in the experimental phase and Clive A. Dove, National Centre for Biotechnology-CSIC (Spain) for proofreading of the manuscript.

Conflict of interest

The authors declare that the research was conducted in the absence of any commercial or financial relationships that could be construed as a potential conflict of interest.

Publisher's note

All claims expressed in this article are solely those of the authors and do not necessarily represent those of their affiliated organizations, or those of the publisher, the editors and the reviewers. Any product that may be evaluated in this article, or claim that may be made by its manufacturer, is not guaranteed or endorsed by the publisher.

Supplementary material

The Supplementary Material for this article can be found online at: <https://www.frontiersin.org/articles/10.3389/fbioe.2023.1176445/full#supplementary-material>

References

- Alterthum, F., and Ingram, L. O. (1989). Efficient ethanol production from glucose, lactose, and xylose by recombinant *Escherichia coli*. *Appl. Environ. Microbiol.* 55 (8), 1943–1948. doi:10.1128/aem.55.8.1943-1948.1989
- Amado, I. R., Vázquez, J. A., Pastrana, L., and Teixeira, J. A. (2016). Cheese whey: A cost-effective alternative for hyaluronic acid production by *Streptococcus zooepidemicus*. *Food Chem.* 198, 54–61. doi:10.1016/j.foodchem.2015.11.062
- Archer, C. T., Kim, J. F., Jeong, H., Park, J. H., Vickers, C. E., Lee, S. Y., et al. (2011). The genome sequence of *E. coli* W (ATCC 9637): comparative genome analysis and an improved genome-scale reconstruction of *E. coli*. *BMC Genomics* 12 (1), 9. doi:10.1186/1471-2164-12-9
- Atsumi, S., Hanai, T., and Liao, J. C. (2008). Non-fermentative pathways for synthesis of branched-chain higher alcohols as biofuels. *Nature* 451 (7174), 86–89. doi:10.1038/nature06450
- Bartek, T., Blombach, B., Lang, S., Eikmanns, B. J., Wiechert, W., Oldiges, M., et al. (2011). Comparative 13C metabolic flux analysis of pyruvate dehydrogenase complex-deficient, L-valine-producing *Corynebacterium glutamicum*. *Appl. Environ. Microbiol.* 77 (18), 6644–6652. doi:10.1128/AEM.00575-11
- Batianis, C., van Rosmalen, R. P., Major, M., van Ee, C., Kasiotakis, A., Weusthuis, R. A., et al. (2022). A tunable metabolic valve for precise growth control and increased product formation in *Pseudomonas putida*. *Metab. Eng.* 75, 47–57. doi:10.1016/j.ymben.2022.10.002
- Blázquez, B., Torres-Bacete, J., San Leon, D., Kniewel, R., Martinez, I., Sordon, S., et al. (2022). Golden standard: A complete standard, portable, and interoperable MoClo tool for model and non-model bacterial hosts. *bioRxiv*, 2022. doi:10.1101/2022.09.20.508659
- Blombach, B., Riester, T., Wieschalka, S., Ziert, C., Youn, J. W., Wendisch, V. F., et al. (2011). *Corynebacterium glutamicum* tailored for efficient isobutanol production. *Appl. Environ. Microbiol.* 77 (10), 3300–3310. doi:10.1128/AEM.02972-10
- Blombach, B., Schreiner, M. E., Holatko, J., Bartek, T., Oldiges, M., and Eikmanns, B. J. (2007). L-valine production with pyruvate dehydrogenase complex-deficient *Corynebacterium glutamicum*. *Appl. Environ. Microbiol.* 73 (7), 2079–2084. doi:10.1128/AEM.02826-06
- Buchholz, J., Schwentner, A., Brunnenkan, B., Gabris, C., Grimm, S., Gerstmeir, R., et al. (2013). Platform engineering of *Corynebacterium glutamicum* with reduced pyruvate dehydrogenase complex activity for improved production of L-lysine, L-valine, and 2-ketoisovalerate. *Appl. Environ. Microbiol.* 79 (18), 5566–5575. doi:10.1128/AEM.01741-13
- Calero, P., and Nikel, P. I. (2019). Chasing bacterial chassis for metabolic engineering: A perspective review from classical to non-traditional microorganisms. *Microb. Biotechnol.* 12 (1), 98–124. doi:10.1111/1751-7915.13292
- Cao, M., Jiang, T., Li, P., Zhang, Y., Guo, S., Meng, W., et al. (2020). Pyruvate production from whey powder by metabolic engineered *Klebsiella oxytoca*. *J. Agric. Food Chem.* 68 (51), 15275–15283. doi:10.1021/ACS.JAFC.0C06724
- Carranza-Saavedra, D., Sánchez Henao, C. P., and Zapata Montoya, J. E. (2021). Kinetic analysis and modeling of L-valine production in fermentation batch from *E. coli* using glucose, lactose and whey as carbon sources. *Biotechnol. Rep.* 31 (9), e00642. doi:10.1016/j.btre.2021.e00642
- Chen, C., Li, Y., Hu, J., Dong, X., and Wang, X. (2015). Metabolic engineering of *Corynebacterium glutamicum* ATCC13869 for L-valine production. *Metab. Eng.* 29, 66–75. doi:10.1016/j.ymben.2015.03.004

- Cigić, I. K., Kosmerl, T., Vodošek, T. V., and Strlič, M. (2008). Amino acid quantification in the presence of sugars using HPLC and pre-column derivatization with 3-MPA/OPA and FMOC-Cl. *Acta Chim. Slov.* 55, 660–664.
- Duncan, D. B. (1955). Multiple range and multiple F tests. *Biometrics* 11 (1), 1. doi:10.2307/3001478
- Erian, A. M., Gibisch, M., and Pflügl, S. (2018). Engineered *E. coli* W enables efficient 2,3-butanediol production from glucose and sugar beet molasses using defined minimal medium as economic basis. *Microb. Cell. Factories* 17 (1), 190–217. doi:10.1186/s12934-018-1038-0
- Fakruddin, M., Mohammad Mazumdar, R., Shahnewaj Bin Mannan, K., Chowdhury, A., and Hossain, M. N. (2013). Critical factors affecting the success of cloning, expression, and mass production of enzymes by recombinant *E. coli*. *ISRN Biotechnol.* 2013, 590587. doi:10.5402/2013/590587
- Feltnagle, E. A., Chaubey, A., Noey, E. L., Houk, K. N., and Liao, J. C. (2012). Engineering synthetic recursive pathways to generate non-natural small molecules. *Nat. Chem. Biol.* 8 (6), 518–526. doi:10.1038/nchembio.959
- Felpeto-Santero, C., Rojas, A., Tortajada, M., Galán, B., Ramón, D., and García, J. L. (2015). Engineering alternative isobutanol production platforms. *Amb. Express* 5 (1), 32. doi:10.1186/s13568-015-0119-2
- Gawin, A., Valla, S., and Brautaset, T. (2017). The XylS/Pm regulator/promoter system and its use in fundamental studies of bacterial gene expression, recombinant protein production and metabolic engineering. *Microb. Biotechnol.* 10 (4), 702–718. doi:10.1111/1751-7915.12701
- Gleiser, I. E., and Bauer, S. (1981). Growth of *E. coli* W to high cell concentration by oxygen level linked control of carbon source concentration. *Biotechnol. Bioeng.* 23 (5), 1015–1021. doi:10.1002/bit.260230509
- Gu, J., Zhou, J., Zhang, Z., Kim, C. H., Jiang, B., Shi, J., et al. (2017). Isobutanol and 2-ketoisovalerate production by *Klebsiella pneumoniae* via a native pathway. *Metab. Eng.* 43, 71–84. doi:10.1016/j.ymben.2017.07.003
- Gudmundsson, S., and Nogales, J. (2021). Recent advances in model-assisted metabolic engineering. *Curr. Opin. Syst. Biol.* 28, 100392. doi:10.1016/j.COISB.2021.100392
- Guurdo, N., Volke, D. C., and Nikel, P. I. (2022). Merging automation and fundamental discovery into the design-build-test-learn cycle of nontraditional microbes. *Trends Biotechnol.* 40 (10), 1148–1159. doi:10.1016/j.TIBTECH.2022.03.004
- Hao, Y., Ma, Q., Liu, X., Fan, X., Men, J., Wu, H., et al. (2020). High-yield production of L-valine in engineered *Escherichia coli* by a novel two-stage fermentation. *Metab. Eng.* 62, 198–206. doi:10.1016/j.ymben.2020.09.007
- Hasegawa, S., Suda, M., Uematsu, K., Natsuma, Y., Hiraga, K., Jojima, T., et al. (2013). Engineering of *Corynebacterium glutamicum* for high-yield L-valine production under oxygen deprivation conditions. *Appl. Environ. Microbiol.* 79 (4), 1250–1257. doi:10.1128/AEM.02806-12
- Heirendt, L., Arreckx, S., Pfau, T., Mendoza, S. N., Richelle, A., Heinken, A., et al. (2019). Creation and analysis of biochemical constraint-based models using the COBRA Toolbox v.3.0. *Nat. Protoc.* 14 (3), 639–702. doi:10.1038/s41596-018-0098-2
- Holátko, J., Elišáková, V., Prouza, M., Sobotka, M., Nešvera, J., and Pátek, M. (2009). Metabolic engineering of the L-valine biosynthesis pathway in *Corynebacterium glutamicum* using promoter activity modulation. *J. Biotechnol.* 139 (3), 203–210. doi:10.1016/j.JBIOTEC.2008.12.005
- Hou, X., Chen, X., Zhang, Y., Qian, H., and Zhang, W. (2012). L-Valine production with minimization of by-products synthesis in *Corynebacterium glutamicum* and *Brevibacterium flavum*. *Amino Acids* 43 (6), 2301–2311. doi:10.1007/S00726-012-1308-9
- Jung, H. M., Han, J. H., and Oh, M. K. (2020). Improved production of 2,3-butanediol and isobutanol by engineering electron transport chain in *Escherichia coli*. *Microb. Biotechnol.* 14 (1), 213–226. doi:10.1111/1751-7915.13669
- Kerem, Z., Bravdo, B. A., Shoseyov, O., and Tugendhaft, Y. (2004). Rapid liquid chromatography-ultraviolet determination of organic acids and phenolic compounds in red wine and must. *J. Chromatogr. A* 1052 (1–2), 211–215. doi:10.1016/j.CHROMA.2004.08.105
- Kim, J., Webb, A. M., Kershner, J. P., Blaskowski, S., and Copley, S. D. (2014). A versatile and highly efficient method for scarless genome editing in *Escherichia coli* and *Salmonella enterica*. *BMC Biotechnol.* 14 (1), 84. doi:10.1186/1472-6750-14-84
- Krause, F. S., Blombach, B., and Eikmanns, B. J. (2010). Metabolic engineering of *Corynebacterium glutamicum* for 2-Ketoisovalerate production. *Appl. Environ. Microbiol.* 76 (24), 8053–8061. doi:10.1128/AEM.01710-10
- Landor, L. A. I., Bratbak, G., Larsen, A., Tjendra, J., and Våge, S. (2023). Differential toxicity of bioorthogonal non-canonical amino acids (BONCAT) in *Escherichia coli*. *J. Microbiol. Methods* 206, 106679. doi:10.1016/J.MIMET.2023.106679
- Lee, S. Y., Kim, H. U., Chae, T. U., Cho, J. S., Kim, J. W., Shin, J. H., et al. (2019). A comprehensive metabolic map for production of bio-based chemicals. *Nat. Catal.* 2 (1), 18–33. doi:10.1038/s41929-018-0212-4
- Lee, W. H., Seo, S. O., Bae, Y. H., Nan, H., Jin, Y. S., and Seo, J. H. (2012). Isobutanol production in engineered *Saccharomyces cerevisiae* by overexpression of 2-ketoisovalerate decarboxylase and valine biosynthetic enzymes. *Bioprocess Biosyst. Eng.* 35 (9), 1467–1475. doi:10.1007/s00449-012-0736-y
- Li, S., Wen, J., and Jia, X. (2011). Engineering *Bacillus subtilis* for isobutanol production by heterologous Ehrlich pathway construction and the biosynthetic 2-ketoisovalerate precursor pathway overexpression. *Appl. Microbiol. Biotechnol.* 91 (3), 577–589. doi:10.1007/s00253-011-3280-9
- Liang, S., Chen, H., Liu, J., and Wen, J. (2018). Rational design of a synthetic Entner-Doudoroff pathway for enhancing glucose transformation to isobutanol in *Escherichia coli*. *J. Industrial Microbiol. Biotechnol.* 45 (3), 187–199. doi:10.1007/s10295-018-2017-5
- Lopes, A. C. A., Eda, S. A., Andrade, R. F., Amorim, J. C., and Duarte, W. F. (2019). New alcoholic fermented beverages—Potentials and challenges, fermented beverages. *Sci. Beverages* 5, 577–603. doi:10.1016/B978-0-12-815271-3.00014-2
- Luo, Y., Zhang, T., and Wu, H. (2014). The transport and mediation mechanisms of the common sugars in *Escherichia coli*. *Biotechnol. Adv.* 32 (5), 905–919. doi:10.1016/j.biotechadv.2014.04.009
- Mano, J., Liu, N., Hammond, J. H., Currie, D. H., and Stephanopoulos, G. (2020). Engineering *Yarrowia lipolytica* for the utilization of acid whey. *Metab. Eng.* 57, 43–50. doi:10.1016/J.YMBEN.2019.09.010
- Martínez-García, E., Fraile, S., Algar, E., Aparicio, T., Velázquez, E., Calles, B., et al. (2022). Seva 4.0: An update of the standard European vector architecture database for advanced analysis and programming of bacterial phenotypes. *Nucleic Acids Res.* 1 (1256879), D1558–D1567. doi:10.1093/NAR/GKAC1059
- Nagata, S. (2001). Growth of *Escherichia coli* ATCC 9637 through the uptake of compatible solutes at high osmolarity. *J. Biosci. Bioeng.* 92 (4), 324–329. doi:10.1016/S1389-1723(01)80234-6
- Nitschel, R., Ankenbauer, A., Welsch, I., Wirth, N. T., Massner, C., Ahmad, N., et al. (2020). Engineering *Pseudomonas putida* KT2440 for the production of isobutanol. *Eng. Life Sci.* 20 (5–6), 148–159. doi:10.1002/elsc.201900151
- Noda, S., Mori, Y., Oyama, S., Kondo, A., Araki, M., and Shirai, T. (2019). Reconstruction of metabolic pathway for isobutanol production in *Escherichia coli*. *Microb. Cell. factories* 18 (1), 124. doi:10.1186/s12934-019-1171-4
- Noronha, S. B., Yeh, H. J., Spande, T. F., and Shiloach, J. (2000). Investigation of the TCA cycle and the glyoxylate shunt in *Escherichia coli* BL21 and JM109 using 13C-NMR/MS. *Biotechnol. Bioeng.* 68 (3), 316–327. doi:10.1002/(SICI)1097-0290(20000505)68:3<316::AID-BIT10>3.0.CO;2-2
- Novak, K., Baar, J., Freitag, P., and Pflügl, S. (2020). Metabolic engineering of *Escherichia coli* W for isobutanol production on chemically defined medium and cheese whey as alternative raw material. *J. Industrial Microbiol. Biotechnol.* 47 (12), 1117–1132. doi:10.1007/S10295-020-02319-Y
- Pandi, K., Chauhan, A. S., Khan, W. H., and Rathore, A. S. (2020). Phosphate starvation controls lactose metabolism to produce recombinant protein in *Escherichia coli*. *Appl. Microbiol. Biotechnol.* 104 (22), 9707–9718. doi:10.1007/s00253-020-10935-y
- Park, J. H., Jang, Y., Lee, J. W., and Lee, S. Y. (2011a). *Escherichia coli* W as a new platform strain for the enhanced production of L-Valine by systems metabolic engineering. *Biotechnol. Bioeng.* 108 (5), 1140–1147. doi:10.1002/bit.23044
- Park, J. H., Kim, T. Y., Lee, K. H., and Lee, S. Y. (2011b). Fed-batch culture of *Escherichia coli* for L-valine production based on *in silico* flux response analysis. *Biotechnol. Bioeng.* 108 (4), 934–946. doi:10.1002/bit.22995
- Park, J. H., Lee, K. H., Kim, T. Y., and Lee, S. Y. (2007). Metabolic engineering of *Escherichia coli* for the production of L-valine based on transcriptome analysis and *in silico* gene knockout simulation. *PNAS* 104 (19), 7797–7802. doi:10.1073/pnas.0702609104
- Radmacher, E., Vaitiskova, A., Burger, U., Krumbach, K., Sahm, H., and Eggeling, L. (2002). Linking central metabolism with increased pathway flux: L-Valine accumulation by *Corynebacterium glutamicum*. *Appl. Environ. Microbiol.* 68 (5), 2246–2250. doi:10.1128/AEM.68.5.2246-2250.2002
- Ren, N., Guo, W., Liu, B., Cao, G., and Ding, J. (2011). Biological hydrogen production by dark fermentation: Challenges and prospects towards scaled-up production. *Curr. Opin. Biotechnol.* 22 (3), 365–370. doi:10.1016/J.COPBIO.2011.04.022
- Schwentner, A., Feith, A., Münch, E., Busche, T., Rückert, C., Kalinowski, J., et al. (2018). Metabolic engineering to guide evolution – creating a novel mode for L-valine production with *Corynebacterium glutamicum*. *Metab. Eng.* 47, 31–41. doi:10.1016/j.ymben.2018.02.015
- Shiloach, J., and Bauer, S. (1975). High-yield growth of *E. coli* at different temperatures in a bench scale fermentor. *Biotechnol. Bioeng.* 17 (2), 227–239. doi:10.1002/bit.260170208
- Silva, A. N. D., Perez, R., Minim, V. P. R., Martins, D. D. S., and Minim, L. A. (2015). Integrated production of whey protein concentrate and lactose derivatives: What is the best combination? *Food Res. Int.* 73, 62–74. doi:10.1016/J.FOODRES.2015.03.009

- Tsermoula, P., Khakimov, B., Nielsen, J. H., and Engelsen, S. B. (2021). Whey - the waste-stream that became more valuable than the food product. *Trends Food Sci. Technol.* 118, 230–241. doi:10.1016/J.TIFS.2021.08.025
- Wang, X., Xia, K., Yang, X., and Tang, C. (2019). Growth strategy of microbes on mixed carbon sources. *Nat. Commun.* 10 (1), 1279–1287. doi:10.1038/s41467-019-09261-3
- Wang, X., Zhang, H., and Quinn, P. J. (2018). Production of l-valine from metabolically engineered *Corynebacterium glutamicum*. *Appl. Microbiol. Biotechnol.* 102 (10), 4319–4330. doi:10.1007/S00253-018-8952-2
- Westbrook, A. W., Ren, X., Moo-Young, M., and Chou, C. P. (2018). Metabolic engineering of *Bacillus subtilis* for l-valine overproduction. *Biotechnol. Bioeng.* 115 (11), 2778–2792. doi:10.1002/bit.26789
- Wu, G., Yan, Q., Jones, J. A., Tang, Y. J., Fong, S. S., and Koffas, M. A. (2016). Metabolic burden: Cornerstones in synthetic biology and metabolic engineering applications. *Trends Biotechnol.* 34 (8), 652–664. doi:10.1016/J.TIBTECH.2016.02.010
- Zhao, K., Tang, H., Zhang, B., Zou, B., Liu, Z., Zheng, Y., et al. (2022). Microbial production of vitamin B5: Current status and prospects. *Crit. Rev. Biotechnol.* 2022, 1–21. doi:10.1080/07388551.2022.2104690
- Zhou, L., Zhu, Y., Yuan, Z., Liu, G., Sun, Z., Du, S., et al. (2022). Evaluation of metabolic engineering strategies on 2-ketoisovalerate production by *Escherichia coli*. *Appl. Environ. Microbiol.* 88 (17), e0097622. doi:10.1128/AEM.00976-22/SUPPL_FILE/AEM.00976-22-S0001.PDF



OPEN ACCESS

EDITED BY

Jiandong Cui,
Tianjin University of Science and
Technology, China

REVIEWED BY

Yejun Han,
Chinese Academy of Sciences (CAS),
China
Abdur Rahim Khan,
University of California, Davis,
United States

*CORRESPONDENCE

Ling Xu,
✉ lxu@ujs.edu.cn

RECEIVED 28 February 2023

ACCEPTED 14 April 2023

PUBLISHED 25 April 2023

CITATION

Wang F, Yu X, Yu Z, Cui Y, Xu L, Huo S,
Ding Z, Zhao L, Du L and Qiu Y (2023),
Improved laccase production by
Trametes versicolor using Copper-
Glycyl-L-Histidyl-L-Lysine as a novel and
high-efficient inducer.
Front. Bioeng. Biotechnol. 11:1176352.
doi: 10.3389/fbioe.2023.1176352

COPYRIGHT

© 2023 Wang, Yu, Yu, Cui, Xu, Huo, Ding,
Zhao, Du and Qiu. This is an open-access
article distributed under the terms of the
[Creative Commons Attribution License](https://creativecommons.org/licenses/by/4.0/)
(CC BY). The use, distribution or
reproduction in other forums is
permitted, provided the original author(s)
and the copyright owner(s) are credited
and that the original publication in this
journal is cited, in accordance with
accepted academic practice. No use,
distribution or reproduction is permitted
which does not comply with these terms.

Improved laccase production by *Trametes versicolor* using Copper-Glycyl-L-Histidyl-L-Lysine as a novel and high-efficient inducer

Feng Wang^{1,2}, Xiaolei Yu¹, Zhuo Yu¹, Yi Cui¹, Ling Xu^{1,2*},
Shuhao Huo¹, Zhongyang Ding³, Liting Zhao³, Lizhi Du⁴ and
Yanguo Qiu⁴

¹School of Food and Biological Engineering, Jiangsu University, Zhenjiang, China, ²Institute of Agricultural Products Processing Engineering, Jiangsu University, Zhenjiang, China, ³Laboratory of Carbohydrate Chemistry and Biotechnology, Ministry of Education, School of Biotechnology, Jiangnan University, Wuxi, China, ⁴Shandong Dehemingxing Biotechnology Co., Ltd., Weifang, China

A highly efficient strategy using Copper-Glycyl-L-Histidyl-L-Lysine (GHK-Cu) as a novel inducer was developed to enhance laccase production by *Trametes versicolor*. After medium optimization, laccase activity increased by 12.77-fold compared to that without GHK-Cu. The laccase production of 1113.8 U L⁻¹ was obtained by scaling-up culture in 5-L stirring tank. The laccase production induced by CuSO₄ was poorer than that of GHK-Cu at the same mole concentration. GHK-Cu could increase the permeability of cell membrane with less damage, and it facilitated the adsorption, accumulation, and utilization of copper by fungal cells, which was beneficial for laccase synthesis. GHK-Cu induced better expression of laccase related genes than that of CuSO₄, resulting in higher laccase production. This study provided a useful method for induced production of laccase by applying GHK chelated metal ion as a non-toxic inducer, which reduced the safety risk of laccase broth and provided the potential application of crude laccase in food industry. In addition, GHK can be used as the carrier of different metal ions to enhance the production of other metalloenzymes.

KEYWORDS

Trametes versicolor, laccase, copper-Glycyl-L-Histidyl-L-Lysine, medium optimization, induction

1 Introduction

Laccase (phenol-oxygen oxidoreductase; EC 1.10.3.2) is a kind of copper containing polyphenol oxidase. Laccase was firstly isolated and purified from lacquer trees of Southeast Asia in 1894 and subsequently it has been identified in fungi, bacteria, and insects (Khatami et al., 2022). Among them, white-rot fungi are good laccase producers (Pisacha et al., 2020). Laccase has a wide range of substrate specificity, and during catalytic reactions, the substrate can be reduced to water and other small molecule substances without causing secondary pollution. This is crucial for environmental maintenance and applications in various industries. So, as an ideal green biocatalyst, laccase has a wide range of applications, including food, textiles, cosmetics, pharma, biofuels, pulp and paper, and bioremediation

(Gomez-Fernandez et al., 2020). The application of laccase in food industry was a hot spot in recent years. However, the large-scale application of laccase in the industry has been limited by the low production and expression levels of natural laccase and the high cost (Su et al., 2020). To improve the laccase expression level, different techniques and methods have been studied, including strain screening, inducer selection, recombinant expression, optimization of medium composition and culture conditions, protein rational design and site-directed mutation (Pardo and Camarero, 2015; Valle et al., 2015; Wang et al., 2017; Wang et al., 2020; Zhang et al., 2021). In addition, new sustainable strategies were developed to improve laccase production, such as physical treatment, and co-culture with other fungi (Wang et al., 2013; Zhang et al., 2020). High enzyme production, high enzyme quality, and excellent performance are the keys to the industrial application of laccase, however, these methods are still far from the industrial wide application (Bertrand et al., 2017). Therefore, it is still attracting the interest of researchers to explore more strategy to improve laccase production.

The most used laccases in the industry were produced by fungi. *T. versicolor* has been recognized as one of the most effective white-rot basidiomycetes to produce large amount of laccase (Fonseca et al., 2016). At present, laccase production of *T. versicolor* has been widely investigated. To improve the activity of laccase, the culture condition of *T. versicolor* was optimized by the orthogonal test in order to improve the activity of laccase (Liu et al., 2019). Researchers found that using cheap substrates to increase laccase production of *T. versicolor* was also an effective strategy, such as tea residues (Xu et al., 2020). In addition, fermentation medium aeration was applied to enhance the laccase production of *T. versicolor* in three types of bioreactors due to the sufficient oxygen supply for microorganisms (Pinheiro et al., 2020).

The selection of inducers in laccase production is an important and interesting work. At present, the reported laccase inducers mainly include phenolic compounds, agro-industrial wastes, natural inducers, aromatic compounds, alcohols, detergents, and metal ions (Wang et al., 2019). Phenolic compounds were often considered effective inducers of laccase, such as guaiacol (Chaurse and Sahay, 2023). The binding of phenolic compounds present in potatoes to starch was believed to be involved in the induced synthesis of laccase in *Pleurotus florida* (Das et al., 1999). Agro-industrial wastes and natural inducers are very economical, and they come from a wide range of sources and provide nutrients (Bertrand et al., 2017). High concentrations of aromatic compounds are toxic to organisms, inhibiting cell growth and enzyme production (BİRhanlı and Yesilada, 2017). Alcohols are cheaper, more readily available, and less toxic. However, laccase activity did not increase significantly (Valle et al., 2015). Recent research has shown that the presence of Pb^{2+} could burst the activity of laccase from *Truncatella angustata* BPF5 (Chaurse and Sahay, 2023). More and more studies have proved that metal ions can promote the production of laccase, and Cu^{2+} is more effective than the other metal inducers. However, high concentration of Cu^{2+} accumulated in cells was toxic to cells (BİRhanlı and Yesilada, 2017). Therefore, the separation and purification operations were generally applied to remove the residual Cu^{2+} residues from culture broth, which increased the production cost and limited its application in food industry.

Copper-Glycyl-L-Histidyl-L-Lysine (GHK-Cu) is a compound formed by the combination of GHK with Cu^{2+} . GHK is non-toxic and occurs naturally in saliva, blood, and urine (Li et al., 2016). Then GHK readily binds copper or zinc cations and was considered as the transporter of metal ions through membranes, which reduced the damage to cells resulted from metal ions (Alshammari and Platts, 2020). In addition, GHK-Cu has antioxidant and anti-inflammatory effects, which can improve the skin and has a wide range of applications in the cosmetics and the skin tissue remodeling industry (Pickart and Margolin, 2018). Therefore, GHK-Cu may be a potential inducer candidate for laccase production from fungi. In this study, laccase production from *T. versicolor* was induced by using GHK-Cu instead of Cu^{2+} . For this purpose, the composition of the culture medium was optimized by one-factor-at-a-time and Box-Behnken design (BBD). And the interaction between medium compositions was analyzed by response surface methodology (RSM). The laccase production in the optimal medium was scaling up in a 5 L stirring reactor. The cell membrane permeability, consumption of copper source, and laccase gene expression were investigated using GHK-Cu and were compared to those under Cu^{2+} induction.

2 Materials and methods

2.1 Materials

2.1.1 Microorganism and chemicals

T. versicolor CICC 14001 was purchased from China Strain Preservation Center and was stored on potato dextrose agar slant at 4°C. TaKaRa MiniBEST Plant RNA Extraction Kit, PrimeScript™ RT reagent Kit with gDNA Eraser (Perfect Real Time) Kit, Green® Premix Ex Taq™ II (Tli RNaseH Plus) Kit was purchased from Shanghai Baisai Biotechnology Co., Ltd. All other chemicals were purchased from Sinopharm Chemical Reagent Co., Ltd.

2.1.2 Medium and culture conditions

The seed culture of *T. versicolor* was prepared according to the procedure described by Xu et al. (2020). The seed pellet mycelia of 5 mL were inoculated into the fermentation medium for laccase production. The pH of the culture broth for laccase production was adjusted with 0.1 mol L⁻¹ NaOH to 4.4 during the fermentation process until the pH rises automatically. The basic fermentation medium was the following composition (per liter): glucose 2 g, KH₂PO₄ 0.2 g, FeSO₄ · 7H₂O 0.035 g, MgSO₄ · 7H₂O 0.05 g, NH₄Cl 0.5 g, CaCl₂ 0.0755 g and sterilized at 121°C for 20 min. The cultures are incubated at 27°C, 150 rpm. One-factor-at-a-time, Box-Behnken design (BBD) and response surface methodology (RSM) were used to optimize the medium of laccase fermentation induced by GHK-Cu (Supplementary Materials and Methods S1). The optimal culture medium were obtained by sampling from the fermentation broth and measuring laccase activity on the 7th day. The scale-up of the reactor culture and exploration of possible mechanisms both were carried out under the optimal medium conditions. This experiment was conducted in a 5 L stirring reactor (GRJB-5D, Zhenjiang Gerui Bioengineering Co., Ltd.) at 27°C, 150 rpm, for 7 days (Supplementary Materials and Methods S2).

2.2 Analytical methods

2.2.1 Determination of intracellular and extracellular Cu content

With the optimal fermentation medium, *T. versicolor* was induced to produce laccase by GHK-Cu and the same amount of CuSO₄ and the control with no inducer. During fermentation (12, 24, 48, 72, 96, 120, 144 h), 50 mL of the broth were collected and centrifugated at 10,000 rpm for 15 min. The supernatant and pelleted mycelium were collected. The pelleted mycelium was washed with sterile distilled water 3 times and vacuum dried. 100 mg of dry mycelium and 3 mL of nitric acid were added into the digestion tube for cold digestion for 1 h, and then, 5 mL water was added into the digestion tube for further digestion according to the following procedure. The digestion temperature rose to 130°C and was maintained for 20 min. After that, the temperature rose to 160°C and was maintained for 10 min, and then the temperature rose to 175°C and was maintained for 20 min. After cooling, constant volume of digestion liquid to 50 mL and used for the test of intracellular Cu content. A certain amount of the supernatant was also digested according to the above procedure and the resulted digestion liquid was used for the test of extracellular Cu content. The Cu content in digestion liquid was detected by ICP-MS. The content of extracellular Cu²⁺ was also determined by ICP-MS using the undigested supernatant directly.

GHK-Cu residues in fermentation were separated and analyzed using an Athena C¹⁸-WP, 100A (150 mm × 4.6 mm, 5 μm) on a Shimadzu LC-10AT system equipped with an SPD-10AUV detector. The mobile phase was 0.1% trifluoroacetic acid (TFA) solution and methanol with an equal gradient of 95:5. The flow rate and injection volume were 0.6 mL min⁻¹ and 20 μL, respectively, and the analytical wavelength was 220 nm.

2.2.2 Microscopic observation of mycelium

As described in Section 2.2.1, the pelleted mycelia of *T. versicolor* were collected on the 7th day of fermentation and washed 3 times with pH 7, 0.2 mol L⁻¹ PBS. Then, they were treated with 2.5% glutaraldehyde and 1% oxide for 2 h before being washed with 0.1 mol L⁻¹ PBS. The rinsed samples were dehydrated overnight with 30% ethanol and rinsed with 0.1 mol L⁻¹ PBS. Next, samples were transferred to a series of ethanol solutions (0, 70, 80, 90, and 100%) for 30 min, respectively. After dehydrating and embedding in Epon 812 resin, ultrathin sections were cut with a diamond knife. Then the slices were double-stained with uranyl acetate and lead citrate quickly. Finally, the slices were prepared and visualized by a transmission electron microscope (Hitachi H-7650, TEM). The experiments were carried out in triplicate. The thickness of the cell wall was measured near the section of the central part of the cell by Image J (V 1.8.0) software.

2.2.3 Determination of laccase gene expression

As described in Section 2.2.1, the pellet mycelia of *T. versicolor* during fermentation process was collected (1, 2, 3, 4, 5, 6 and 7th day) and washed 3 times with sterile water, and the pelleted mycelium was dried with sterile cloth and stored at -80°C. RNA was extracted using TaKaRa MiniBEST Plant

RNA Extraction Kit. gDNA removal and reverse transcription to cDNA synthesis was performed according to the Prime Script™ RT Reagent Kit with gDNA Eraser (Perfect Real Time). The synthesized cDNA was stored at -20°C. The primer sequences of 3 target genes laccase (*TvLac*) and housekeeping gene *18s* were standardized. The primers used in this study are shown in [Supplementary Table S1](#). Real-time fluorescence quantitative PCR (RT-qPCR) was used in this study with the TB Green® Premix Ex Taq™ II (Tli RNaseH Plus) Kit to perform the PCR reaction in the Step One Plus Real-time PCR System, and the reaction system was shown in [Supplementary Table S2](#). The reaction was continued under the following conditions, 40 denaturation cycles at 95°C for 30 s, annealing, and extension steps at 60°C for 30 s. The melting curves ranged from 60°C to 95°C. The Bio-Rad CFX Manager 3.0 software was used to process the Ct (Threshold cycle) values and the 2^{-ΔΔCT} method was used to calculate the experimental results.

2.3 Other determination methods

Samples are taken daily from the fermentation broth, the culture broth was separated by centrifugation for 10 min at 8000 rpm, at 4°C. And then, cell-free supernatant was used to determine glucose content, extracellular protein content, and laccase activity. The glucose concentration was measured by an SBA-40E glucose tester. Extracellular protein was determined by [Bradford. \(1976\)](#), and bovine serum albumin was used as standard. The measurement of biomass and laccase activity was prepared according to the procedure described by [Wang et al. \(2014\)](#). In addition, to observe the leakage of intracellular substances, intracellular macromolecular leakage and conductivity were determined ([Supplementary Materials and Methods S3](#)).

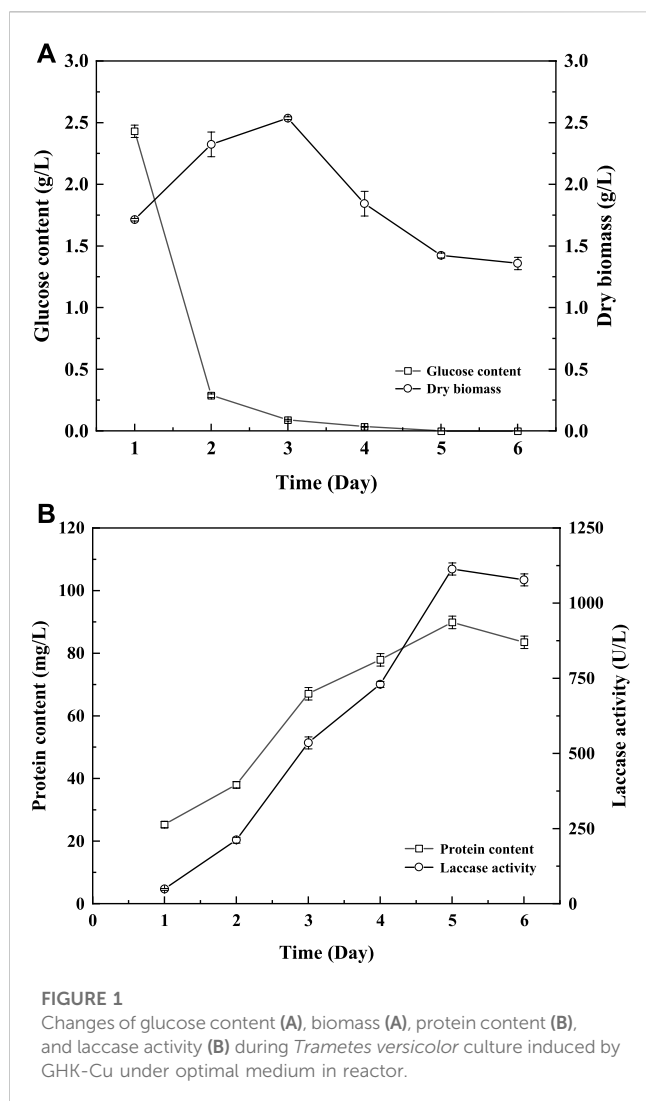
2.4 Statistical analysis

All experiments were repeated three times, and results were analyzed using SPSS16.0 software (SPSS, Inc., Chicago, IL, United States) and expressed as mean ± standard deviation. The data were analyzed by one-way analysis of variance (ANOVA), and the difference between the means was tested by Tukey test ($p < 0.05$).

3 Results

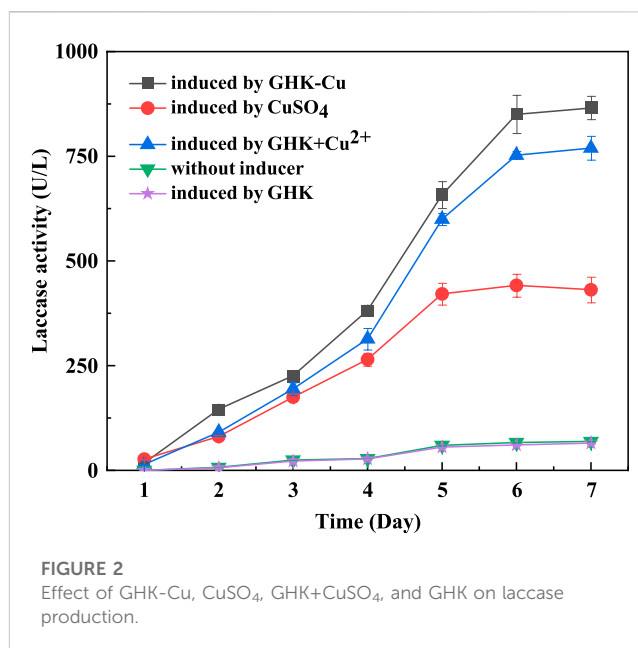
3.1 Effects of GHK-Cu on laccase production

When the concentration of GHK-Cu was 50–200 μmol L⁻¹, the production of laccase increased gradually, reaching the maximum value of 605.61 U L⁻¹ at 200 μmol L⁻¹. After that, laccase production remained stable with the increase of GHK-Cu concentration ([Supplementary Figure S1](#)). Therefore, GHK-Cu is an effective inducer of laccase of *T. versicolor*, and the expression of laccase was not affected by the high concentration of GHK-Cu, which may be due to its low cytotoxicity.



3.2 Screening of other important variables affecting laccase production

Seven variables were tested for the better laccase production by *T. versicolor* (Supplementary Figures S1, S2) using one-factor-at-a-time, GHK-Cu 200 $\mu\text{mol L}^{-1}$, glucose 5 g L^{-1} , NH_4Cl 0.2 g L^{-1} , KH_2PO_4 0.2 g L^{-1} , CaCl_2 0.04 g L^{-1} , $\text{FeSO}_4 \cdot 7\text{H}_2\text{O}$ 0.03 g L^{-1} , and $\text{MgSO}_4 \cdot 7\text{H}_2\text{O}$ 0.05 g L^{-1} . According to the ANOVA, GHK-Cu, glucose, NH_4Cl , KH_2PO_4 , CaCl_2 , and $\text{FeSO}_4 \cdot 7\text{H}_2\text{O}$ were significant factors affecting laccase production with $p < 0.05$ (Supplementary Table S3). The production of laccase was improved and reached the maximal production at 200 $\mu\text{mol L}^{-1}$ of GHK-Cu. Glucose of 10 g L^{-1} and NH_4Cl of 0.2 g L^{-1} caused a maximum laccase production that was 635.48 and 533.27 U L^{-1} , respectively. Different C/N is needed by different microorganisms, it leads to different glucose and NH_4Cl contents in the culture medium. Laccase production was caused by a significant effect of KH_2PO_4 , which plays an important role in cell growth and reproduction. The production of laccase reached 636.02 U L^{-1} with KH_2PO_4 of 0.2 g L^{-1} . The effect of each parameter on laccase production was studied in the form of one-factor-at-a-time. However, the interaction between various factors is also very important in



fermentation. Therefore, the composition of the fermentation medium was further optimized by BBD and RSM.

3.3 Optimization of screened variables by BBD-RSM

In a set of 54 trials, the optimal level of each component and their interactions were determined by BBD (Supplementary Table S4, S5). The quadratic model illustrated a mathematical relationship between the factors and laccase production as Supplementary Eq. SA6.

AVONA of the BBD was shown in Supplementary Table S4. A, B, C, AB, BF, and CE in the medium components were all significant. GHK-Cu, glucose, and NH_4Cl were more influential than the other variables. In Supplementary Table S6, the F-value for “Lack of fit” was 2.51, indicating that the “Lack of fit” was not significant. The model had linear correlation coefficient (R^2) and the adjusted correlation coefficients (R^2_{adj}) were 0.95 and 0.91, respectively (Supplementary Tables S6, S7). A significant correlation between the predicted and the actual value of laccase production also was proved (Supplementary Figure S3). 3-D response surface (Supplementary Figure S4) was plotted through the optimal level of each variable and the effect of their interactions on laccase production. The interaction between glucose and GHK-Cu indicated that higher activity of laccase was observed at higher GHK-Cu concentration with increased glucose concentration until at the central level (Supplementary Figure S4A). The interaction between NH_4Cl and KH_2PO_4 (Supplementary Figure S4B) showed that KH_2PO_4 and NH_4Cl at the central level resulted in higher laccase production. As from Supplementary Figure S4C, D, the optimum laccase activity was obtained at high NH_4Cl concentration with low concentration of CaCl_2 and $\text{FeSO}_4 \cdot 7\text{H}_2\text{O}$ and this result is consistent with Supplementary Figure S4G. The response surface curve showed maximal laccase activity at the middle level of

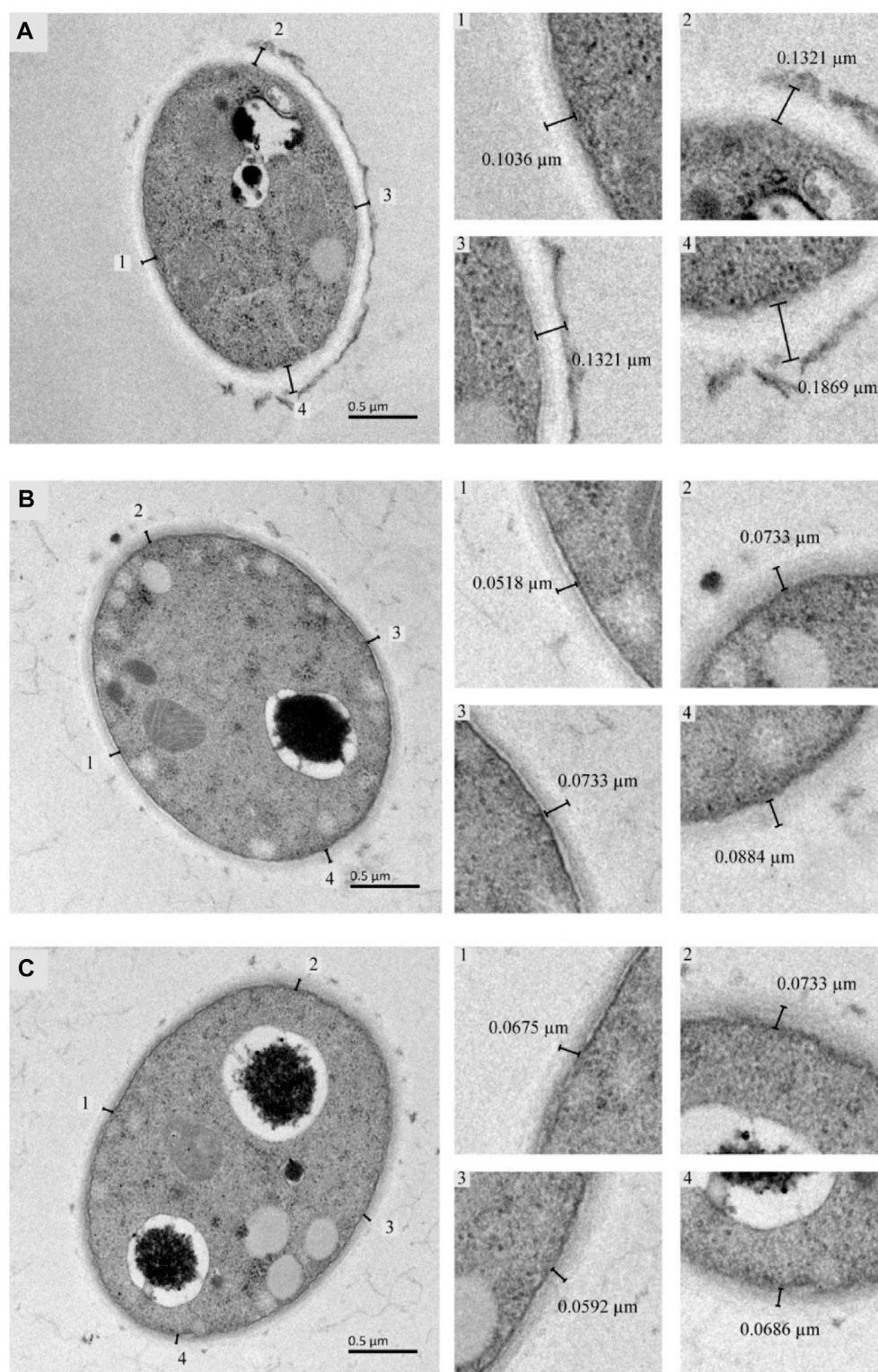


FIGURE 3

TEM analysis of *Trametes versicolor* cultured under different inducers [(A) Control, (B) GHK-Cu, (C) CuSO₄].

KH₂PO₄, CaCl₂, and FeSO₄·7H₂O content (Supplementary Figures S4E, F).

Based on the above results, the formula was differentiated by software Design-Expert (Version 13, Stat-Ease Inc., United States), and the optimal

medium formula was obtained as follows, GHK-Cu 290 $\mu\text{mol L}^{-1}$, glucose 4.21 g L^{-1} , NH₄Cl 0.31 g L^{-1} , KH₂PO₄ 0.18 g L^{-1} , CaCl₂ 0.047 g L^{-1} , FeSO₄·7H₂O 0.043 g L^{-1} , and MgSO₄·7H₂O 0.0526 g L^{-1} . The maximum response value of the model is 830.233 U L⁻¹.

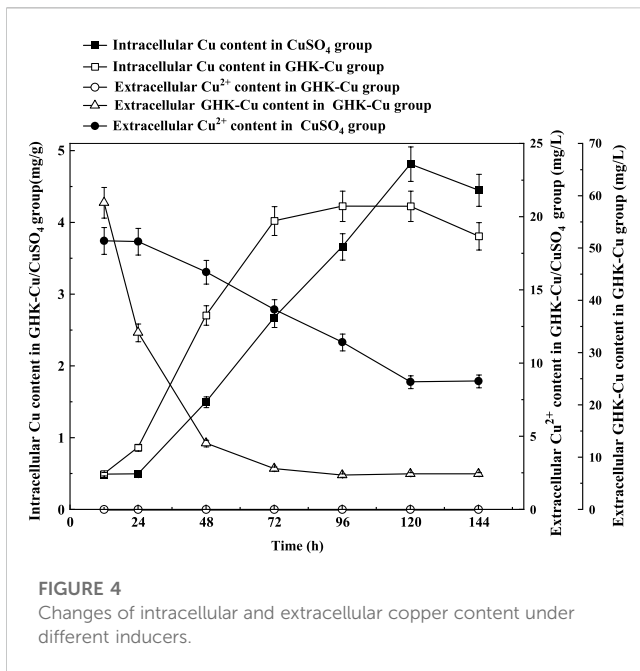


FIGURE 4
Changes of intracellular and extracellular copper content under different inducers.

To verify the induction of GHK-Cu on laccase production by *T. versicolor*, the laccase activity was 850.05 U L^{-1} (Supplementary Figure S5) at the 7th day of culture under optimal conditions, which was consistent with the predicted value. The production of laccase was 12.77-fold higher than that of the basal fermentation medium with the final enzyme activity of 66.59 U L^{-1} flask.

3.4 Laccase production in a 5 L reactor

To further verify the feasibility of laccase production by fermentation induced by GHK-Cu, the scaling-up fermentation of *T. versicolor* in 5 L reactor was carried out. As shown in Figure 1, the growth trend of *T. versicolor* under amplification culture in the reactor is basically consistent with a shake flask (Supplementary Figure S5). In the first 72 h, *T. versicolor* grew rapidly, biomass reached the peak of 2.33 g L^{-1} on the 3rd day. At the same time, glucose was consumed rapidly until the 3rd day, which was consistent with the time when the maximum biomass of *T. versicolor* appeared. Laccase activity reached the maximum value of 1113.57 U L^{-1} on the 5th day. At the early stage of fermentation, with the cell growth and laccase production, the protein content was increased and reached the peak of 89.86 mg L^{-1} on the 5th day. Compared to the results in the shake flask, the peak of biomass and laccase production in a 5 L reactor was 1 day earlier than those in shake flask. And, the laccase production in bioreactor was 1.31-fold higher than that of the shake.

3.5 Possible mechanisms

3.5.1 Effects of different inducer component and combination on laccase production

Based on the optimal medium without GHK-Cu, the same amount of GHK-Cu, CuSO_4 , GHK+ CuSO_4 , and GHK was added

separately, and the control was without inducer. The laccase production of the five groups was compared and results are shown in Figure 2. It can be seen that the addition of GHK-Cu, CuSO_4 and GHK+ CuSO_4 could promote the laccase production by the *T. versicolor*, while GHK exhibited no promotion effect. Among them, GHK-Cu provided the highest laccase production of 850.05 U L^{-1} , followed by GHK+ CuSO_4 complex solution with the laccase production of 752.52 U L^{-1} , and CuSO_4 exhibited the worst induction effect with the laccase production of 441.57 U L^{-1} on the 6th day. This suggested that GHK-Cu was the best inducer for laccase production by *T. versicolor* at the same concentration of Cu^{2+} .

The effects of different concentrations of GHK-Cu and CuSO_4 on the laccase production were also investigated and the results were shown in Supplementary Figure S6. Both GHK-Cu and CuSO_4 could induce the laccase production when the concentration of Cu^{2+} was in the range of $50\text{--}300 \mu\text{mol L}^{-1}$. The laccase production reached the maximum of 850.05 U L^{-1} at $290 \mu\text{mol L}^{-1}$ GHK-Cu, while CuSO_4 induced the peak laccase activity of 513.56 U L^{-1} at $400 \mu\text{M}$. It indicated that the GHK-Cu exhibited high induction efficiency since higher laccase production was obtained at lower inducer concentration. In addition, further increase in inducer concentration resulted in no significant change in laccase production of the GHK-Cu group. However, the laccase production in the CuSO_4 group significantly decreased at high concentration.

3.5.2 Effect of GHK-Cu on membrane permeability

Supplementary Figure S7 showed the changes in leakage of protein and nucleic acid from the cells during the culture period of *T. versicolor*. The leakage of protein and nucleic acid from the same amount of cells increased with respect to the culture time. It indicated that the cell membrane permeability increased with the prolonged culture time. The treatment with CuSO_4 or GHK-Cu could promote the cell membrane permeability of *T. versicolor* and CuSO_4 showed the most serious destroy of cell membrane resulting in the largest amount of leakage. As shown in Supplementary Figure S8, the conductivity and mass transfer diffusion coefficient (R_c) also increased with the increase of culture time and CuSO_4 showed the best performance.

The cell wall thickness of *T. versicolor* was observed by TEM (Figure 3). There was a significant difference in mycelial cell wall thickness. The control cell wall ($0.139 \pm 0.030 \mu\text{m}$) was approximately 1.95-fold and 2.07-fold the thickness of the cells treated with GHK-Cu ($0.071 \pm 0.013 \mu\text{m}$) and CuSO_4 ($0.067 \pm 0.005 \mu\text{m}$), respectively. This result proved that GHK-Cu and CuSO_4 had an inhibitory effect on the cell wall synthesis of *T. versicolor* and CuSO_4 exhibited more serious effect.

3.5.3 Change of intracellular and extracellular Cu concentration

According to the results in Figure 4, no extracellular Cu^{2+} was detected in the GHK-Cu group, indicating that GHK-Cu in the broth was not disassociated or degraded into free Cu^{2+} during culture period. The consumption of extracellular GHK-Cu was faster, which tended to be stable after 72 h, and the consumption percentage reached 89.8% at 48 h, while that of Cu^{2+} in the CuSO_4

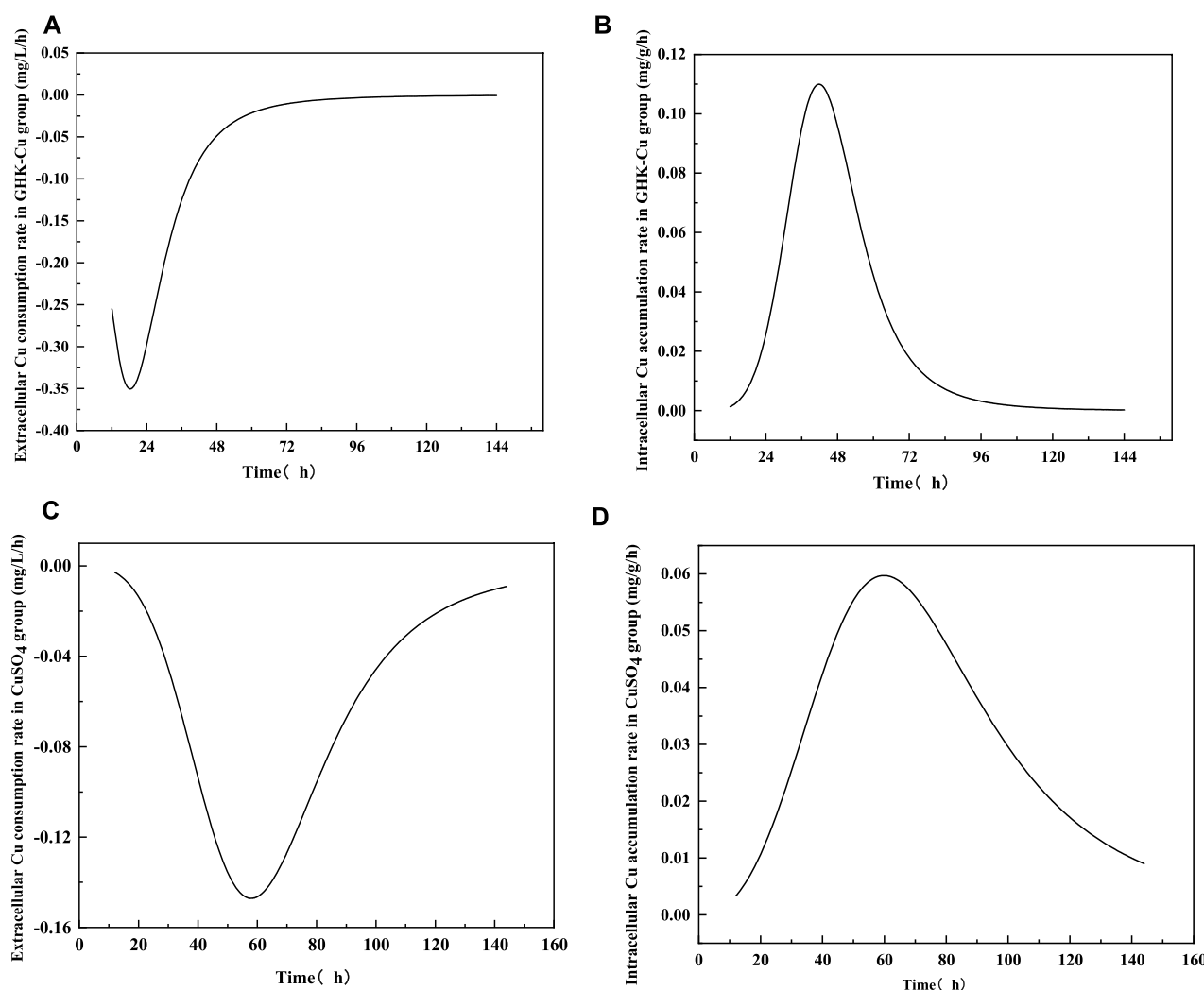


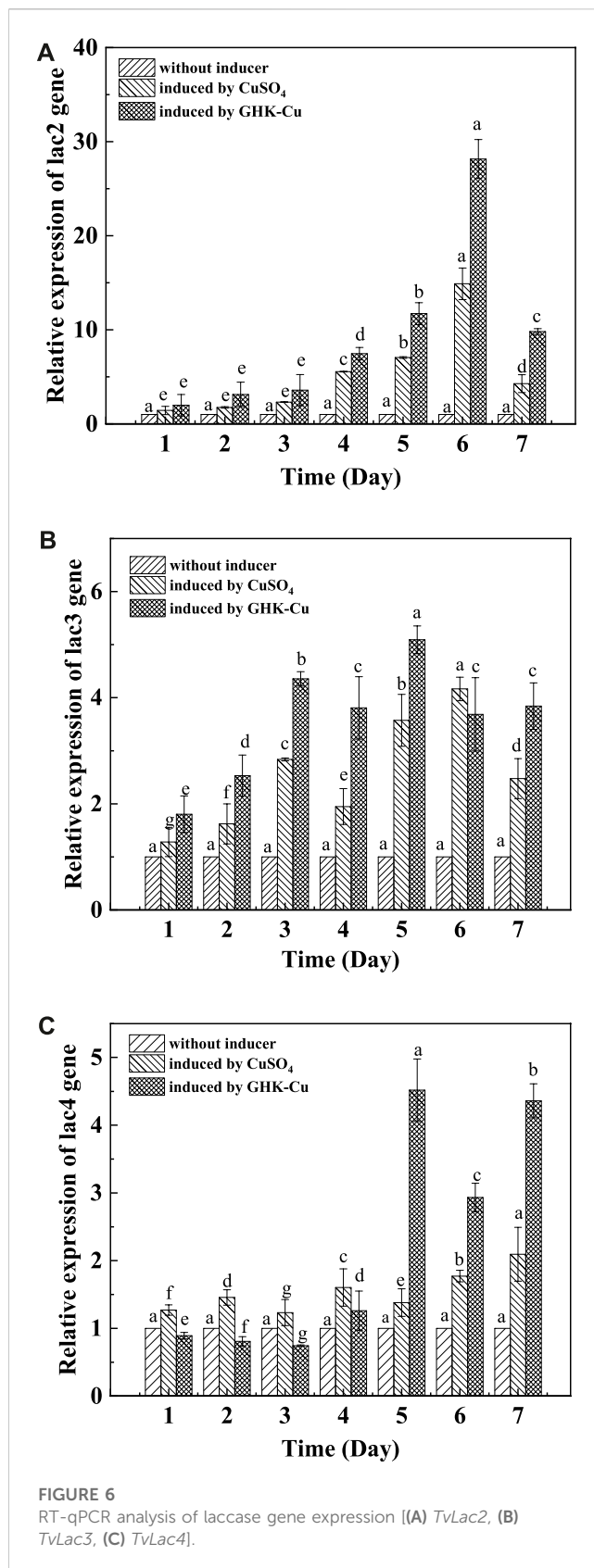
FIGURE 5
Consumption rates of extracellular Cu and accumulation rates of intracellular Cu treated with different inducers [(A) consumption rate in GHK-Cu group, (B) accumulation rate of Cu in GHK-Cu group, (C) consumption rate in CuSO₄ group, (D) accumulation rate of Cu in CuSO₄ group].

group was only 12.7%. In this study, GHK-Cu, as a complex of small molecular protein and metal ions, facilitated the transportation of Cu into fungal cells in liquid culture. With the prolonged culture time, intracellular Cu showed a downward trend during 120–144 h in both treatment groups, which may be due to the leakage of intracellular Cu into the broth resulted from cell aging and autolysis. At 144 h, the mole concentration of the extracellular GHK-Cu in GHK-Cu group and the extracellular Cu²⁺ in CuSO₄ group was 20 and 137 $\mu\text{mol L}^{-1}$, respectively. However, the Cu content in mycelium was 3.73 and 4.45 mg g^{-1} for GHK-Cu group and CuSO₄ group, respectively, where the biomass was 1.36 g L^{-1} in GHK-Cu group and 1.41 g L^{-1} in CuSO₄ group (data not shown). These results indicated more Cu in the GHK-Cu group was consumed, which may be resulted from higher laccase production. The consumption rate of Cu and the accumulation rate of Cu in mycelium were also calculated (Figure 5). The maximal consumption rate and accumulation rate

of Cu in the GHK-Cu group were 0.35 $\text{mg L}^{-1} \text{h}^{-1}$ and 0.11 $\text{mg g}^{-1} \text{h}^{-1}$ (Figures 5A, B). The peak of Cu consumption rate and Cu accumulation rate in CuSO₄ group was 0.15 $\text{mg L}^{-1} \text{h}^{-1}$ and 0.06 $\text{mg g}^{-1} \text{h}^{-1}$ (Figures 5C, D). The maximal consumption and accumulation rates of Cu in GHK-Cu group were higher than those in the CuSO₄ group and occurred in the earlier stage. The content of intracellular Cu in the GHK-Cu group also increased more rapidly than that in the CuSO₄ group, and tended to be stable after 72 h.

3.5.4 Analysis of laccase gene expression

The differential regulation of laccase gene expression (*TvLac2*, *TvLac3* and *TvLac4*) during the fermentation period of *T. versicolor* was shown in Figure 6. The relative expression level of the tested laccase genes was relatively low in the early culture stage, and it increased gradually and reached the peak on the 5th and 6th day. The induced expression levels of *TvLac2* exhibited the highest



relative increase multifold in both the GHK-Cu group and CuSO_4 group, where it was 28.15 and 14.88 times higher than that of the control on the 6th day. The expression levels of *TvLac3* and *TvLac4* genes in the GHK-Cu group were 5.09 and 4.51 times than that of the control on the 5th day, respectively. The expression levels of *TvLac3* and *TvLac4* genes in the CuSO_4 group were 4.16 and 2.09 times higher than those in the control on day 6 and day 7, respectively. Combined with [Supplementary Figure S5](#), it can be seen that the dynamic trend of gene expression level was basically the same as that of laccase production.

4 Discussion

4.1 Optimization of medium and scale-up of 5 L reactor for laccase production

In the exploration of the optimal composition of the culture medium, compared with other variables, GHK-Cu had a significant effect on laccase production. Cu^{2+} has been proved to be a good inducer of laccase production by *T. versicolor* ([BİRhanlı and Yesilada, 2017](#)). This may be due to adding Cu^{2+} could upregulate the transcription level of the laccase gene ([Xu et al., 2020](#)). Metal ions have positive effects on laccase production ([Akpınar and Öztürk Urek, 2017](#)). In addition, inorganic salts play an important role in buffer and regulation between strain and culture medium, and are closely related to microbial growth and metabolism. Among them, laccase production was affected by KH_2PO_4 , because it played an important role in the mass transfer of nutrients during microbial growth ([Nandal et al., 2013](#)). And, the same conclusion as Xu et al., was obtained, cell growth and metabolism were affected by C/N ([Xu et al., 2020](#)). Studies have shown that a higher concentration of glucose results in the faster growth of microbes and the better the products ([Nandal et al., 2013](#)). The results of this study are different from theirs. For different microorganisms, appropriate nitrogen source and carbon source both are important reason for increasing the laccase production ([Wang et al., 2019; Su et al., 2020](#)). Due to the different strains and media, the interaction between the various components of the medium is discrepant, so the optimal medium formulations to obtain the laccase production are diverse. Studies have proved that reasonable optimization of medium components can increase laccase production in fermentation ([Patil et al., 2020](#)). In 5 L reactor, the peak of biomass and laccase production was 1 day earlier than that in shake flask, and higher laccase production was obtained. The laccase production increased rapidly during the period of rapid glucose consumption. A similar phenomenon was also observed in the culture of *Aquatic Hyphomycetes*, which indicated a correlation between glucose consumption and biomass production ([Charcosset and Chauvet, 2001](#)). The better laccase production obtained in the bioreactor was due to the accurate

control of temperature, pH, and effective supply of oxygen in the stirring reactor. Studies have shown that the supply and transfer of oxygen is an efficient strategy to promote the normal metabolism and product production of fungi (Meneghel et al., 2014).

4.2 Possible mechanisms

The effects of different inducers on laccase production were compared, and it was found that GHK-Cu had a better effect, which benefited from the characteristics of CHK-Cu. When GHK was coupled with copper, the peptide may quench the redox activity of copper, facilitating the non-toxic delivery of Cu^{2+} into the hepatoma cells (Pickart et al., 1980). This could be the reasons for the best laccase production induced by GHK-Cu. In case of GHK+ CuSO_4 addition, the complex GHK-Cu could be formed due to the high affinity GHK for Cu^{2+} (Alshammari and Platts, 2020). And thus, GHK+ CuSO_4 showed partly induction effect of GHK-Cu, resulting enhanced laccase production compared to that in CuSO_4 group.

It can be found by analyzing the results of macromolecule leakage and Rc in the cells of *T. versicolor*. The increase of cell membrane permeability in CuSO_4 group and GHK-Cu group was beneficial for the secretion of laccase, which can be one of the reasons for the enhanced laccase production. The same results can be obtained in TEM images, both GHK-Cu and CuSO_4 could reduce cell wall thickness and enhance cell membrane permeability, while CuSO_4 had a stronger effect. A significant decrease of cell wall's thickness may be beneficial to the secretion of intracellular substance (Ma et al., 2019). However, the production of laccase induced by CuSO_4 was lower, indicating that CuSO_4 had a negative effect on laccase activity. These results proved that CuSO_4 showed higher toxicity to *T. versicolor* cells than that of GHK-Cu. It has been reported that laccase production of *Ganoderma* sp. increased with the increasing Cu^{2+} concentration in the medium (Sharma et al., 2015) and high concentration of Cu^{2+} affected cell growth and laccase production of *Trametes* sp. due to its toxicity (Akpınar and Öztürk Urek, 2017). GHK-Cu showed no cytotoxicity to skin cells in the range of $0.0058\text{--}5,800\text{ }\mu\text{mol L}^{-1}$, while Cu^{2+} substantial cytotoxicity at $5,800\text{ }\mu\text{mol L}^{-1}$ after 30 min treatment (Li et al., 2016). It is maybe due to the promoted production of free radicals induced by excessive copper interfered with fatty acid and protein metabolism, respiration, and membrane integrity, resulting in the change of cell membrane permeability and the leakage of electrolyte (Shi-Sheng, 2007). It can be concluded that GHK-Cu was a good laccase inducer with high efficiency and low toxicity.

The content of copper inside and outside the cells of the suppository was determined. It indicated that GHK-Cu can enter cells quickly and be used efficiently compared to the Cu^{2+} from CuSO_4 . Lysine on the GHK side chain of GHK-Cu could participate in the recognition of liver cancer cell receptors, and these receptors played an important role in the absorption of Cu, the transport of Cu into cells was be promoted (Pickart et al., 1980). Therefore, the high-efficient

absorption, accumulation and utilization of Cu could be one of the reasons for the good laccase expression induced by GHK-Cu. In fact, the promoter region of laccase gene may contain elements responding to Cu^{2+} regulation, which regulated laccase gene expression in a strain-dependent manner (Degerli et al., 2019; Pawlik et al., 2021). It has been proved that the increase in laccase gene expression level contributed to the increase in laccase production (Rodrigues et al., 2019). It can be concluded that GHK-Cu provided better expression level of laccase gene compared to CuSO_4 at the same Cu^{2+} concentration, resulting in enhanced laccase production. It may be related to the quick and high accumulation of intracellular Cu.

All the above results indicate that GHK-Cu was more conducive to the secretion of laccase. This fact may be due to that GHK is considered to be the transporter of metal ions through membranes, and the exchange kinetics and REDOX behavior of GHK are stable in biological systems, which makes copper much safer for cells when transported into them (Alshammari and Platts, 2020). Moreover, glutathione chelating with Cu can be involved in repairing membrane damage caused by Cu (Freedman et al., 1899). It was speculated that GHK and glutathione have the same effect on reducing the damage of Cu to the cell membrane. Therefore, high production laccase was induced by GHK-Cu with less damage and toxicity to cells.

5 Conclusion

To obtain the efficient laccase production from *T. versicolor*, non-toxic GHK-Cu was used as a new inducer instead of CuSO_4 . The laccase production was greatly improved after the optimization of medium composition by one-factor-at-a-time, BBD and RSM, and it was scaled-up in 5 L stirring reactor. To reveal the possible mechanism, cell membrane permeability, copper consumption and accumulation and laccase gene expression were characterized. It was found that GHK-Cu was a low toxicity and high-efficient laccase inducer, which may expand the application of laccase in food industry by using the culture broth directly. Besides it, GHK chelated metal ions can also be a potential strategy for the induced expression of other metal enzymes.

Data availability statement

The original contributions presented in the study are included in the article/Supplementary Material, further inquiries can be directed to the corresponding author.

Author contributions

FW: conceptualization, methodology, funding acquisition, writing-review and editing. XY: methodology, validation, data curation, and writing-original draft preparation. ZY: investigation. YC: validation. LX: resources, software, formal

analysis, funding acquisition, and supervision. SH: funding acquisition and validation. ZD: conceptualization. LZ: visualization. LD: project administration. YQ: funding acquisition. All authors have read and agreed to the published version of the manuscript.

Funding

This work was supported by the National Key Research and Development Program of China, grant number 2020YFA0907300; the National Natural Science Foundation of China, grant number No. 21978120; the Key R&D project in Jiangsu Province, grant number BE2020405 and the Senior Talent Scientific Research Initial Funding Project of Jiangsu University, grant numbers 15JDG17 and 15JDG061.

Acknowledgments

The authors would like to thank Ou Xianjin (Institute of Biophysics, CAS) for the technical assistance.

References

- Akpinar, M., and Ozturk Urek, R. (2017). Induction of fungal laccase production under solid state bioprocessing of new agroindustrial waste and its application on dye decolorization. *3 Biotech.* 7, 98. doi:10.1007/s13205-017-0742-5
- Alshammari, N., and Platts, J. A. (2020). Theoretical study of copper binding to GHK peptide. *Comput. Biol. Chem.* 86, 107265. doi:10.1016/j.compbiolchem.2020.107265
- Bertrand, B., Martinez-Morales, F., and Trejo-Hernandez, M. R. (2017). Upgrading laccase production and biochemical properties: Strategies and challenges. *Biotechnol. Prog.* 33, 1015–1034. doi:10.1002/btpr.2482
- Birhanli, E., and Yeşilada, Ö. (2017). The effect of various inducers and their combinations with copper on laccase production of *Trametes versicolor* pellets in a repeated-batch process. *Turk J. Biol.* 41, 587–599. doi:10.3906/biy-1608-44
- Bradford, M. M. (1976). A rapid and sensitive method for the quantitation of microgram quantities of protein utilizing the principle of protein-dye binding. *Anal. Biochem.* 72, 248–254. doi:10.1016/0003-2697(76)90527-3
- Charcosset, J. Y., and Chauvet, E. (2001). Effect of culture conditions on ergosterol as an indicator of biomass in the aquatic hyphomycetes. *Appl. Environ. Microbiol.* 67, 2051–2055. doi:10.1128/AEM.67.5.2051-2055.2001
- Chaurse, V. K., and Sahay, S. (2023). Laccase from *Truncatella angustata* showing Pb²⁺ induced burst of activity and dye decolorization without mediator and carbon footprint in cold climate. *Bioresour. Technol. Rep.* 21, 101305. doi:10.1016/j.biteb.2022.101305
- Das, N., Chakraborty, T. K., and Mukherjee, M. (1999). Role of potato extract in extracellular laccase production of *Pleurotus florida*. *J. Basic Microbiol.* 39, 299–303. doi:10.1002/(SICI)1521-4028(199912)39:5/6<299:AID-JOBM299>3.0.CO;2
- Degerli, E., Yangin, S., and Cansaran-Duman, D. (2019). Determination of the effect of RBBR on laccase activity and gene expression level of fungi in lichen structure. *3 Biotech.* 9, 297. doi:10.1007/s13205-019-1832-3
- Fonseca, M. I., Tejerina, M. R., Sawostjanik-Afanasiuk, S. S., Giorgio, E. M., Barchuk, M. L., Zapata, P. D., et al. (2016). Preliminary studies of new strains of *Trametes sp.* from Argentina for laccase production ability. *Braz J. Microbiol.* 47, 287–297. doi:10.1016/j.bjm.2016.01.002
- Freedman, J. H., Ciriolo, M. R., and Peisach, J. (1989). The role of glutathione in copper metabolism and toxicity. *J. Bio Chem.* 264, 5598–5605. doi:10.1016/s0021-9258(18)83589-x
- Gomez-Fernandez, B. J., Risso, V. A., Rueda, A., Sanchez-Ruiz, J. M., and Alcalde, M. (2020). Ancestral Resurrection and Directed Evolution of Fungal Mesozoic Laccases. *Appl. Environ. Microbiol.* 86, e00778–20. doi:10.1128/AEM.00778-20
- Khatami, S. H., Vakili, O., Movahedpour, A., Ghesmati, Z., Ghasemi, H., and Taheri-Anganeh, M. (2022). Laccase: Various types and applications. *Biotechnol. Appl. Biochem.* 69, 2658–2672. doi:10.1002/bab.2313
- Li, H., Toh, P. Z., Tan, J. Y., Zin, M. T., Lee, C. Y., Li, B., et al. (2016). Selected biomarkers revealed potential skin toxicity caused by certain copper compounds. *Sci. Rep.* 6, 37664. doi:10.1038/srep37664
- Liu, H. Y., Zhang, Z. X., Xie, S. W., Xing, H., Zhu, Y. N., Li, H. Y., et al. (2019). Study on transformation and degradation of bisphenol A by *Trametes versicolor* laccase and simulation of molecular docking. *Chemosphere* 224, 743–750. doi:10.1016/j.chemosphere.2019.02.143
- Ma, Z. B., Xu, M. M., Wang, Q. O., Wang, F., Zheng, H. H., Gu, Z. H., et al. (2019). Development of an efficient strategy to improve extracellular polysaccharide production of *Ganoderma lucidum* using L-phenylalanine as an enhancer. *Front. Microbiol.* 10, 2306. doi:10.3389/fmicb.2019.02306
- Meneghel, L., Reis, G. P., Reginatto, C., Malvessi, E., and da Silveira, M. M. (2014). Assessment of pectinase production by *Aspergillus oryzae* in growth-limiting liquid medium under limited and non-limited oxygen supply. *Process Biochem.* 49, 1800–1807. doi:10.1016/j.procbio.2014.07.021
- Nandal, P., Ravella, S. R., and Kuhad, R. C. (2013). Laccase production by *Corioliopsis caperata* RCK2011: Optimization under solid state fermentation by taguchi DOE methodology. *Sci. Rep.* 3, 1386. doi:10.1038/srep01386
- Pardo, I., and Camarero, S. (2015). Laccase engineering by rational and evolutionary design. *Cell. Mol. Life Sci.* 72, 897–910. doi:10.1007/s00018-014-1824-8
- Patil, N. D., Chopade, L. R., Narkhede, K. P., Chaudhari, B. L., and Mahajan, R. T. (2020). Bioprocess optimization of laccase production through solid substrate fermentation using *Perenniporia tephropora*-L168 and its application in bioremediation of triaryl-methane dye. *Biotechnol. Prog.* 36, e2916. doi:10.1002/btpr.2916
- Pawlik, A., Ciolek, B., Sulej, J., Mazur, A., Grela, P., Staszczak, M., et al. (2021). Cerrena unicolor laccases, genes expression and regulation of activity. *Biomolecules* 11, 468. doi:10.3390/biom11030468
- Pickart, L., Freedman, J. H., Loker, W. J., Peisach, J., Perkins, C. M., Stenkamp, R. E., et al. (1980). Growth-modulating plasma tripeptide may function by facilitating copper uptake into cells. *Nature* 288, 715–717. doi:10.1038/288715a0
- Pickart, L., and Margolin, A. (2018). Regenerative and protective actions of the GHK-Cu peptide in the light of the new gene data. *Int. J. Mol. Sci.* 19, 1987. doi:10.3390/ijms19071987
- Pinheiro, V. E., Michelin, M., Vici, A. C., de Almeida, P. Z., and Teixeira de Moraes Polizeli, M. L. (2020). *Trametes versicolor* laccase production using agricultural wastes: A comparative study in erlenmeyer flasks, bioreactor and tray. *Bioprocess Biosyst. Eng.* 43, 507–514. doi:10.1007/s00449-019-02245-z
- Pisacha, I. M., Perkasa, T. A. B., Amnelia, T., Miranti, M., Puspita, F., Nurulita, Y., et al. (2020). Screening for potential laccase producers from *Trichoderma* strains isolated from riau citrus rhizosphere and palm tree plant parts. *J. Phys. Conf. Ser.* 1655, 012039. doi:10.1088/1742-6596/1655/1/012039

Conflict of interest

Authors LD and YQ were employed by the company Shandong Dehemingxing Biotechnology Co., Ltd.

The remaining authors declare that the research was conducted in the absence of any commercial or financial relationships that could be construed as a potential conflict of interest.

Publisher's note

All claims expressed in this article are solely those of the authors and do not necessarily represent those of their affiliated organizations, or those of the publisher, the editors and the reviewers. Any product that may be evaluated in this article, or claim that may be made by its manufacturer, is not guaranteed or endorsed by the publisher.

Supplementary material

The Supplementary Material for this article can be found online at: <https://www.frontiersin.org/articles/10.3389/fbioe.2023.1176352/full#supplementary-material>

- Rodrigues, E. M., Karp, S. G., Malucelli, L. C., Helm, C. V., and Alvarez, T. M. (2019). Evaluation of laccase production by *Ganoderma lucidum* in submerged and solid-state fermentation using different inducers. *J. Basic Microbiol.* 59, 784–791. doi:10.1002/jobm.201900084
- Sharma, A., Shrivastava, B., and Kuhad, R. C. (2015). Reduced toxicity of malachite green decolorized by laccase produced from *Ganoderma sp.* rckk-02 under solid-state fermentation. *3 Biotech.* 5, 621–631. doi:10.1007/s13205-014-0258-1
- Shi-Sheng, K. E. (2007). Effects of copper on the photosynthesis and oxidative metabolism of amaranthus tricolor seedlings. *Agr. Sci. China* 6, 1182–1192. doi:10.1016/S1671-2927(07)60162-X
- Su, Y., Seguinot, P., Sanchez, I., Ortiz-Julien, A., Heras, J. M., Querol, A., et al. (2020). Nitrogen sources preferences of non-*Saccharomyces* yeasts to sustain growth and fermentation under winemaking conditions. *Food Microbiol.* 85, 103287. doi:10.1016/j.fm.2019.103287
- Valle, J. S., Vandenberghe, L. P., Oliveira, A. C., Tavares, M. F., Linde, G. A., Colauto, N. B., et al. (2015). Effect of different compounds on the induction of laccase production by *Agaricus blazei*. *Genet. Mol. Res.* 14, 15882–15891. doi:10.4238/2015.December.1.40
- Wang, F., Hu, J. H., Guo, C., and Liu, C. Z. (2014). Enhanced laccase production by *Trametes versicolor* using corn steep liquor as both nitrogen source and inducer. *Bioresour. Technol.* 166, 602–605. doi:10.1016/j.biortech.2014.05.068
- Wang, F., Ma, A. Z., Guo, C., Zhuang, G. Q., and Liu, C. Z. (2013). Ultrasound-intensified laccase production from *Trametes versicolor*. *Trametes versicolor Ultrason. Sonochem* 20, 118–124. doi:10.1016/j.ultsonch.2012.05.003
- Wang, F., Xu, L., Zhao, L. T., Ding, Z. Y., Ma, H. L., and Terry, N. (2019). Fungal laccase production from lignocellulosic agricultural wastes by solid-state fermentation: A review. *Microorganisms* 7, 665. doi:10.3390/microorganisms7120665
- Wang, J. Y., Lu, L., and Feng, F. J. (2017). Combined strategies for improving production of a thermo-alkali stable laccase in *Pichia pastoris*. *Electron J. Biotechnol.* 28, 7–13. doi:10.1016/j.ejbt.2017.04.002
- Wang, J. Y., Yu, S. Y., Li, X. Y., Feng, F. J., and Lu, L. (2020). High-level expression of *Bacillus amyloliquefaciens* laccase and construction of its chimeric variant with improved stability by domain substitution. *Bioprocess Biosyst. Eng.* 43, 403–411. doi:10.1007/s00449-019-02236-0
- Xu, L., Sun, K., Wang, F., Zhao, L. T., Hu, J. H., Ma, H. L., et al. (2020). Laccase production by *Trametes versicolor* in solid-state fermentation using tea residues as substrate and its application in dye decolorization. *J. Environ. Manage* 270, 110904. doi:10.1016/j.jenvman.2020.110904
- Zhang, Q., Zhao, L. T., Li, Y. R., Wang, F., Li, S., Shi, G. Y., et al. (2020). Comparative transcriptomics and transcriptional regulation analysis of enhanced laccase production induced by co-culture of *Pleurotus eryngii* var. *ferulae* with *Rhodotorula mucilaginosa*. *Appl. Microbiol. Biotechnol.* 104, 241–255. doi:10.1007/s00253-019-10228-z
- Zhang, Z. C., Shah, A. M., Mohamed, H., Tsiklauri, N., and Song, Y. D. (2021). Isolation and screening of microorganisms for the effective pretreatment of lignocellulosic agricultural wastes. *Biomed. Res. Int.* 2021, 1–16. doi:10.1155/2021/5514745

Frontiers in Bioengineering and Biotechnology

Accelerates the development of therapies,
devices, and technologies to improve our lives

A multidisciplinary journal that accelerates the
development of biological therapies, devices,
processes and technologies to improve our lives
by bridging the gap between discoveries and their
application.

Discover the latest Research Topics

See more →

Frontiers

Avenue du Tribunal-Fédéral 34
1005 Lausanne, Switzerland
frontiersin.org

Contact us

+41 (0)21 510 17 00
frontiersin.org/about/contact



Frontiers in
Bioengineering
and Biotechnology

